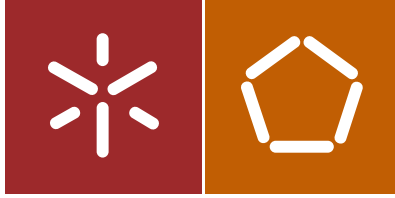




Universidade do Minho
Escola de Engenharia

João Manuel Matias

Infrared stereolithography



Universidade do Minho
Escola de Engenharia

João Manuel Matias

Infrared stereolithography

Tese de Doutoramento
Ciência e Engenharia de Polímeros e Compósitos

Trabalho efectuado sob a orientação do
Professor Doutor António José Vilela Pontes
Professor Doutor Paulo Jorge da Silva Bártolo

DECLARAÇÃO

Nos exemplares das teses de doutoramento ou de mestrado ou de outros trabalhos entregues para prestação de provas públicas nas universidades ou outros estabelecimentos de ensino, e dos quais é obrigatoriamente enviado um exemplar para depósito legal na Biblioteca Nacional e, pelo menos outro para a biblioteca da universidade respectiva, deve constar uma das seguintes declarações:

É AUTORIZADA A REPRODUÇÃO INTEGRAL DESTA TESE APENAS PARA EFEITOS DE INVESTIGAÇÃO, MEDIANTE DECLARAÇÃO ESCRITA DO INTERESSADO, QUE A TAL SE COMPROMETE.

Universidade do Minho, ___/___/_____

Assinatura: _____

STATEMENT OF INTEGRITY

I hereby declare having conducted my thesis with integrity. I confirm that I have not used plagiarism or any form of falsification of results in the process of the thesis elaboration.

I further declare that I have fully acknowledged the Code of Ethical Conduct of the University of Minho.

University of Minho, _____

Full name: _____

Signature: _____

Acknowledgements

To my Ph.D. Advisor, Professor António José Vilela Pontes, from the Department of Polymer Engineering at the University of Minho, for his wise supervision, guidance, great wisdom, extensive knowledge and experience. Thanks to him, this research work was kept on track, properly focused on the good results obtained.

To my Ph.D. Advisor, Professor Paulo Jorge da Silva Bártolo, from the Mechanical Engineering Department of the Polytechnic Institute of Leiria, for his wise supervision, guidance, great wisdom, extensive knowledge and experience. More than an advisor, it is also a lifetime friend. Some difficulties were overcome but stronger values will prevail.

To Professor André Jardini from the UNICAMP (Campinas, Brazil) for his knowledge and cooperation on experimental work carried out in his labs.

To the Portuguese Foundation for Science and Technology, for supporting this research work and the result dissemination activities under the grant SFRH/BD/39288/2007.

To the University of Minho and to the Polytechnic Institute of Leiria, for the cooperation protocol established between both institutions under which this research work was developed. University of Minho has provided me full access to his labs in order to carry out some of the experimental work. Also the Polytechnic Institute of Leiria has provided the necessary conditions for the execution of the mask irradiation apparatus.

To Professor António Pouzada for his support. His leadership of the cooperation protocol was crucial to overcome difficulties encountered.

To my colleagues of the Mechanical Engineering Department at the Polytechnic Institute of Leiria, for their companionship and mutual support throughout this period, António Selada, Mário Correia, Mário Pereira, Nuno André, Pedro Martinho and Rui Carvalho.

To my good friend and department colleague, Rui Rúben, for always be there with good advices. His expertise was support in terms of simulation and modeling were a significantly contribute to the success of this work.

To my good friend and department colleague, Paulo Gameiro, for “keeping me afloat” in the bad moments.

To my wife, Susana, she has paid the higher price...

To my daughters, Mariana e Catarina, there are no words to describe what you mean to me.

Abstract

Stereolithography is an important rapid prototyping process that creates three-dimensional solid objects in a multi-layer procedure. This technology involves the curing or solidification of a liquid photo or thermo sensitive polymer through the use of an irradiation light source, which supplies the energy needed to induce a chemical reaction, bonding large numbers of small molecules and forming a highly cross-linked polymer. This reaction determines the resin morphology that, in turn, defines the physical, electrical, and mechanical properties of the cured material. The cure reaction is highly exothermic and, the temperature and the reaction rate can vary considerably within the curing material due to polymers low thermal conductivity.

The main goal of this thesis is to study the process of microstereolithography by infrared radiation and the corresponding polymeric systems. Thermal effects were used over an appropriated polymeric resin to induce a phase change in the material, known as cure reaction, and consequently to obtain solid shapes or patterns. Cure kinetics was characterised and the effects of resin composition were determined. The knowledge of parameters and material composition influence over the process is of great importance to predict both the final geometry and mechanical properties.

Resumo

A estereolitografia é um importante processo de prototipagem rápida que permite criar objectos sólidos tridimensionais através de um processo camada a camada. Esta tecnologia envolve a cura ou solidificação de uma resina polimérica líquida, termo ou foto sensível através da utilização de uma fonte de irradiação, que fornece a energia necessária para provocar uma reacção química, ligando um grande número de pequenas moléculas e levando à formação de um polímero altamente reticulado. Esta reacção determina a morfologia de resina que, por sua vez, define as propriedades físicas, eléctricas e mecânicas do material curado. A reacção de cura é altamente exotérmica e a temperatura e velocidade da reacção podem variar consideravelmente no interior do material curado devido à baixa condutividade térmica dos polímeros.

O objetivo principal deste trabalho é estudar o processo de micro estereolitografia por radiação infravermelha e os sistemas poliméricos correspondentes. Efeitos térmicos foram utilizados sobre uma resina polimérica apropriada para induzir uma mudança de fase no material, conhecido como reacção de cura, e, conseqüentemente, para obter formas ou padrões sólidos. A cinética da cura foi caracterizada e os efeitos da composição da resina foram determinados. O conhecimento da influência dos parâmetros e da composição do material no processo é de grande importância para prever a geometria final e as propriedades mecânicas.

Index

Chapter 1 – Introduction	1
1.1 – Research context	2
1.2 – Research aims	5
1.3 – Thesis structure	6
1.4 – References	7
Chapter 2 – Micro additive manufacturing processes	9
2.1 – Introduction	10
2.2 – Information flow	11
2.3 – Micro additive processes	19
2.3.1 – Stereolithographic processes	19
2.3.1.1 – Stereolithography	20
2.3.1.2 – Scanning microstereolithography	44
2.3.1.3 – Integral microstereolithography	46
2.3.1.4 – Two-photon sub-micron microstereolithography	48
2.3.2 – Laser sintering processes	53
2.3.2.1 – Introduction	53
2.3.2.2 – Fabrication strategies	53
2.3.2.3 – Laser Micro Sintering	55
2.3.3 – Extrusion-based processes	56
2.3.3.1 – Introduction	56
2.3.3.2 – Fabrication strategies	56
2.4 – Summary	57
2.5 – References	58

Chapter 3 – Materials and characterisation techniques	65
3.1 – Resin systems used in stereolithography	66
3.2 – Photo polymerisation reactions	67
3.2.1 – Technological significance of photo-initiated reactions	68
3.2.2 – Radical photo-initiated reactions	69
3.2.3 – Cationic photo-initiated reactions	70
3.2.4 – Hybrid photo-initiated reactions	70
3.3 – The cure mechanism	71
3.3.1 – Introduction	71
3.3.2 – Modelling approaches to simulate the curing reaction	72
3.4 – The polymeric system	75
3.4.1 – The pre-polymer	75
3.4.1.1 – The curing reaction of unsaturated polyester resins	75
3.4.2 – The initiator	77
3.4.3 – Additives	78
3.5 – Material characterisation	81
3.5.1 – Experimental techniques to study cure kinetics	81
3.6 – Summary	82
3.7 – References	83
Chapter 4 – The cure reaction: Mechanism and modelling	87
4.1 – Introduction	88
4.2 – Experimental results	88
4.2.1 – Procedure	88
4.2.2 – Results and discussion	89
4.2.2.1 – Case I: the effect of curing temperature	89
4.2.2.2 – Case II: the effect of initiator concentration	105
4.2.3 – Vyazovkin model	112

4.2.3.1 – Results and discussion	113
4.2.3.2 – Results and discussion (with the use of silica)	124
4.2.3.3 – Case III: the effect of initiator concentration	133
4.2.3.4 – Case IV: the effect of silica concentration	135
4.2.3.5 – Case V: the effect of silica particle size	137
4.3 – Modelling the curing kinetics	141
4.3.1 – Reaction order	142
4.3.2 – The activation energy	148
4.3.3 – The dependence of the rate constant with the initiator concentration	150
4.3.4 – Prediction of fractional conversions	152
4.4 – Summary	164
4.5 – References	164
Chapter 5 – Fabrication process by infrared microstereolithography	167
5.1 – Introduction	167
5.2 – The infrared stereolithography system	171
5.2.1. – Light source	171
5.2.2 – Optical system	172
5.2.3 – Vat control	173
5.2.4 – Operating parameters and layer thickness	174
5.3 – Experimental results	175
5.4 – Summary	180
5.5 – References	180
Chapter 6 – Conclusions and further work	181
6.1 – Introduction	181
6.2 – Summary and conclusions	182
6.3 – Further work	185

1

Introduction

1

Due to the high competition in global market, it is increasingly important, for producing value-additive products, to realize clear differentiation from other products. Product differentiation can be achieved by new functionality and innovative technology [1].

Additive processes, which generate in a layered way, have around 20 years of history. These processes, started in the late 80's with stereolithography are not exclusively used for prototyping any longer. New opportunities and applications in appropriate manufacturing tasks open up, even though the economic impact is still modest [2]. Time-to-market was originally the strongest inspiration and economical driving force in additive fabrication. Product life cycle becomes shorter and builds up interest. The production of long term usable components and tooling increases the interest in this technology [3].

Stereolithography is one of the most relevant additive technologies currently available, but still in its infancy. Many research studies are being carried out to understand and model process parameters and novel fabrication strategies and new materials have been proposed. The knowledge of both fabrication and material parameters are particularly important in order to optimise both the process and the obtained parts.

Infrared Stereolithography

The main goal of this thesis is to study the process of stereolithography by infrared radiation and the corresponding polymeric systems. Special effort has been placed in obtaining small parts in an attempt to establish the bridge to microstereolithography. Thermal effects were used over an appropriated polymeric resin to induce a phase change in the material, known as cure reaction, and consequently to obtain solid shapes or patterns. Cure kinetics was characterised and the effects of resin composition were determined. The knowledge of parameters and material composition influence over the process is of great importance to predict both the final geometry and mechanical properties.

This chapter introduces the main goals of the thesis and presents a brief research context. The structure of the thesis is described, providing the readers a general overview of the document.

1.1 – Research context

The evolution of the world economy to a global market has lead to significant changes in the main characteristics of products and services. Nowadays, products are more complex with a wide range of features and functions regarding consumer expectations. Customization, quality policies and more demanding consumers require new manufacturing techniques providing products with shorter life cycle and reducing the time to market. Global competitiveness can be achieved through products and services involving complexity, integration and interconnectivity. As a consequence new fabrication techniques emerged to support product development and rapid manufacturing. The rapid prototyping processes were sustained by the development and introduction into the manufacturing sector of advances in technology, computers and information management.

As pointed out by the Rapid Manufacturing (RM) Platform, the European economy is facing a growing challenge to survive against low wage regions to keep (or bring back) production inside the Union. The manufacturing sector has to be transformed into high-tech industries in order to regain competitiveness by [4]:

- Moving from resource based manufacturing to knowledge based manufacturing;
- Moving from mass produce single use products to new concepts of higher added value, custom made, eco efficient and sustainable products, processes and services.

One of the most unique technologies to achieve these goals is additive manufacturing, which integrates computer automated production with the intrinsic technology characteristic to make individual products in small volumes without the need of tooling, with a high added value, and environment friendly process and a much shorter time to market.

The demand for microproducts and components has been rapidly increasing in electronics, optics, medicine, biotechnology, automotive, communication and avionics [5, 6]. The miniaturised products require the production of components with features in the range of a few

to several hundred micrometers. Researchers in academia and industry worldwide are striving to develop innovative manufacturing technologies to meet this demand.

Miniaturisation plays a key role in the demand for competitiveness because it means more features, less weight, handy size, less resources employment, more mobility and low price. Microsystems-based products are recognized as an important contributor to industrial and economic future representing a key value-adding element. While the late 20th century has seen a silicon-based microelectronics revolution, the 21st century looks forward to the adoption of micro- and nano- manufacturing technologies making use of a variety of materials, components and knowledge-based technologies that provide functionality and intelligence to highly miniaturised systems [7]. Micro- and nanomanufacturing is a highly resource and knowledge intensive sector and capitalising on the latest technological developments can only be achieved by a concerted effort of industrial stakeholders, research and academic organisations and public bodies [8].

A general classification of micromanufacturing processes is indicated in Figure 1.1. Microcomponents can be made by material addition, shape change or by selective material removal. Material additive processes can be subdivided into lamination and deposition according to the formation of material addition during the process. Typical lamination additive processes include microstereolithography and micro selective laser sintering.

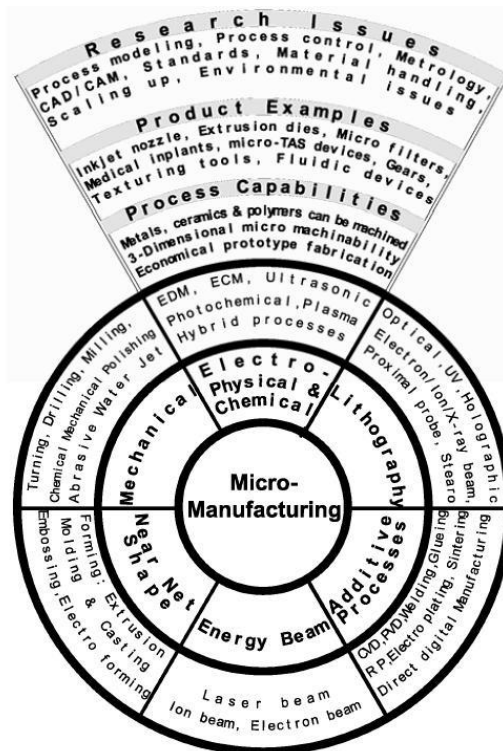


Figure 1.1 – A general classification of micro-manufacturing processes [9]

Additive technologies comprise different techniques using different materials (Figure 1.2). However, all of these techniques consist on the construction layer-by-layer of a three-

Infrared Stereolithography

dimensional object based on the information contained in a geometric CAD model. The main advantages of this technology are that they allow to obtain a complex solid model without requiring planning of process sequences or specific tools to handle the material and with reduced hand labour.

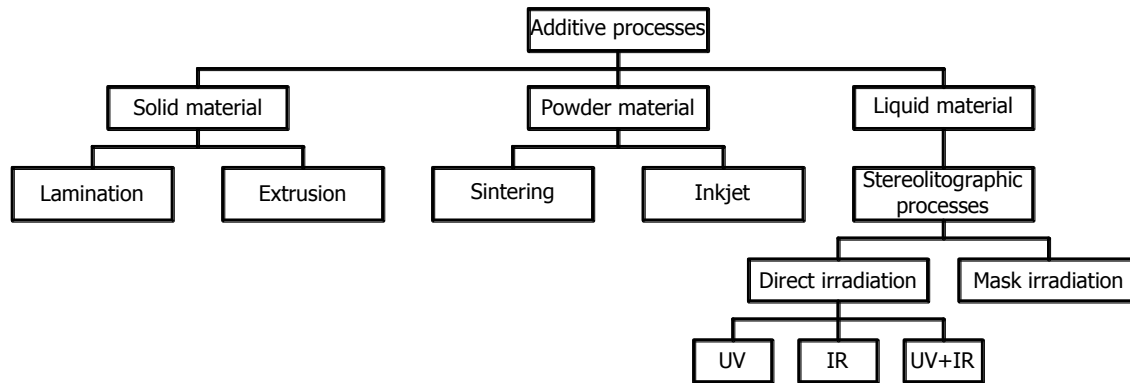


Figure 1.2 – Additive rapid prototyping classification

The most relevant technology currently available is stereolithography (SL) [3]. The stereolithographic processes consist in the selective solidification (cure) of a liquid photo or thermo sensitive polymer when activated by an appropriated source of energy, mainly a laser beam. This energy induces a chemical reaction, bounding together large quantities of small molecules forming a highly cross-linked polymer. The viscosity increases until the vitrification phenomenon. When the layer is completed, defining the intended cross-section of the model, the construction platform is lowered allowing the liquid material to recoat a new layer, and then positioned in the correct level. The process is repeated, with each new layer adhering to the previous one, until the complete solid model is defined. Finally, the model is submitted to a post-cure operation to increase fractional conversion (the amount of solid material) improving mechanical properties.

Although SL became a wide spread and well accepted technology, is a recent process and have a large possibility of development and improvement. Many of the technology and operating procedures are based on empirical correlations and work experience and there are a reduced knowledge about the physical and chemical changes that occurs in the material as a consequence of the irradiation. A more accurate understanding of the cure process is important to improve both the precision and the quality of the model.

One major problem consists in the materials used in SL, with repercussion in the mechanical properties of the fabricated parts. Despite of SL be a process with wide acceptance, parts created by the existing apparatus exhibit weak mechanical properties and significant shrinkage. It is expected that research on new material compositions and characterization, together with appropriate design and control of the associated process parameters, will play increasingly crucial role in SL, particularly regarding the direct fabrication of parts for engineering applications [10].

Micro additive technologies started as a miniaturisation process of the existing additive technologies. These processes, described in detail in Chapter 2, include processes like microstereolithography, laser sintering and extrusion based processes. Microstereolithography, one of the most versatile and flexible technology, started in 1993 with different strategies to improve the vertical and lateral resolution of the stereolithography process. As the resolution of microstereolithography is far better than other micro additive techniques, it has aroused interest in both the rapid prototyping domain where it can be used to produce high resolution prototypes and in the micro engineering field. It is a highly promising microfabrication process to produce small objects with complicated shapes and intricate details. Nevertheless microstereolithography, which uses ultraviolet (UV) radiation, cannot be used to produce composite structures due to the high diffraction effects that compromise the accuracy of the process. To solve this problem this thesis proposes a novel stereolithographic strategy based on the use of infrared (IR) radiation to obtain small parts. This fabrication process, detailed in Chapter 5, uses a dynamical pattern generator to shape the light beam according to the image of the layer to be build. The system uses the thermal energy by IR radiation to selectively solidify a liquid resin that contains a certain amount of thermal initiator. An in-depth study on the appropriate polymeric composition and a study of the curing kinetics can be found in Chapter 4 and represents a core part of this thesis.

1.2 – Research aims

The aim of this research is to investigate the theoretical basis of a new microstereolithographic approach using infrared radiation. The main concern will be to reach a small dimension scale that represents a step in the direction of subsequent developments leading to the micro scale. To reach these aims this thesis covers a wide range of scientific fields, namely engineering, polymer science and optics. The main research objectives can be listed as follows:

- To develop a better understanding relating to the physical and chemical transformations associated with the cure;
- Study and development of polymeric systems suitable for being used in the construction of prototype models obtained by infrared microstereolithography. An extensive experimental work was carried out in order to study the effect of the major material and process parameters: light intensity (temperature), irradiation time, initiator concentration, styrene concentration and the effect of silica;
- To develop a prototype system of infrared stereolithography capable of produce parts with small size resolution. This task include the selection of the irradiation source, the definition and selection of the dynamic mask generator device, the development of control software for the dynamic mask generator device, the design and manufacture of the equipment structure and elevation platform;

Infrared Stereolithography

- To develop mathematical models to describe thermal-initiated curing reactions and shrinkage effects associated with the polymerisation phenomena. These models make it possible to control several kinds of information: the progress of the cure reaction for estimating the time to produce a physical model, the spatial solidification profile for controlling the precision of the process and diffusion control effects to evaluate the need of post-curing operations.

1.3 – Thesis structure

The thesis is composed by six chapters which progress in accordance with the identified research objectives. The first chapter contains an introduction and also briefly describes the context of the research and his key objectives. The contents of the remaining chapters are summarised below.

Chapter 2 – Micro additive manufacturing processes

This chapter gives a review of the state of the art of current micro additive technologies. The importance of a microcomponent is outlined and the additive technologies currently available described. The advantage and limitations of current micro additive technologies are summarised. Finally a new approach to microstereolithography is introduced in order to offer improvements to current microstereolithography.

Chapter 3 – Materials and characterisation techniques

The properties and characteristics of the polymeric system selected for this research study are described in this Chapter. The main characterisation techniques used to study the polymeric system are also summarised.

For the design, control and optimisation of microstereolithography it is necessary to obtain adequate information about the reaction kinetics of the selected polymeric systems. This Chapter describes the theoretical aspects of thermosetting cure reactions and presents a review of models developed to describe the relation between the process parameters and the fractional conversion.

Chapter 4 – The cure reaction: Mechanism and modelling

Experimental techniques to study the cure kinetics are described and experimental results are presented and discussed. The effect of parameters, such as the temperature, the initiator concentration, and the silica content are discussed as well as the dependence between the curing kinetic parameters and those factors. Heat of reaction and glass transition temperatures are evaluated through the use of differential scanning calorimetry.

Chapter 5 – Fabrication process by infrared microstereolithography

This Chapter describes the implementation of an infrared stereolithography system designed to obtain small size prototypes. For this purpose a device was manufactured and tested. The equipment is composed by a light source, a shutter to switch on-off the radiation, a set of filters and lenses that ensure control over the wavelength, a DMD™ to define the micro-image of each layer of the model, a ZEISS® lens to reduce the layer image (maximum 10x) and the construction area.

Chapter 6 – Conclusions and further work

The aim of this chapter is to provide an overall summary of the thesis. The conclusions derived from the research study are listed and analysed. Finally, possible future directions for research following on from this thesis are indicated.

1.4 – References

1. Kimura, F., *Issues in Styling and Engineering Design*. CIRP Annals - Manufacturing Technology, 1997. **46**(2): p. 527-534.
2. Levy, G.N., R. Schindel, and J.P. Kruth, *Rapid manufacturing and rapid tooling with layer manufacturing (LM) technologies, state of the art and future perspectives*. CIRP Annals - Manufacturing Technology, 2003. **52**(2): p. 589-609.
3. Wohlers, T., *Rapid Prototyping and Tooling, State of the Industry*. 2008, Annual Worldwide Progress Report, Wohlers Associates.
4. *A Vision Paper*. 2006, Rapid Manufacturing Platform.
5. Masuzawa, T. and H.K. Tönshoff, *Three-Dimensional Micromachining by Machine Tools*. CIRP Annals - Manufacturing Technology, 1997. **46**(2): p. 621-628.
6. Alting, L., et al., *Micro Engineering*. CIRP Annals - Manufacturing Technology, 2003. **52**(2): p. 635-657.
7. Dimov, S.S., et al., *A roadmapping study in Multi-Material Micro Manufacture*, in *4M 2006 - Second International Conference on Multi-Material Micro Manufacture*. 2006, Elsevier: Oxford. p. xi-xxv.
8. Ehmann, K.F., et al., *International Assessment of Research and Development in Micromanufacturing*. 2005, World Technology Evaluation Centre (WTEC): Baltimore.
9. Rajurkar, K.P., et al., *Micro and Nano Machining by Electro-Physical and Chemical Processes*. CIRP Annals - Manufacturing Technology, 2006. **55**(2): p. 643-666.
10. Lu, L., J. Fuh, and Y.S. Wong, *Laser-Induced Materials and Processes for Rapid Prototyping*. 2001: Springer.

2

Micro additive manufacturing processes

The recent advances in technology led to the miniaturization of products and components, emphasizing the role of micro additive manufacturing processes as a mass production technique of small parts. This chapter presents an overview of micro additive manufacturing processes, namely microstereolithography, micro laser sintering and micro extrusion-based processes. The genesis of some of these processes was associated with an attempt to improve the resolution of traditional prototyping techniques by a method of downscale. However, for the development of these micro techniques was necessary to introduce innovative concepts and technological advances recently obtained.

This chapter also addresses the pre-processing stage, common to all additive fabrication techniques. The information flow issues are related to a computational phase of the manufacturing process, and have decisive influence over the entire process in terms of quality, time and cost.

2.1 - Introduction

The number and heterogeneity of fabrication processes proposed for making three-dimensional micro-scale features is vast. They can be classified in [1]:

- Subtractive processes;
 - Micro mechanical machining;
 - Electro physical and chemical machining;
- Near-Net-Shape processes;
- Additive processes.

However, regarding only for micro additive processes, they can be organized in stereolithographic processes, laser sintering processes and extrusion-based processes.

The stereolithographic processes are divided in mono-photonic and bi-photonic according to the excitation mechanisms of reactive species.

Microstereolithography is a recent technology that uses the same principle as conventional stereolithography (SL) to produce, layer-by-layer, micro-components with high resolution. Usually, microstereolithography uses ultraviolet radiation to start the curing reaction in a polymeric medium containing a certain amount of photo-initiator. This research focuses on the, so-called infrared microstereolithography, which represents a step forward in terms of costs and energetic efficiency. Bi-photonic processes allow manufacturing objects in a real three-dimensional way promoting the polymerisation inside the reactive medium.

Laser micro sintering is a novel freeform technique based on selective laser sintering (SLS) by which micro parts with an overall resolution of 30 μm can be produced from powder materials. Due to the used materials, metals and ceramics, functional micro bodies can be generated. Developed at Laserinstitut Mittelsachsen e.V. (Germany) in 2003, this new technique has shifted the resolution of selective laser sintering below the limits of commercial SLS devices. To achieve these goals, two major innovations were necessary; a novel technique and equipment for the handling and coating of sub- μm sized metal powders, and a new laser sintering technique employing q-switched pulses. The technique and the equipment is marketed under the brand name microSINTERING by 3D-Micromac AG, Chemnitz, Germany [2].

Extrusion-based micro processes are based in conventional forming technologies, such as extrusion. However, at microscale, these processes have encountered new challenges due to the influence of "size effects" that tend to be predominant at this length scale. The micro-extrusion of organic inks for direct-write assembly is a highly versatile microfabrication technique used to create microfluidic networks by the robotic deposition of a fugitive ink onto a moving stage [3]. To obtain an optimized result in the shape of the deposited material, the translational speed of the moving stage has to closely match the linear velocity of the fugitive ink at the micro-nozzle

exit. The continuous ink pattern generating technique is especially promising due to its material flexibility, low cost and capability for self-supporting features [3].

2.2 - Information flow

The growing complexity of technology, products and services has strongly affected the landscape of the high-tech industry. The reduction of life-cycles for technology innovations has influenced the product development and manufacturing processes, increasing market demand for first-time-right and zero-defect products. The role of additive fabrication technologies in product development becomes essential, not only for the reduction of iterations but also allowing process stages to become simultaneous and consequently accelerating the product development process, increasing quality and minimizing errors, costs and time-to-market. It is a multi-disciplinary design environment, involving researchers and technicians from different educational areas. Due to the representation and manipulation of complex forms and features exclusively within a computational environment it is possible that product research and development, and manufacturing are not on a single site.

Additive fabrication processes are techniques for direct conversion of three-dimensional CAD (Computer-Aided Design) data into a physical model, using fully automatic processes. The entire process for product fabrication is illustrated in Figure 2.1 and summarized in this section.

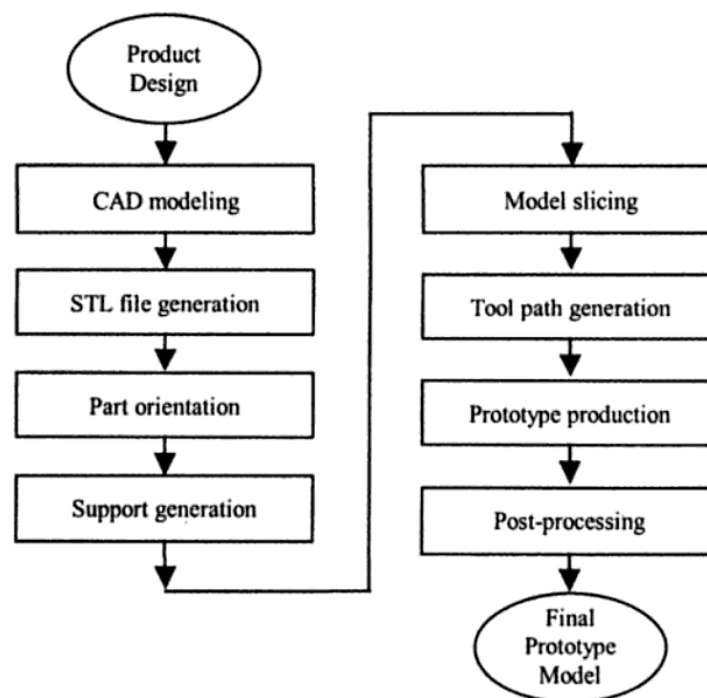


Figure 2.1 – Overview of the entire process of additive fabrication [4]

CAD modelling

The first step in any additive fabrication process is to prepare a CAD model of the object to be fabricated. CAD models contain the mathematical definition of an object or a set of objects assembled together, allowing validating geometric and functional aspects of the product without physical fabrication of the model. Solid modelling provides a framework to model and represent an object's shape in the computer to perform computational operations such as rheological, mechanical and functional analyses. A group of independent application geometric tools and algorithms can be used to query and analyse the model to obtain unambiguous results [5].

In computer aided geometric design, a variety of mathematical surfaces are available. The simplest surfaces are algebraic surfaces, such as plane, cylinder, cone or sphere. Commonly used surfaces for free-form geometry are parametric surfaces such as Bézier, B-spline and Non-Uniform Rational B-Spline (NURBS) surfaces [6, 7]. Subdivision surfaces are also becoming popular for CAD applications, especially for modelling shapes with arbitrary topology, for animation, data compression and texture mapping (Figure 2.2) [8].

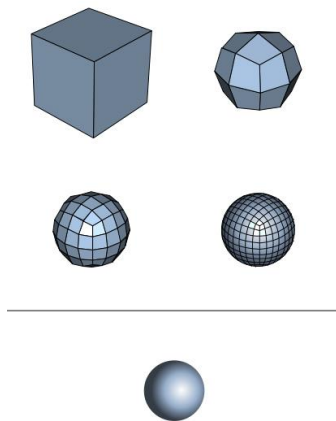


Figure 2.2 - First three steps of a cube subdivision [9]

CAD surfaces can also be obtained by reverse engineering techniques. Starting from an existing solid model, 3D measuring techniques are used for data acquisition which is processed and converted into a solid model through the use of appropriated CAD software's.

Surface representations are the main building blocks for solid modelling. To convert a CAD surface model into a solid model, often the surfaces needs to be extended, intersected, trimmed, and applied chamfers and fillets to them. Finally they are stitched together forming a closed volume, which corresponds to a solid model representation.

There are also a variety of schemes for solid modelling, namely Constructive Solid Geometry (CSG) consisting in three key building blocks: solid primitives (standard solid features, such as block, cylinder, sphere or solid wedge), transformation operations (such as translation, rotation, shearing, scaling and their combinations) and Boolean operations (union, intersection and subtraction). Very complex engineering parts can be obtained starting from a solid primitive,

which is easily defined through just a few parameters, and then combining transformation and or Boolean operations (Figure 2.3).

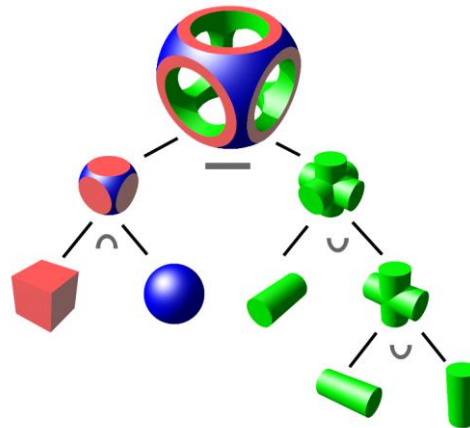


Figure 2.3 – Example of CSG technique for solid modelling

Although CSG is a very intuitive and user-friendly solid modelling scheme, the limited availability of solid primitives, depending on the particular CAD modelling system, affect the capability of shapes that can be obtained. Boundary representation (B-rep) is an alternative solid modelling scheme that is entirely complimentary to CSG in solid modelling activities [10].

B-rep is a very powerful and flexible scheme that can be used to model any object found in the physical world. The objects are defined by a set of boundary faces that can be either planar or freeform surfaces. Topologically, each boundary face is enclosed by a loop of boundary curves which can be a simple line segment or a freeform curve, but should have two end/boundary points and their characteristic geometric parameters [4].

Most of the Computer-Aided Design and Manufacturing systems use a hybrid solid modelling scheme, combining the flexible model representation of B-rep with the simplified user interfacing of CSG.

STL file generation

STL (STereo-Lithography) is a file format for interfacing a CAD model with an additive fabrication system. In the STL file format, the precise geometrical model is described through an involving mesh of triangles (similar to a finite elements mesh), that from a mathematical point of view is the simplest polynomial mode to describe a surface [11, 12]. This file contains the Cartesian coordinates (xyz) of each triangle nodes and the respective exterior facet normal which indicates to the system where the solid material is. Developed by 3D Systems in 1987, it was accepted by all manufacturers as the standard file format for additive fabrication systems. Nowadays, all CAD systems commercially available have a post-processor capable of generate STL files.

Therefore, the STL file consists of a list of facet data which define the surface of a three-dimensional object. Each facet is uniquely identified by a line perpendicular to the triangle and

with a length of 1.0, called unit normal, and by three vertices. These elements are specified by three coordinates each resulting in a total of 12 numbers stored for each facet. Since the facets are the boundary between the interior and exterior, its orientation is important to define the inside and outside of the object. The orientation of the facets is specified redundantly in two ways which must be consistent; the direction of the normal is outward and the vertices are listed in counter-clockwise order when looking at the object from the outside (right-hand rule) (Figure 2.4).

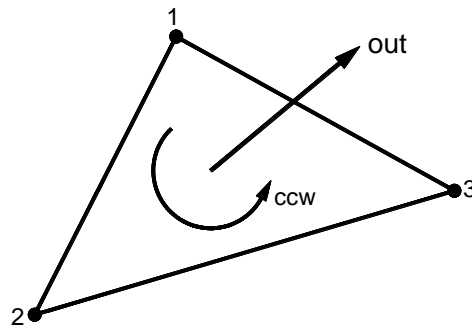


Figure 2.4 – STL facet

Each triangle must share two vertices with each of its adjacent triangles. In other words, a vertex of one triangle cannot lie on the side of another (Figure 2.5). The object represented must be located in the all-positive octant, i.e., all vertex coordinates must be positive-definite (nonnegative and nonzero) numbers. The STL file does not contain any scale information; the coordinates are in arbitrary units. In order to optimize the performance of the slice program it is recommended, but not required, to sort the triangles in ascending z-value order using the z maximum of each triangle. There are specialized STL-handling software's available that are able to repair some problems, such as minor gaps or inconsistencies, sort out the connectivity of the facets, remove duplicate nodes, and correct overlapping triangles; however more significant problems usually require modifications on the original CAD model.

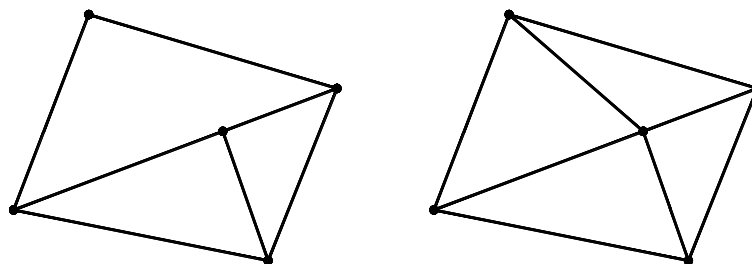


Figure 2.5 – The vertex-to-vertex rule (violation of the rule and correct configuration)

The STL standard format includes two data formats, ASCII and binary. Binary files are more common, since they are more compact. Thus the ASCII format is primarily intended for testing new CAD interfaces because the large size of its files makes it impractical for general use. The syntax for these formats are presented and described separately below (Figures 2.6 and 2.7).

```

solid name
    {
    facet normal ni nj nk
        outer loop
            vertex v1x v1y v1z
            vertex v2x v2y v2z
            vertex v3x v3y v3z
        endloop
    endfacet
    }
endsolid name
    
```

Figure 2.6 – Syntax for an ASCII STL file

In the data structure for STL ASCII format, note that: bold face indicates a keyword and must appear in lower case; “facet normal” and “outer loop” have a space between words while there is no space in any of the keywords beginning with “end”; indentation must be done with spaces since tabs are not allowed; the content inside the brace brackets describes one facet and will be repeated for each existing facet; symbols in italics are variables which are to be replaced with user-specified values using floating point numerical representation, for instance 1.23456E+789; only facet normal coordinates may have a leading minus sign because vertex coordinates are positive-definite.

Bytes	Data type	Description
80	ASCII	Header. No data significance.
4	unsigned long integer	Number of facets in file
}	4 float	<i>i</i> for normal
	4 float	<i>j</i>
	4 float	<i>k</i>
	4 float	<i>x</i> for vertex 1
	4 float	<i>y</i>
	4 float	<i>z</i>
	4 float	<i>x</i> for vertex 2
	4 float	<i>y</i>

Figure 2.7 – Syntax for a binary STL file

In the data structure for STL binary format, note that: the content inside the brace brackets describes one facet and will be repeated for each existing facet; the attribute byte count should be set to zero. A binary STL file has an 80 character header followed by a 4 byte unsigned integer indicating the number of triangular facets in the file and by the data describing each triangle.

The file simply ends after the last triangle. Each triangle is described by twelve 32-bit-floating point numbers, three for the normal and three for the xyz coordinate of each vertex, and by a two byte unsigned “short” integer that is the “attribute byte count”.

One obvious limitation of STL files is that a faceted model is an approximation of the original surface geometry. However to guarantee an appropriated accuracy can be used very small facets for the tessellated model with tolerances in the range of 0.001 mm. By other hand, to accurately approximate a 3D complex form, a large size STL file will be generated due to the number of triangles involved.

The STL files contain a great volume of redundant information because the vertex coordinates of every triangle are stated individually. Since any vertex will be shared with two or more adjacent triangles, each point will be stated two, three or more times.

Additionally, some useful information will be lost when surfaces are converted to a faceted model, such as surface boundaries, for example.

Validate and repair the models defined in STL format is extremely important because during the triangle mesh generation some errors can be introduced to the geometry causing geometric anomalies or inconsistency of the model.

Part orientation and support generation

When the STL file is ready, after repair and validation of the model, several factors must be considered such as adjustments due to shrinkage and distortions effects, and also the introduction of structural supports [4, 13]. Additional operations over the model comprise scaling and orientation at the working zone of the equipment. Since physical parts shrink and deform under processing, models must to anticipate and compensate for these shape changes. Most users follow a trial-and-error procedure, iterating through several trial runs before achieving the desired part [14]. The orientation of the model is a fundamental issue with direct influence over the surface quality, construction time, need of structural supports, shrinkage and distortions [15]. This issue will be addressed once more in another section, particularly for stereolithography.

Structural supports are used to avoid that solidified layers became in suspension, due to the liquid environment of the construction area. In the past, the structural supports were projected in CAD systems, but this was a highly time consuming task. To make this process stage more efficient and save time, who is an essential question in this kind of technology, were developed algorithms to obtain the structural supports specification in an automatic way [4]. This subject will also be addressed in a following section of this chapter.

Model slicing

After being prepared, the STL model is divided in layers generating a SLI (SLIce) file [15]. The information contained in this file will then allow the construction of the physical model. The time

necessary to slice the model depends on the geometric shape and size, number of triangles used in its representation and the number of layers considered. The lower the thickness of each layer the greater the accuracy achieved, but will also increase substantially the time spent in the operation of slicing, and later in the building process of the model.

The common method for model slicing is the uniform layer thickness method, in which all layers have equal thickness. However some theoretical and software works have been proposed using adaptive layer thickness as slicing technique, where the slicing thickness varies according to the part geometry complexity. Theoretically, has been proven that this method can produce parts with higher accuracy, less deviation from the CAD model, and shorter fabrication time [16-18]. Although because of technical difficulties, the implementation of this method on the current commercial RP processes has not been reported [19].

The model and the support features described in a STL file are sliced from bottom to top generating thin parallel cross sections along the vertical z-axis. An algorithm is incorporated in the SLI generator to determine if each contour is internal or external. The data is stored in SLI files which are merged together creating additional files that in turn will be read by a computer that controls the movements of the laser and elevator mechanism.

Tool path generation (scanning strategies)

The slicing contour data will be used to define the tool path for the rapid prototyping application. In general, the tool path for all rapid prototyping processes can be classified into the following basic categories (Figure 2.8) [4]:

- Raster scanning: refers to scanning along the coordinate axis and can be applied to processes such as SL, SLS and some 3D printing processes for internal hatching (Figure 2.8a).
- Perimeter scanning: is used for producing external surfaces and is applicable to almost all rapid prototyping processes involving skin region solidification and also for cutting in LOM (Laminated Object Manufacturing) process (Figure 2.8b,c).
- Directional scanning: is an alternative to raster scanning, when it might be advantageous to perform scanning along arbitrary paths due to the contour of the model or to improve mechanical properties (Figure 2.8d). Is used by SL machines of 3D systems.
- Zigzag tool path: is used in FDM (Fused Deposition Modeling), 3D welding, extruding type and 3D printing processes (Figure 2.8e,f).
- Contouring and spiral paths: for parts with specific geometry, these approaches may produce parts with improved mechanical properties (Figure 2.8g).

- Line by line scanning: a line component is sweep along the principal scanning direction. Is used for some inkjet type printing processes, such as the process used by ThermoJet 3D printer of 3D systems (Figure 2.8h).
- Area by area solidification: some processes such as SGC (Solid Ground Curing) from Cubital solidify the all layer by integral exposure to an irradiation source through a mask previously prepared from sliced contours data (Figure 2.8i).
- Boundary cutting tool paths: it's a variant from perimeter scanning developed for be used in LOM (Figure 2.8j). The orthogonal xy-hatching pattern is necessary for cutting waste and supporting materials during LOM process.

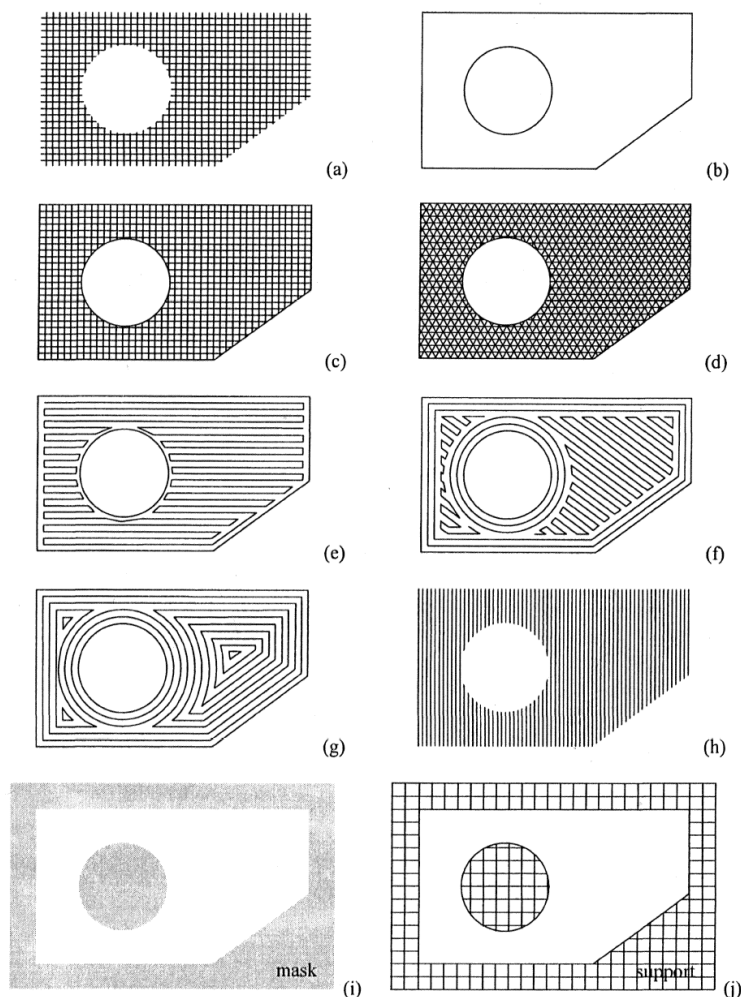


Figure 2.8 – Typical tool paths for model prototyping: a) x- and y-raster scanning for internal hatching (may be used separately); b) perimeter scanning; c) single perimeter surface scanning and orthogonal internal xy-hatching; d) single perimeter surface scanning with internal directional hatching; e) single perimeter with internal horizontal zigzag paths; f) three perimeters with internal inclined zigzag paths; g) contouring equidistant paths; h) line-by-line scanning; i) area/based solidification using masks; j) boundary cutting with orthogonal cross/cutting for LOM [4]

Most of the rapid prototyping systems use vectors for the various types of scanning paths, however it is possible to use direct contouring based on exact parameterisation, such as circular movements. Scanning strategies are a main issue due to the influence over parameters such as time spent, quality and accuracy of the models.

2.3 - Micro additive processes

In the last years research institutes and universities around the globe have focused on research in micro- and nanoscale phenomena, devices and systems. Although this research has resulted in an advanced knowledge in micro- and nanomanufacturing, it is evident that the lack of industrial implementation of this know-how is the key in strengthening the future growth of these technologies. Even though progress has been made in mass production concerning these areas the main production environment for micro- and nanomanufacturing technologies remains in the lab. This results in an unfamiliarity of large scale production environments to micro- and nanotechnologies, leading industries to hesitate adapting technologies that might import unpredicted factors affecting the performance and quality of the manufacturing chain. At this point investing in the development of concepts, such as higher modularisation, flexibility and scalability might allow a reduction of production costs and are vital for success of new production platforms. This will allow a strong industrial involvement with leading research labs to take micro- and nanoproducts to the next level [20].

Most of the micro manufacturing processes have been developed based on downsizing strategies of conventional rapid manufacturing processes. Thus, in the following sections of this chapter will be addressed micro additive manufacturing processes and their source conventional rapid manufacturing processes.

2.3.1 - Stereolithographic processes

Stereolithography consists in the solidification (cure) of photo-sensitive or thermo-sensitive resins with low viscosity using a proper energy source, commonly a laser device. This process is widely applied in the fabrication of conceptual and functional models, as well as in the fabrication of models to be used in the rapid production of tools, having an important role in the product development process.

Obtaining high quality stereolithographic models in a fast and efficient manner and the use of new polymeric systems of high performance are fundamental issues to the development of this technology. This will be decisive for the integration of these processes in the manufacturing chain to produce directly parts or components.

Classification

The stereolithographic processes can be classified in two groups (Figures 2.9 and 2.10) [21-24]:

- Direct irradiation processes with the use of a laser device;
- Mask irradiation processes.

The direct irradiation processes can be mono-photonic or bi-photonic initiation (Figure 2.9) [25].

The direct irradiation process of mono-photonic can be separated in [25, 26]:

- Processes involving ultraviolet radiation – conventional stereolithography;
- Processes involving infrared radiation – CO₂ stereolithography;
- Processes involving ultraviolet and infrared radiation – stereo-thermal-lithography.

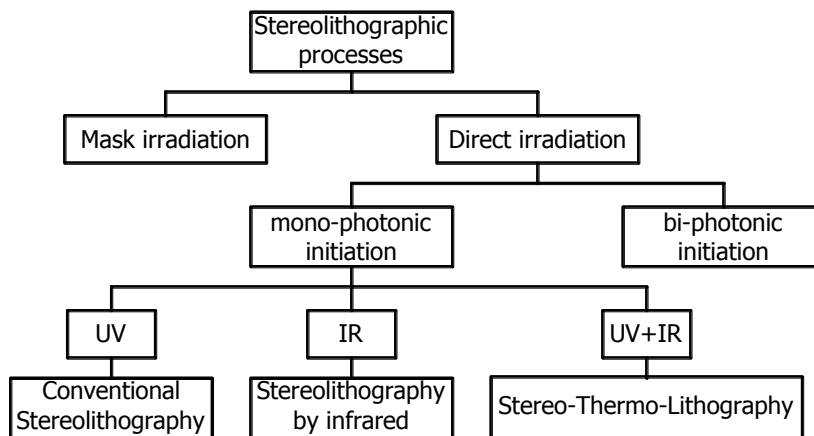


Figure 2.9 – Classification of stereolithographic processes

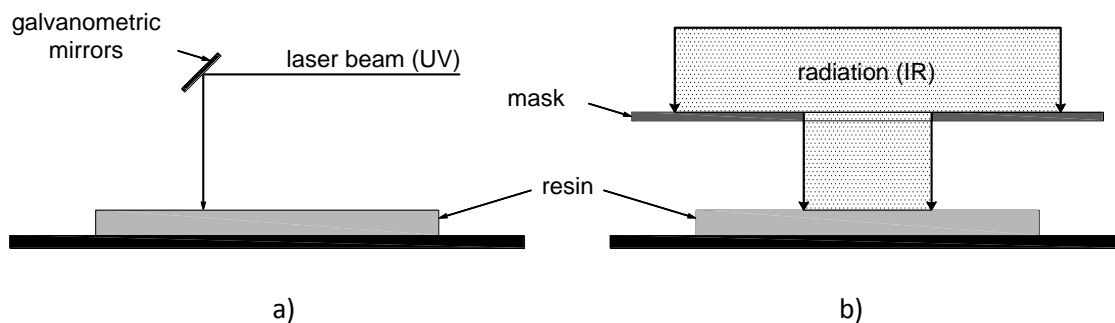


Figure 2.10 – Stereolithographic processes: a) Direct irradiation; b) Mask irradiation

2.3.1.1 - Stereolithography

Conventional stereolithography

The stereolithography process, currently commercialized by 3D Systems, was initially developed and patented by Hull [27, 28] (Figure 2.11) as a result of separated researches works presented in 70 and 80 from past century, mainly by Swainson [29-35], Kodama [36, 37], Herbert [38] and Hull [27, 28]. This process consists in the use of a laser source emitting in the ultraviolet domain to solidify, point by point, a surface of a liquid resin. The solidified spots are small volume elements with parabolic profiles, usually named voxel (tri-dimensional pixel). When a layer

corresponding to a transversal section of the 3D model is solidified, the construction platform goes down a value equal to the thickness of the next layer, and the laser scanning process is repeated. This strategy, corresponding to the descendent construction method, is used by the majority of occidental manufacturers of stereolithography apparatus. Hull [27] also proposed the ascendant construction method (Figure 2.12), which is nowadays used by the Japanese manufacturers. In this last case, the irradiation is done through a glass window located at the bottom of the vat which contains the resin. The 3D model is produced from top to bottom with ascension of the movable platform after the solidification of each layer. In fact, the difference in the descendent method, come out in the necessity of a leveller to reduce the surface tensions of the model and stabilize the surface of the liquid resin, making the thickness of the layer uniform, but in other hand increasing the complexity of the equipment and the fabrication time [27]. This does not happen in the ascent method because the window guarantees the stabilisation of each resin layer.

Recently, was proposed another system which allows the resin solidification spot by spot, directly in the interior of the vat, due to the formation of an air bobble at the extremity of an optical fibre [39]. The radiation is conducted through the optic fibre and promotes the cure of the photo-polymer only at the air bobble region. It's a system, not yet commercialized, who enables the fabrication of the model with a three-axis scanning strategy, in opposition to the traditional methods of layer by layer fabrication. However, the system reveals low scanning velocities [40].

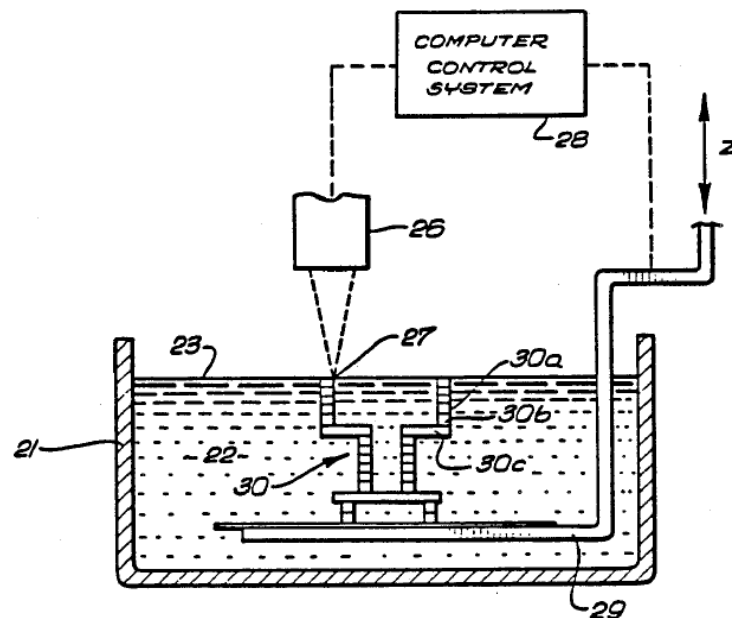


Figure 2.11 – Stereolithographic process of descendent fabrication [27]

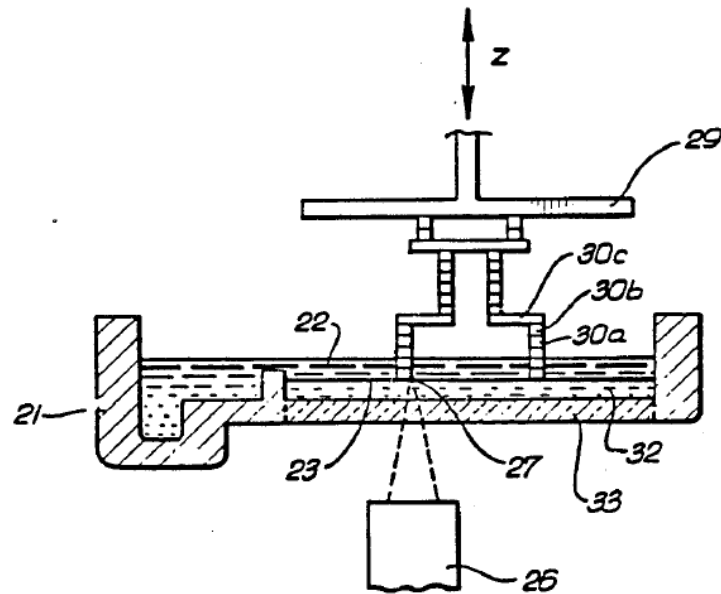


Figure 2.12 – Stereolithographic process of ascendant fabrication [27]

Since the fabrication of prototypes in stereolithography is done in liquid environment, it is necessary to build structural supports to ensure the correct replication of the 3D model geometry without limitations, sustaining with efficiency the solidified layers avoiding that they become in suspension. Other function of the supports is to grab the model to the elevation platform. This way the model is not built directly on the platform and after the fabrication process it can be removed without damage. The structural supports also allow to compensate position errors that could exist between the model and the movable platform, besides of reducing curl and deformations originated by the material shrinkage [4, 41]. However, the supports increase the volume of solidified material and therefore the construction time and the quantity of material spent, since this is not a reusable material.

In his patent, Hull [27], specifies a solution to reduce the structural supports need, adding one more degree of freedom to the movable platform (Figure 2.13). However, this device was never introduced in a commercially available apparatus.

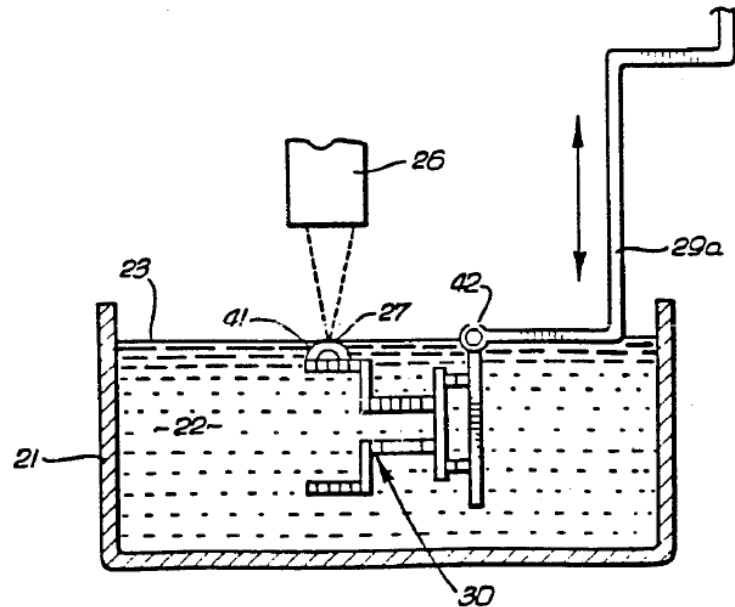


Figure 2.13 – Stereolithographic process with rotation of the movable platform [27]

More recently were developed techniques to generate perforated supports (Figure 2.14) without significant lost in the mechanical properties of the models [39]. This way, preserving the performance and functionality, significant savings of material and time are achieved, as well as support removal in post-processing operations is easier [4]. The Tokyo University at Japan has proposed a more drastic modification, developing a system where the liquid resin at the construction area is cooled and frozen. This way, the frozen material acts as a support to the next layers avoiding the necessity of build conventional structural supports [39]. This process is very complex and was never implemented in commercial apparatus.

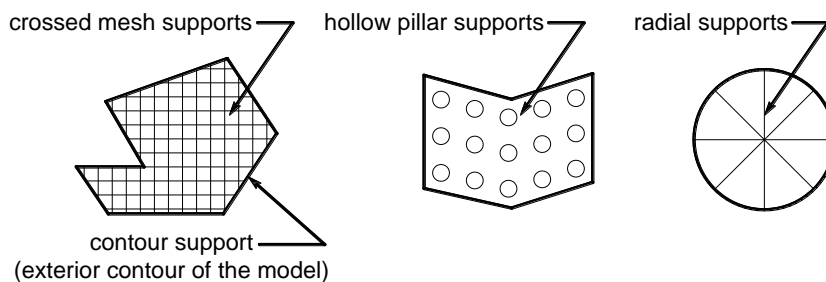


Figure 2.14 – Examples of structural supports

The most relevant parameters to project the structural supports are the geometry, orientation and surface area of the model. However, the model orientation is chosen in order to minimize shape errors, therefore it is proper to orientate the model in a position that place the curved surfaces perpendicular to the movable platform (Figure 2.15), and also to avoid very high dimensions of fabrication who causes high bending moments and warping [4, 41]. Consequently, the main factor is the model orientation and the structural supports will have to be adapted.

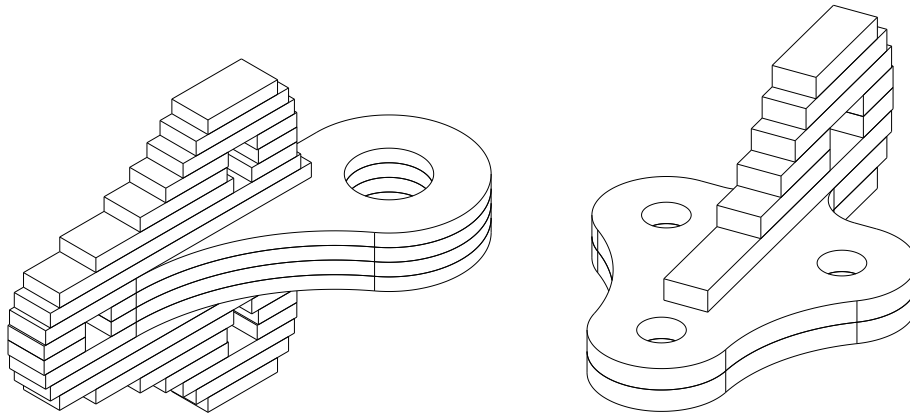


Figure 2.15 – Comparison of the shape deviation due to the model orientation

As a consequence of the layer by layer fabrication process, the models have a geometric difference when compared with the original CAD model. This error with the shape of stair steps, usually called stairs effect, is a chordal deviation and is directly related to the layer thickness (Figures 2.16 and 2.17) [4, 41].

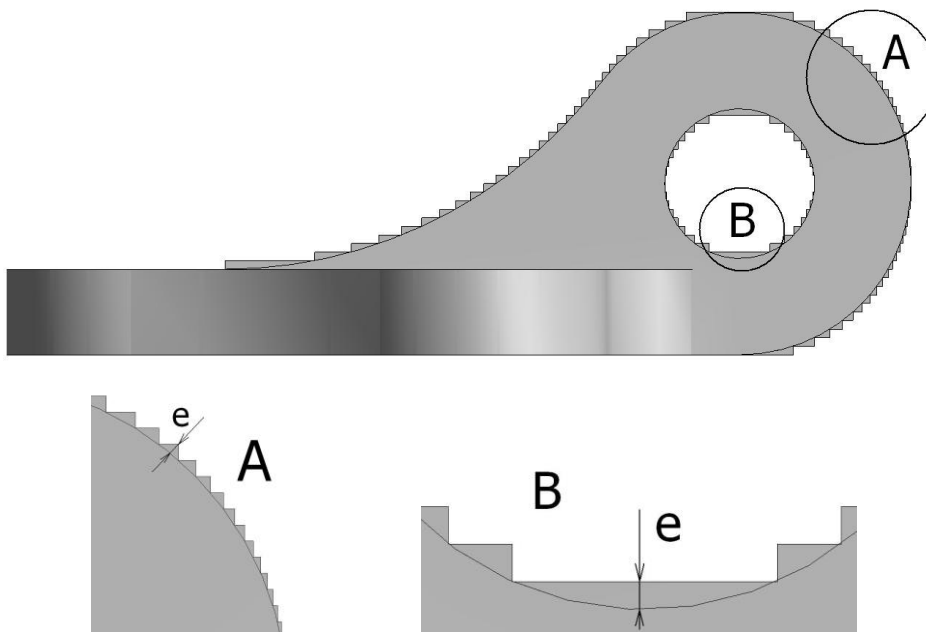


Figure 2.16 – Errors related to the layer by layer fabrication process

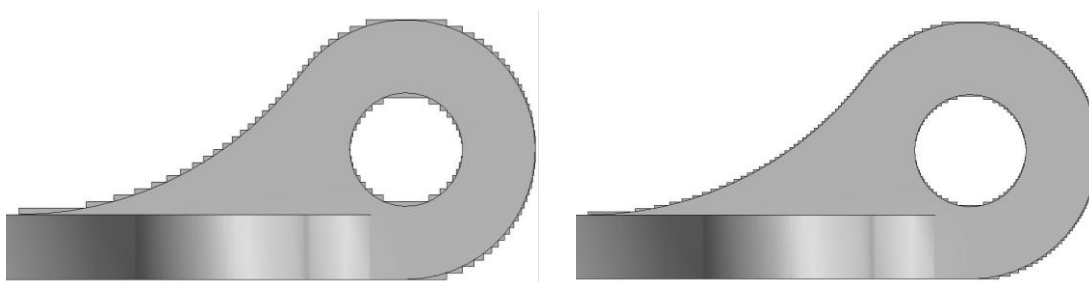


Figure 2.17 – Comparison of the shape deviation due to the layer thickness

Generically, the stereolithography apparatus is composed by a computer with the function of control unit, a vat which contains the thermoset resin in liquid state, a laser device emitting in ultraviolet domain, an optical system to guide the laser beam, and a movable platform which allows the layer by layer fabrication. It is a very complex process and depends of several adjustable parameters. Each stage of the process, between CAD model and the final physical model, contributes to the final result. To control and optimize the process parameters, simulation models supported by experimental works, were developed. This simulation is divided in three main areas: modelling of the laser source, modelling of the free-radical polymerization and modelling of heat transfer involved in the process [42].

The result of this models includes the spatial and temporal variation of monomer and polymer concentration, the consume of initiator, and the variations of temperature in the spot exposed to the laser beam and surrounding areas [25].

The process of stereolithography is based in the selective cure of a resin photo or thermo sensitive obtained with the exposure to an ultraviolet or infrared radiation. The ultraviolet radiation is provided by a laser device of He-Cd (or Nd:YVO₄ in most recent apparatus) which solidifies a thin layer or resin [4]. The cure process occurs in the presence of species initiator/catalytic of reaction, and is called polymerisation. Basically, it is the bonding of small molecules (monomers) that become cross-linked, creating this way a tri-dimensional molecular chain of larger dimensions (pre-polymers), and ending in the achievement of a solid structure (Figure 2.18). The obtained solid it is a thermoset, so the material can be processed only once and therefore is not recyclable [43].

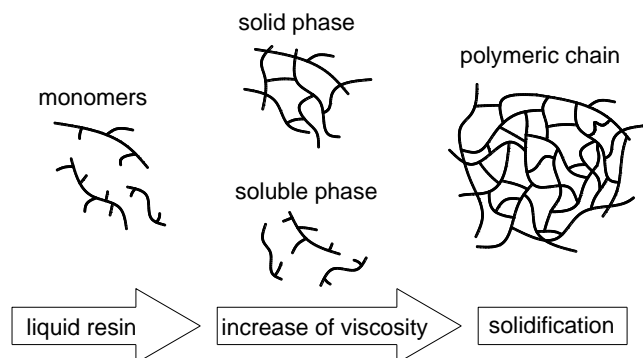


Figure 2.18 – Solidification steps of a liquid resin during the cure process

To start this highly exothermic reaction is necessary the presence of initiators species, which can be of free radicals or cationic types. Once started the reaction, occurs a propagation phase, corresponding to grow of polymeric chain due to the consecutive links between reactive species and oligomers [44, 45]. This phase ends when the reactive centres are annulled by one of the characteristic termination processes: combination or un-proportionality [44, 46-48].

During the cure process very important phenomenons occur [25, 44, 48, 49]:

- gelation;

- vitrification.

The gelation occurs due to a suddenly and huge increase of viscosity. Since the beginning of this phenomenon, the molecular chains starts to lose their mobility and consequently being confined, causing uni-molecular termination phenomenon because of the impossibility of happening propagation and reaction of two polymeric chains. Since the flux of material is affected, it will be composed by two different phases, one soluble and the other solid, corresponding this way to a heterogeneous polymeric chain (Figure 2.18). The vitrification it is a phenomenon that occurs after the gelation and it leads to the material solidification and in sequence to the raise of molecular weight. This phenomenon is related to the increase of glass transition temperature and causes a decrease in reaction rate consequence of limitations on the polymeric chains mobility. The decrease of mobility, resulting from diffusion phenomenon will determinate the fractional conversion (percentage of cured material) obtained in fabrication process and the necessity and extension of post-processing procedures. It is also responsible for the formation of heterogeneous structures with a negative influence in properties and durability of the cured polymer, and generating specific volume modifications with consequences in inducing internal tensions. Because of all these factors, the characterisation of a proper polymeric system to use in stereolithographic applications is a main issue, in order to prevent the vitrification phenomenon with direct consequences in the cured material percentage obtained.

The increase of fractional conversion can be achieved with higher initial concentration of initiator and with higher radiation intensity [25, 50, 51]. However, when a critical value of the first parameter is exceeded the radiation ability to penetrate the resin is reduced with negative consequences in the thickness of cured material obtained. The second parameter, have also disadvantages since that the higher intensity radiation is provided by more powerful laser devices which will result in the use of more expensive systems.

Hence, higher energy supplied to the polymeric system will causes higher penetration capacity and therefore the increase of cured material layer thickness, according to the equation [42]:

$$e_c = P_p \cdot \ln\left(\frac{E}{E_c}\right) \quad (2.1)$$

where e_c is the layer thickness of cured material, P_p is the penetration depth of radiation, E is the energy supplied to the exposed area and E_c is the critical energy to start the cure reaction.

Sometimes it is necessary an additional post-processing operation called post-cure with the aim of increase the percentage of cured material. In this operation, the models are exposed to an intense ultraviolet radiation, heat, or immersion in a chemical bath containing an accelerator agent. This way is obtained an additional reaction in some reactive centres that were captive due to vitrification phenomenon's or due to scanning techniques [25].

The shrinkages, bends and distortions of the models depends of the materials, but can be also originated by equipment impreciseness, bad position of the mirrors system and small power discontinuity of laser device. Is not easy to quantify these imperfections, however Gargiulo and Belfiore [52] based in experimental work have established, from heuristic way, an equation to quantify the material shrinkage:

$$\Delta = -1.227 \times 10^{-3} d \quad (2.2)$$

where d is the intended dimension and Δ the expected shrinkage.

The Table 2.1 shows the main advantages and disadvantages of the stereolithography process.

<i>Advantages:</i>	<i>Disadvantages:</i>
Possibility of obtain parts with complex geometries;	Necessity of post-cure;
Good dimensional accuracy;	Necessity of structural supports;
Good details definition;	Shrinkages and distortions of the fabricated models;
Very good surface finishing;	Toxic materials;
Allows to obtain models partially hollowed, decreasing the fabrication cost;	Expensive materials;
Prototypes can be used to lose-models techniques.	Use of lasers devices.

Table 2.1 – Advantages and disadvantages of the SL process [4, 15, 25]

The polymerisation processes using ultraviolet radiation have advantages when compared with the thermal cure, mainly in [49, 53]:

- cure in a short period of time;
- better quality products;
- Absence of solvents emissions.

CO₂ Stereolithography

The infrared stereolithography is a recent process that uses the radiation from a CO₂ laser device emitting infrared radiation with wavelength of 10.6 μm to solidify thermo-sensitive resins (Figure 2.19) [24]. The main difference to the conventional systems is that the polymerisation reaction is thermo-initiated. The infrared radiation solidifies, in a selective way, a liquid resin containing a proper thermo-initiator concentration (peroxide). Maintaining the cure zone focused is a problem in this process because of reactive species diffusion mechanisms and due to thermal conduction phenomenon's [54-56]. This problem can be solved by adding silica in proper proportions.



Figure 2.19 – Stereolithography system using infrared radiation [57]

Stereo-thermal-lithography

In stereo-thermal-lithography (STGL) optical and thermal effects are simultaneously used to locally induce a phase change in a liquid resin [58]. The resin contains thermo-initiator and photo-initiator in concentrations precisely controlled in order to avoid any polymerisation mechanism by isolated action of temperature (produced, for example, by infrared radiation) or ultraviolet radiation. However in the interception zone of the two effects, the radical population is enough to initiate the cure reaction. The temperature causes the production of free radicals through the fragmentation of thermo-initiators and contributes simultaneously to increase the photo-initiated reaction rate.

This process has significant advantages with direct implications in fabrication time but also in the final model properties [25]. The use of temperature to control the reaction kinematics allows the possibility of eliminate the necessity of post-cure since that the raise of temperature will permit to obtain higher cured material percentage. It is an important advantage because besides the benefits of reducing fabrication time, the post-cure operations are responsible for distortions and bends in the models.

Other advantage in consequence of using temperature is the raise of reaction rate, which allow reducing the intensity of ultraviolet radiation necessary to polymerisation process. The use of laser devices with less power makes the system less expensive [25, 26].

The combined effect of both initiators allows reducing significantly their concentration in the resin. The penetration of the radiations is deeper since there is less quantity of initiators in his way causing the solidification of larger thickness layers [25].

The increase of reaction rate as a result of temperature will cause a better control over the cure process and this way the cure zone will be more focused. The more effective control of the

kinematics cure reaction increases the versatility of this system when compared to the systems mentioned previously [58].

Laser

The laser is a device who controls how excited atoms release photons [59, 60]. It's a fundamental element to the rapid prototyping technologies since many of them were not even possible without the existence of proper laser devices.

At the beginning of stereolithography were used laser devices of HeCd, with power under 40 mW to wavelengths of 325 nm [4]. However, those laser devices are being replaced by higher power devices, first of Argon-Ion (power under 600 mW to wavelengths of 351 nm) and more recently by solid state laser devices (Nd:YAG and Nd:YVO4) [4]. With the use of more powerful laser devices the processing velocity starts to depend mainly of maximum velocity of scanning allowed by the optical system. This way, research and development was made in this subject, leading to the substitution of conventional galvanometric mirrors by rotational hexagonal mirrors or by illuminating systems based in optical fibers [61, 62].

The working principle of a laser device is the stimulated emission of photons in consequence of an energetic level transition of atoms when returning to his fundamental level [4, 60]. Each atom has a particular internal energy and his spatial distribution reflects the tendency to the fundamental state be the one that minimizes the total energy. When a light beam is pointed to the optical system, the photons can be absorbed by the atoms, making them go to an excited energetic state, which will be a superior energetic level if the photons energy was enough [4, 59, 60]. This process, called population inversion, make the atoms population that before were mainly in is fundamental state go to localizations in higher energetic levels. In opposite, an atom who were in excited state can travel to a lower energetic level, not necessarily is fundamental state, through two different mechanisms, both involving a photon emission: the spontaneous or stimulated emission [4].

According to the minimum energy principle, after a short period of time (usually about 10^{-8} s), the excited electrons return to is fundamental energetic state emitting photons with energy equal to the previously absorbed [4]. This is the spontaneous light emission and the emitted photons are animated exactly with the same energy (therefore same wavelength) and phase then the previous absorbed photons, however the emission occurs in a random direction. Thus, in the spontaneous emission the photon is propagated in a random direction and the atoms are irradiated independently, the emitted photons have not any stable phase with relation between each other. Therefore, this is an incoherent beam of light.

The principle of stimulated emission was established by Einstein in 1917, but only about thirty years later Townes e Prokhorov, independently, starting to use it in practical applications, taking them to win the Nobel Prize of Physics [63]. However only in 1960 Maiman as resolved the practical problems and invented the first laser device [63].

Assuming that a medium was previously excited originating that N_u atoms are in the higher energetic level W_u , there are a lower energetic level available, W_i , and considering that this excited medium is irradiated with a laser beam with photons of energy equal to $(W_u - W_i)$, Einstein found that in this conditions the received photons of the optical signal originates that the atoms of the higher energetic level, W_u , starts vibrating forcing his transition to the lower energetic level, W_i [4]. Although of the interaction with the excited atom, the incident photon passes without being modified, but because it has stimulated the atom to return to his fundamental state a second photon is emitted with identical energy (therefore same wavelength), direction and phase to the incident photon [4, 53]. This way, the light was not amplified because were supplied two photons, one to excite the atom and other to stimulate is return to the lower energetic level, and as a result were emitted also two photons. However, in proper conditions, the photon resulting from the stimulated emission can resonate with others excited atoms in his path leading to a chain reaction. This way is achieved the light amplification [4, 59].

In stimulated emission case, the emission of energy is started by the presence of electromagnetic radiation with appropriated frequency. The emitted photons have the same phase, polarisation and propagating direction of the stimulating radiation. This way, a laser device generates a light beam extremely focused which do not diverge when gets far from the source.

Every laser is composed by three main elements [59]: an active medium, constituted by a set of atoms, ions or molecules capable of emitting optical radiation; a source of energy capable of exciting the atoms from the active medium; and a resonating cavity composed by two mirrors in which the radiation beam is successively reflected, forcing it to pass many times through the active medium [59].

There are several types of laser devices used in stereolithographic applications [62]. The solid lasers are constituted by tri-valence ions of rare earth metals inside of solid matrices, crystalline garnets of yttrium and aluminium (YAG – Yttrium and Aluminium Garnet) or glass. They emit wavelengths between 170 nm and 3900 nm and can produce laser beams of high power (Figure 2.20).

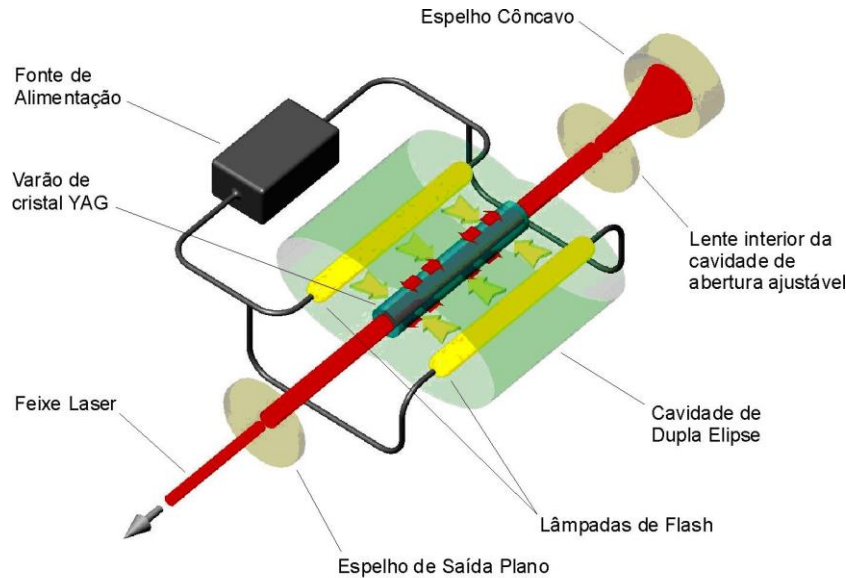


Figure 2.20 – Solid state laser device Nd:YAG [64]

The gaseous lasers more used are [59]: the argon laser which radiates between 488 nm and 514,5 nm in pulsed or continuous regimen and with low exit power but that can reach 150 W; the carbon dioxide laser that radiates in the infrared (10,6 nm) and which have an exceptionally high energetic efficiency; and the continuous helium-cadmium laser that radiates in 325 nm and 441,6 nm, wavelength corresponding to electronic transitions at cadmium ion from excited states, originated for collision with helium atoms.

31

Recent developments in laser technology have greatly enhanced the spatial precision of laser microprocessing and are given access to new interaction mechanisms that can be utilized to alter materials in new ways. This kind of lasers, femtosecond lasers, are lasers which emits optical pulses with a duration in the domain of femtoseconds ($1 \text{ fs} = 10^{-15} \text{ s}$).

The laser power necessary to induce the resin polymerisation is obtained by the equation [62]:

$$P = \frac{E \cdot A \cdot e}{t \cdot \eta} \quad (2.3)$$

where E is the specific energy required by the photo-polymer (in J/m^2), A is the area of the spot defined by laser beam, e is the irradiating layer thickness, t is the exposure time by spot, and η is the optical system efficiency (between 0,5 and 1).

The majority of irradiation systems by laser beam emits in ultraviolet domain, however recent research works are using other spectrum zones. An example is the use of infrared radiation proposed by Campinas University in Brazil and by CNRS in France (CO_2 stereolithography), and the simultaneously use of ultraviolet and infrared radiation proposed by CDRSP in Portugal and by Reading University in United Kingdom (stereo-thermal-lithography).

To maximize parameters such as processing velocity, quality and accuracy of the obtained models, developments are being achieved in matters of scanning strategies of the laser beam over the resin surface. This way, the scanning strategies can be [65-68]:

- Star-Weave: the scanning path has very wide spread lines and therefore are achieved high production velocities. However, between the solidified lines stays closed a very large quantity of resin not polymerised.
- ACES (Accurate Clear Epoxy Solid): as a result of superposed laser beam scanning lines, with this scanning strategy are obtained massive prototypes.
- QuickCast, TetraCast: through the definition of a reticulated internal structure, allows the attainment of models with partial hollows. The not polymerized resin is drained by gravity effect because there are, in the model, drain and ventilation holes. With this scanning strategy is intended to obtain less expensive models.

Recently, Hon *et al* [68] have proposed a new scanning strategy named Bisector (scanning by sectors), which uses a strategy usually used in CNC fabrication (Figure 2.21). It was carried out detailed research work, using numeric simulation, about the effects of this scanning strategy when compared to Star-Weave. It was developed a thermo-mechanical model to analyse tensions, bends and distortions induced by each strategy. The model was implemented through the commercial software of finite elements ABAQUS. The obtained results shows that structures polymerized through Bisector scanning have lower bends and distortions (Figure 2.22).

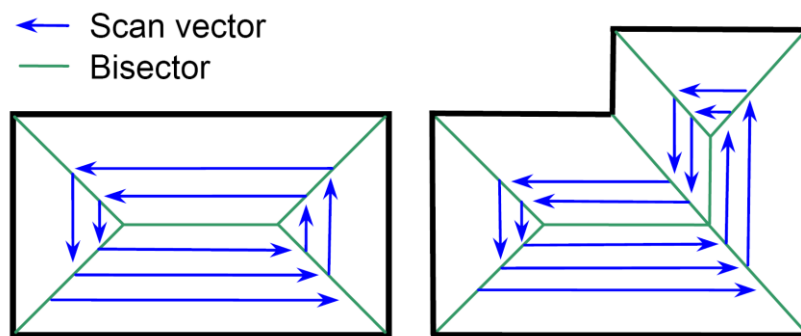


Figure 2.21 – Principle of the scanning strategy Bisector [68]

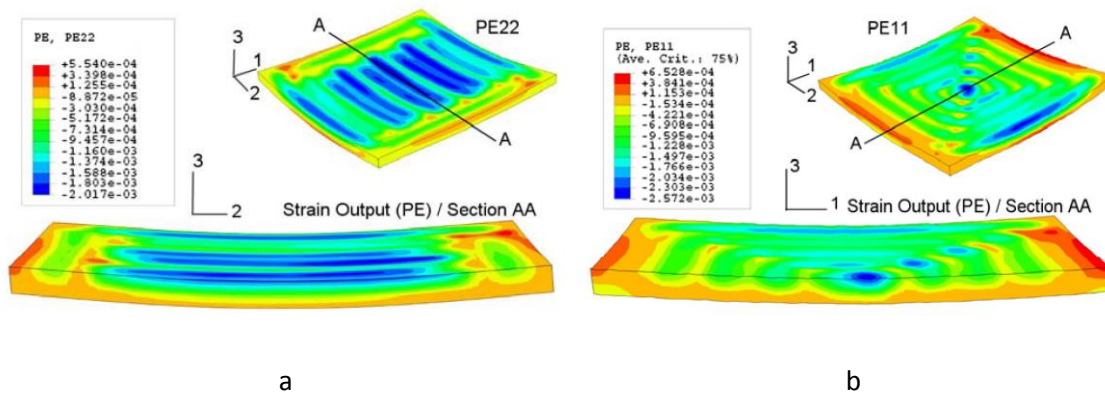


Figure 2.22 – Results obtained with the scanning strategies Star-Weave (a) and Bisector (b) to plastic deformations in directions x (1) and y (2) after processing [68]

Optic systems

Between the laser irradiation source and the resin surface, the light beam can be submitted to an intensity modulation system [61, 62]. However, the majority of stereolithography apparatus do not have this modulating system, being the control of optical exposition done with the scanning velocity [62, 68].

The orientation and control of laser beam can be done by several methods, being the selection of the deflector system depending of the pretended scanning velocity, resolution and accuracy. The deflection systems classified as reflective is constituted by galvanometric or rotating mirrors [61].

The galvanometric mirrors are small mirror attached to a filament winding between two poles of a permanent magnet. The rotation of the mirrors resulting from the current flux in that filament winding, will generate the reflection of incident light with an angle twice of the one submitted to the mirrors [61]. The maximum operation velocities are determined according to the physical limits of the material, such as distortions due to centripetal accelerations, limits of thermal dissipation and linear deflections. The main advantages of this kind of mirrors are the simplicity, reliability and low cost. Besides, the optical distortion is low because the radiation is reflected by one surface only. However, these systems have the disadvantage of having a limited scanning rate [61].

On the other hand, the rotating mirrors (Figure 2.23) allows high scanning rates without prejudice to the number of spots or incident points [13, 61]. The maximum scanning rate is limited by material tensions generated by high velocities of rotation of these planar mirrors. These tensions can exceed permissible limits of the material originating distortions or even fracture, being themselves a limiting factor [61]. This way, the tangential tension at the centre of each mirror face must be less than the permissible tension of the material. The disadvantage of this kind of mirror is the fact of the high velocities involved originate problems of misalignment of the mirror faces, which compels to the production of high precision mirrors and to the use of

additional compensation optic systems, all this with direct consequences in the increase of equipment cost [61].

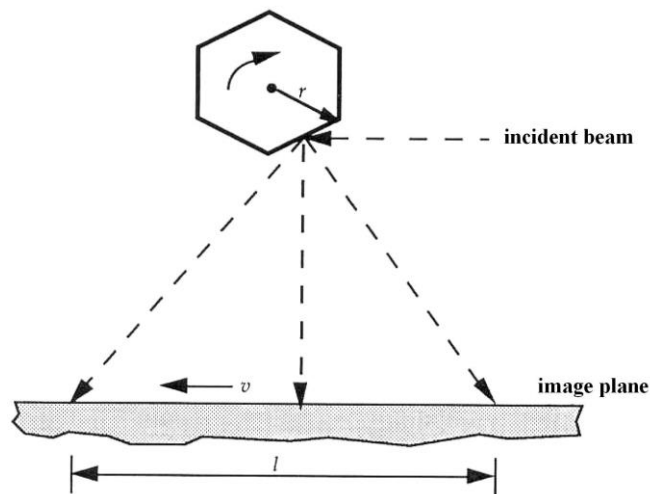


Figure 2.23 – Schematic representation of rotating mirrors [61]

The use of mirrors for laser beam deflection originates distortions that require compensations or corrections. The optics used by the system besides of acting as focalization agents are responsible for the correction of these distortions [13, 61].

A linear deflection x in the image plan requires a specific rotation of the mirror (Figure 2.24):

$$\theta = \tan^{-1} \frac{x}{r} \tag{2.4}$$

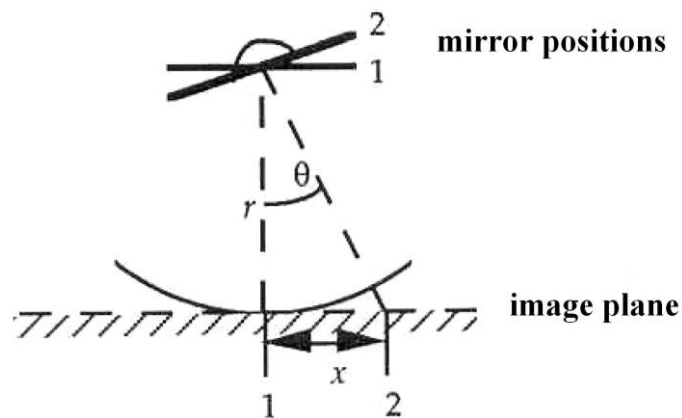


Figure 2.24 – Distortions originated by mirrors rotation [61]

For each indication of position received by the optic system must be associated the calculation of a nonlinear compensation, process that is called beam shaping [61].

Mask irradiation

Initially proposed by Fudim [21, 22, 69, 70] and Pomerantz [71, 72], the stereolithographic processes of mask irradiation, consists in a mask located between an ultraviolet bulb and the layer of resin to be solidified. This mask, fabricated by xerographic techniques, is a negative image of the transversal section pretended. This way, the irradiation that occurs simultaneously to the entire layer, only hits the desired areas of the resin under polymerisation. However, besides less efficiency from the energetic point of view when compared with the direct irradiation processes, experimentally was verified that in larger thickness layers the monochromatic radiation produced by laser beams polymerises the entire layer more uniformly [73].

Osaka University, in Japan, is developing a system that projects the radiation of a halogen bulb in the resin using a LCD projector and a mirror. This method is faster for the irradiation of each resin layer and do not need to use an equipment to align the mask, which is a characteristic of traditional systems [25]. The mask irradiation process was commercialised during the 1990 by the Israelite company Cubital [13]. In Figure 2.25 is shown the fabrication process of prototypes used by this company. At (1), the area of the resin layer below the mask which is exposed to the radiation is solidified by the action of an ultraviolet radiation. Then, the model is cleaned from the material not cured (2). A wax is applied in the areas where the resin not cured was removed and is thermally hardened (3), in order to works like a support to the next layer. At (4), the surface of the resin/wax is milled to guarantee the planar shape and the correct thickness, and then the process restarts fabricating the next layer, with the deposition of photo-sensitive resin (5).

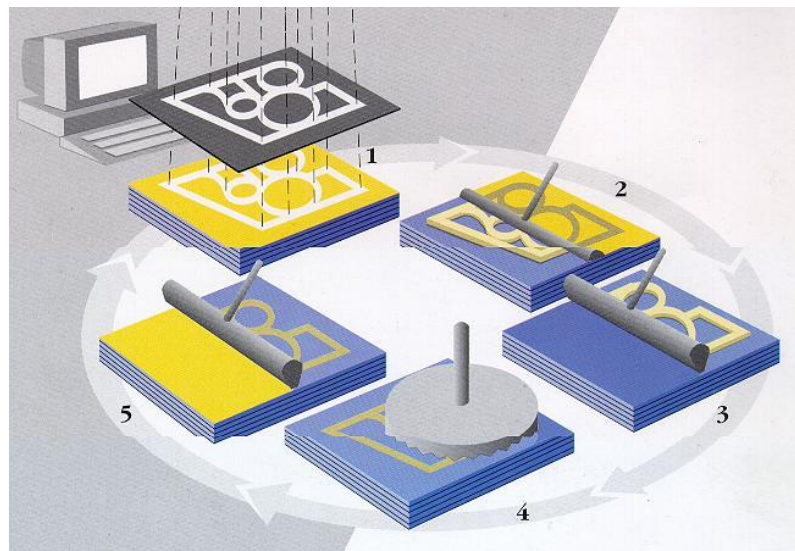


Figure 2.25 – Irradiation mask process from Cubital (Solid Ground Curing)

Light-polymeric system interaction

The photo-polymerisation process starts with the molecular luminescence phenomenon, which consist on the emission of electromagnetic radiation at ultraviolet (UV) spectrum derived from molecules previously excited in the returning to their original state of energy (fundamental state). The molecules excitation is done through the absorption of photons and results in the displacement of the valence electrons to a more energetic orbital, process designated by population inversion.

Depending on the excitation process involved, the molecular luminescence can be classified in fluorescence and phosphorescence. The fluorescence occurs when the state is singlet, which is when the excited electron spin maintain the same direction. When an inversion of the spin is verified, triplet excited state, is named phosphorescence (Figure 2.26).

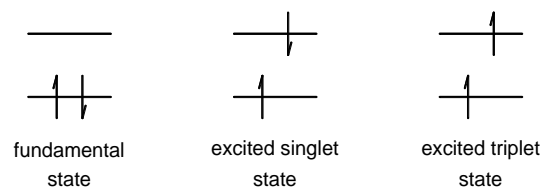


Figure 2.26 – Excited states

36

The Jablonski diagram (Figure 2.27) represents the principal types of electronic transitions. When a photon has enough energy to excite an electron from the fundamental level (S_0) to a superior level (S_n) it is absorbed and occurs an optic transition between those states. The photon with less energy that is absorbed by the molecule has energy equal to the minimum energy difference between S_0 and S_1 [74].

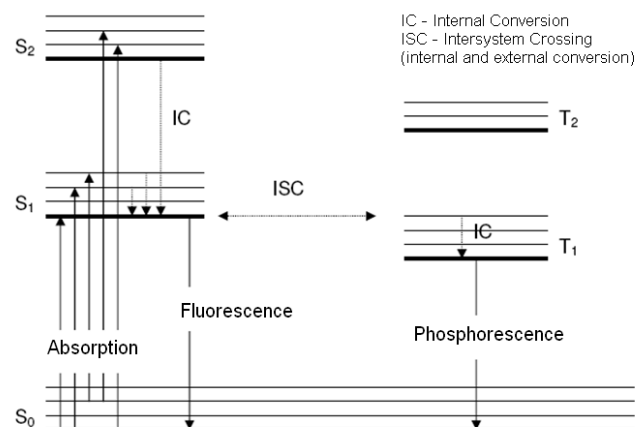
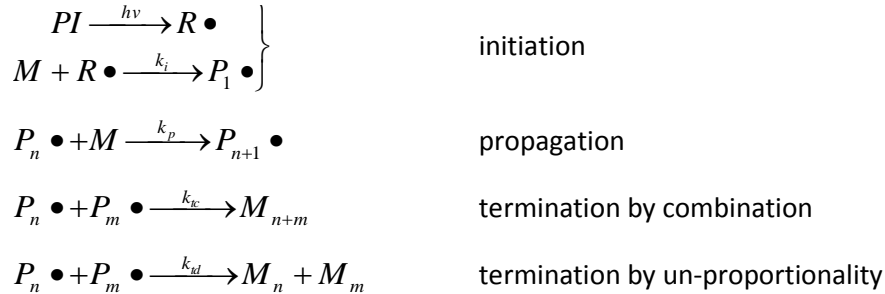


Figure 2.27 – Jablonski diagram [74]

Photo-polymerisation is a chain reaction consisting in three main stages: photo-initiation, propagation and termination. The photo-initiation occurs when photons provided by a laser irradiation source collide with a photo-initiator molecule originating free radicals by a process of excitation and transformation of energy. The propagation stage consists in the growing of

molecular polymeric chain by addition of monomer molecules and will end by several mechanisms called termination.

The radicalar photo-polymerisation process can be described by [46, 75]:



where PI and M represents the photo-initiator and the monomer, $R \bullet$ is the primary radical, $P_n \bullet$ is the polymeric radical with a chain length of n units of monomer (macro-radical).

During the initiation stage, will be formed reactive species that will unite to the monomer molecules [46, 76]. For stereolithographic applications the initiation of polymerisation can be achieved by action of UV radiation, IR radiation or thermal effects [25].

The propagation is then processed by the successive addition of monomers, resulting in the growth of the polymer chain.

The termination always involves the reaction of two macro-radicals, and can take place by two different ways. The first corresponds simply to the formation of a bound between two macro-radicals, called termination by combination. In the termination by un-proportionality mechanism, a proton is transferred originating a double bound [46, 76].

The reactions of inhibition are considered negligible. Ignoring the small percentage of monomers consumed during the initiation, the rate of polymerisation obtained is [46, 76]:

$$-\frac{d[M]}{dt} = R_p = k_p [M][P \bullet] = k_p [M]_0 (1 - \alpha) [P \bullet] \quad (2.5)$$

The total polymeric radical's concentration $[P]$ is given by:

$$\frac{d[P \bullet]}{dt} = R_i - R_t = \phi_i I_a - k_t [P \bullet]^b \quad (2.6)$$

where ϕ_i is the quantum efficiency for the initiation and I_a is the absorbed radiation. The exponent $b=2$ for bimolecular termination; $b=1$ for monomolecular termination (trapping of radicals) [53]. Both termination mechanisms take place in stereolithography [25]. At the initial stage of reaction, when the system viscosity is low, the bimolecular termination dominates. As the viscosity becomes increasingly high the mobility of chains is reduced, increasing the chances of radical chains becoming imprisoned between the cross links of the polymeric network [77-79].

The cure mechanism of stereolithographic resins is a highly exothermic reaction, which results in a significant increase in the temperature of the resin. The energy balance, in transient regime, is a result of the terms of heat generation and conduction. These are the terms that determine the distribution of temperatures in the resin, assuming that the heat generated by other processes than the stage of propagation is negligible [46].

Prototype construction

The stereolithography was the first commercially available technology that allows the fabrication layer by layer, by an additive process, of physical objects obtained directly from information contained in a CAD system. The process starts with the definition of a CAD model from the intended object to be manufactured. Then, the triangulation of the model is made, in which the information is reduced to triangular planar elements connected each other (STL format). Thereafter, is made the slicing of the model, consisting in the separation of information in geometric layers (SLI format), which will be used to the physical fabrication of the model. Then, the stereolithography apparatus prints the various layers generating the solid model. During this step, the control unit adjusts the mirrors to focus the light beam in the desired spot, following a scanning strategy who leads to the solidification of the pretended geometry. Then the movable platform moves a value equal to the layer thickness and the scanning process is repeated. When the fabrication of the model is finished, the model is removed from the platform, the structural supports are also removed and the model is submitted to post-cure operations to increase the percentage of cured material (fractional conversion). The prototype, now completely solidified, can be then submitted to finishing operations or painted in accordance with the pretended effect (Figure 2.28).

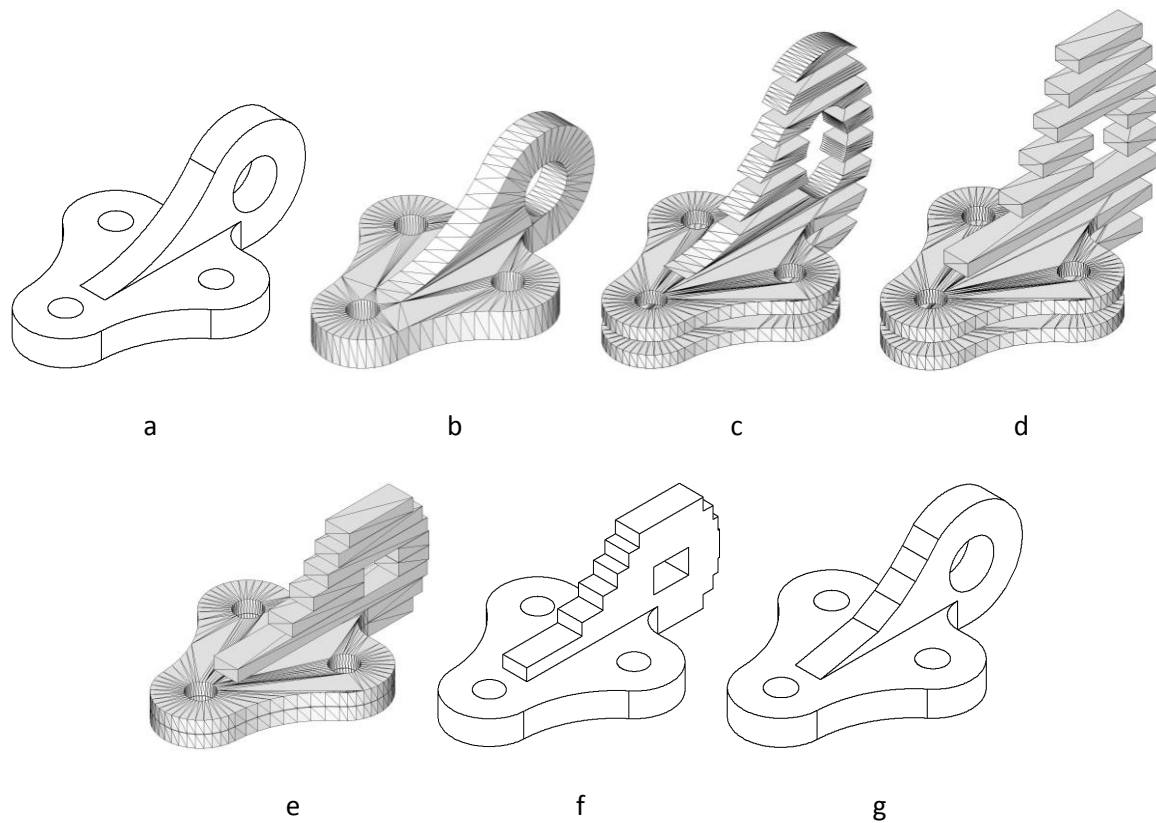


Figure 2.28 – Fabrication layer by layer: a) CAD model; b) STL; c) cut the model in sections; d) layers definition; e) SLI; f) physical model; g) model after finishing

It is useful to estimate with accuracy the time necessary to manufacture the prototype in order to optimize the process parameters, such as layer thickness and model orientation. Thus, this information is important to make a correct budget of the model, to plan and organize the work execution and by a question of strategy and marketing. The stereolithography, like other processes of rapid prototyping, is constituted by three stages that contribute to the time spent in the transformation of CAD model in to a three-dimensional object [13, 42]:

- Pre-processing
- Construction
- Post-processing

Pre-processing stage

The pre-processing stage consists in the preparation of the CAD file in to a format that will able the stereolithography apparatus to fabricate the model. During this preparation is done the model orientation, the slicing of CAD model, the generation of structural supports and the definition of laser beam paths. The time spent in this tasks depends of the used software (for example: QuickSlice, MagicsRP, Buildstation, Maestro, etc.), of the STL file size, which depends of the physical dimensions and the geometric complexity of the model, of the accuracy pretended for the model construction [13]. Calculate the time necessary to the pre-processing stage is difficult to obtain analytically.

Construction

The time actually spent in the construction of the model depends of factors like the model dimensions and geometry, is orientation, and the used process parameters of the rapid prototyping process [13, 73]. During this stage several processes occur successively. The laser beam scans the resin generating the cure reaction, then is done the resin deposition, after that is necessary a waiting time to levelling the resin that depends essentially on the viscoelastic behaviour of the resin and its time of relaxation [39, 42]. Therefore, to estimate with precision the duration of this stage some parameters must be known with anticipation.

For the calculation of the time consumed during the scanning of the laser device, is important to know exactly the total distance covered and the velocity of displacement. The total distance is dependent of the characteristics of the scanning type, which includes parameters such as: orientation, layer thickness, distance between scanning lines, configuration of the scanning lines, etc., besides geometry and characteristics of the model [65, 67, 68]. All the information about geometric definition is contained in a STL file or by layers in a SLI file (the model is divided in parallel sections with the exact shape of the layers used in the fabrication, as previously described). The currently considered analytical models to estimate time consumed can use directly the information of STL model or the representation by layers. The precision of the calculations will be higher in the second case because this type of files supplies detailed information about the area to be covered with the exact path and information referring to the recoat process, generated by the stereolithography apparatus during the preparation of the model process [42].

A very important construction parameter is the scanning velocity of the laser beam, which depends on the laser device power and on the physical characteristics of the resin [13]. This velocity is not constant during all the irradiation process since the laser source cannot supply a constant power. This way, the laser device power and the diameter of irradiation are detected before the fabrication of each layer, and the PLC controller determines the optimum velocity of scanning.

Theoretically, an average velocity of the laser scanning can be calculated assuming that the laser presents a Gaussian distribution at the surface, and that the resin absorption of the laser radiation in depth, follows the law of Beer-Lambert. Based on that, is calculated the maximum depth of cured material. Considering relation between the maximum exposition, the power of the laser device, the irradiation diameter and the velocity of scanning, necessary for the solidification of a specific material thickness, the scanning speed is calculated by the following equation [42]:

$$V_s = \sqrt{\frac{2}{\pi}} \left[\frac{P_L}{r_0 E_C} \right] \exp\left(-\frac{C_d^S}{D_p}\right) \quad (2.7)$$

where V_S is the velocity of laser scanning, P_L is the laser device power, r_0 is the radius of laser beam, E_C the critical laser exposition to initiate the polymerization, C_d is the maximum depth of cured material and D_p is the depth of penetration (characteristic of the material).

The scanning direction does not have influence in the scanning time, remaining constant for one specified thickness of cure. Furthermore, is confirmed that the velocity of displacement of the laser beam in the periods that is not curing the liquid resin is approximately $9,3 \text{ m}\cdot\text{s}^{-1}$ and it depends only of the reflection mirrors rotation [42].

For the construction of each layer occurs a series of operations that are successively repeated [13, 73]:

- levelling the resin;
- platform submersion to resin deposition;
- platform elevation;
- translational movement to the construction position;
- positioning off Z level according to the value layer thickness specified;
- laser scanning;
- Repetition of the previous steps until the attainment of the final prototype.

All these steps involve time consumption, relatively simple to calculate because the time consumption depends on specific constant parameters of each machine or parameters defined by the operator. The time consumed is calculated considering the total number of layers.

There are several simulation models capable of calculating the construction time as a result of the scanning velocity of the laser radiation defined as a function of the scanning strategy pretended [42]. The models have in consideration if the laser is defining the contour of the model or its interior and how it is filled. Furthermore, the time necessary to the auxiliary operations is calculated for each task based on the constant parameters previously referred.

Post-processing stage

The post-processing stage includes the follow steps:

- model removal;
- model cleaning;
- post-cure;
- Finishing operations.

The time necessary to the post-processing tasks like removal and cleaning are function of the complexity and dimensions of the model. For the post-cure, it depends on the dimensions of the model, characteristics of the resin and cure conditions that have direct influence in the process and in consequence in the solidification percentage obtained. This operation represents an

important parcel of time consumption and it is used to complete the cure process and to improve the mechanical properties of the model [13, 58]. However, during this stage is released heat that added to the heat produced by the ultraviolet bulbs used, induces important tensions with thermal origin and consequently bends on the model. The time necessary to finishing operations depends on the intended quality and use for the model.

Quality of the model

In stereolithography there are more than twenty parameters that can be modified with direct influence in the quality of the model obtained, therefore is a highly adjustable process. Quality of a model fabricated by rapid prototyping means basically two factors: surface finishing and dimensional accuracy [13]. They depend on the process parameters, as mentioned previously, but also on the apparatus parameters.

Surface finishing quality

The stairs effect is an inevitable consequence of the fabrication processes based on additives techniques (construction layer by layer) and results in an extremely high surface roughness. All the used techniques to improve the superficial quality represent time consumption and are performed after the production of the model.

42

Experimental research works demonstrate that the main factors with influence in surface roughness are [42]:

- model orientation;
- layer thickness;
- resin properties;
- scanning strategy.

Several analytic models were proposed to predict the surface roughness based in trigonometric concepts [42]. However, some of them were not verified experimentally and others were but with some limitations referring to model geometry.

Other perspective of this problem proposes the application of coverings over the model surfaces. There are a great variety of proposed solutions however all of them represents increase in time consumption and cost of the model [42].

Finally, other solution was presented at programming level. An alternative software to generate the layers (slices) from CAD file using slope surfaces on the steps vertices. This strategy called adaptive slicing allows an improvement on the surface finishing and reduction in the construction time (Figure 2.29) [80, 81]. These strategies are very interesting due to improvement of the surface quality, however, nowadays is not possible to implement them in commercial systems.

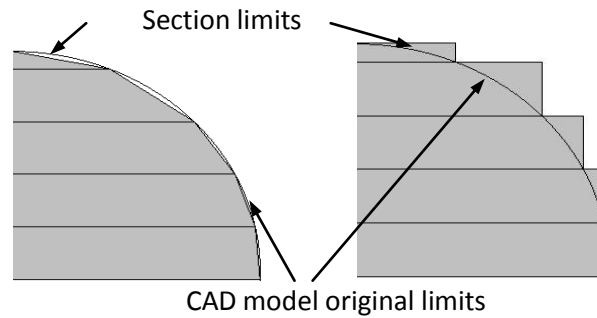


Figure 2.29 – Slicing adaptive and conventional [26]

Dimensional accuracy

The dimensional accuracy has been subject of several experimental studies. Some models semi-empiricists were developed based in statistical analysis of experimental methods and in analytical processes. These models demonstrate the influence of specific parameters of the process in the quality characteristics of the models produced by stereolithography [42].

Additionally some theoretical works had been published, presenting a model capable to predict the dimensional accuracy based in [42]:

- physical properties of the resin;
- laser beam compensation;
- post-cure;
- finishing processes;
- accuracy of stereolithography apparatus.

The main error sources are explained by the shrinkage effect. The photo-sensitive resins used in stereolithography are exposed to a volumetric contraction during the cure process, and this phenomenon is asymmetric in relation to the middle plane of the layers and model. The volumetric contraction is the main cause of dimensional and geometrical inaccuracy, and it happens during three successive stages of fabrication: construction of the model, removal of structural supports and post-cure.

The effects of shrinkage are being studied, experimentally and theoretically, to make possible a better understanding of the inaccuracy and distortion that it causes in the model.

Recently, was elaborated a theoretical model that calculates the value of the expected shrinkage for a plastic filament obtained by stereolithography. Later it was complemented with an analytical model capable of predicting the residual shrinkage based on the fractional conversion. From this model results that resins allowing a faster shrinkage generates minor values of general shrinkage, and this was experimentally verified by Salonitis *et al* [42].

2.3.1.2 - Scanning microstereolithography

Micro-stereolithography (μ -SL) is a recent manufacturing technology that, using the same principle of conventional stereolithography, enables to produce small parts or features with micro precision by the use of additive techniques, not only layer by layer but also using 3D fabrication methods. Usually, μ -SL uses ultraviolet radiation to start the curing reaction in a polymeric medium containing a certain amount of photo-initiator.

At the beginning μ -SL was an evolution of the stereolithographic processes intending to obtain micro-components or components with micro-features. This way, it has started to be a miniaturisation process of the conventional technology (small spot stereolithography technique), however the particularities of the micro domain originated that the developments achieved have distinguished the two processes, not only in terms of equipment but also at the materials point of view.

In microstereolithography two major groups can be identified, according to the construction method; layer-by-layer processes and three-dimensional processes where the solidification occurs inside the liquid resin.

In layer-by-layer construction method, similar to conventional stereolithography, the three-dimensional object is sliced in layers containing the 2D cross section of the model. The irradiation can be done by vector scanning or by mask, where the whole section of the model is submitted to the irradiation by a single integral exposition. These processes can be divided in free-surface method and constrained-surface method. In the first case, the polymeric resin is submitted to the irradiation source from above and the resin at the surface is solidified. The fixed-surface method consists in the irradiation of the resin through a flatly transparent window immersed in the resin, promoting the solidification at the surface defined by this window. This method has a higher resolution [82, 83] than the free-surface method however the adhesion between the solidified resin and the window causes often destruction of the model, thus it is not suitable for production proposes.

Due to the similarities, at the beginning the experimental work done at μ -SL field was obtained with the use of traditional equipment of conventional SL by Takagi and Nakajima [84], Ikuta and Hirowatari [85] and André and Corbel [86]. They had proven that small objects could be built by this method. In this process, the laser beam is reflected by two galvanometric mirrors and focused, through a dynamic lens, at the surface of an acrylate resin containing an ultraviolet photo-initiator [87] (Figure 2.30). The main conclusion was that, in order to improve the focalization of the laser beam at the resin surface it would be necessary to reduce the number of movable components of the process. Therefore, this came to be the basic principle followed by the research groups later involved in the development of μ -SL experimental equipment.

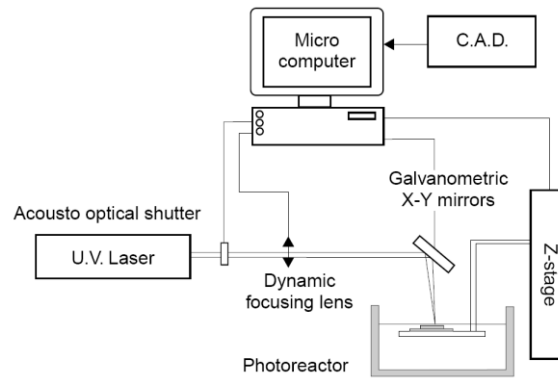


Figure 2.30 – Classic equipment of SL adapted to μ -SL [87]

To improve the accuracy of the μ -SL equipment Ikuta and Hirowatari [85] built a machine at the Kyushu Institute of Technology (Japan), in which the energy source was an ultraviolet lamp irradiating through a glass window (Figure 2.31). The light beam was focused directly over the glass / resin interface without the need of galvanometric mirrors or optic devices. The focus point of the irradiation remain stopped during the construction of each layer, and the movement necessary for the scanning of the area to polymerize was made by the construction platform, which had two degrees of freedom corresponding to the x and y axes. During the x-y movements without polymerization and the level increments, the light is blocked by a shutter. This way, was obtained a focalization point with lesser dimension, however, for more complex geometries the construction time was significantly increased.

45

As a consequence of the glass window, the layer thickness is easily assured avoiding the problems inherent to the distribution of the polymer over each layer. However, does not allow an effective control over the polymerised resin thickness, since it depends from physical and chemical parameters like the irradiation source power, the spotlight diameter and the composition of the reactive medium. Another disadvantage of this construction method is the adhesion between the glass window and each new polymerized layer over it, leading frequently to the partial or total destruction of the model during the construction process. Therefore, this method is inadequate to be adopted as a direct manufacturing process of components.

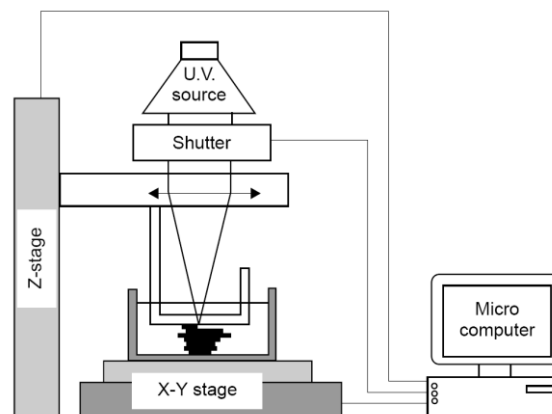


Figure 2.31 – Equipment of μ -SL through a glass window (constrained surface technique) [85]

Later, Zissi *et al* [88] proposed a μ -SL equipment, in which all degrees of freedom (x, y and z) were located in the construction platform, remaining stopped the optic device responsible for focusing the irradiation beam (Figure 2.32). In order to obtain with accuracy the location of the resin surface, was used a position sensor equipped with a diode laser, allowing this way to control the focus point exactly over it.

Unlike the previous methods, it allows to obtain good quality models at the first attempt avoiding unnecessary repetitions. However, since the recoat time depends on the rheological properties of the resin, it is recommended the use of low viscosity resins. The main disadvantages of this method are related with the use of a laser as irradiation source. Since it is required a micrometric accuracy there are focalisation problems. Besides, the spotlight must be extremely small so that the interaction photon / material is focused in the smallest volume as possible, and the density of the light flux, sometimes is so high that induces undesirable polymerisations, for example due to thermal effects. These problems could be avoided using new polymeric systems with appropriated compositions adapted to micro-fabrication.

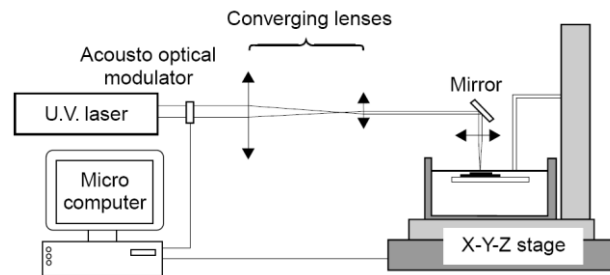


Figure 2.32 – Equipment of μ -SL developed by Zissi *et al* (free surface technique) [88]

2.3.1.3 - Integral microstereolithography

Bertsch *et al* [87] have developed and applied a new concept in μ -SL, the irradiation of whole resin layer simultaneously. The free surface of the polymeric system is irradiated through a matrix of liquid crystals (LCD – Liquid Crystal Display) that acts like a dynamic mask generator (Figure 2.33).

Like the previous methods the model is built layer by layer but, in this case, the whole layer is polymerised with one unique irradiation not depending on the geometry to solidify. The profile is generated in a computer which controls the LCD. The liquid crystal pixels in the opaque state block the light, and in opposition the pixels in transparent state allows the passage of the light instigating the cure of the resin in the correspondent region. Therefore, when light passes through the LCD assumes the shape of the layer defined by the computer (mask). Then, with the use of an appropriated optic device the light is reduced and focused at the surface resin promoting the selective cure of the area corresponding to the transparent pixels. To obtain a high accuracy it is necessary to irradiate the largest LCD area, this is done by the expansion of the laser beam with an appropriated lens.

The mobility of the equipment is therefore reduced to a single degree of freedom (z-axis) which allows the positioning of the construction platform at the desired level.

Comparing with the vector scan methods, the energy flux density is smaller allowing a better control of the cure zone and reducing the occurrence of undesirable polymerisations. Other advantage of this process is the reduction of elements with mobility, avoiding the focusing problems related with translation movements (x and y axes). The irradiation time is significantly reduced and independent from the geometry to obtain. Typically an integral process can produce one to five layers per minute [89] leading to a short manufacturing time. The irradiation time of the integral process can be as short as one second but the necessary time for the recoat leads to a characteristic maximum vertical construction time of one millimetre per hour.

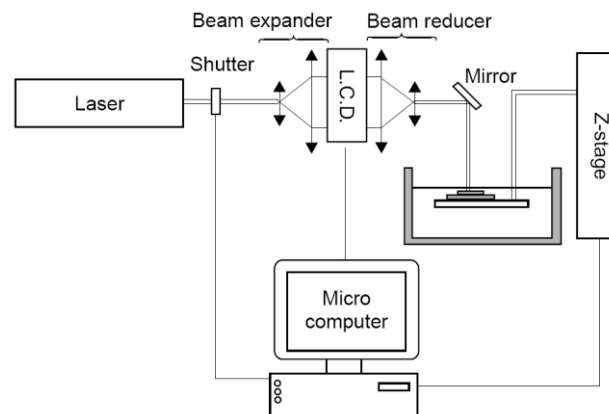


Figure 2.33 – Equipment of μ -SL with dynamic mask generator [87]

The LCD has the disadvantage of not blocking entirely the light at the opaque pixels, allowing the passage of around 20% of the incident beam. This problem can be solved with the composition of the polymeric medium using threshold energy systems. The electric wires net that controls the LCD is opaque to the light, which associated to diffraction phenomenon originates that the cured material surface is not totally smooth. Furthermore, the four glass lenses involving the LCD are opaque to ultraviolet radiation compelling to the use of light sources emitting in visible spectrum and polymeric systems that reacts with these wavelengths.

More recent developments in the μ -SL equipment field were achieved due to the possibility of using more efficient systems as dynamic mask generators, such as DMDTM (Digital Micromirror Devices) produced and commercialised by Texas Instruments[®]. This component is a MEMS (Micro-Electro-Mechanical System) device that works as a light switch, reflecting in the intended direction at the transparent zones of the mask and deviating around 30 degrees at the opaque zones.

The suitability of this kind of component has started to be proven by Beluze *et al* [90]. It was used a micro-mirror matrix with VGA resolution (640 x 480) to produce a model with irradiation in the visible spectrum. The average construction speed obtained, depending of the layers

geometry, was 200 to 300 layers per hour, and the maximum resolution achieved was $3 \times 3 \times 3 \mu\text{m}^3$.

Latter developments in the DMD™ devices commercially available allows to expand the use of this kind of technology to others wavelengths.

Some authors have investigated the use of microstereolithography as a collective manufacturing technology (Figure 2.34). Ikuta *et al* [91] has presented a collective microstereolithography process at the MEMS conference, where an array of multiple optical fibres distributes the UV light provided by a xenon lamp for the surface of the resin. The *x-y-z* movements are in the construction platform and the irradiation light remains stopped. This technique allows manufacturing multiple parts simultaneously however the final result shows a lower resolution when compared with the others methods.

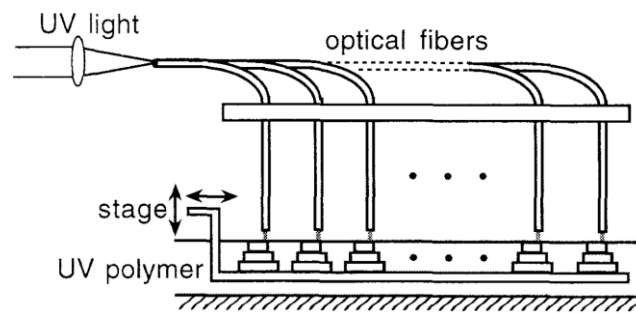


Figure 2.34 – Vector scanning microstereolithography allowing manufacturing several components simultaneously [91]

The surface roughness in the layer-by-layer processes is defined by the stair effect. It can be reduced by using thinner layers, however with implications on construction time. Smoother surfaces can be obtained in three-dimensional processes using very small increments in the vertical direction.

2.3.1.4 - Two-photon sub-micron microstereolithography

The use of supports to prevent displacement of the first suspended layer, common in conventional stereolithography, cannot be used to manufacture micro components because it is almost impossible to remove such small structures without damage the final part. This limitation in the complexity of components can be solved with real three-dimensional construction processes inside the polymeric resin, two photon polymerisation and more recently multi photon polymerisation. Another major advantage results from the fact that there is no need of spreading or recoating of new layers, significantly speeding the process. These methods can produce micro components with very good resolutions but are inadequate to the manufacture of bigger objects.

The technical development achievements in the ultra-short laser systems have created exciting possibilities for very precise localisation of laser energy in time and space. These have triggered novel laser applications based on nonlinear interaction processes [92].

Two photon polymerisation (TPP) techniques take advantage of the quadratic dependence of the rate of two-photon absorption with photon intensity. This absorption occurs when two photons interact with a molecule to induce an electronic transition from the ground state to an excited state with twice the energy of each photon. Regarding that two near infrared photons cause the same transition as a single ultraviolet photon and selecting an appropriated resin transparent to IR it is possible to focus the light beam inside the resin without polymerisation at the surface (Figure 2.35). The first two photon microstereolithography apparatus was presented by Maruo *et al* in 1996 [93] and it was the first microstereolithography process with a submicron resolution.

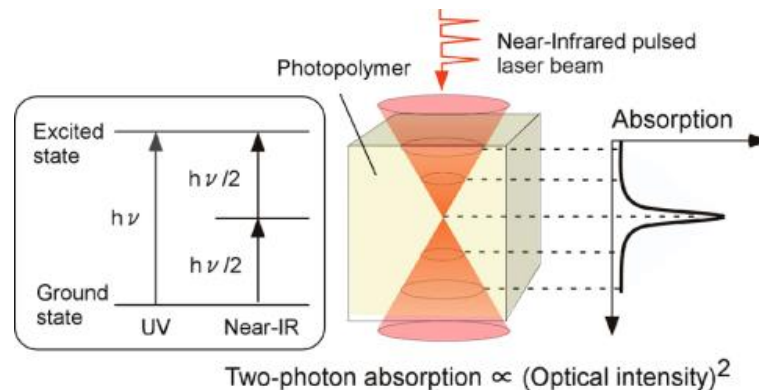


Figure 2.35 – Fundamentals of multiphoton polymerisation generated by a focused laser beam [94]

There are two different mechanisms of two photon absorption (TPA): sequential excitation and simultaneous two-photon excitation. The first case involves the excitation of the absorbing species to a real intermediate state. This first excited state becomes populated by the first absorbed photon and has a well-defined lifetime, typically 10^{-4} to 10^{-9} sec; this state then absorbs a second photon (Figure 2.36 (a)). In the other mechanism (Figure 2.36 (b)) there is no real intermediate state, but a virtual intermediate state is created by the interaction of the absorbing species with the first photon. Only if the second photon arrives within the virtual state lifetime, about 10^{-15} sec, can it be absorbed. Therefore, it is apparent that higher intensities are required for the second approach, which usually requires a femtosecond laser [74].

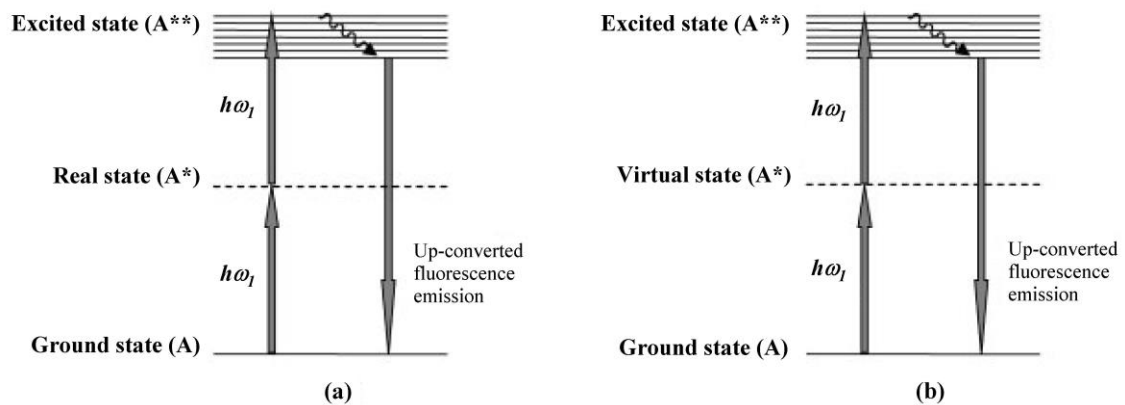


Figure 2.36 – Two mechanisms of TPA: (a) sequential excitation and (b) simultaneous excitation [74]

The single-photon process is based in the nonlinearity of the photo polymerisation reaction in response to the radiation intensity. In the presence of oxygen solved in the resin the polymerisation reaction is inhibited and if the intensity of the radiation is low the reaction does not start. Controlling the radiation intensity level it is possible to polymerise inside the resin and only at the desired spots corresponding to the focal point [95]. This process was introduced by Maruo *et al* at the MEMS conference in 1998 [96].

The resolution of three-dimensional processes depends on the dimensions of energy voxel and is controlled by the value of energy emitted and by the number of laser impulses. These processes enable excellent resolution and dimensional accuracy due to the use of piezoelectric systems for high precision displacements (Figure 2.37). However these systems have very limited working envelope (hundreds of microns) originating difficulties to manufacture components with dimensions over 1 millimetre [92].

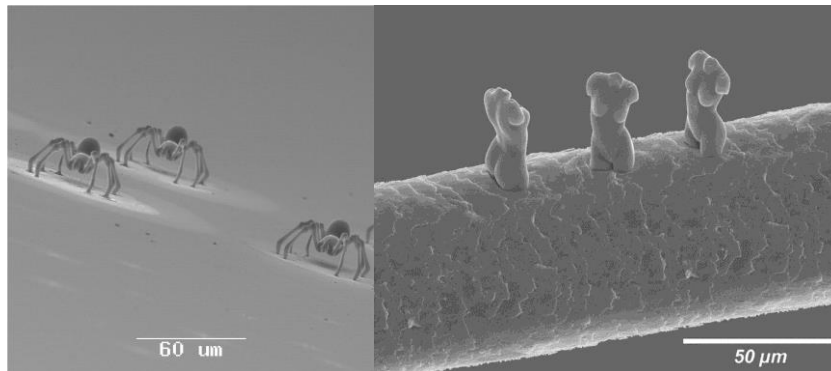


Figure 2.37 – Examples of objects polymerised by TPP technique at Laser Zentrum Hannover [97]

In early stages of development of multi photon microfabrication techniques were used commercially available materials such as urethane acrylates and epoxies [94]. However these photopolymers were originally developed for 3D modelling of macro-scale plastics and their chemical and mechanical properties are insufficient for many practical applications at micro scale. Therefore, several kinds of materials, including inorganic-organic hybrid polymers, biopolymers, photoresists, and hybrid polymers containing metal ions, have been developed for multi-photon fabrication. For biological applications, proteins have been utilized, such as bovine serum albumin and collagen. The resultant structures are porous, and show promise for use as drug delivery devices or sustained release devices. Collagen microstructures will enable the fabrication of 3D scaffolds for tissue engineering [94].

Several kinds of photosensitive materials have been used for photonic applications, including inorganic-organic hybrid polymers (ORMOCER), a negative photoresist (SU-8) and hybrid materials containing metallic ions [94]. An important element component of materials used for multi-photon fabrication is also the photoinitiators, whose suitability depends of factors such as two-photon absorption cross section, initiation velocity, and solubility. While some groups have used commercially available photoinitiators, considerable effort has also been devoted to the

design and synthesis of new photoinitiators with enhanced two-photon absorption cross sections [94] (Figure 2.38).

Table 2.2 shows the single-photon and two-photon photo physical parameters of TPA materials.

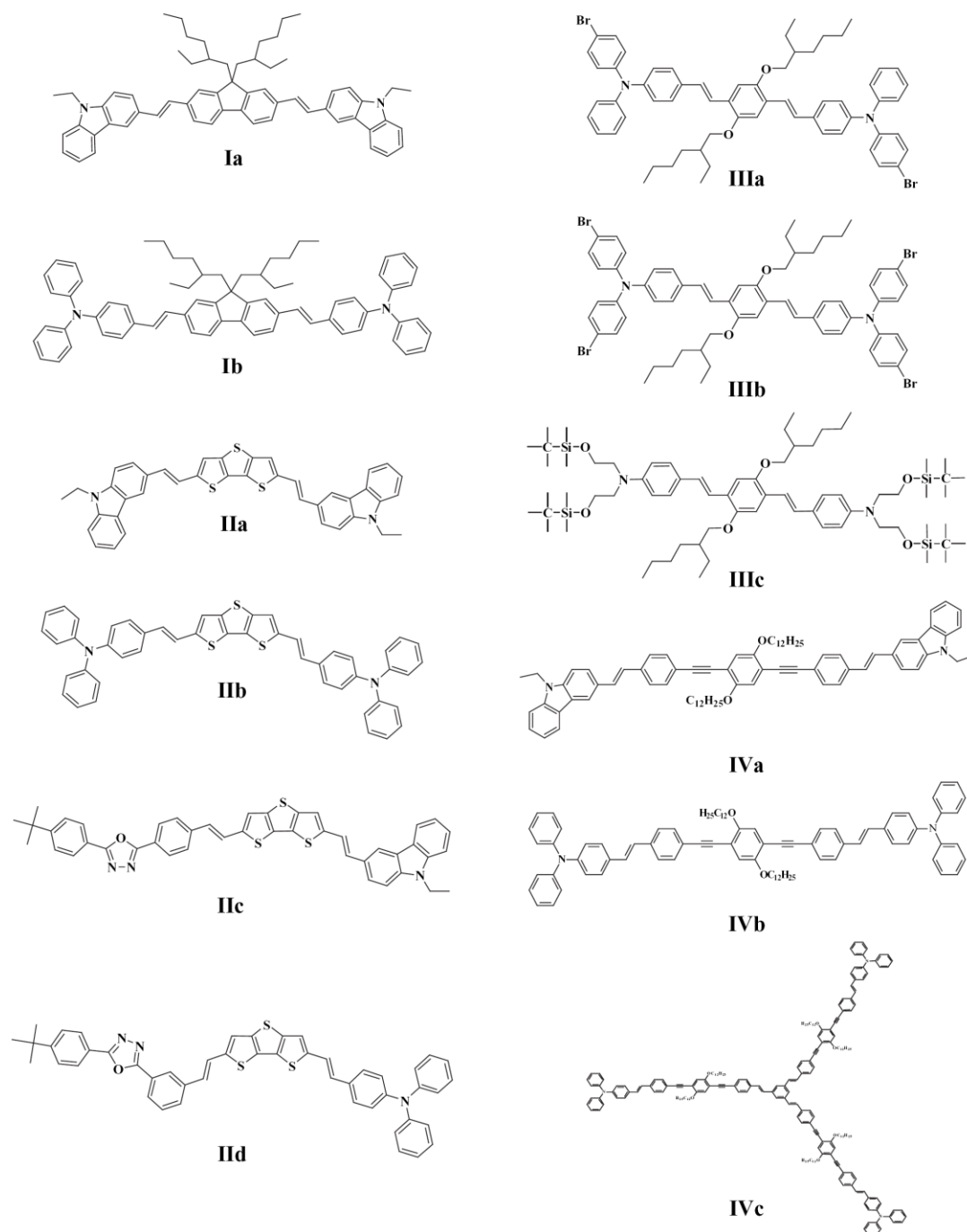


Figure 2.38 – Molecular structures of two-photon absorbing materials [74]

Chromophore	$\lambda_{\max}(\text{abs})$ (nm)	$\lambda_{\max}(\text{PL})$ (nm)	Φ^a	σ^b (GM)	λ_{\max} (TPA) (nm)
Ia	398	434	0.80	290 (80 fsec)	≤ 735
Ib	411	452	0.78	954 (80 fsec)	740
IIa	441	486	0.69	740 (80 fsec)	740
IIb	453	503	0.70	1140 (80 fsec)	785
IIIa	424	507	0.81	470 (80 fsec)	780
IIIb	423 ^c	480 ^c	0.80	470 (180 fsec)	780
IIIc	423 ^c	480 ^c	0.81	190 (80 fsec)	740
IVa	403	446	0.81	960 (80 fsec)	704
IVb	412	464	0.89	1184 (80 fsec)	704
IVc	408	476	0.89	5219 (80 fsec)	700

^a Fluorescence quantum yield determined relative to fluorescein in 0.1 N NaOH.

^b TPA cross-section; 1 GM = $10^{-50} \text{ cm}^4 \text{ sec photon}^{-1}$ measured in two-photon fluorescence method.

^c Solution in CH_2Cl_2 and the others are tetrahydrofuran solution.

Table 2.2 - Single-photon and two-photon photo physical parameters of TPA materials [74]

Applications

Due to the increasing demand of small parts with micro definitions, microstereolithography is starting to be a commercially available manufacturing process, both at prototypes and also equipment markets. The first company that started to sell this kind of prototype products was microTEC at Duisburg (Germany) [98]. Also in Germany, at Laser Zentrum Hannover, a two photon polymerisation microstereolithography equipment can be produced by demand (Figure 2.39). The number of units installed is kept in secret but there are reports that refer the use of these equipment both with research and manufacturing purposes. However, the majority of the produced micro components is obtained with research purposes and is designed to test and develop the capacities of the processes.



Figure 2.39 – Two photon polymerisation microstereolithography equipment developed at Laser Zentrum Hannover [92]

To make possible the use of microstereolithography as a manufacturing process is necessary to solve a very important issue related with the materials limitation regarding that only a few polymers can be used, like acrylates in general and possibly epoxies. Trying to accomplish final components or systems with adequate mechanical, chemical and physical properties, several works are being made using polymeric/ceramic composites but none have reported completely satisfactory results. Bertsch *et al* [99] have reported the fabrication of ceramic micro-components by microstereolithography using a reactive medium composed by 75 wt% of alumina nano sized powder. Despite of a shrinkage value of 20% resulting from the debinding and sintering stages, no visible cracks or deformations were observed in the obtained parts.

2.3.2 - Laser sintering processes

2.3.2.1 - Introduction

The sintering process, usually called Selective Laser Sintering (SLS), was developed in the Texas University by Deckard and Bourell, and consists in the use of infrared radiation to bond particles of powder material, through melting/fusing mechanisms (Figure 2.40) [4, 100]. The laser selectively fuses powdered material by scanning on the surface of a chamber containing the material. The scanning path of each layer defines a cross-section of the model under fabrication. After the fabrication of the all layer, the powder bed is lowered one layer thickness and a new layer of material is applied on top. The process is repeated until the part is completed.

Striving to improve the resolution of selective laser sintering below the limits of commercial SLS devices, a newly development was achieved for the selective fusion of sub- μm sized metal powders. Initially, this technique called laser micro sintering, has been successfully adapted to the processing of 10 μm grained metals applying 10 μm thick sinter layers, and heretofore to the laser micro sintering of 1 μm size grain material [101].

2.3.2.2 - Fabrication strategies

A laser emitting in the infrared zone of spectrum is used to raise the temperature, of a localized point, until the limit value to occur fusion of the material and this way bond it particle by particle. After the fabrication of a layer, a piston is raised supplying a certain quantity of powder material (feeding stage). A levelling roller is used to distribute the material by the working area making a uniform layer (levelling stage), and the process restarts with the laser promoting the solidification and consequent adhesion to the lower layer. The unsintered material works like a support to the model under fabrication. Some apparatus are equipped with a pre-heater system, by infrared radiation, to raise the construction chamber temperature closer to the fusion point of the material. This way, the shrinkage value of the model is lower.

It is a complex apparatus, but it allows to obtain functional models, fabricated in materials similar to the ones intended to the final parts and therefore with identical mechanical properties. However, due to the fabrication process the models show a high superficial roughness and worst dimensional accuracy when compared with models obtained by other

rapid prototyping techniques [4]. As a consequence of the powder material sintering, the model reveals porosity. In the case of direct sintering, the powder material is involved with an adhesive material that is removed after the fabrication of the models. Therefore, is necessary a subsequent infiltration operation with others materials to increase the density of models. In consequence, the mechanical properties and superficial roughness are also improved.

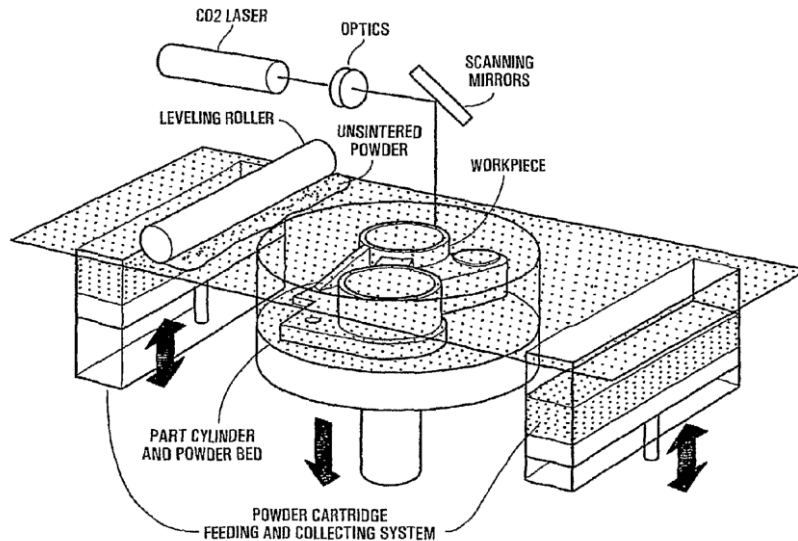


Figure 2.40 – Sintering process [102]

The Table 2.3 shows the advantages and disadvantages of the sintering process.

<i>Advantages:</i>	<i>Disadvantages:</i>
Does not need structural supports;	Porosity of models;
Large diversity of suitable materials;	Significant time invested in heating and cooling the construction chamber;
Possibility of grouping several models in the same setup;	Distortions and warpage;
Models with good mechanical and thermal resistance;	Possibility of toxic emissions using some materials;
Allows the fabrication of parts to clutch or fix, flexible parts and hinges;	High energy consumption during the sintering;
The model can be converted in powder by smashing, to reuse of material.	Worst surface finishing compared to others processes;
	Expensive raw materials (especially in metallic alloys case).

Table 2.3 – Advantages and disadvantages of SLS process [4, 15, 103]

More recently was proposed an alternative to this process, named Selective Inhibition Sintering (SIS) [104]. The difference consists in the fact that after the deposition of a powder material layer is also deposited an inhibitor of sintering. The inhibition is achieved by moisten the intended areas of construction material using an inkjet printer. In this process is possible the thermal irradiation of a complete layer of powder using an infrared light bulb. This way is

achieved an improvement in some properties, like reducing distortions and increase the mechanical resistance of the model [104].

The main advantages and disadvantages of this process are shown in Table 2.4.

<i>Advantages:</i>	<i>Disadvantages:</i>
Low cost of production and rapidity of process; Good dimensional accuracy and surface quality; Multicolor models; Absence of polymeric adhesives.	Process is in early development stage.

Table 2.4 – Advantages and disadvantages of SIS process [104]

2.3.2.3 - Laser Micro Sintering

This technique is an additive freeform fabrication method based on selective laser sintering by which micro parts with an overall resolution of 30 μm can be produced from powder materials. Functional micro bodies can be generated from metals and ceramics without geometric limitations allowing to produce hollows and undercuts [2, 105].

Laser Micro Sintering (LMS) has been successfully applied by the Laser Institut Mittelsachsen e.V in Mittweida, Germany. It was developed a procedure and a device to produce functional micro tools or micro-components for tools from powders of refractory as well as lower melting metals in steps of 1 μm thick sintered layers [106]. Structures were obtained with a resolution of less than 30 μm for overall resolution, of 20 μm for ligaments and of 10 μm for notches at aspect ratios of 12 and above, and a minimal roughness R_a of 1.5 μm . Two main innovations were necessary to achieve those goals: a novel technique and equipment for the handling and coating sub- μm sized metal powders, and a new laser sintering technique employing q-switched pulses [2].

For each layer, the powder material is coated and sintered by a laser beam scanning over the planned cross section. Two important novelties were introduced to the power handling and processing: it allows performing SLS with powder under vacuum or a controlled process atmosphere, and secondly, it is suited to spread sub-micron sized powder layers with sufficient densities.

Two or more racks sweep the powder material in a circular motion onto the sample piston. This technique allows vertical gradients of material blends or grain sizes in the sinter part. The pistons are tight and therefore suitable for powder and liquid materials and also suitable for slurries. The chamber can be evacuated down to pressures of 10^{-3} Pa [2].

The laser pulses are derived by a Q-switched source (Nd:YAG, $\lambda=1064$ nm) although multimode pulses and other lasers with various wavelengths are used.

2.3.3 - Extrusion-based processes

2.3.3.1 - *Introduction*

The rapid prototyping process of extrusion was developed by Crump under the name of Fused Deposition Modelling (FDM), and commercially introduced by the company Stratasys in 1991 [107]. Using this process it is possible to obtain models with good mechanical properties, durable and fully functional. The model is made layer by layer from filaments of polymeric material that is fused and extruded (Figure 2.41).

2.3.3.2 - *Fabrication strategies*

The extrusion head is assembled to a support capable of doing movements in the construction at high velocity under the control of a computer. The polymeric filament is unwound from a coil under the action of a pair of drive wheels, pass through a zone of thermal resistances where is heated to near is fusion point, and then is supplied to the extrusion nozzle. The cold material introduced works like a piston and pushes the liquefied material forcing is exit through the end of extrusion tip [4]. As the material is heated slightly above is flow point but under is melt point, it solidifies quickly adhering to the lower layer. The extrusion head have a mechanism that is able to interrupt the fused material flux and is assembled to a mechanic platform with horizontal and vertical movements. The position of this platform over the working area is controlled according to a STL file provided to the FDM apparatus.

Unlike the lamination process (LOM) there are, in this case, the needs of construct structural supports, which will compel to make a supplementary hand-labour finishing operation to the models. As materials could be used machinable resins or waxes, proper resins to build models to investment casting (also known as lost-wax process), ABS and polyamides [4, 15].

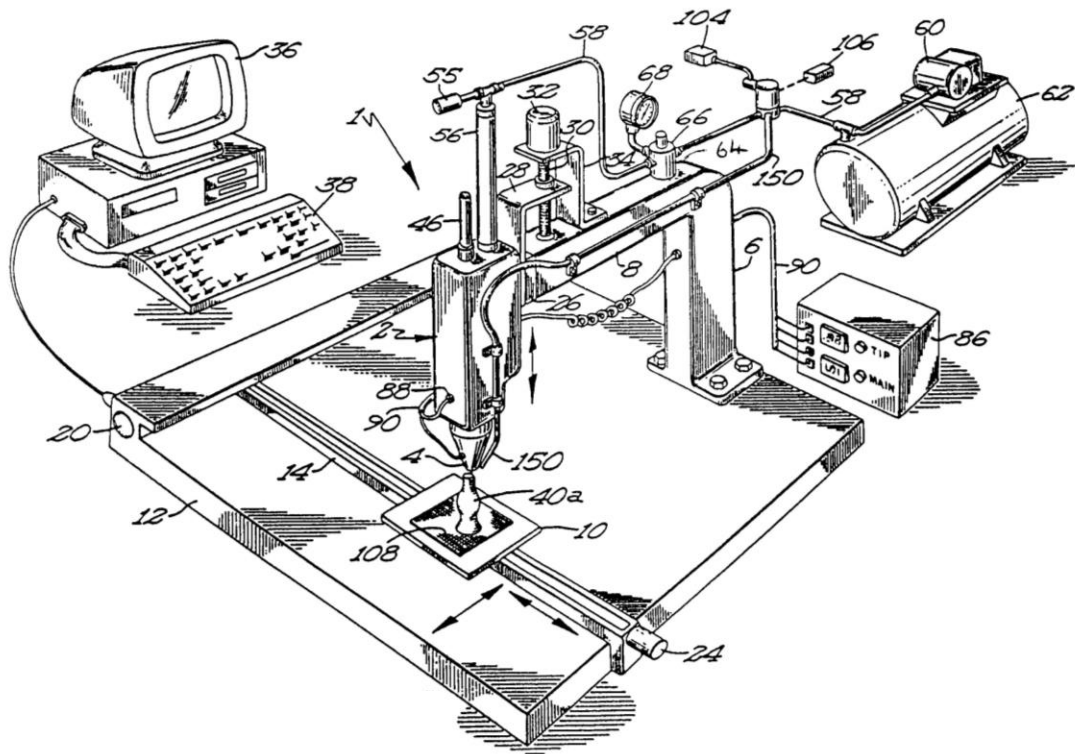


Figure 2.41 – Extrusion process [107]

The main advantages and disadvantages of this process are pointed in Table 2.5.

<i>Advantages:</i>	<i>Disadvantages:</i>
Possibility of obtain fully functional models;	Necessity of structural supports;
Multi-material or multi-colour parts due to the possibility of changing the material during the construction process;	Slow construction for huge volume parts;
Large variety of suitable materials;	Poor mechanical resistance in vertical direction;
Non-toxic materials;	Worst surface finishing compared to others processes;
Absence of a laser device;	Reduced dimensional accuracy;
Desktop apparatus proper to an office ambience;	Variations on temperature during construction process could instigate delaminating phenomenon.
Low waste of material.	

Table 2.5 – Advantages and disadvantages of FDM process [4, 15]

2.4 - Summary

This chapter gives a review of the state of the art of current additive technologies emphasizing the stereolithographic processes. The importance of micro components is outlined and therefore the aim of this research work is to be more focused in small sized components. Thus, special attention was given to micro additive processes.

Others additive technologies currently available were described in order to establish a parallel with stereolithography. The advantage and limitations of current micro additive technologies are summarised.

Stereolithographic techniques and parameters were also described in order to understand the process and therefore design a new apparatus for the intended purpose, including the control system. This way is also possible to predict the result of the prototype in terms of mechanical properties and geometric accuracy.

Current scanning microstereolithography systems denote loss of accuracy due to the movable components. Efforts should be made to reduce the impact of this problem. The integral expose could represent an advantage, from this point of view, since it has less movable components.

Sub-micron microstereolithography allows real 3D construction, polymerising selectively inside the resin and avoiding problems and disadvantages resulting of recoat process. Despite of being able to produce micro components with very good resolution, this process cannot be used to produce bigger objects. Also, there are few suitable materials and in consequence the objects produced have poor mechanical properties.

Small sized objects can be produced, more appropriately, using microstereolithography based on more conventional processes. The working envelope and the volume rate of production are important advantages. Even more significant benefits can be achieved due to the use of other types of materials. In fact, it is possible to produce small objects with good mechanical properties, or even with other intended specific properties using appropriated additives.

Finally a new approach to stereolithography for creating small sized products was introduced in order to offer improvements to current microstereolithography.

2.5 - References

1. Rajurkar, K. and M. Madou, *Processes*, in *Micromanufacturing*. 2007, Springer Netherlands. p. 53-87.
2. Regenfuß, P., R. Ebert, and H. Exner, *Laser Micro Sintering – a Versatile Instrument for the Generation of Microparts*. *Laser Technik Journal*, 2007. **4**(1): p. 26-31.
3. Julien, B. and et al., *Micro-extrusion of organic inks for direct-write assembly*. *Journal of Micromechanics and Microengineering*, 2008. **18**(11): p. 115020.
4. Venuvinod, P.K. and W. Ma, *Rapid Prototyping Laser-Based and Other Technologies*. 2003, Massachusetts: Kluwer Academic Publishers.
5. Kamrani, A.K. and E.A. Nasr, eds. *Rapid Prototyping - Theory and Practice*. 2005, Springer.
6. Farin, G., *Curves and Surfaces for CAGD: a Practical Guide*. 2002, San Francisco: Morgan Kaufmann Publishers.

7. Piegler, L. and W. Tiller, *The NURBS Book*. 1995, Berlin: Springer-Verlag.
8. Zorin, D. and P. Schröder. *Subdivision for Modeling and Animation*. in *SIGGRAPH 2000 Course Notes*. 2000: ACM.
9. Romainbehar. Available from: www.Wikipedia.com.
10. Zeid, I., *CAD/CAM Theory and Practice*. 1991: McGraw Hill.
11. Wood, L., *Rapid Automated Prototyping: An Introduction*. 1993: Industrial Press.
12. Bohn, H. *File Format Requirements for the Rapid Prototyping Technologies of Tomorrow*. in *International Conference on Manufacturing Automation*. 1997. Hong Kong.
13. Chua, C.K., K.F. Leong, and C.S. Lim, *Rapid Prototyping - Principles and Applications*. Second ed. 2004: World Scientific.
14. Prinz, F.B., et al., *Rapid Prototyping in Europe and Japan*. 1997, JTEC/WTEC.
15. Noorani, R., *Rapid Prototyping - Principles and Applications*. 2006, New Jersey: John Wiley & Sons.
16. Dolenc, A. and I. Mäkelä, *Slicing procedures for layered manufacturing techniques*. *Computer-Aided Design*, 1994. **26**(2): p. 119-126.
17. Vouzelaud, T. and A. Bagchi, *An adaptive lamina generation for shape dependent process control and/or object decomposition*. 1995: US Patent 5 432 704.
18. Kulkarni, P., A. Marsan, and D. Dutta, *A review of process planning techniques in layered manufacturing*. *Rapid Prototyping Journal*, 2000. **6**(1): p. 18-35.
19. Hayasi, M. and B. Asiabanpour, *Machine path generation using direct slicing from design-by-feature solid model for rapid prototyping*. *The International Journal of Advanced Manufacturing Technology*, 2009. **Published online**.
20. Ratchev, S. and M. Turitto, *Micro- and Nanomanufacturing Strategic Research Agenda*. 2008, MINAM.
21. Fudim, E.V., *Method and Apparatus for Production of Three-Dimensional Objects by Photosolidification*. 1988: US Patent 4 752 498.
22. Fudim, E.V., *Method and Apparatus for Production of Three-Dimensional Objects by Photosolidification*. 1989: US Patent 4 801 477.
23. Yan, X. and P. Gu, *A review of rapid prototyping technologies and systems*. *Computer-Aided Design*, 1996. **28**(4): p. 307-318.
24. Jardini, A.L., et al., *The Development in Infrared Stereolithography Using Thermosensitive Polymers*, in *Advanced Research in Virtual and Rapid Prototyping*. 2003. p. 273-277.
25. Bártolo, P.J., *Optical Approaches to Macroscopic and Microscopic Engineering*. 2001, Reading University, UK.

26. Bártolo, P.J. and A.L. Jardini, *Stereolithographic Processes: Materials, Techniques and Applications*, in *10th European Forum on Rapid Prototyping*. 2004: Paris, France.
27. Hull, C.W., *Apparatus for Production of Three-Dimensional Objects by Stereolithography*. 1986: US Patent 4 575 330.
28. Hull, C.W., *Method for Production of Three-Dimensional Objects by Stereolithography*. 1990: US Patent 4 929 402.
29. Swainson, W.K., *Method, Medium and Apparatus for Producing Three-Dimensional Figure Product*. 1977: US Patent 4 041 476.
30. Swainson, W.K. and S.D. Kramer, *Three dimensional systems*. 1978: US Patent 4 078 229.
31. Swainson, W.K., *Method, Medium and Apparatus for Producing Three-Dimensional Figure Product*. 1980: US Patent 4 238 840.
32. Swainson, W.K. and S.D. Kramer, *Three dimensional systems*. 1981: US Patent 4 288 861.
33. Swainson, W.K. and S.D. Kramer, *Three-Dimensional Pattern Making Methods*. 1982: US Patent 4 333 165.
34. Swainson, W.K. and S.D. Kramer, *Three-Dimensional Patterned Media*. 1984: US Patent 4 466 080.
35. Swainson, W.K. and S.D. Kramer, *Method and Media for Accessing Data in Three Dimensions*. 1984: US Patent 4 471 470.
36. Kodama, H., *A Scheme for Three-Dimensional Display by Automatic Fabrication of Three-Dimensional Model*. IECE, 1981. **J64-C(4)**: p. 237-241.
37. Kodama, H., *Automatic method for fabricating a three-dimensional plastic model with photo-hardening polymer*. Review of Scientific Instruments, 1981. **52(11)**: p. 1770-1773.
38. Herbert, A.J., *Solid Object Generation*. Journal of Applied Photographic Engineering, 1982. **8(4)**: p. 185-188.
39. Kruth, J.P., M.C. Leu, and T. Nakagawa, *Progress in Additive Manufacturing and Rapid Prototyping*. CIRP Annals - Manufacturing Technology, 1998. **47(2)**: p. 525-540.
40. Bártolo, P.J. and A. Mateus, *O Estado da Arte dos Processos Aditivos de Prototipagem Rápida: Processos Estereolitográficos*, in *O Molde*. 2002 Set. p. 24-28.
41. Grimm, T., *User's Guide to Rapid Prototyping*. 2004, Michigan: Society of Manufacturing Engineers.
42. Salonitis, K., et al., *A Critical Review of Stereolithography Process Modeling*, in *Advanced Research in Virtual and Rapid Prototyping*. 2003. p. 377-384.
43. Biron, M., ed. *Thermosets and Composites: Technical Information for Plastics Users*. 2003, Elsevier.
44. Drobny, J.G., *Radiation Technology for Polymers*. 2002: CRC Press.

45. Belfield, K.D. and J.V. Crivello, eds. *Photoinitiated Polymerization*. 2004, American Chemical Society Publication: Washington.
46. Odian, G., *Principles of Polymerization*. 1981, New York: John Wiley & Sons Inc.
47. Scranton, A.B., C.N. Bowman, and R.W. Peiffer, *Photopolymerization: Fundamentals and Applications*. 1998: American Chemical Society Publication.
48. Fouassier, J.P., ed. *Photochemistry and UV Curing: New Trends 2006*. 2006, Research Signpost.
49. Pappas, S.P., ed. *UV Curing: Science and Technology*. 1985, Technology Marketing Corp.
50. Bártolo, P.J., *Photo-curing modelling: direct irradiation*. International Journal of Advanced Manufacturing Technology, 2007. **32**(5-6): p. 480-491.
51. Gaspar, J., *Study of the Flow and Curing Behavior of the Reinforced Polymeric Systems for Stereolithography*. 2006, Minho University, Portugal.
52. Gargiulo, E.P. and D.A. Belfiore, *Photopolymer Solid Imaging Process Accuracy*. Intelligent Design and Manufacturing for Prototyping ASME, 1991. **PED 50**: p. 81-95.
53. Fouassier, J.P., *Photoinitiation, Photopolimerization, and Photocuring: Fundamentals and Applications*. 1995: Hanser Gardner Pubns.
54. A. L. M. Jardini, R.F.M., M. A. F. Scarparo, S. R. Andrade, L. F. M. Moura,, *Advances in stereolithography: A new experimental technique in the production of a three-dimensional plastic model with an infrared laser*. Journal of Applied Polymer Science, 2004. **92**(4): p. 2387-2394.
55. Jardini, A.L.M., et al., *Improvement of the spatial resolution of prototypes using infrared laser stereolithography on thermosensitive resins*. Journal of Materials Processing Technology, 2006. **172**(1): p. 104-109.
56. S. R. Andrade, A.L.J., M. R. Wolf Maciel, R. Maciel Filho,, *Numerical simulation of localized cure of thermosensitive resin during thermo stereolithography process (TSTL)*. Journal of Applied Polymer Science, 2006. **102**(3): p. 2777-2783.
57. Jardini, A.L., et al., *Development of Nanocomposite Material for Rapid Manufacturing: Application in Microreactor Technology*, in *Virtual and Rapid Manufacturing - Advanced Research in Virtual and Rapid Prototyping*, P.J. Bártolo, et al., Editors. 2008, Taylor & Francis. p. 325-329.
58. Bartolo, P.J. and G. Mitchell, *Stereo-thermal-lithography: a new principle for rapid prototyping*. Rapid Prototyping Journal, 2003. **9**(3): p. 150-156.
59. Ferreira, M., *Óptica e Fotónica*. 2003, Lisbon: Lidel.
60. Steen, W.M., *Laser Material Processing*. 2005, London: Springer.
61. Johnson, J.L., *Principles of Computer Automated Fabrication*. 1994: Palatino Press.

62. Lu, L., J. Fuh, and Y.S. Wong, *Laser-Induced Materials and Processes for Rapid Prototyping*. 2001: Springer.
63. Hecht, E., *Optics*. 2001: Addison Wesley.
64. Vasco, J., *A Micro-fabricação Aplicada ao Processo de Micro-injecção*. 2006, Minho University, Portugal.
65. Onuh, S.O. and K.K.B. Hon, *An Experimental Investigation into the Effect of Hatch Pattern in Stereolithography*. CIRP Annals - Manufacturing Technology, 1998. **47**(1): p. 157-160.
66. Hull, C.W., et al., *Method and Apparatus for Production of Three-Dimensional Objects by Stereolithography with Reduced Curl*. 1992: US Patent 5 104 592.
67. Hull, C.W., et al., *Stereolithography using Different Types of Vector Scanning*. 2002: EP 1 217 438.
68. Hon, K.K.B., C. Han, and S.P. Edwardson, *Investigations on New Scanning Pattern for Stereolithography*. CIRP Annals - Manufacturing Technology, 2006. **55**(1): p. 217-220.
69. Fudim, E.V., *A New Method of 3-D Micromachining, in Mechanical Engineering*. 1985 Sep. p. 54-59.
70. Fudim, E.V., *Sculpting with Light, in Machine Design*. 1986 Mar. p. 102-106.
71. Pomerantz, I., et al., *Three Dimensional Modelling Apparatus*. 1990: US Patent 4 961 154.
72. Pomerantz, I., et al., *Three Dimensional Modelling Apparatus*. 1991: US Patent 5 031 120.
73. Burns, M., *Automated Fabrication: Improving Productivity in Manufacturing*. 1993: Prentice-Hall.
74. Kwang-Sup Lee, D.-Y.Y., Sang Hu Park, Ran Hee Kim, *Recent developments in the use of two-photon polymerization in precise 2D and 3D microfabrications*. Polymers for Advanced Technologies, 2006. **17**(2): p. 72-82.
75. Painter, P.C. and M.M. Coleman, *Fundamentals of polymer science - an introductory text*. Second ed. 1997: Technomic Publishing Co.
76. Rodrigues, M.R. and M.G. Neumann, *Fotopolimerização: princípios e métodos*. Polímeros: Ciência e Tecnologia, 2003. **13**(4): p. 276-286.
77. Rosu, D., et al., *Cure kinetics of epoxy resins studied by non-isothermal DSC data*. Thermochemica Acta, 2002. **383**(1-2): p. 119-127.
78. Schawe, J.E.K., *A description of chemical and diffusion control in isothermal kinetics of cure kinetics*. Thermochemica Acta, 2002. **388**(1-2): p. 299-312.
79. Macan, J., et al., *Study of cure kinetics of epoxy-silica organic-inorganic hybrid materials*. Thermochemica Acta, 2004. **414**(2): p. 219-225.

80. Zhou, M., *Adaptive Slicing of Functionally Graded Material Objects for Rapid Prototyping*. The International Journal of Advanced Manufacturing Technology, 2004. **24**(5-6): p. 345-352.
81. Unnanon, K., *Adaptive Slicing for the Three-Dimensional Plotting Rapid Prototyping Process*. 2000, North Carolina State University, USA.
82. Kobayashi, K. and K. Ikuta. *Development of free-surface microstereolithography with ultra-high resolution to fabricate hybrid 3-D microdevices*. in *Micro-NanoMechatronics and Human Science, 2005 IEEE International Symposium on*. 2005. Nagoya, Japan.
83. Kobayashi, K. and K. Ikuta. *Advanced free-surface microstereolithography with 10 μ m resolution for hybrid microstructures*. in *Advanced intelligent mechatronics, 2007 IEEE/ASME international conference on*. 2007. Zurich, Switzerland.
84. Takagi, T. and N. Nakajima. *Photoforming applied to fine machining*. in *Proceedings of 4th International Symposium on Micro Machine and Human Science (MHS'93)*. 1993. Nagoya, Japan.
85. Ikuta, K. and K. Hirowatari. *Real three dimensional micro fabrication using stereo lithography and metal molding*. in *Micro Electro Mechanical Systems, 1993, MEMS '93, Proceedings An Investigation of Micro Structures, Sensors, Actuators, Machines and Systems. IEEE*. 1993. Fort Lauderdale, USA.
86. André, J.C. and S. Corbel, *Stéréophotolithographie Laser*. 1994, Paris, França: Polytechnia Ed.
87. Bertsch, A., et al., *Microstereophotolithography using a liquid crystal display as dynamic mask-generator*. *Microsystem Technologies*, 1997. **3**(2): p. 42-47.
88. Zissi, S., et al., *Stereolithography and microtechniques*. *Microsystem Technologies*, 1996. **2**(2): p. 97-102.
89. Bertsch, A., H. Lorenz, and P. Renaud, *3D microfabrication by combining microstereolithography and thick resist UV lithography*. *Sensors and Actuators A: Physical*, 1999. **73**(1-2): p. 14-23.
90. Beluze, L., A. Bertsch, and P. Renaud. *Microstereolithography: a new process to build complex 3D objects*. in *Design, Test, and Microfabrication of MEMS and MOEMS*. 1999. Paris, France: SPIE.
91. Ikuta, K., et al. *Development of mass productive micro stereo lithography (Mass-IH process)*. in *Micro Electro Mechanical Systems, 1996, MEMS '96, Proceedings. 'An Investigation of Micro Structures, Sensors, Actuators, Machines and Systems'. IEEE, The Ninth Annual International Workshop on*. 1996. San Diego, USA.
92. Ostendorf, A. and B.N. Chichkov, *Two-Photon Polymerization: A New Approach to Micromachining*, in *Photonics Spectra*. 2006, Laurin Publishing.
93. Maruo, S., O. Nakamura, and S. Kawata. *Three-Dimensional Microfabrication with Two-Photon Absorbed Photopolymerization*. in *Society of Photo-Optical Instrumentation Engineers (SPIE) Conference*. 1996. Taejon, South Korea.

94. S. Maruo and J.T. Fourkas, *Recent progress in multiphoton microfabrication*. Laser & Photonics Review, 2008. **2**(1-2): p. 100-111.
95. Maruo, S. and K. Ikuta, *Three-dimensional microfabrication by use of single-photon-absorbed polymerization*. Applied Physics Letters, 2000. **76**(19): p. 2656-2658.
96. Ikuta, K., S. Maruo, and S. Kojima. *New micro stereo lithography for freely movable 3D micro structure-super IH process with submicron resolution*. in *Micro Electro Mechanical Systems, 1998. MEMS 98. Proceedings., The Eleventh Annual International Workshop on*. 1998. Heidelberg, Germany.
97. *Two-photon polymerization (2PP) technique*. [cited 2009 2009/07/23]; Available from: http://www.laser-zentrum-hannover.de/en/fields_of_work/material_processing/nanotechnology/2pp.php.
98. Bohlman, H. and R. Götzen. *High aspect ratio components through RMPD*. in *4th International Workshop on High Aspect Ratio Micro Structure Technology (HARMST'01)*. 2001. Baden-Baden, Germany.
99. Bertsch, A., S. Jiguet, and P. Renaud, *Microfabrication of ceramic components by microstereolithography*. Journal of Micromechanics and Microengineering, 2004. **14**(2): p. 197-203.
100. Deckard, C.R., *Selective Laser Sintering*. 1988, The University of Texas at Austin, Texas.
101. Regenfuss, P., et al. *Advancements in Laser Micro Sintering*. in *Third International WLT-Conference on Lasers in Manufacturing 2005*. 2005. Munich.
102. Böhler, P. and R. Martinoni, *Selective Laser Sintering and Polymer Used Therein*. 2005: WO 2005/097475.
103. Bártolo, P.J. and H.M. Bártolo, *The Use of Computer-Based Technology for Architectural Concurrent Design*, in *Housing Construction - An Interdisciplinary Task*. 2002, Wide Dreams: Coimbra.
104. Asiabanpour, B., B. Khoshnevis, and K. Palmer, *Advancements in the selective inhibition sintering process development*. Virtual and Physical Prototyping, 2006. **1**(1): p. 43 - 52.
105. Exner, H., et al., *Laser micro sintering: A new method to generate metal and ceramic parts of high resolution with sub-micrometer powder*. Virtual and Physical Prototyping, 2008. **3**(1): p. 3-11.
106. Regenfuß, P., et al. *Industrial Laser Micro Sintering*. in *4th LANE 2004*. 2004. Erlangen, Germany.
107. Crump, S.S., *Apparatus and Method for Creating Three-Dimensional Objects*. 1990: EP 0 833 237 A2.

3

Materials and characterisation techniques

Stereolithographic resins are usually composed by a pre-polymer, photo-initiators and additives. Depending on pre-polymer and photo-initiator different solidification or curing reactions can be considered. The curing kinetics, mechanical properties of the final parts and accuracy of the produced models strongly depend on the type of polymerisation mechanism.

In order to achieve high quality products it is fundamental to understand the curing mechanism of stereolithographic resins and the effect of the major parameters (resin composition, light intensity, temperature) on both the curing process and model properties. During the fabrication process it is important to achieve high degree of solidification in order to avoid cost and time consuming post curing operations.

This chapter describes the major stereolithographic resins and the different curing mechanisms available to produce stereolithographic parts. The material selected for the research work is

described in detail. Finally the major techniques used to characterise both non-processed and processed resins are detailed.

3.1 - Resin systems used in stereolithography

In the stereolithographic processes involving cure by polymerisation are used, acrylic resins with polymerisation by free radicals, epoxy resins with polymerisation from the cationic type, and more recently hybrid resins. In stereolithography the curing reaction is usually initiated by supplying appropriated energy from an ultraviolet radiation (conventional stereolithography), infrared radiation (CO₂ stereolithography) or through the combination of both radiations (stereo-thermo-lithography), and propagates by chain reaction processes transforming low molecular weight liquid polymers into highly reticulated and insoluble structures.

As the polymeric systems do not generate *per si* initiating species, it is necessary to add an initiator that allows the initiation of the polymerisation process when stimulated by an appropriated source of energy. Thus, it is important to select a suitable photo-initiator for the wavelength of the laser source being used. This way, stereolithographic resins are composed by [1-6]:

- oligomer or pre-polymer – determines the mechanical properties of the model;
- diluent (monomer of low molecular weight) – controls the viscosity, and both the physical and mechanical properties of the produced model;
- photo-initiator – absorbs the energy supplied by a laser source, initiating the polymerisation through the formation of reactive species (free radicals or cations);
- Additives.

A proper polymeric system for stereolithographic applications should have the following properties [4, 5]:

- high reactivity when submitted to the irradiation;
- controlled viscosity;
- low volatileness;
- low toxicity;
- low shrinkage. The material shrinkage is a consequence of an increase of material density occurring during the solidification process and can generate significant internal tensions and distortions that affect the quality of the model in terms of both dimensional and geometrical accuracy [2, 7];
- high cure level;
- Good mechanical properties after solidification.

Depending on the combination between the pre-polymer and the photo-initiator different polymerisation mechanisms can be considered. The most common reactions are the so-called free radical polymerisation reactions typically involving acrylic resins and unsaturated polyester resins as well as ketones (acetophenones, benzophenones, etc) as photo-initiators. Free radical polymerisations are highly inhibited by the presence of oxygen, presenting high shrinkage levels during the curing process (5 to 8 % of shrinkage in volume), as indicated in Table 3.1. Free radical polymerisations are progressively substituted by cationic systems [7-10]. These systems, usually epoxy resins, despite of being more expensive and requiring higher energy values to initiate the polymerisation reaction, show low shrinkage values (2 a 3 %) and the produced solid models have better mechanical and thermal properties [8]. Hybrid polymeric formulations were recently introduced to take the advantage of the best characteristics of both free radical and cationic polymerisations.

Table 3.1 - Main characteristics of polymeric systems used in stereolithography

	<i>Radicalar systems</i>	<i>Cationic systems</i>
<i>Cost</i>	low	high
<i>Mechanical properties</i>	poor	good
<i>Shrinkage</i>	high	low
<i>Inhibition</i>	O ₂	H ₂ O
<i>Efficiency</i>	high	low

The first materials used in stereolithography were polymerisation systems of free radicals, where the pre-polymers were unsaturated polyester resins and acrilate based resins, and the photo-initiators were ketones (acetophenones, benzophenones, etc.) [6]. However, due to the fact of the free radical polymerisations be highly inhibited by oxygen presence, besides having high shrinkage levels during the cure process (5 to 8 % of shrinkage in volume), were progressively substituted by cationic systems [8-11]. These systems (epoxy resins) despite of being more expensive and having the necessity of higher energy values to initiate the polymerisation reaction, have lower shrinkage values (2 a 3 %) and the fabricated solid models have better mechanical and thermal properties (see Table 3.1) [9]. The hybrid polymeric formulations, recently introduced, are constituted by different types of pre-polymers that cure with simultaneous reactions of polymerisation by free radicals and cationic polymerisation.

3.2 - Photo polymerisation reactions

Photo polymerisation is the synthesis of polymers by chain reactions that are initiated upon the absorption of light by a polymerisable system.

It is necessary to add small amounts of photo-initiators to the formulations for being polymerised. Both radical and ionic chain polymerisations can be photo-initiated, providing that appropriated initiators and monomers are employed [12].

3.2.1 - Technological significance of photo-initiated reactions

Photo polymerisation is the basis of some very important practical applications in the areas of surface coating and printing plates, in the manufacturing of optical discs and aspheric lenses, in the inline coatings of optical fibres, in the production of printed circuit boards, and in the generation of 3-D models [12]. Photo-induced curing reactions are also used in photolithography and microphotolithography, in stereolithographic processes and in holography [2].

The main industrially applied photo curing processes are based on four chemical systems that are converted into three-dimensional networks upon irradiation [12, 13]:

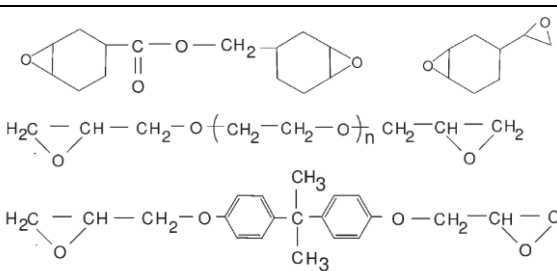
1. Unsaturated maleic/fumaric acid-containing polyesters (UPEs) dissolved in styrene;
2. acrylate/methacrylate systems;
3. thiol/ene systems;
4. epoxide- or vinyl ether-containing systems.

In the case of systems (1)–(3), free radical polymerisations are used, while in case (4) cationic species are involved. Typical di- and tri-functional compounds used for photo curing applications are indicated in Table 3.2.

Table 3.2 - Typical di- and tri-functional compounds used for photocuring [12]

<i>Class</i>	<i>Chemical structure</i>	<i>Mode of polymerisation</i>
Trifunctional acrylates	$ \begin{array}{c} \text{CH}_2-\text{O}-\text{C}(=\text{O})-\text{CH}=\text{CH}_2 \\ \\ \text{H}_3\text{C}-\text{CH}_2-\text{C}-\text{CH}_2-\text{O}-\text{C}(=\text{O})-\text{CH}=\text{CH}_2 \\ \\ \text{CH}_2-\text{O}-\text{C}(=\text{O})-\text{CH}=\text{CH}_2 \end{array} \quad \begin{array}{c} \text{CH}_2-\text{O}-\text{C}(=\text{O})-\text{CH}=\text{CH}_2 \\ \\ \text{HO}-\text{CH}_2-\text{C}-\text{CH}_2-\text{O}-\text{C}(=\text{O})-\text{CH}=\text{CH}_2 \\ \\ \text{CH}_2-\text{O}-\text{C}(=\text{O})-\text{CH}=\text{CH}_2 \end{array} $ <p style="text-align: center;">Trimethylolpropane triacrylate Pentaerythritol triacrylate</p>	Free radical
Oligomeric diacrylates	$ \text{H}_2\text{C}=\text{CH}-\text{C}(=\text{O})-\text{O}-\text{X}-\text{O}-\text{C}(=\text{O})-\text{CH}=\text{CH}_2 $ <p>X: Polyester, Polyether, Polyurethane, Polysiloxane</p>	Free radical
Thiol/Enes	$ \text{C}(\text{X}-\text{SH})_4 / \text{H}_2\text{C}=\text{CH}-\text{X}'-\text{CH}=\text{CH}_2 $	Free radical

(continuation)

<i>Class</i>	<i>Chemical structure</i>	<i>Mode of polymerisation</i>
Difunctional epoxides		Cationic
Epoxidized siloxanes	$\text{H}_2\text{C}=\text{CH}-\text{O}-\text{CH}_2-\text{CH}_2-\text{O}-\text{CH}_2-\text{CH}=\text{CH}_2$	Cationic
Difunctional vinyl ethers	$\text{H}_2\text{C}=\text{CH}-\text{O}-\text{X}-\text{O}-\text{CH}=\text{CH}_2$ <p>X: Polyester, Polyether, Polyurethane, Polysiloxane</p>	Cationic

3.2.2 - Radical photo-initiated reactions

The UV curing of certain monomers, such as acrylate, methacrylate and maleate/vinyl ether systems, is initiated by free radicals [14]. In this cases, the initiating radicals are generated from electronically excited photoinitiator molecules [5, 15].

The synthesis of macromolecules by the free radical chain polymerisation of low molar mass compounds, the monomers, starts with the generation of free radicals, usually through photo fragmentation reactions of initiator molecules. The subsequent processes, comprise propagation, including chain transfer, and termination mechanisms. The simplified overall mechanism is described in Figure 3.1 [12].

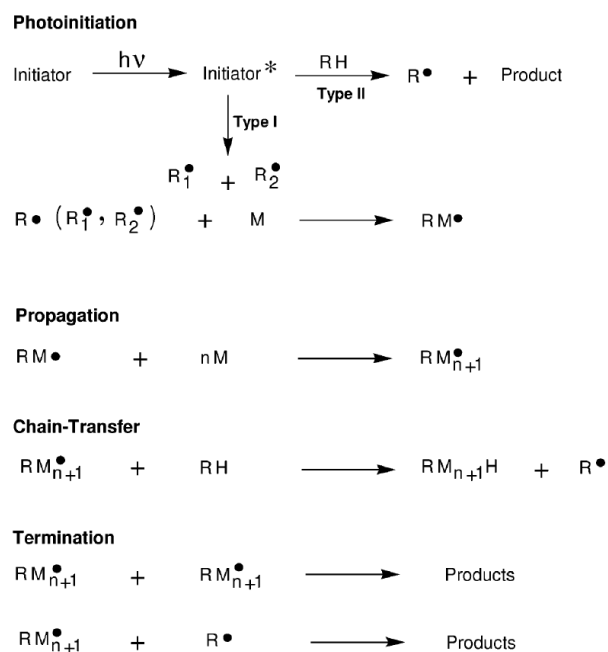


Figure 3.1 – Reaction scheme illustrating the photoinitiated free radical polymerisation of monomer M, commonly a compound with a C=C bound [12]

3.2.3 - Cationic photo-initiated reactions

Cationic photo-initiators are compounds that release an acid under the influence of UV or visible radiation, that in turn, catalyses the desired polymerisation process.

The advantages of photo-initiated cationic polymerisation are the rapid polymerisation without oxygen inhibition, and the ability to polymerise vinyl ethers, oxiranes (epoxides), and other heterocyclic monomers that do not polymerise by a free radical mechanism [12].

Similarly to free radical polymerisations, cationic processes proceed as chain reactions involving initiation and propagation. However, in many cases, there is no termination by neutralization, and the growing chains are only terminated by nucleophilic impurities contained in the system [12].

A major difference between cationic and free radical curing is the degree of shrinkage caused by the polymerisation. Cationic ring-opening polymerisation leads to a shrinkage of 1–2%, as compared to 5–20% for radical polymerisation [12].

3.2.4 - Hybrid photo-initiated reactions

A mode of dual curing involves the simultaneous occurrence of free radical and cationic radiation-induced cross-linking polymerisation of formulations containing appropriate initiators [16-18]. This method, which is called hybrid curing, leads to coatings with unique properties. A typical hybrid-cure system contains a diacrylate and a diepoxide, the former polymerising by a free radical and the latter by a cationic mechanism. Exposure of the system to intense UV radiation results in the formation of interpenetrating networks (IPNs, see Figure 3. 2) [12].

Often, IPN polymers combine the main features of the different networks. For example, elasticity and rigidity are combined in the case of interpenetrating networks formed from a vinyl ether and an acrylate, respectively [12].

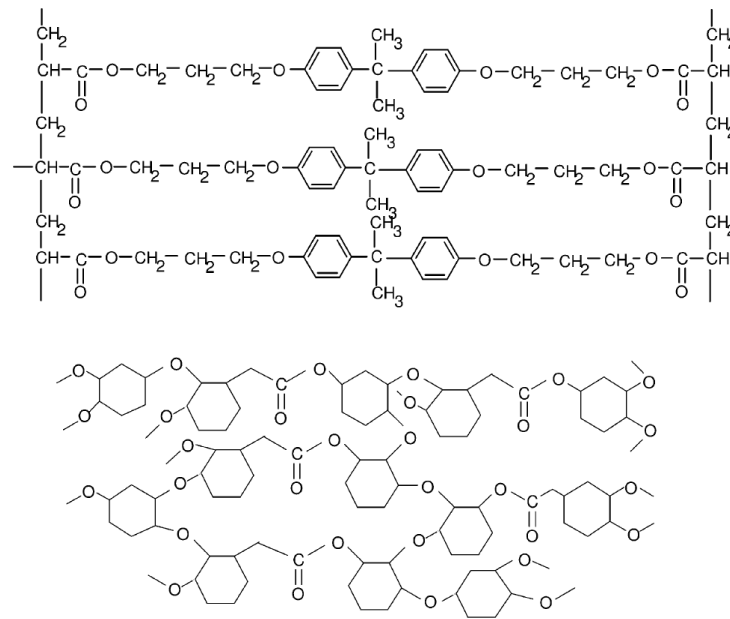


Figure 3. 2– Segments of network structures formed by the radical polymerisation of a diacrylate (top) and the cationic polymerisation of a bis(cycloaliphatic) diepoxide (bottom) [19]

3.3 - The cure mechanism

3.3.1 - Introduction

The curing reactions of thermosetting resins is a polymerisation process characterised by chemical cross-linking reactions that create infusible, insoluble and highly cross-linked three-dimensional network [2, 20]. The process, consisting in an exothermic reaction, is initiated by supplying an appropriate energy source, such as heat, light (commonly ultraviolet light) or an electric potential. In some cases, pressure is also used to enhance cure [21].

The properties of a thermosetting polymer depend on the extent of reaction. Therefore, it is essential understanding the mechanism and kinetics of the cure reaction for a better knowledge of structure relationships.

Two main aspects of the curing reactions of thermosetting resins are gelation and vitrification. Gelation is a non-reversible event and corresponds to the incipient formation of an infinite network during the epoxy curing reaction, which is related with a dramatic increase of viscosity [2, 22, 23]. The molecular chains start to lose their mobility and consequently being confined causing unimolecular termination phenomenon's due to the impossibility off occurring propagation and reaction of two polymeric chains. The polymeric system stops flowing and occur the coexistence of two phases: a soluble phase and a solid phase (or gel phase) corresponding to a heterogeneous polymeric chain (Figure 3.3). The gel corresponds to the formation of an infinite network in which polymer molecules have been cross-linked to each other to form a macroscopic molecule [23]. The non-gel portion remains soluble and can be extracted with solvents. A dramatic physical change occurs during the process of gelation

leading to the transformation of the initial liquid polymeric mixture into a polymer of infinite viscosity.

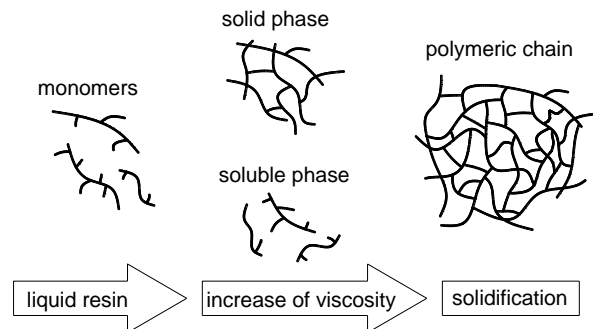


Figure 3.3 – Solidification steps of a liquid resin during the cure process

Vitrification is a phenomenon that, usually, occurs after gelation, and is associated to the transformation from a liquid state to a glassy state as a result of increase in both, the molecular weight and the cross-linking density. It is related to the increase of glass transition temperature and causes a decrease in the reaction rate as a consequence of the polymeric chain mobility limitations. The decrease of mobility, resulting from diffusion limitations of the reactive species will determine the fractional conversion and the need and extension of post-processing operations. This phenomenon is responsible for the formation of heterogeneous structures with a negative influence in both properties and durability of the cured polymer, generating specific volume modifications that induce internal stresses. Therefore, the characterisation of a proper polymeric system to be use in stereolithographic applications is a critical issue, being fundamental to prevent the vitrification phenomenon.

3.3.2 - Modelling approaches to simulate the curing reaction

Three different approaches were developed to model the curing reaction:

- Energetic models,
- Mechanistic and semi-mechanistic models, and
- Phenomenological models.

Energetic models

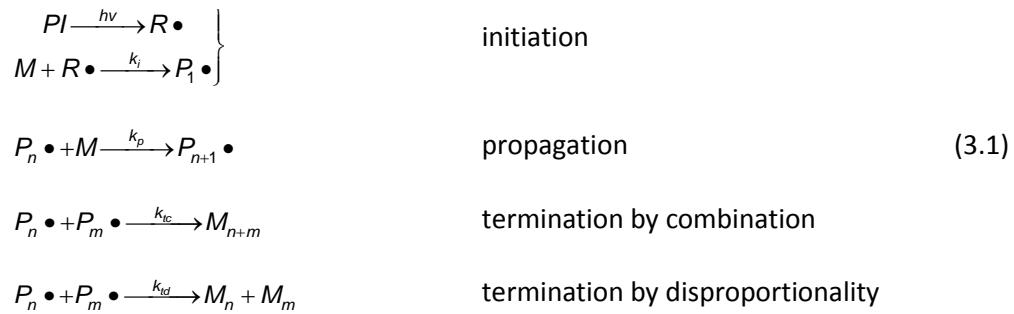
The energetic models were proposed by Yamaguchi and Nakamoto [24] assuming that the cure process begins only when a critical value of energy is reached, which depends on the material being used. These models are based on a direct relation between the radiation intensity, radiation profile, and energy, developed to simulate both direct irradiation and mask irradiation processes.

Mechanistic and semi-mechanistic models

Mechanistic models are based on both the concept of free radical polymerisation and mechanisms of reactions with diffusion [25-27]. These approaches require several assumptions

and approximations to simplify the complexity of the curing reaction. The rate constants in the free radical polymerisation reactions have been modified by introducing the molecular parameters of free volume and glass transition temperature incorporating the effect of diffusion. In this way, these models have pointed out that the model equations often include many parameters that must be determined using numerical optimisation schemes.

Typical radical polymerisation mechanisms can be described as follows [23, 28]:



where PI and M are respectively the photo-initiator and the monomer, $R\bullet$ is the primary radical, $P_n\bullet$ is the polymeric radical with a chain size of n units of monomer.

The rate of monomer depletion, called rate of polymerisation, is given by the following equation [23, 29]:

$$-\frac{d[M]}{dt} = R_P = k_P [M][P\bullet] = k_P [M]_0 (1-\alpha)[P\bullet] \tag{3.2}$$

73

The total concentration of polymeric radicals $[P\bullet]$ is given by:

$$\frac{d[P\bullet]}{dt} = R_i - R_t = \phi_i I_a - k_t [P\bullet]^b \tag{3.3}$$

where ϕ_i is the quantum efficiency of the initiation and I_a is the light intensity. The exponent b is equal to 2 for bimolecular termination processes, and equal to 1 either for unimolecular termination or radical trapping mechanisms.

Phenomenological models

Phenomenological models were developed assuming that only one reaction can represent the whole curing process and are given by the following equation:

$$\frac{d\alpha}{dt} = k_c(T) f(\alpha) \tag{3.4}$$

where $d\alpha/dt$ is the reaction rate, $f(\alpha)$ is a function of conversion, and $k_c(T)$, the chemical-controlled rate constant is a function of temperature.

The simplest and most common analytical form of $f(\alpha)$ is given by:

$$f(\alpha) = (1 - \alpha)^n \quad (3.5)$$

where n is a constant that corresponds to the reaction order. Substituting equation (3.5) into equation (3.4), the following equation is obtained:

$$\frac{d\alpha}{dt} = k_c(T) \cdot (1 - \alpha)^n \quad (3.6)$$

which corresponds to the so-called n th order kinetic model.

The rate constant is supposed to observe an Arrhenius law, so it can be expressed by:

$$k_c(T) = k_0 \exp\left(\frac{-E}{R(\Delta + T)}\right) \quad (3.7)$$

where k_0 is a pre-exponential factor or frequency factor, E is the activation energy, R is the gas constant, T is the temperature in °C, and $\Delta + T$ is the absolute temperature ($\Delta = 273$ °C), indicated hereafter as T_{abs} .

Considering the rate constant expression, equation (3.6) is given by:

$$\frac{d\alpha}{dt} = k_0 \exp\left(-\frac{E}{R T_{abs}}\right) \cdot (1 - \alpha)^n \quad (3.8)$$

For an isothermal reaction, the n th order kinetic equation (3.8) predicts the maximum of the reaction rate, at time $t = 0$. However, if an isothermal process is characterised by a thermogram showing a maximum value of the reaction rate at any point, rather than the reaction starting point, the n th order kinetic model cannot be applied. In these cases, the n th order models are usually replaced by the so-called autocatalytic models, which were initially proposed by Kamal and Sourour [30, 31]:

$$\frac{d\alpha}{dt} = (k_{c1}(T) + k_{c2}(T) \alpha^m) (1 - \alpha)^n \quad (3.9)$$

where $k_{c1}(T)$ and $k_{c2}(T)$ are rate constants expressed by equation (3.7), m and n are constants whose sum is the overall reaction order. The order of the reaction, according to its definition, indicates the number of atoms, molecules, or reactive groups whose concentration determines the reaction rate.

The Kamal model was modified by Bártolo [2] for stereolithographic processes, incorporating the effects of radiation over the curing process. In Bártolo's model, the kinetics parameters are defined as functions of temperature, resin composition, light intensity and fractional conversion. Diffusion-controlled effects due to the vitrification phenomena are also considered [2, 26, 27]:

- thermal-initiated curing reactions:

$$\frac{d\alpha}{dt} = \frac{1}{1 + \exp[\xi(\alpha - \alpha_d)]} \varphi \exp\left(\frac{-E}{R T_{abs}}\right) [\beta]^q \alpha^m (1 - \alpha)^n \quad (3.10)$$

- photo-initiated curing reactions:

$$\frac{d\alpha}{dt} = \frac{1}{1 + \exp[\xi(\alpha - \alpha_d)]} \varphi I^p \exp\left(\frac{-E}{R T_{abs}}\right) [\beta]^q \alpha^m (1 - \alpha)^n \quad (3.11)$$

where ξ is the diffusion constant, α_d is the critical value of fractional conversion corresponding to the beginning of vitrification, φ is a pre-exponential factor, I is the light intensity, E is the activation energy, R is the gas constant, T_{abs} is the absolute temperature, p and q are constants, and m and n exponents represent the reaction order.

These models were experimentally tested with unsaturated polyester resins [2], and recently extended to other radical and cationic systems, as well to highly reinforced resins [32].

3.4 - The polymeric system

3.4.1 - The pre-polymer

3.4.1.1 - The curing reaction of unsaturated polyester resins

The curing reaction of unsaturated polyester (UP) resins with styrene is a free radical polymerisation and comprises three major reactions: styrene-polyester vinylene, styrene-styrene and polyester vinylene-polyester vinylene [33-38]. The styrene homopolymerisation forms a soluble polystyrene segment, which does not contribute to the network formation [35, 38].

Studies on copolymerisation of styrene and diethyl fumarate suggest that homopolymerisation of styrene monomer is significant in relation to the copolymerisation between styrene and polyester vinylene [39]. Therefore, the styrene monomer in UP resins is always present in stoichiometric excess when compared with the polyester vinylenes [40]. The styrene homopolymerisation, however, proceeds much less readily than the styrene-polyester vinyl copolymerisation [38, 40].

The polyester vinylene homopolymerisation is much more difficult to achieve than the other reactions because of the relative immobility of the long polyester chains [34, 35, 38, 40]. Nevertheless, if the concentration of polyester vinylenes becomes much higher than the concentration of styrene monomer, at a local site, the polyester vinylene homopolymerisation may be more favourable than the co-polymerisation between styrene and polyester at that location [34, 38]. This was indicated by Cook and Delatycki [41], whose results showed that, in addition to styrene fumarate copolymerisation, a fumarate-fumarate crosslinking reaction

occurred when the styrene monomer concentration was low. Yang et al. [42] studied the cure kinetics of UP resins and also found that at low conversions, the polyester reaction was more favourable than the styrene reaction because of the intramolecular cyclisation of polyester chains, whereas at high conversions, the styrene reaction became predominant.

The UP resin system can be described as a collection of coiled polyester chains swollen in the styrene monomer [35, 38]. The size of these coils depends on several factors such as the polyester molecular chain length, the chain stiffness, the compatibility of UP molecules with the styrene monomer, and the concentration of the polyester chain [38]. A chemical reaction may occur inside, outside, and at the surface of the coils (Figure 3.4) [35, 38].

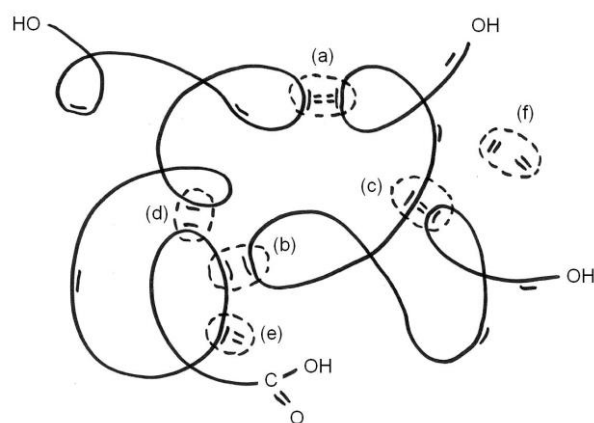


Figure 3.4 – Possible reactions in the styrene–UP copolymerisation. These reactions can be divided into four mechanisms: intermolecular crosslinking (Reactions a and b), intramolecular cyclisation (Reactions c and d), branching growth (Reaction e), and styrene homopolymerisation (Reaction f).

Before the start of the curing reaction, the resin system usually contains UP molecules, styrene monomers, inhibitors and initiators [2, 43, 44]. Under irradiation, the initiator splits into free radicals. At the very beginning of the reaction, most of the free radicals are consumed by the inhibitor, which acts as a retarder of the polymerisation, and reacts with the radicals until it is exhausted [2, 43, 44]. Very little polymerisation occurs at this stage, which is called the inhibition or induction stage [2]. When the inhibitor concentration becomes low, the vinyl bonds (i.e. C=C bonds) on the polyester and styrene molecules are able to compete for the initiator radicals [43]. After this stage, the free radicals will start the reaction by linking adjacent UP molecules and form long-chain molecules through the connection of styrene monomers, by both inter and intramolecular reactions [45].

These long-chain molecules tend to form spherical structures, called microgels or primary polymers, because of the intramolecular crosslinking reactions [35, 38]. Dusek [46] described these microgels as high cyclisation and crosslinking density structures. Moreover, due to the high crosslinking of microgels, many pendant vinyl's are buried inside these structures [35]. This phenomenon, called the “molecular shielding” effect, causes the diffusion-controlled termination reaction effect, which means that termination among the polymer radicals may not be an important factor [2].

As the reaction proceeds, interparticle reactions among microgels will occur with the formation of larger clusters [35, 38]. These reactions will occur through polyester vinyl bonds at, or near, the surface core of the microgels, with styrene monomers serving as chain extenders. Finally, more and more domains are formed and connected, forming a continuous structure.

3.4.2 - The initiator

Two different types of thermal-initiator were investigated, according to procedure described in section 4.2.1, a methyl ethyl ketone and a benzoyl chloride, submitted to an isothermal situation (Figure 3.5).

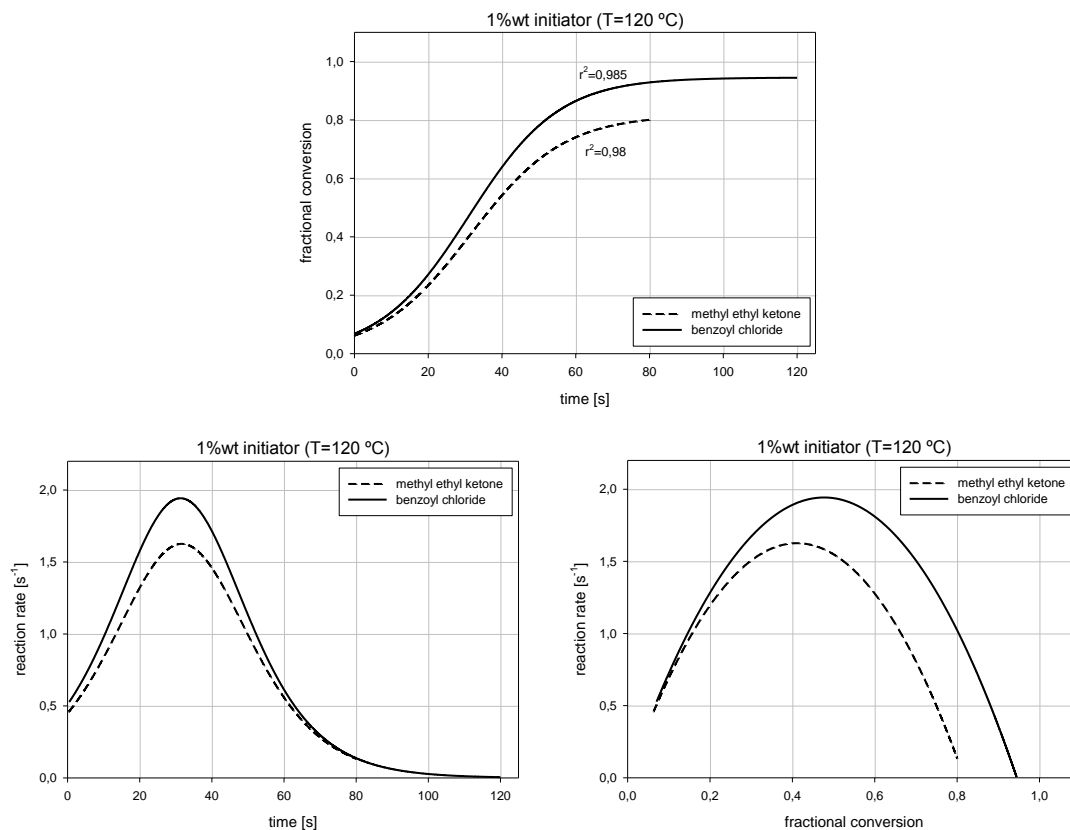


Figure 3.5 – Variation of the fractional conversion versus heating time (first graphic), conversion rate versus time (second graphic), and conversion rate versus fractional conversion (third graphic) for two types of thermal-initiator (1% wt of thermal-initiator, temperature of 120 °C)

The results obtained shown that the resin containing benzoyl chloride thermal-initiator has achieved higher values of fractional conversion for the same curing time. The curing reaction has started earlier, therefore with a shorter inducing period. Also during the propagation phase of the reaction, the resin containing benzoyl chloride has revealed faster conversion rates. For the time periods investigated, the same polymeric compound has achieved higher fractional conversion values at final stages of reaction.

The analysis of the results obtained lead to the conclusion that, at similar conditions, the use of benzoyl chloride thermal-initiator with the polyester resin under investigation has revealed

better performance during the curing reaction and allowed to obtain higher values of fractional conversion for shorter times of thermal exposure.

For the time period investigated the use of methyl ethyl ketone has led to unsatisfactory results in terms of fractional conversion achieved. In addition to longer times of exposure stemming to lower reaction rates, also lower values of fractional conversion were attained. Therefore, the cured samples have worst mechanical properties and it will be necessary to perform additional post curing operations to raise fractional conversion.

Better final results and less time consumed for the same level of applied energy indicate that the use of benzoyl chloride is more appropriate for being used as initiator for polymeric resin tested and therefore it will be used henceforward.

3.4.3 - Additives

Intending to control the curing spot, the use of silica plays an important role since it acts as an energy absorptive medium within the sample reagents. Silica hinders heat diffusion to zones outside the irradiated area. However, the amount of silica is understood to be critical in the process of localized cure because if it is excessively present in the resin composition, silica restricts the curing of reagents absorbing excessively the energy. Not only the kinematic parameters of the cure reaction are influenced but also the layer thickness of cured material is determined by the amount of silica used [47].

Two types of silica were considered to this research work, a colloidal silica and a fumed silica. The colloidal silica was characterized using a Mastersizer and the results shown that, although containing particles between 4 and 190 μm (Figure 3.6), the average size of the particles is around 70 μm , as can be seen in Figure 3.7.

78

Result: Analysis Table

ID: Silica Coloidal R3		Run No: 12		Measured: 18/9/09 10:22			
File: 180909		Rec. No: 30		Analysed: 18/9/09 10:22			
Path: C:\USUARIOS\ANDREJ-1\				Source: Analysed			
Range: 300RF mm		Beam: 2.40 mm		Sampler: MS14			
Presentation: 3OHD		Analysis: Polydisperse		Obs': 11.7 %			
Modifications: None				Residual: 0.261 %			
Conc. = 0.0785 %Vol		Density = 1.120 g/cm ³		S.S.A. = 0.1154 m ² /g			
Distribution: Volume		D[4, 3] = 71.09 μm		D[3, 2] = 46.42 μm			
D(v, 0.1) = 25.26 μm		D(v, 0.5) = 64.48 μm		D(v, 0.9) = 125.96 μm			
Span = 1.562E+00		Uniformity = 4.843E-01					
Size (um)	Volume Under%	Size (um)	Volume Under%	Size (um)	Volume Under%	Size (um)	Volume Under%
0.05	0.00	0.67	0.00	9.00	1.04	120.67	88.33
0.06	0.00	0.78	0.00	10.48	1.61	140.58	93.59
0.07	0.00	0.91	0.00	12.21	2.35	163.77	97.03
0.08	0.00	1.06	0.00	14.22	3.29	190.80	99.03
0.09	0.00	1.24	0.00	16.57	4.48	222.28	100.00
0.11	0.00	1.44	0.00	19.31	6.02	258.95	100.00
0.13	0.00	1.68	0.00	22.49	8.03	301.68	100.00
0.15	0.00	1.95	0.00	26.20	10.71	351.46	100.00
0.17	0.00	2.28	0.00	30.53	14.25	409.45	100.00
0.20	0.00	2.65	0.00	35.56	18.92	477.01	100.00
0.23	0.00	3.09	0.00	41.43	24.94	555.71	100.00
0.27	0.00	3.60	0.01	48.27	32.41	647.41	100.00
0.31	0.00	4.19	0.03	56.23	41.22	754.23	100.00
0.36	0.00	4.88	0.07	65.51	51.04	878.67	100.00
0.42	0.00	5.69	0.16	76.32	61.41		
0.49	0.00	6.63	0.34	88.91	71.92		
0.58	0.00	7.72	0.62	103.58	81.06		

Figure 3.6 – Table of results obtained with Mastersizer for the colloidal silica

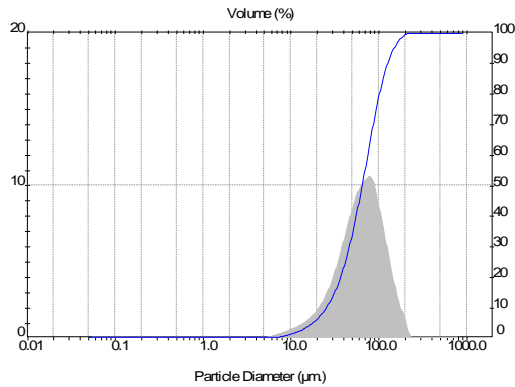


Figure 3.7 – Graphic of results obtained with Mastersizer for the colloidal silica

The untreated fumed silica used was CAB-O-SIL® M-5, from Cabot GmbH, that is a synthetic, amorphous, colloidal silicon dioxide. This silica has extremely small particle size, with enormous surface area, high purity, and excellent chain-forming tendencies. The typical properties of this silica are presented in Table 3.3.

Table 3.3 – Typical properties of silica CAB-O-SIL, as indicated by Cabot GmbH

Typical Properties	
<i>B.E.T. Surface Area</i>	200 m ² /g
<i>pH (4% aqueous slurry)</i>	3.7–4.3
<i>325 Mesh Residue (44 microns)</i>	0.02% max.
<i>Bulk Density*</i>	3.0 lb/ft ³ max.
<i>(Pour Density)</i>	(50 g/l Tap Density)
<i>Loss on Heating*</i>	< 1.5% max.
<i>Loss on Ignition* (@ 1000°C)</i>	< 2 wt. %
<i>Specific Gravity</i>	2.2 g/cm ³
<i>Wt. per gallon</i>	18.3 lb
<i>Refractive Index</i>	1.46
<i>X-ray Form</i>	Amorphous
<i>Assay (% SiO₂)</i>	> 99.8
<i>Oil Adsorption</i>	~350 g/100 g oil
<i>Average Particle (Aggregate) Length</i>	0.2–0.3 microns

*At time of packaging

Non-isothermal cure reactions were performed using a DSC apparatus to investigate the effect of silica particle size on the cure kinetics. The results were analysed with Model Free Kinetics software based on Vyazovkin model allowing the prediction of the reaction rate and fractional conversion. The method is described in detail in section 4.2.3.

Two different temperatures were investigated (100 °C and 120 °C). The results for fractional conversion and reaction rate are shown in Figures 3.8 to 3.10.

Infrared Stereolithography

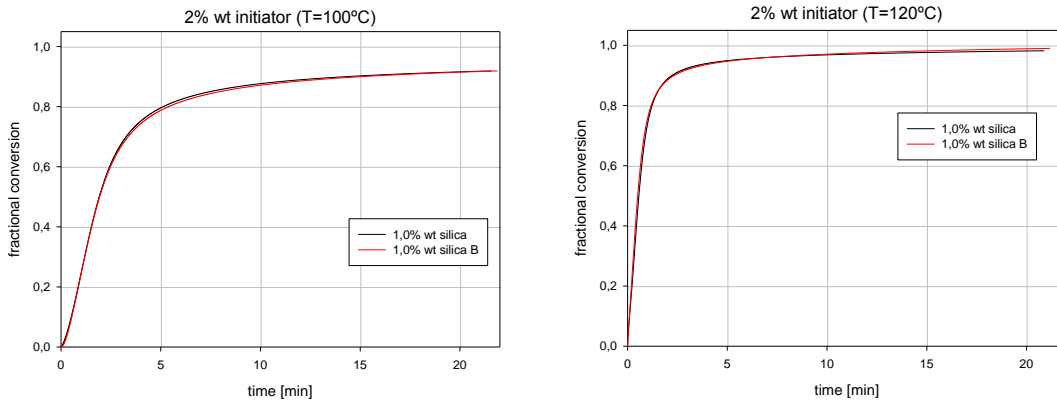


Figure 3.8 – Variation of the fractional conversion versus heating time for the two kinds of silica at different temperatures (2% wt of thermal-initiator)

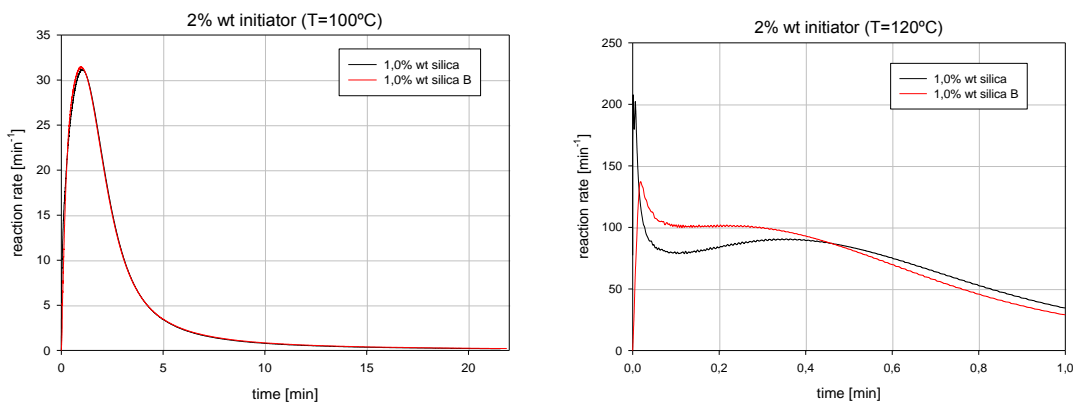


Figure 3.9 – Variation of the the reaction rate versus heating time for the two kinds of silica at different temperatures (2% wt of thermal-initiator)

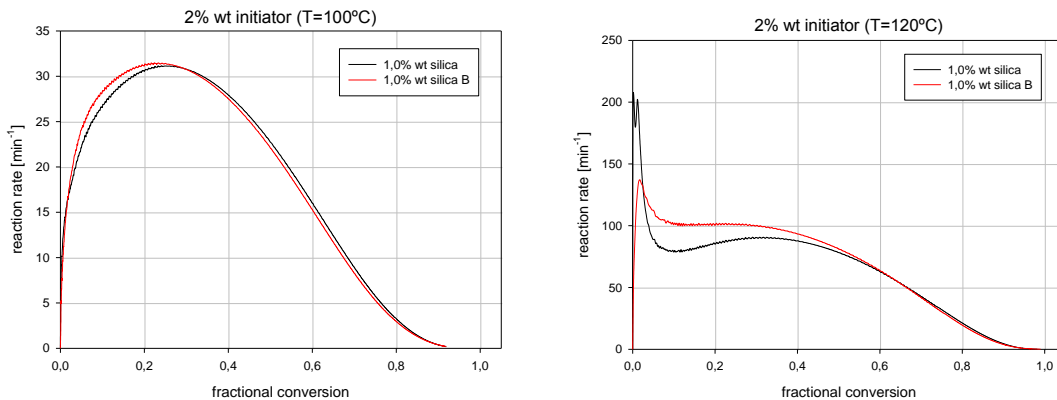


Figure 3.10 – Variation of the reaction rate versus fractional conversion for the two kinds of silica at different temperatures (2% wt of thermal-initiator)

The results shown an induction time slight reduced when silica M-5 was used, outcome from the smaller particle size. Due to the size there are more, although smaller, particles dispersed throughout the resin. The thermal energy is captured by silica particles and this way more reactive points are available in this silica allowing a faster induction of reaction. This effect has repercussions on the following stage of propagation because more active reactions are present. However, the vitrification phenomenon occurs with more consequences in this case for the

reason that the energy is concentrated in more, but smaller points. This way the mobility of reactive chains is less affected with the use of colloidal silica. In this case, the thermal energy is retained in larger spots and this way dispersed by larger areas.

Described effects were more notorious at higher temperature ($T = 120\text{ }^{\circ}\text{C}$). The reactions occur faster and the several stages of reaction are anticipated. The fractional conversion obtained is higher since more energy was induced to the polymeric system.

Small sized particles will have also positive impact in the resolution of the cured models since will allow retaining the thermal energy in more localised spots, therefore improving the accuracy of the cured geometry.

3.5 - Material characterisation

3.5.1 - Experimental techniques to study cure kinetics

A variety of experimental analysis techniques are used for the study of the cure kinetics of thermosetting resins [2]:

- Calorimetry techniques, such as differential scanning calorimetry (DSC) and differential photocalorimetry (DPC);
- Thermogravimetric analysis (TGA);
- Ultrasonic measurements;
- Spectroscopic methods, such as infrared and Raman spectroscopy, nuclear magnetic resonance, fluorescence, Brillouin scattering and photon correlation spectroscopy;
- Dielectric analysis;
- Dynamic mechanical analysis.

Throughout this research work two techniques were used, DSC and a gel content method.

Differential Scanning Calorimetry (DSC) means the measurement of the change of the difference in the heat flow rate to the sample and to a reference sample while they are subjected to a controlled temperature program [48]. In Figure 3.11, S is the sample, R is the reference sample, F is the furnace, A is the cross section of the heat conductor between furnace and S and R, Δl is the distance between temperature measurement point and furnace.

In the study of cure kinetics, two different approaches can be used to perform the experimental measurements. The dynamic analysis consists in submitting the sample to heating or cooling at a constant rate with measurement of the properties as a function of temperature. On the other hand, at the isothermal approach the sample is kept at a constant temperature, with the measurement of properties as a function of time.

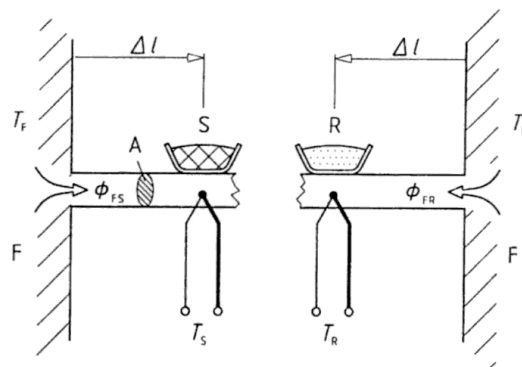


Figure 3.11 – Heat flux DSC (disk-type), model for zeroth approximation (linear model) [48]

A gel content method was used to evaluate the fractional conversion during the polymerisation reaction. This is a major factor, which determines the properties of the processed material. The fractional conversion was determined by soaking the sample in solvent (dichloromethane) for four days at room temperature. Periods of one, four and eight days were evaluated and similar results for conversion fraction were obtained for the last two periods. The insoluble polymer was recovered by filtration, at room temperature, and the solid fraction was evaluated from the weight ratio of insoluble polymer to the initial sample.

3.6 - Summary

The properties and characteristics of the polymeric system selected for this research study are described in this Chapter. The main characterisation techniques used to study the polymeric system are also summarised.

For the design, control and optimisation of microstereolithography it is necessary to obtain adequate information about the reaction kinetics of the selected polymeric systems. In this Chapter was described the theoretical aspects of thermosetting cure reactions and presented a review of models developed to describe the relation between the process parameters and the fractional conversion. Understanding process parameters is crucial in order to control the final properties of cured parts.

The polymeric system used in this research study was analysed. Two different types of initiators were tested and the results were presented and analysed in order to determine the composition of the resin to submit to an extensive experimental work. The results obtained led to the conclusion that using benzoyl chloride as thermal-initiator with the polyester resin under investigation allows achieving better performance during the cure reaction and also allows to obtain higher values of fractional conversion for shorter periods of thermal exposure.

Likewise, two types of silica were researched to be used as heat concentrator agent. The CAB-O-SIL[®] M-5 silica, mainly due to its smaller particle size has revealed several advantages, improving cure kinetics. Despite of worst results in terms of vitrification phenomenon, huge advantages could be attained in accuracy of cured geometry as a consequence of very small sized particles and also due to minor variations in dimensions.

Finally, experimental techniques to be used in the extensive experimental work were described in detail. This experimental work will be carried out with the aim of study and understand the parameters of cure kinetics and the influence of resin composition.

3.7 - References

1. Lu, L., J. Fuh, and Y.S. Wong, *Laser-Induced Materials and Processes for Rapid Prototyping*. 2001: Springer.
2. Bártolo, P.J., *Optical Approaches to Macroscopic and Microscopic Engineering*. 2001, Reading University, UK.
3. Bártolo, P.J. and A.L. Jardini, *Stereolithographic Processes: Materials, Techniques and Applications, in 10th European Forum on Rapid Prototyping*. 2004: Paris, France.
4. Fouassier, J.P., ed. *Photochemistry and UV Curing: New Trends 2006*. 2006, Research Signpost.
5. Fouassier, J.P., *Photoinitiation, Photopolymerization, and Photocuring: Fundamentals and Applications*. 1995: Hanser Gardner Pubns.
6. Burns, M., *Automated Fabrication: Improving Productivity in Manufacturing*. 1993: Prentice-Hall.
7. Bartolo, P.J. and G. Mitchell, *Stereo-thermal-lithography: a new principle for rapid prototyping*. *Rapid Prototyping Journal*, 2003. **9**(3): p. 150-156.
8. Steinmann, B. and A. Schulthess, *Liquid, Radiation-Curable Composition, Especially for Stereolithography in my Patents List*. 1999: US Patent 5 972 563.
9. Coats, A.L. and J.P. Harrison, *Stereolithography Resins and Methods in my Patents List*. 2004: US Patent 4 135 292.
10. Corcione, C.E., A. Greco, and A. Maffezzoli, *Photopolymerization kinetics of an epoxy-based resin for stereolithography*. *Journal of Applied Polymer Science*, 2004. **92**(6): p. 3484-3491.
11. Hague, R., et al., *Materials analysis of stereolithography resins for use in Rapid Manufacturing*. *Journal of Materials Science*, 2004. **39**(7): p. 2457-2464.
12. Schnabel, W., *Polymers and Light, Fundamentals and Technical Applications*. 2007, Weinheim, Germany: WILEY-VCH Verlag GmbH & Co.
13. Dufour, P., *State-of-the-Art and Trends in the Radiation Curing Market*. Vol. I of [7].
14. Drobny, J.G., *Radiation Technology for Polymers*. 2002: CRC Press.
15. Dietliker, K.K., ed. *Chemistry and technology of UV and EB formulation for coatings, inks and paints*. Vol. 3 (Oldring, P.K.T., Ed.). 1991, SITA Technology: London.
16. Decker, C., *Photoinitiated Curing of Multifunctional Monomers*. *Acta Polym.*, 1994. **45**: p. 333.

17. Peeters, S., *Overview of Dual-Cure and Hybrid-Cure Systems in Radiation Curing*.
18. Decker, C., *Photoinitiated Crosslinking Polymerization*. Prog. Polym. Sci., 1996. **21**: p. 593.
19. Decker, C., F. Masson, and R. Schwalm, *Macromol. Mater. Eng.*, 2003(288): p. 17.
20. Selli, E. and I.R. Bellobono, *Radiation Curing in Polymer Science and Technology*, in *Polymerisation Mechanisms*, J.P. Fouassier and J.F. Rabek, Editors. 1993, Elsevier Applied Science: London. p. 1-32.
21. Stevens, M.P., *Polymer Chemistry : An Introduction*. 1999, Oxford: Oxford University Press.
22. Barral, L., et al., *Kinetics of curing reaction of a diglycidyl ether of bisphenol A/1,3-bisaminomethyl-cyclohexane (DGEBA/1,3-BAC) epoxy resin system*. Journal of Thermal Analysis and Calorimetry, 1996. **46**(2): p. 387-395.
23. Odian, G., *Principles of Polymerization*. 1981, New York: John Wiley & Sons Inc.
24. Yamaguchi, K. and T. Nakamoto, *Microfabrication by UV Laser Photopolymerization*. Memoirs of the School of Engineering, Nagoya University, 1998. **50**(No 1/2): p. 33-82.
25. Yousefi, A., P.G. Lafleur, and R. Gauvin, *Kinetic studies of thermoset cure reactions: A review*. Polymer Composites, 1997. **18**(2): p. 157-168.
26. Bartolo, P.J. and E. Lenz, *Computer simulation of stereolithographic curing reactions: phenomenological versus mechanistic approaches*. CIRP Annals - Manufacturing Technology, 2006. **55**(1): p. 221-225.
27. Bártolo, P.J., *Photo-curing modelling: direct irradiation*. International Journal of Advanced Manufacturing Technology, 2007. **32**(5-6): p. 480-491.
28. Painter, P.C. and M.M. Coleman, *Fundamentals of polymer science - an introductory text*. Second ed. 1997: Technomic Publishing Co.
29. Rodrigues, M.R. and M.G. Neumann, *Fotopolimerização: princípios e métodos*. Polímeros: Ciência e Tecnologia, 2003. **13**(4): p. 276-286.
30. Kamal, M.R. and S. Souror, SPE ANTEC Technical Paper, 1972. **18**(93).
31. Kamal, M.R. and S. Souror, *Kinetics and thermal characterization of thermoset cure*. Polymer Engineering & Science, 1973. **13**(1): p. 59-64.
32. Gaspar, J., *Study of the Flow and Curing Behavior of the Reinforced Polymeric Systems for Stereolithography*. 2006, Minho University, Portugal.
33. Liu, S.B., J.L. Liu, and T.L. Yu, *Microgelation in the curing reaction of unsaturated polyester resins*. Journal of Applied Polymer Science, 1994. **53**(9): p. 1165-1177.
34. Huang, Y.J., J.D. Fan, and L.J. Lee, *A free radical copolymerization model for simulating reactive processing of unsaturated polyester resins*. Polymer Engineering & Science, 1990. **30**(11): p. 684-692.

35. Yang, Y.S. and L.J. Lee, *Microstructure formation in the cure of unsaturated polyester resins*. Polymer, 1988. **29**(10): p. 1793-1800.
36. Martin, J.L., *Kinetic analysis of two DSC peaks in the curing of an unsaturated polyester resin catalyzed with methylethylketone peroxide and cobalt octoate*. Polymer Engineering & Science, 2007. **47**(1): p. 62-70.
37. Kosar, V., Z. Gomzi, and S. Antunovic, *Cure of polyester resin in a cylindrical mould heated by air*. Thermochimica Acta, 2005. **433**(1-2): p. 134-141.
38. Yang, Y.S. and L.J. Lee, *Rheokinetic studies of unsaturated polyester resins*. Polymer Process Engineering, 1987-1988. **5**(3&4): p. 327-356.
39. Horie, K., I. Mita, and H. Kambe, *Calorimetric investigation of polymerization reactions. II. Copolymerization of diethyl fumarate with styrene*. Journal of Polymer Science Part A-1: Polymer Chemistry, 1969. **7**(9): p. 2561-2573.
40. Lee, L.J., *Curing of compression molded sheet molding compound*. Polymer Engineering & Science, 1981. **21**(8): p. 483-492.
41. Cook, W.D. and O. Delatycki, *Re-examination of the Crosslinking Process in Styrene-Unsaturated Polyester Systems*. Journal of Macromolecular Science: Part A - Chemistry, 1978. **12**(5): p. 769-787.
42. Yang, Y.S., et al., *Monitoring the cure of unsaturated polyester resins by pressure DSC and FTIR-PLC*. Journal of Applied Polymer Science, 1989. **37**(8): p. 2313-2330.
43. Stevenson, J.K., *Free radical polymerization models for simulating reactive processing*. Polymer Engineering & Science, 1986. **26**(11): p. 746-759.
44. Boenig, H.V., *Unsaturated Polyesters: Structure and Properties*. 1964, Amsterdam, New York: Elsevier Pub. Co. 222.
45. Muzumdar, S.V. and L.J. Lee, *Prediction of gel-time in the cure of unsaturated polyester resins: Phenomenological modeling vs. statistical analysis*. Polymer Engineering & Science, 1991. **31**(23): p. 1647-1656.
46. Dusek, K., in *Developments in polymerisation - 3*, R.N. Haward, Editor. 1982, Applied Science Publishers: Barking, UK. p. 143-206.
47. Munhoz, A.L.J.W., P.R.; Ierardi, M.C.F.; Kiel, A.; Scarparo, M.A.F., *Optical and thermal parameters characterization in CO² laser application in thermosensitive resins using stereolithography processes*. Revista Brasileira de Ciências Mecânicas, 1998. **XX**(2): p. 146-155.
48. Höhne, G., W.F. Hemminger, and H.-J. Flammersheim, *Differential Scanning Calorimetry*. 2nd ed. 2003, Berlin: Springer.

4

The cure reaction: Mechanism and modelling

Stereolithography is an important rapid prototyping process that creates three-dimensional solid objects in a multi-layer procedure. This technology involves the curing or solidification of a liquid photo or thermo sensitive polymer through the use of an irradiation light source, which supplies the energy needed to induce a chemical reaction, bonding large numbers of small molecules and forming a highly cross-linked polymer. This reaction determines the resin morphology that, in turn, defines the physical, electrical, and mechanical properties of the cured material. The cure reaction is highly exothermic and, the temperature and the reaction rate can vary considerably within the curing material due to polymers low thermal conductivity.

Simulations of stereolithography require analytical models describing accurately the curing kinetics. The use of appropriate irradiation, energetic and kinetic models is a critical issue to study photo or thermal-initiated curing reactions in stereolithographic applications. The proposed models for modelling the reaction kinetics are both theoretically rigorous and practical in its implementation, consisting of the resolution of a set of partial differential equations accurately describing the heat transfer mechanism, irradiation conditions and chemical reactions

involved. These models are integrated and solved using the finite element method. The proposed simulation tool includes effects of initiator concentration, temperature and light intensity, to predict the diffusion-controlled effects occurring after vitrification, the phenomenon of unimolecular termination.

4.1 - Introduction

The stereolithography apparatus consists of a computer, a vat containing a photosensitive polymer, a moveable platform on which the model is built, a laser to irradiate and cure the polymer, and a dynamic mirror system to orientate the laser beam. The computer uses a sliced model information to control the mirrors, which guide the laser beam over the polymer surface, “writing” the cross-section of one slice of the model, by polymerising a set of elementary volumes called voxels. After drawing a layer, the platform dips into the polymer vat, leaving a thin film, from which the next layer is created. The next layer is drawn after a waiting period to re-coat the surface of the previous layer. The process is repeated, with each new layer adhering to the previous one. Finally, a post-cure operation could be required to complete the curing process.

The use of stereolithography is still in its infancy. Much of the technology and operating procedures are based on empirical correlations and work experiences and very little is known about the physical and chemical changes occurring in the material owing to the irradiation. A good understanding of the curing process is an important factor to improve both the precision and quality of the models, and to develop well-adapted polymeric systems. Therefore a novel computational tool using the finite element method was developed to study, simulate and optimize stereolithography. The model, which is theoretically rigorous and practical in its implementation, describes both the heat transfer effects and the chemical reaction course.

4.2 - Experimental results

4.2.1 - Procedure

Thermal-initiated cure reactions were performed using the Mettler FP80 Thermal Analysis System with the FP82 Thermal Microscopy Hot Stage (Figure 4.1).

The FP82 Thermal Microscopy Hot Stage uses the principle of heating both sides of the sample with an accuracy of ± 0.6 °C for the range of temperatures used. The sample is inserted on a slide located at a flat rectangular chamber and is submitted to a homogenous temperature field between two heating plates. The furnace is built in a double-walled housing and effective heat insulation is achieved through a mirror finish on the internal housing. Cooling air is blown by a fan located between the internal and external housing. A resistance sensor measures the temperature of the chamber.

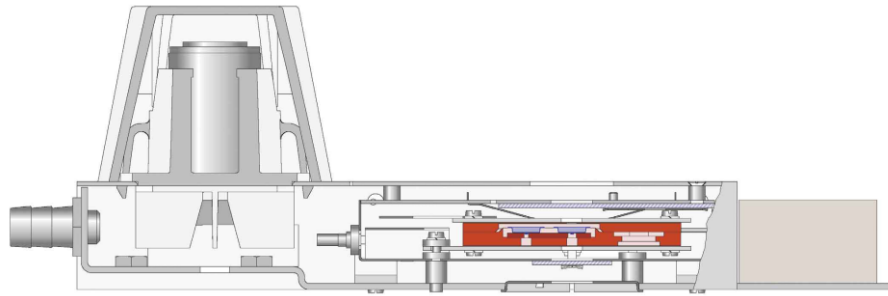


Figure 4.1 – Cross-section of the hot-stage cell

To evaluate the fractional conversion was used the gel content method. In this method, the fractional conversion value is determined by soaking the sample in solvent (dichloromethane) in a closed recipient for a period of time at room temperature. The period of time was estimated by preliminary studies. These studies indicated that four days was adequate because for longer periods the same result was obtained. The insoluble polymer was filtrated at room temperature and the solid fraction was evaluated considering the initial weight of the sample.

4.2.2 - Results and discussion

Thermal-initiated reactions were performed to evaluate and model the effect over the cure process of the following parameters:

- Case I: the effect of curing temperature;
- Case II: the effect of initiator concentration;
- Case III: the effect of initiator concentration (Vyazovkin model);
- Case IV: the effect of silica concentration;
- Case V: the effect of silica particle size.

4.2.2.1 - Case I: the effect of curing temperature

Samples of polyester resin AROPOL FS 6902 (Ara Ashland), with different amounts of thermal-initiator Peroxan BP-Paste 50 PF (Pergan), were cured at different isothermal cure temperatures: 160, 140, 120, 100 and 80 °C. Fractional conversion was determined using the gel content method.

For the study of the thermo-initiated cure reactions under isothermal conditions, four different initial concentrations of thermo-initiator were considered (1, 3, 6 and 9% in weight). Thus, was intended to evaluate the effect of this parameter on the cure kinetics. The results are compared and analysed in Chapter 4.2.2.2.

The results obtained for fractional conversion versus heating time for the isothermal temperatures investigated are shown in Figures 4.2 to 4.5. For the temperature of 80 °C, results were inconclusive due to the low value of fractional conversion obtained. Therefore, only the

results of the other four temperatures are analysed hereafter. The experimental discrete values obtained with gel content method were fitted using sigmoidal equation due to characteristic “s” or sigmoidal-shape profile typically verified in cure profile [1]. These procedures allow obtaining a continuous range of values to better evaluate the cure process. From this technique results that $t=0$ moment is not well defined due to the velocity of reactions.

In Figures 4.2 to 4.5 are shown the profiles of fractional conversion versus heating time for different temperatures and initial concentration of thermo-initiator. The results indicate that after a starting period of induction [1], more meaningful for low temperatures and low concentrations of initiator, reaction develops rapidly to approximate the maximum degree of cure. For values of fractional conversion above 0,8 the reaction rate slows down and the profile of fractional conversion versus time tends to become leveled. This effect is associated with increasing of molecular weight of polymer structure and the consequent reduction of the mobility of polymer chains. Also the reduction of reactive centers due to consumption of initiator species contributes to the described effect.

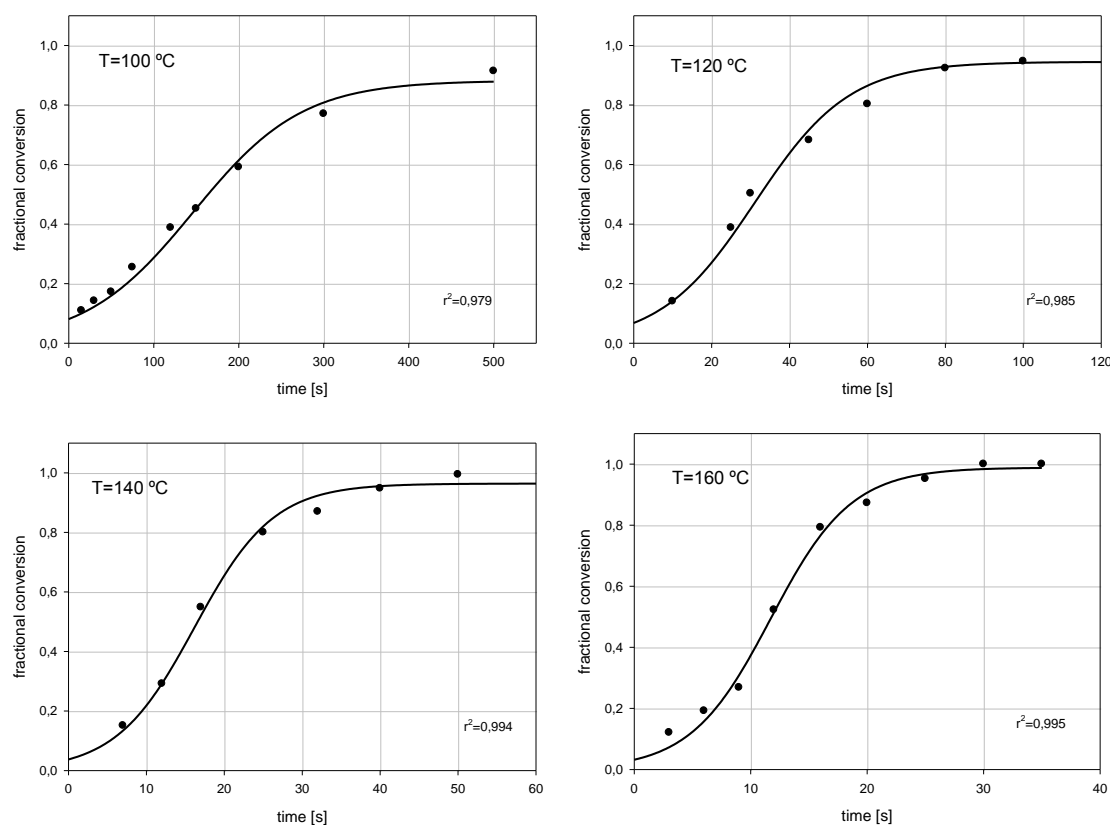


Figure 4.2 – Case I: variation of the fractional conversion versus heating time for different isothermal temperatures (1% wt of thermal-initiator)

The results reveal that the final value obtained for fractional conversion increases for higher temperatures. In fact, for the lowest temperature investigated, fractional conversion obtained is clearly inadequate because it is far below total conversion. On the opposite, it is clear that for the higher temperature value ($T= 160\text{ }^{\circ}\text{C}$) the fractional conversion achieved is very satisfactory, getting closer to one.

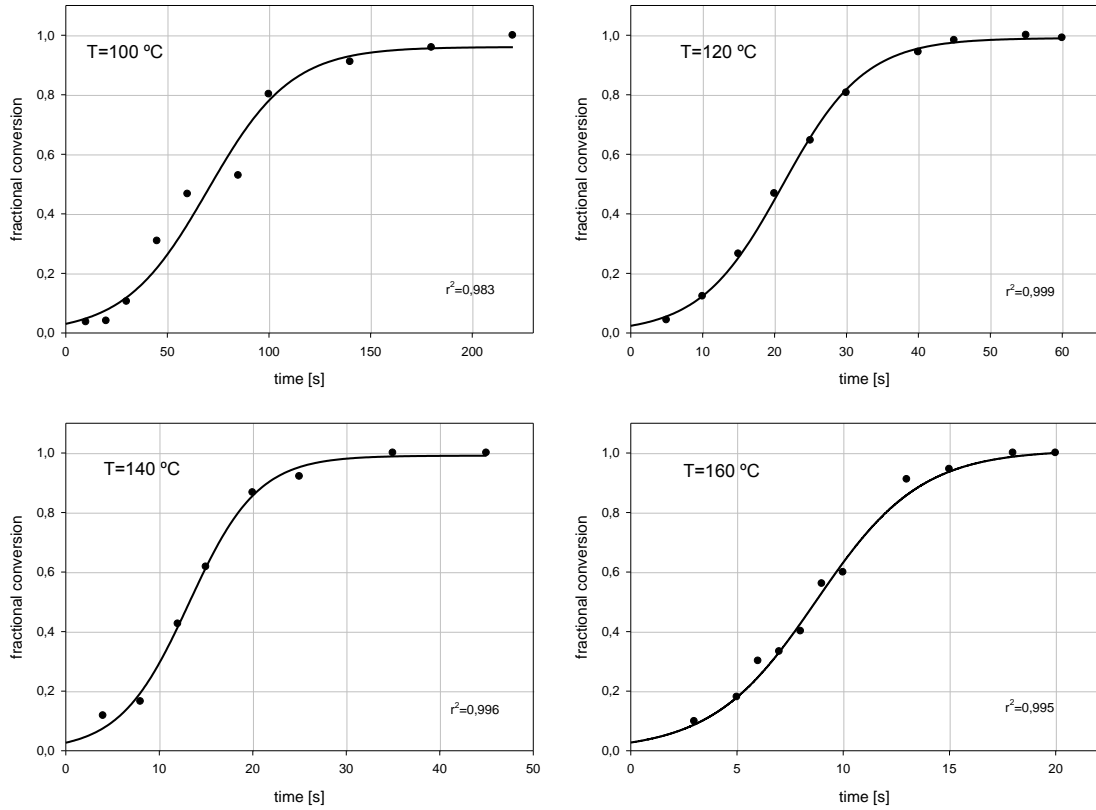


Figure 4.3 – Case I: variation of the fractional conversion versus heating time for different isothermal temperatures (3% wt of thermal-initiator)

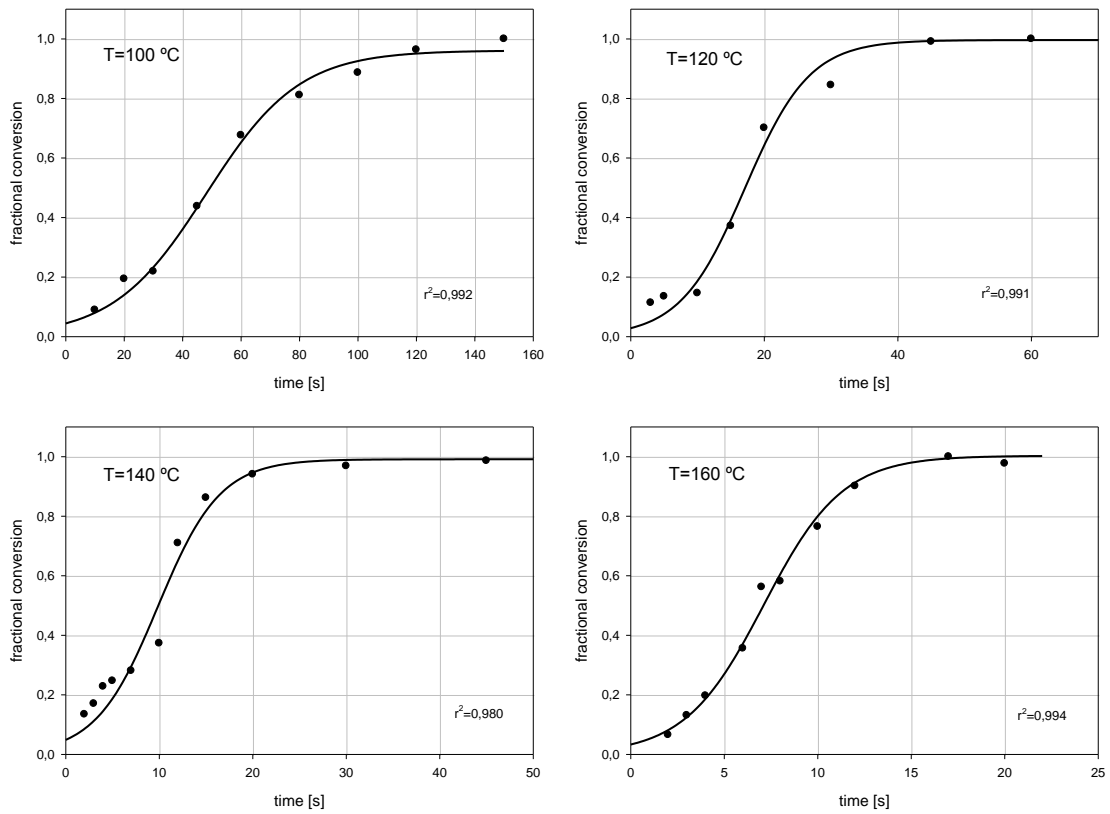


Figure 4.4 – Case I: variation of the fractional conversion versus heating time for different isothermal temperatures (6% wt of thermal-initiator)

The presented results also show that increasing temperature and concentration of initiator increases the speed of cure reaction, reduces the induction time and increase the percentage of cured material decreasing the need for post-curing operations. The results for higher values of initiator concentration point to a behaviour similar to the one previously described for the lowest value of initiator but diverse numerical values are achieved. This effect will be analysed in detail on the following section.

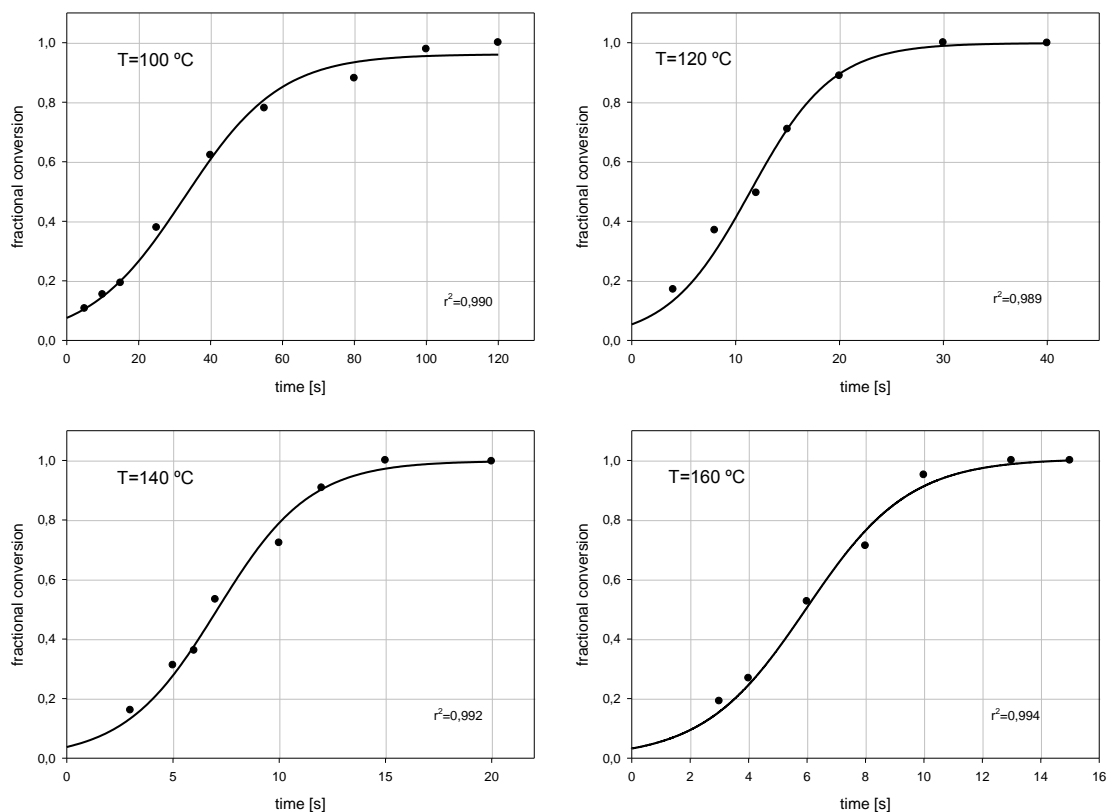


Figure 4.5 – Case I: variation of the fractional conversion versus heating time for different isothermal temperatures (9% wt of thermal-initiator)

The profile of the conversion rate versus time of cure for different temperatures and polymeric compositions used is shown in Figures 4.6 to 4.9, whereas the variation in conversion rate versus conversion fraction for the same parameters is shown in Figures 4.9 to 4.13. The results also show that increasing temperature and initiator concentration accelerates the reaction. The results show that above a certain value of curing temperature, the increasing of temperature does not have significant effects in terms of final conversion rate obtained. In fact, values near total conversion are achieved and this way there are no more reactive centres available to continue the reactions. In this case, there is not useful to increase the energy levels because it will not cause better final results and it will represent energy consumption.

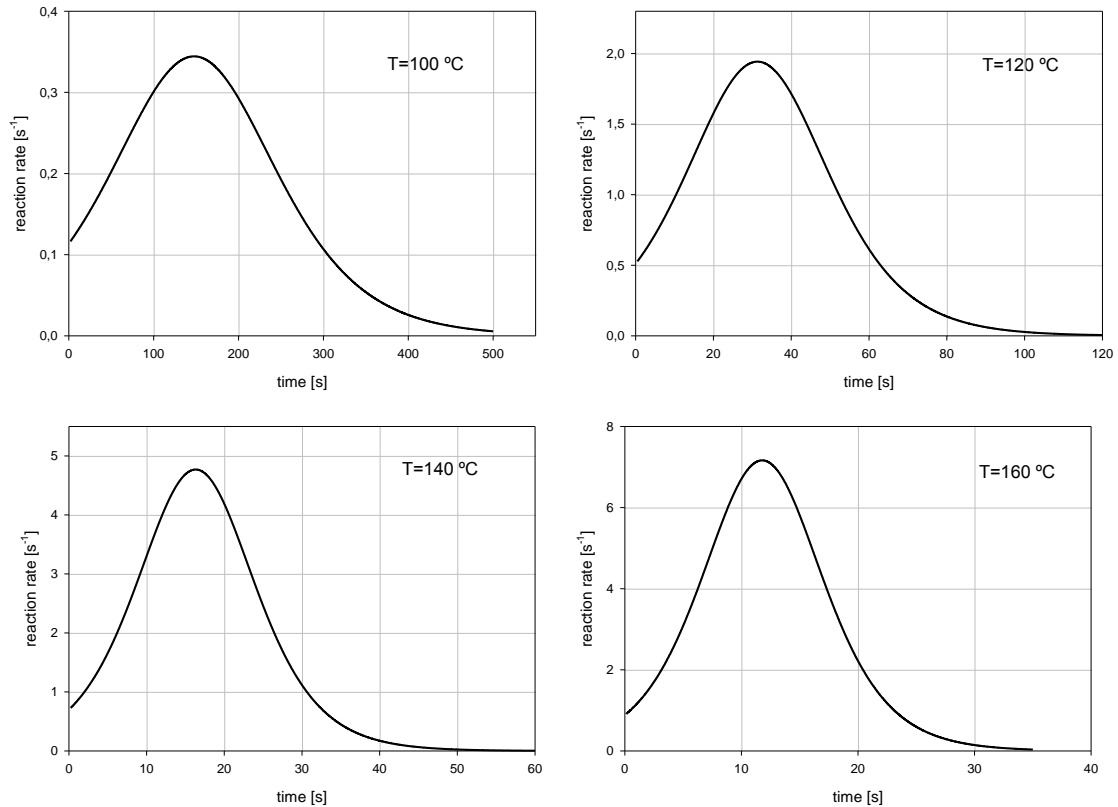


Figure 4.6 – Case I: variation of the reaction rate versus heating time for different isothermal temperatures (1% wt of thermal-initiator)

Analysing the results, it is notorious the initial induction time followed for a strong increase in the reaction rate, corresponding to the propagation stage. A peak value is attained and the reaction evidences a progressive deceleration, since there are less reactive species available, consumed during the previous period. Then, there is an abrupt and severe deceleration corresponding to the vitrification phenomenon period consequence of increased molecular weight and loss of mobility. Finally the reaction rate reaches zero, *i. e.*, the reaction stops.

The results also shown that higher peak values of reaction rate are achieved for higher temperatures, direct consequence of the presence of more energy in the system. It is also clear that those values are attained for shorter periods of time, in other words, the maximum value of reaction rate occurs earlier.

Once more, it should be mentioned that $t=0$ moment is not well defined due to the velocity of reactions and the procedure of this experimental technique.

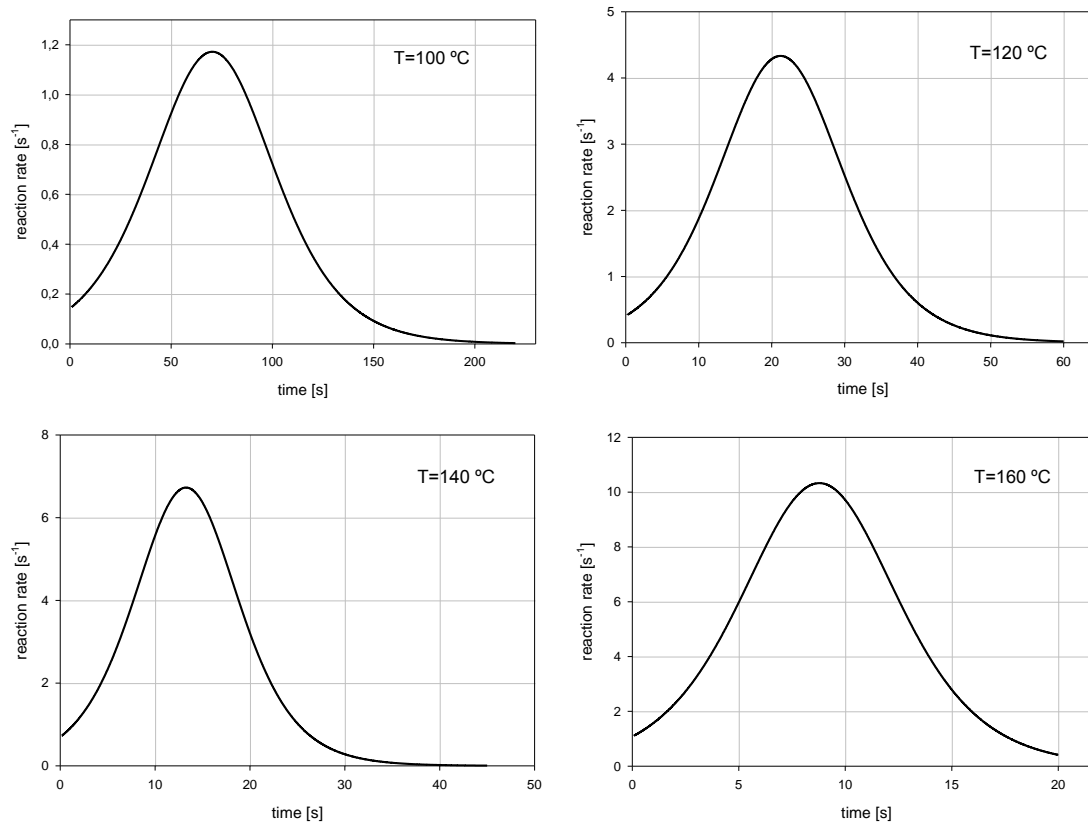


Figure 4.7 – Case I: variation of the reaction rate versus heating time for different isothermal temperatures (3% wt of thermal-initiator)

Similar behaviour was detected for 3% wt of thermal-initiator when compared with the previous case. However, the values involved are, in this case, more pronounced. In fact, higher values of peak reaction rates were achieved and the time consumed to reach those points was significantly reduced. The presence of more reactive centres, and therefore more active reactions, explains this fact. The induction time is reduced, and the propagation stage occurs with higher reaction rates since the number of initiated reactions is higher. Also, the vitrification phenomenon is attained earlier due to the consumption of reactive species and the decrease of chains mobility.

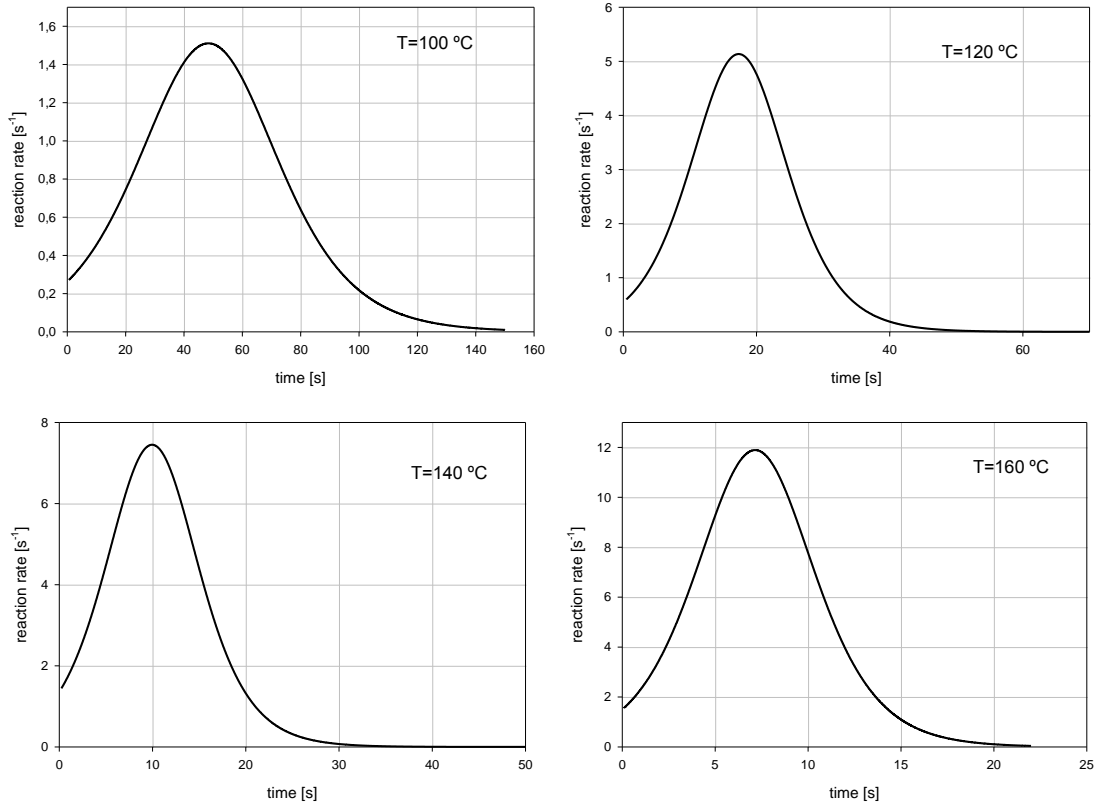


Figure 4.8 – Case I: variation of the reaction rate versus heating time for different isothermal temperatures (6% wt of thermal-initiator)

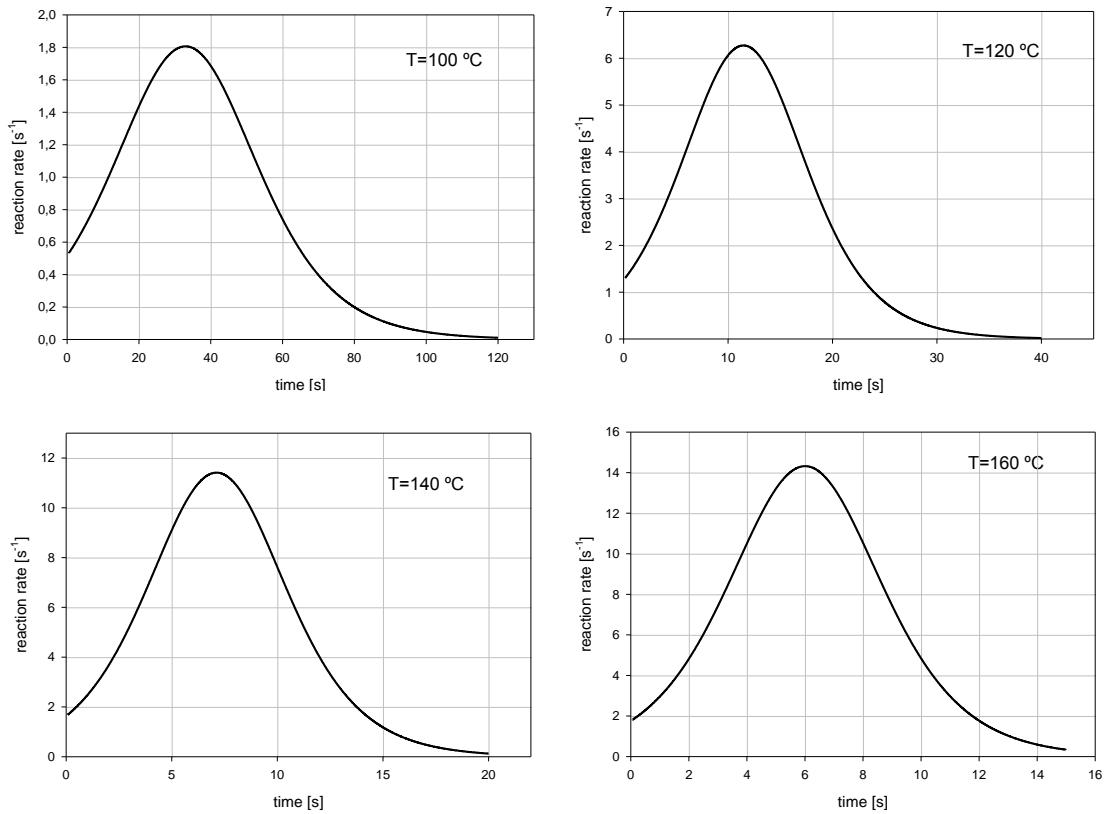


Figure 4.9 – Case I: variation of the reaction rate versus heating time for different isothermal temperatures (9% wt of thermal-initiator)

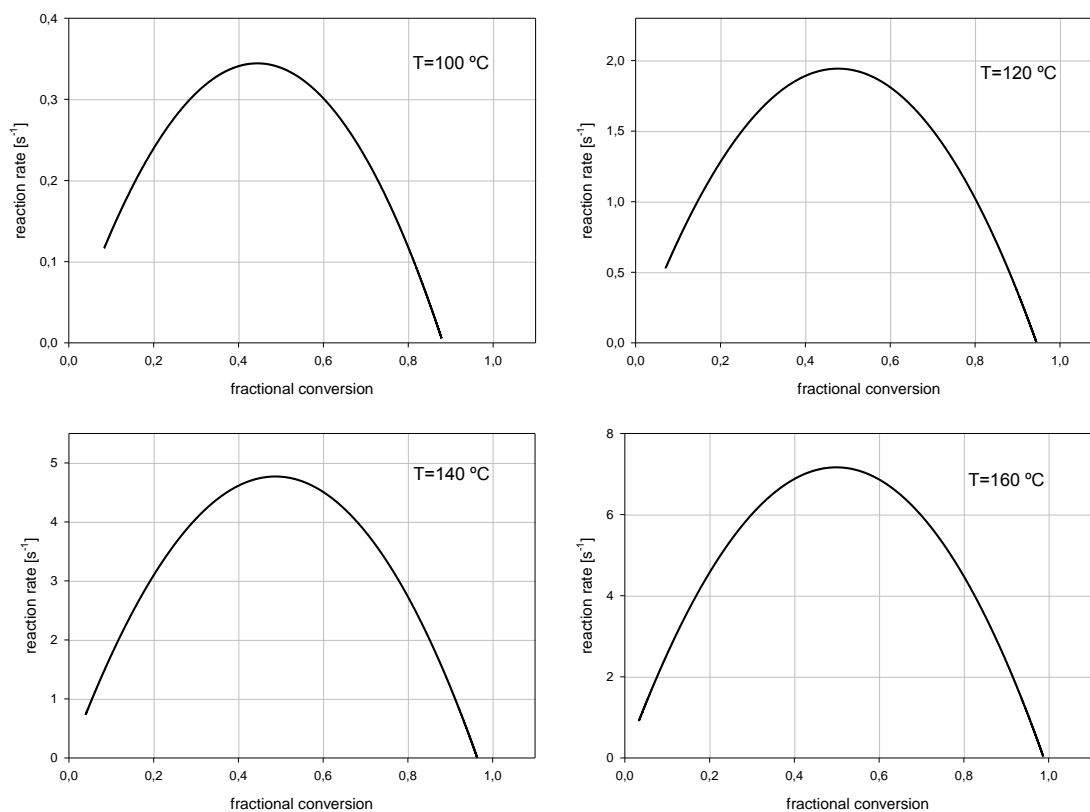


Figure 4.10 – Case I: variation of the reaction rate versus fractional conversion for different isothermal temperatures (1% wt of thermal-initiator)

In the presented results (Figure 4.10), it can be observed that during an initial period, the reaction rate significantly increases with the increasing of fractional conversion. Then, a maximum value is achieved, from which the opposite relation is detected. Two remarks must be done to the profile of graphics, once more $t=0$ moment is not well defined, and the maximum value is attained not in a sharp peak way but in a smoothed curve shape.

The described tendencies can be explained by the presence of reactive species available to the propagation of cure reactions. Initially, the abundance of reactive centres allows the reaction to happens quickly and progressively accelerated. Consequently, the fractional conversion grows and the initiator species are consumed. A balanced zone is reached where the effect of conversion starts to slow down the reaction. Then, the decrease of chains mobility and the consumption of reactive species has a predominant influence and the reaction rate starts to decline, increasingly sharply until the reaction stops.

It is notorious that higher values of maximum reaction rate are achieved for higher temperatures and also the accelerations and decelerations are more pronounced. Reaction rate starts to decrease at similar but increasing values of fractional conversion for higher values of temperature. These values vary between nearby 0,45 and 0,50 for temperatures, respectively of $100\text{ }^{\circ}\text{C}$ and $160\text{ }^{\circ}\text{C}$. Results also shown that, when the reactions stops (reaction rate equal to zero), increasingly higher values of fractional conversion were achieved for higher temperatures.

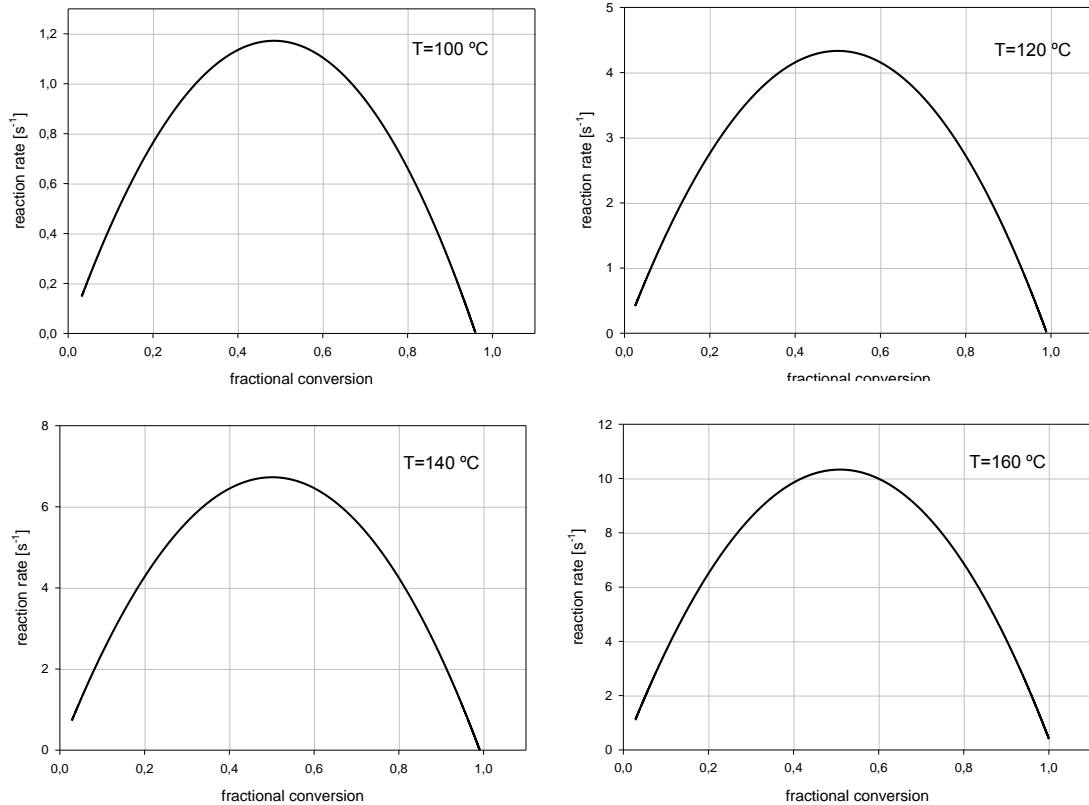


Figure 4.11 – Case I: variation of the reaction rate versus fractional conversion for different isothermal temperatures (3% wt of thermal-initiator)

With a higher value of initial thermal-initiator concentration it is verified that the maximum values of reaction rate as increased significantly. These values are attained for similar values of fractional conversion, in the vicinity of 0,50. Moreover, it can be seen that the reactions stop achieving higher values of fractional conversion. This fact can be explained with the presence of more reactive species and therefore more reactive spots. Although the effects of vitrification also being present, the existence of a larger number of reactive spots spread for larger areas of the resin reduces the outcome of the loss of mobility.

The reaction kinetics at different temperatures denotes similar behaviour to the one previously described for the other concentration of initiator. Furthermore, the effect of temperature will be discussed in detail forward in the current chapter.

Infrared Stereolithography

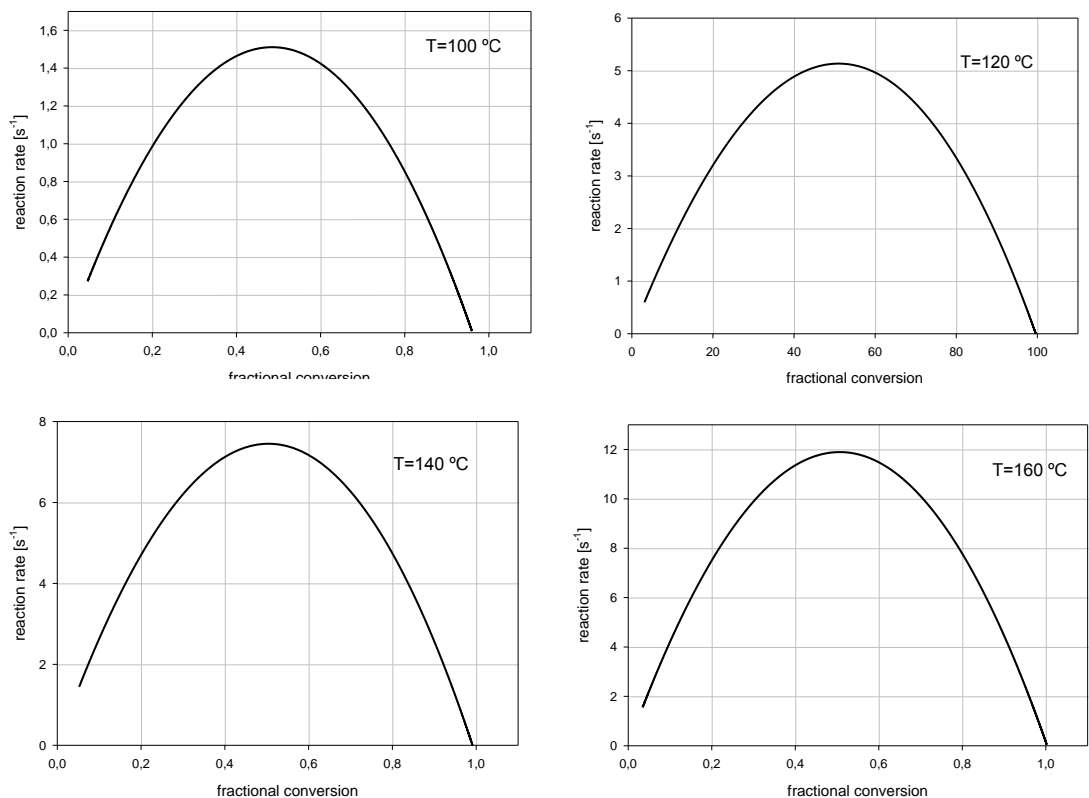


Figure 4.12 – Case I: variation of the reaction rate versus fractional conversion for different isothermal temperatures (6% wt of thermal-initiator)

98

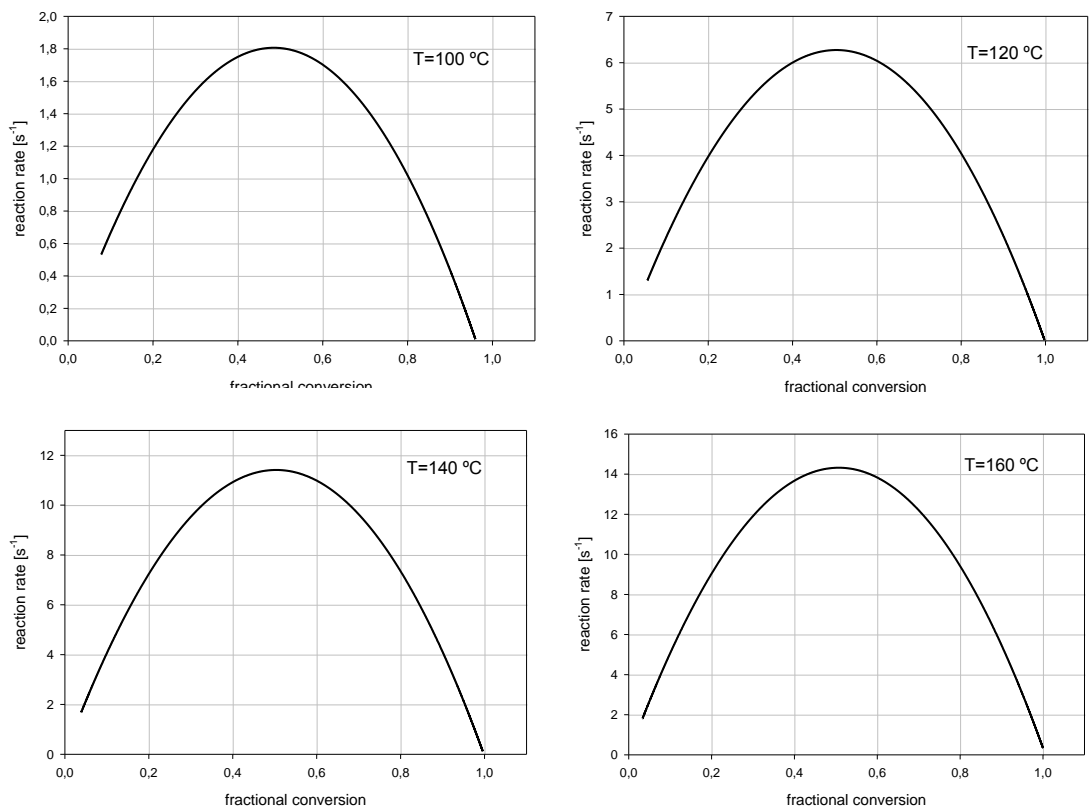


Figure 4.13 – Case I: variation of the reaction rate versus fractional conversion for different isothermal temperatures (9% wt of thermal-initiator)

Results obtained for fractional conversion and reaction rate for different conditions of temperature and initiator concentration used are compared in Figures 4.14 to 4.25. The results shown that increasing the concentration of initiator and temperature, accelerates the cure process allowing achieving higher values of maximum fractional conversion. Furthermore, the maximum conversion rate occurs for shorter curing times because polymerisation reaction is accelerated. Also, higher values of fractional conversion are achieved when using resins containing higher concentrations of initiator and submitted to higher curing temperatures.

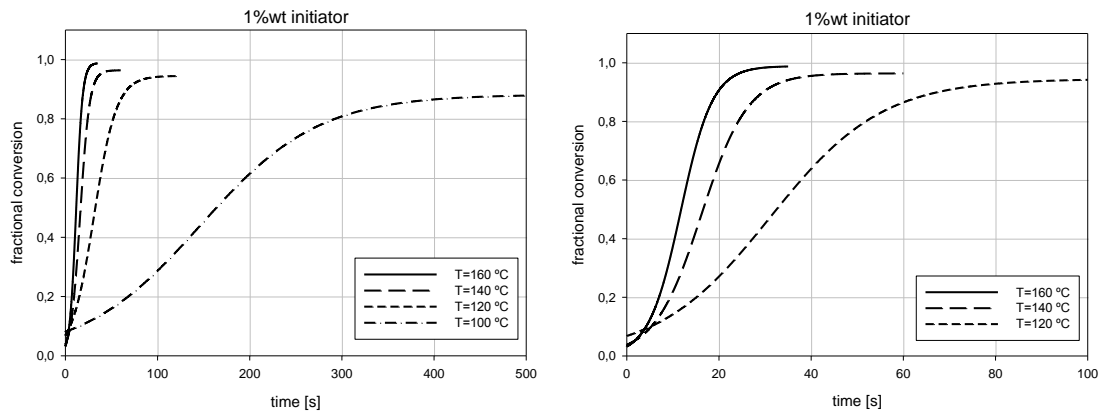


Figure 4.14 – Case I: variation of the fractional conversion versus heating time for different isothermal temperatures (1% wt of thermal-initiator)

Figure 4.14 denotes the effect of temperature on cure kinetics. Increasing the temperature strongly accelerates the reactions since more energy is supplied to the polymeric system. This effect is more accentuated for lower temperatures. In fact, the same increment for higher temperatures tends to influencing in a lesser extent the reactions due to the already existing high velocity of the reactions.

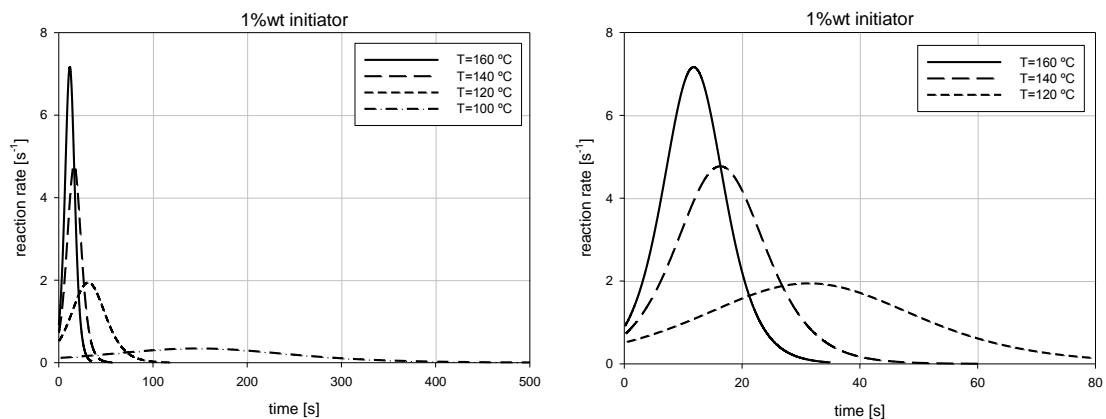


Figure 4.15 – Case I: variation of the reaction rate versus heating time for different isothermal temperatures (1% wt of thermal-initiator)

Results shown in Figure 4.15 demonstrate that the increase of temperature greatly accelerates the reaction, since higher values of reaction rate are attained for shorter periods of time. For higher temperatures, the same increment of temperature as a strong effect on peak value of

reaction rate but a more moderate influence in the absolute value of time necessary to reach that point. However, if the relative value is analysed, it is found that the decrement in time is almost halved. The absolute value of time to reach the peak value of reaction rate cannot be dramatically reduced because it is already a low value due the high velocity of the reaction.

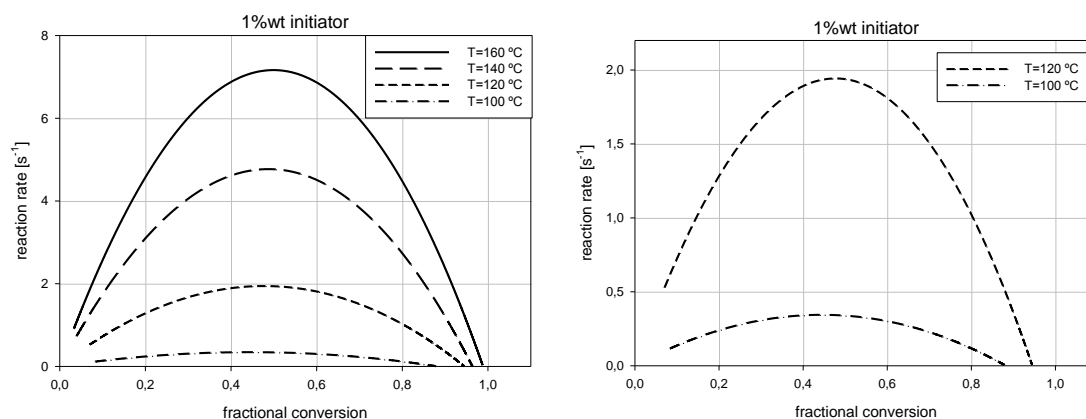


Figure 4.16 – Case I: variation of the fractional conversion versus reaction rate for different isothermal temperatures (1% wt of thermal-initiator)

Some major conclusions can be done by the analysis of Figure 4.16, where is stated the reaction rate versus fractional conversion for different temperatures. Firstly, as previously concluded, the increment of temperature has a strong effect on the reaction rate, strongly accelerating the reaction. Further, the maximum value of reaction rate is achieved for similar but slightly increasing fractional conversion values (between 0,45 and 0,50). In fact, this inversion point is reached sooner but is the consumption of reactive species and the decreasing of reactive chains mobility, expressed by the fractional conversion already achieved who determines the turning point where reaction starts to decelerate. Finally, the increase of temperature clearly benefits the final value of fractional conversion obtained, approaching to the perfect value of 1. For higher values of temperature, more energy is present in the polymeric system, with benefits in the mobility of the chains, and this way allowing the reactive centres to interact.

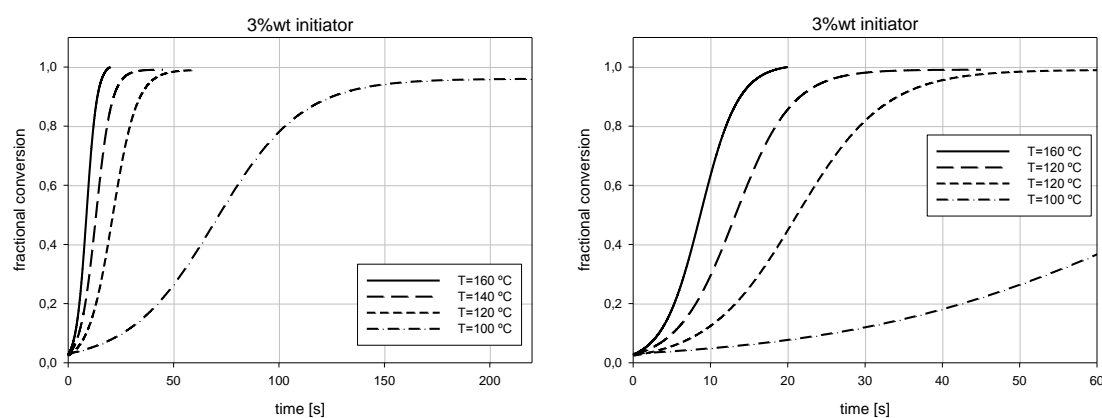


Figure 4.17 – Case I: variation of the fractional conversion versus heating time for different isothermal temperatures (3% wt of thermal-initiator)

Once more the increase of temperature, using 3% in weight of thermal initiator, has a strong effect on cure kinetics accelerating the reaction (Figure 4.17). Clearly separated curves were obtained, and despite of similar final values of fractional conversion, the time consumed to reach those values was noticeably shortened. All the stages of reaction were accelerated, starting with a clear reduction of induction time and assuming special prominence the effect on propagation stage denoted by the increasing angle of the curve. Also in the final stage of reaction, the effect of vitrification is more pronounced and abrupt due to higher extension of reaction already achieved.

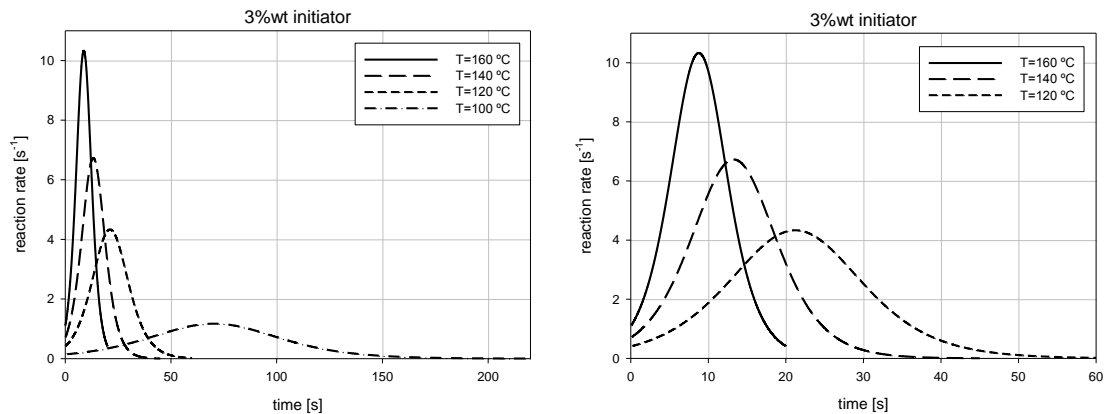


Figure 4.18 – Case I: variation of the reaction rate versus heating time for different isothermal temperatures (3% wt of thermal-initiator)

Progressively higher peaks of reaction rate are attained in consequence of higher levels of energy available (Figure 4.18). The time consumed to reach those peaks is significantly reduced in accordance with the previously stated acceleration of propagation stage. It is during this stage that the peak value occurs, and the beginning of deceleration is due to consumption of reactive species. Only later the loss of mobility of the polymeric chains will apply its influence.

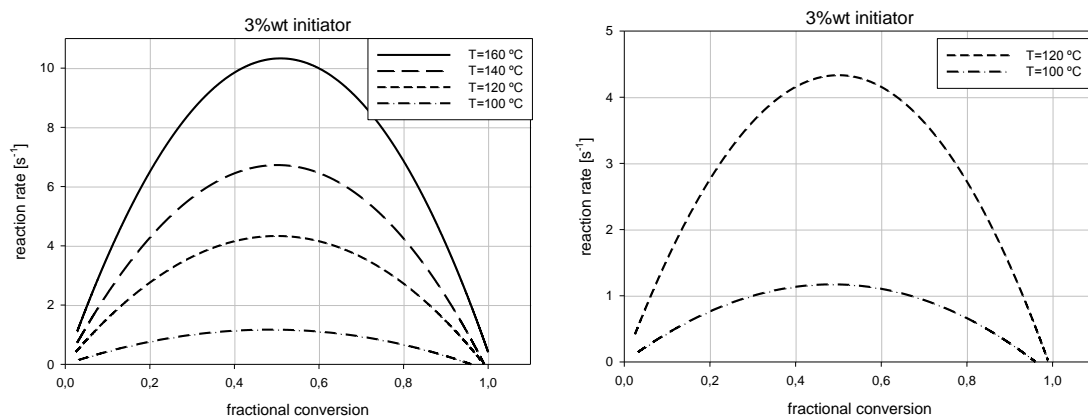


Figure 4.19 – Case I: variation of the fractional conversion versus reaction rate for different isothermal temperatures (3% wt of thermal-initiator)

Reaction rate versus fractional conversion is progressively higher with the increase of temperature (Figure 4.19). The highest values of reaction rate are achieved for similar values or

fractional conversion, around 0.5, almost independently of the temperature value. Therefore, the temperature has a strong effect in the value of reaction rate attained; however, the maximum value is reached for similar values of fractional conversion without visible dependence on temperature. The deceleration of the reaction is related with the extent of reaction, and therefore occurs as a consequence of the consumption of reactive species.

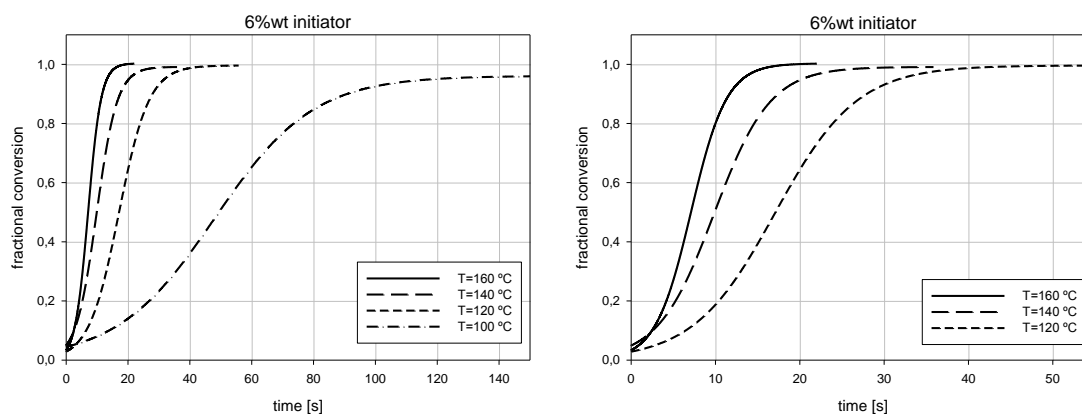


Figure 4.20 – Case I: variation of the fractional conversion versus heating time for different isothermal temperatures (6% wt of thermal-initiator)

Figure 4.20 shows a marked influence of temperature on the cure kinetics of a resin containing 6% in weight of thermal initiator. The effect is more pronounced at lower temperatures since the presence of lower level of energy does not enable a strong opposition to the effect of vitrification, which thereby leads to fractional conversion below 1. For higher temperatures, the reaction is accelerated but the final values of fractional conversion are not strongly affected since almost total conversion is attained. In those cases, the energy is sufficient to promote the mobility of the polymeric chains and to enable the reaction occurs in such way that the initiator can be activated and almost all the material solidifies.

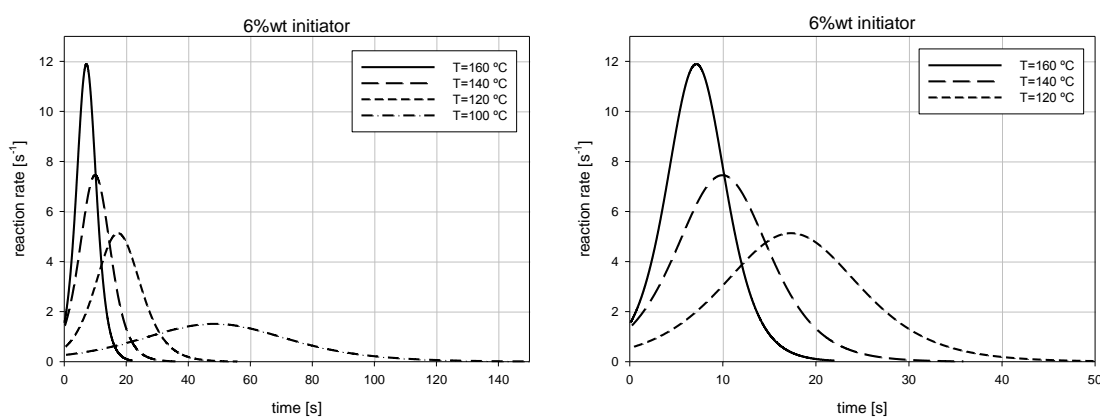


Figure 4.21 – Case I: variation of the reaction rate versus heating time for different isothermal temperatures (6% wt of thermal-initiator)

The temperature increases significantly the values of reaction rate obtained (Figure 4.21). The peak value is more pronounced and the curve is sharper in the vicinity, in other words, the

transition between acceleration, peak value, and deceleration of reaction rate is more abrupt than in previous cases.

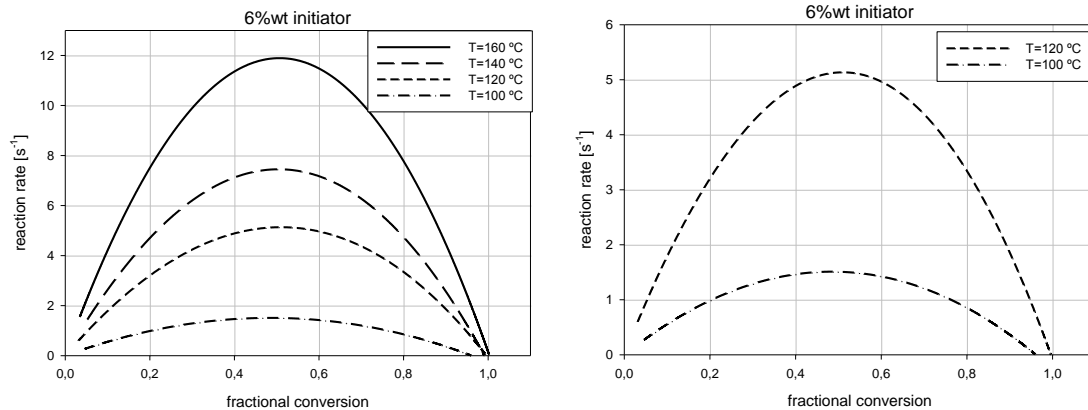


Figure 4.22 – Case I: variation of the fractional conversion versus reaction rate for different isothermal temperatures (6% wt of thermal-initiator)

According to the previous cases, the temperature has a clear influence on the value of the reaction rate but does not affect significantly the value of the fractional conversion from which the reaction begins to decelerate (Figure 4.22). This inversion point is verified slightly above 0.5.

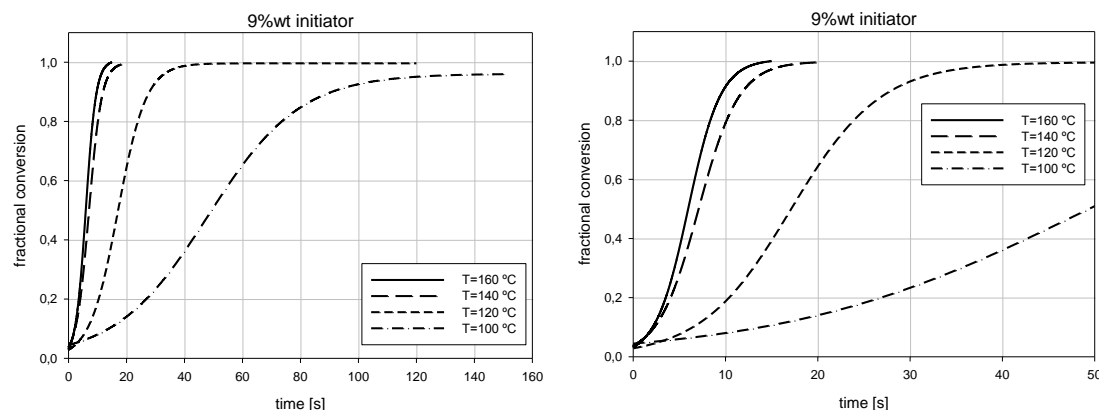


Figure 4.23 – Case I: variation of the fractional conversion versus heating time for different isothermal temperatures (9% wt of thermal-initiator)

Resin compositions containing 9% in weight of thermal initiator were also investigated (Figure 4.23). Despite of the large amount of initiator present in the resin, for the lower temperature ($T=100\text{ }^{\circ}\text{C}$) was not obtained total conversion. In fact, the energy was not enough to promote mobility of reactive chains in opposition to the higher viscosity of the resin and the vitrification effect during polymerisation.

The increase of temperature highly accelerate the reaction and leads to total conversion since energy levels become sufficient to ensure that initiator is activated and reactive spots can continue to react. For the higher values of temperature, the effect is less evident once the reaction is already quite fast. Thus, the increase of temperature, which means more energy

supplied to the process, does not result in a significant benefit in terms of reaction time or fractional conversion obtained.

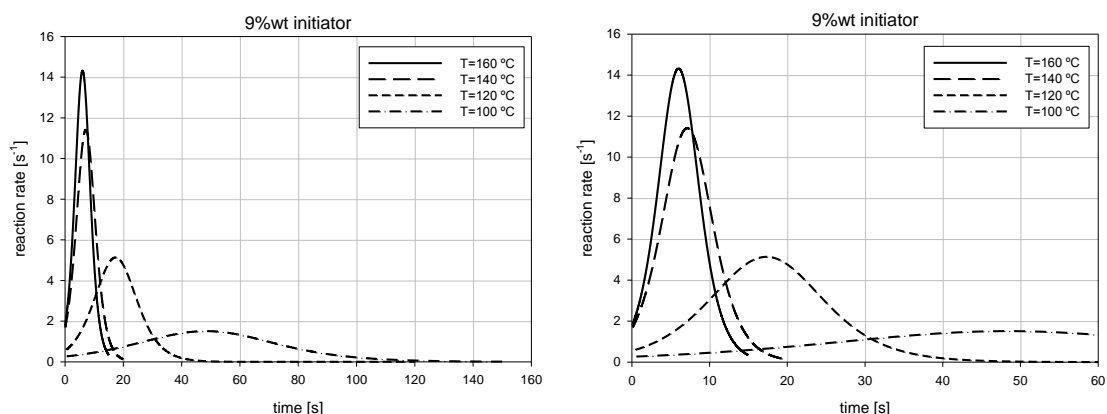


Figure 4.24 – Case I: variation of the reaction rate versus heating time for different isothermal temperatures (9% wt of thermal-initiator)

Figure 4.24 shows that higher values of reaction rate are attained when higher temperatures are used, and those peak values occur sooner and more sharpened due to the high value of reaction rate. Above T=140 °C, the increase in reaction rate is less significant since already high values are obtained. Also the time necessary to reach the peak value is just slightly reduced.

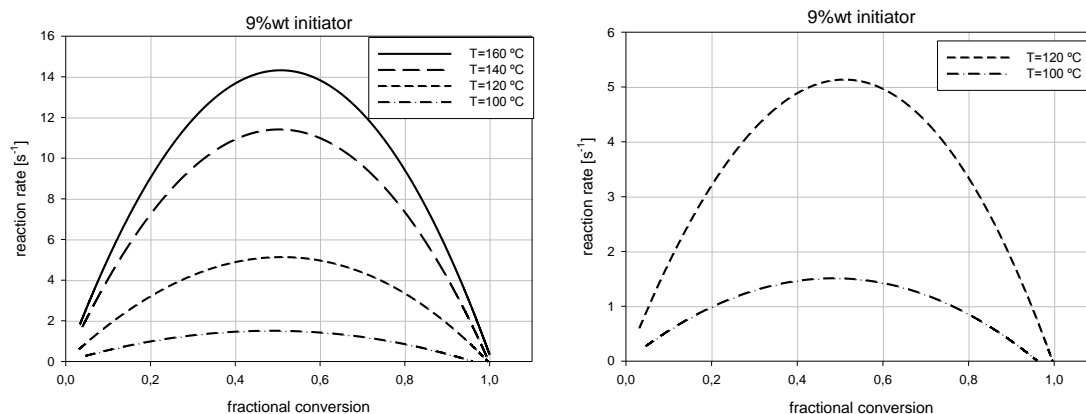


Figure 4.25 – Case I: variation of the fractional conversion versus reaction rate for different isothermal temperatures (9% wt of thermal-initiator)

The reaction rate versus fractional conversion increases with the temperature more substantially for lower values of temperature (Figure 4.25). For higher values of temperature, the same increment of temperature has a more attenuated effect because already very high values are attained. Once more, the value of the fractional conversion from which the reaction begins to decelerate is practically unaffected by temperature, registering values near 0.5.

To evaluate the effect of curing temperature, different concentrations of thermal initiator were investigated and the results were analysed and explained individually for each case. Similar

behaviours were detected from the point of view discussed. The effect of initiator concentration on the cure kinetics is analysed in detail in the next section.

4.2.2.2 - Case II: the effect of initiator concentration

Results obtained for different amounts of thermal-initiator concentration are presented in Figures 4.26 to 4.37. Likewise the previous case, the $t=0$ moment is not well defined due to the velocity of reactions and to the experimental technique used.

Obtained results shown that, for the same temperature, the reaction is faster for higher values of thermal-initiator concentration (see Figure 4.26). The induction time is reduced since there are more reactive centres available to start the polymerisation reaction. Therefore, more reactions were started and more thermo-sensitive species are available to the evolution of the polymeric chains, consequently the propagation stage is in advance and faster for higher values of thermal-initiator concentration. Hence, the vitrification occurs sooner for higher initiator concentrations as a result of consumption of initiator species and decreasing mobility of polymeric chains. Although all stages of polymerisation reactions occur sooner and faster, the effect of the initiator concentration in the fractional conversion obtained is evident for lower percentages of initiator but not so obvious for higher amounts. In that case, there is a slightly increase due to near 1 values are already achieved.

Since initiator species are thermo-sensitive and heat source was not irradiation, but rather isothermal chamber, shadows effects were not detected, *i.e.* the heat energy could reach the inside zones of resin without being blocked by more external initiator species. This way, fractional conversion has not decreased for high values of initiator, as is often the case for irradiated samples. Thus, there are evident benefits for increasing the percentage in weight of thermal-initiator from 1% wt to 3% wt, but for higher values, the increase yields irrelevant gains in terms of fractional conversion.

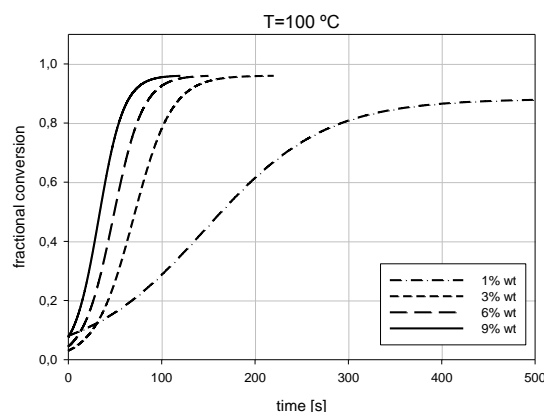


Figure 4.26 – Case II: variation of the fractional conversion versus heating time for different initial concentrations of initiator (temperature of 100 °C)

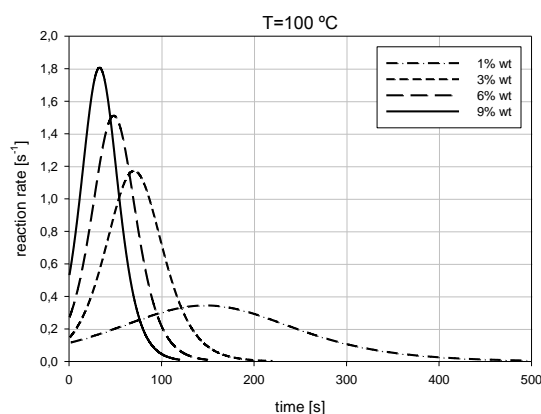


Figure 4.27 – Case II: variation of the reaction rate versus heating time for different initial concentrations of initiator (temperature of 100 °C)

Figure 4.27 presents the results obtained for reaction rate versus curing time for several samples with different compositions submitted to an isothermal temperature of 100 °C. Results shown that reaction rate is highly dependent of initiator concentration present in the sample. In fact, the reaction rate begins to rise sooner and more sharply for higher values of initiator concentration due the presence of more reactive centers. A more accentuated effect is detected for increments at lower values of initiator concentration, but unlike the previously effect described for fractional conversion, for higher values there is also a significant increase in the reaction rate.

The peak value of reaction rate is higher and is attained sooner for higher percentages of initiator. This point occurs when propagation stage ends and vitrification phenomenon starts to occur. Then reaction slows down due to consumption of reactive species and to loss of mobility of polymeric chains. More reactive centers were present for higher values of initial concentration but due to the higher reaction rate they were consumed sooner, anticipating the time of peak value.

At final stages, the deceleration smooth up until finally stops. This happens later for lower values of initial concentration of initiator, reflecting the fact of the reaction rate being substantially lower in this case. Despite of, initially there were fewer reactive species, they were consumed more slowly due to reaction rate and this way they were present in the polymeric compound until later.

Figure 4.28 shown the reaction rate versus fractional conversion for different resin compositions submitted to an isothermal temperature ($T= 100\text{ }^{\circ}\text{C}$). Once more, it is obvious that for smaller percentages of initiator the effect of this parameter in reaction kinetics is stronger. The presence of more initiator species (in weight percentage) originates further polymerisation reactions to start and consequently propagate with direct consequences in the reaction rate.

The maximum value of reaction rate increases with initial percentage of initiator. In fact, increasingly high values are attained although the impact of this parameter is progressively

attenuated for higher values. The reaction continues to be accelerated, however for lower amounts of initiator, smaller increments lead to larger increases in the reaction rate.

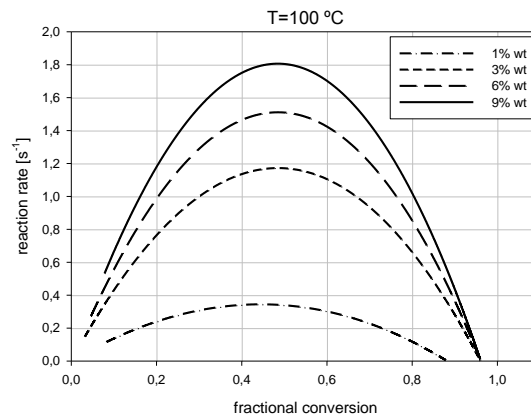


Figure 4.28 – Case II: variation of the reaction rate versus fractional conversion for different initial concentrations of initiator (temperature of 100 °C)

Although the maximum value of reaction rate increases with the concentration of initiator, were detected slight variations to the point where it happens. This point slightly increases from a value of fractional conversion around 0,45 (for 1 %wt of initiator) to values near 0,50 for the remaining cases. This demonstrates the dependence of the reaction rate relatively to the fractional conversion, due to vitrification phenomenon by loss of mobility of the polymeric chains.

Figure 4.28 also show that the final value of fractional conversion obtained increase with the concentration of initiator. However, above 3 %wt of initiator, and despite the presence of more reactive spots dispersed in the resin, the thermal energy existent in the system is not enough to promote the mobility of polymeric chains. This way, the effect of vitrification prevails leading to final results for fractional conversion around 0.96.

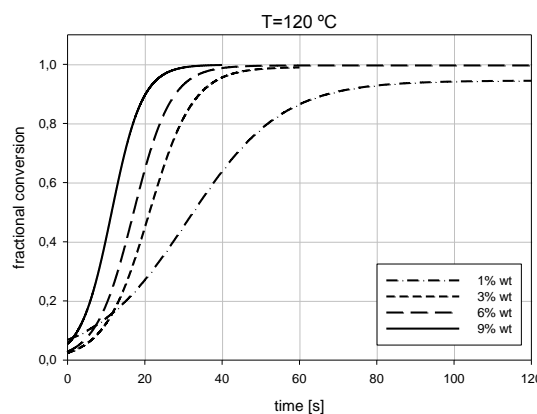


Figure 4.29 – Case II: variation of the fractional conversion versus heating time for different initial concentrations of initiator (temperature of 120 °C)

For isothermal conditions with $T = 120\text{ °C}$, total conversion was achieved for the larger concentrations of initiator (Figure 4.29). In fact, only for 1 %wt of initiator was not obtained total

conversion due to the lower number of reactive spots present in the resin. The advantage of using more than 3 %wt of initiator was mainly verified on the time spent during the polymerisation reaction. The reaction is faster, particularly in the induction time which is significantly reduced due to the presence of more initiator dispersed in the resin. Also the propagation of reaction is accelerated because more polymeric chains are reacting. Consequently, the vitrification is anticipated, but the presence of enough amounts of reactive species and energy level lead to a fractional conversion value of practically 1.

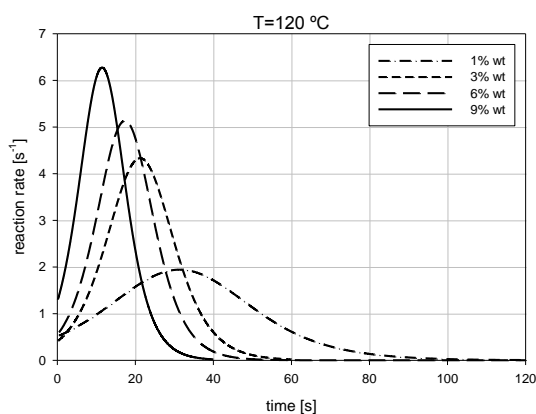


Figure 4.30 – Case II: variation of the reaction rate versus heating time for different initial concentrations of initiator (temperature of 120 °C)

With the increase of thermal initiator concentration, the reaction becomes faster. Not only the induction time is shortened, anticipating the raise of reaction rate, but also higher values of reaction rate are attained in shorter periods of time (Figure 4.30). This effect is more evident for lower concentrations of initiator.

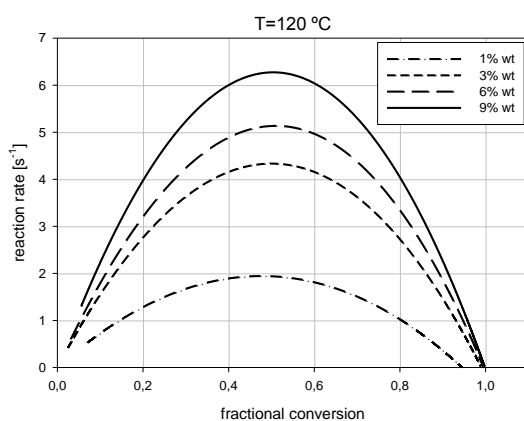


Figure 4.31 – Case II: variation of the reaction rate versus fractional conversion for different initial concentrations of initiator (temperature of 120 °C)

Reaction rate versus fractional conversion increases with the concentration of initiator in accordance with the previous analyses. The maximum value obtained is progressively superior and occurs for fractional conversion of approximately 0.45 for 1 %wt of initiator and 0.5 for the remaining concentrations (Figure 4.31).

The results also show that the final value of fractional conversion obtained increase with the initiator concentration (Figure 4.31). However for higher values of initiator concentration, fractional conversion slightly increases since values near to 1 are already achieved. This is due to the large amount of initiator present in the resin, allowing the existence of several reactive centres widely dispersed, and thus the polymerisation can occur without great mobility of the polymeric chains.

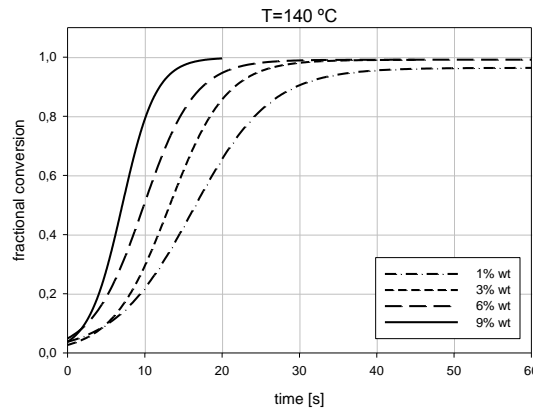


Figure 4.32 – Case II: variation of the fractional conversion versus heating time for different initial concentrations of initiator (temperature of 140 °C)

For higher values of temperature ($T= 140\text{ °C}$) the effect of the concentration of initiator is more progressive and constant than in previous cases (Figure 4.32). It is noticeable that the curves are more equidistant, which leads to the conclusion that the energy level is high enough to oppose to the vitrification phenomena. Thus, the presence of more reactive species has direct correspondence in reaction rate since there are more reactive spots occurring simultaneously. At the same time, there is enough energy present to promote the mobility of the polymeric chains and delay and reduce the effects of vitrification. Almost total conversion is achieved except for lower concentrations of initiator (1 %wt).

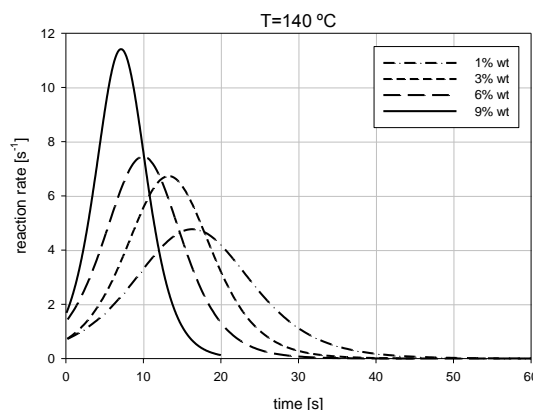


Figure 4.33 – Case II: variation of the reaction rate versus heating time for different initial concentrations of initiator (temperature of 140 °C)

Reaction rate is progressively higher and its peak value occurs sooner for higher values of initiator concentration (Figure 4.33). There is a marked difference for the higher concentration of initiator (9 %wt). The combination of two factors contributed to this, the presence of large amounts of initiator and the adequate level of energy to activate them and promote the polymerisation. The so high value of reaction rate leads to the fast consumption of reactive components and along with the level of conversion already obtained explains the fact of the reaction starts to slowdown earlier for higher concentrations of initiator.

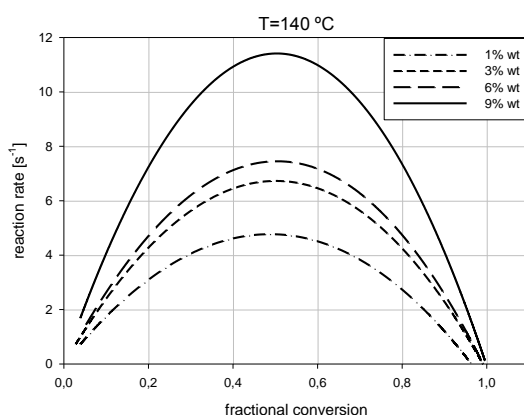


Figure 4.34 – Case II: variation of the reaction rate versus fractional conversion for different initial concentrations of initiator (temperature of 140 °C)

In the sequence of previous observations, also for the reaction rate versus fractional conversion is for the higher value (9 %wt) that the results denote more impact of the concentration of initiator (Figure 4.34). For all the concentrations, reaction rate starts to slow down at similar values of fractional conversion (approximately 0.50). For higher concentrations of initiator almost total conversion was achieved.

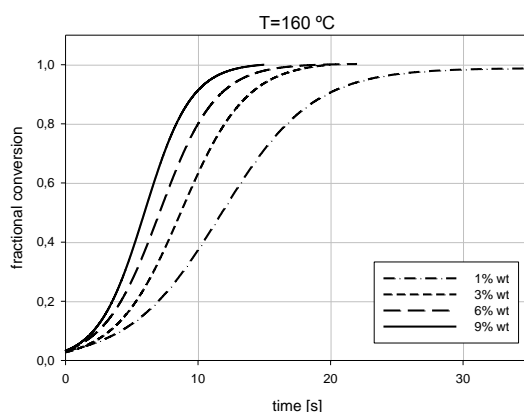


Figure 4.35 – Case II: variation of the fractional conversion versus heating time for different initial concentrations of initiator (temperature of 160 °C)

As can be deduced by the proximity of the curves, for high values of thermal energy ($T= 160\text{ °C}$) the effect of initiator concentration is gradual, accelerating the reaction of polymerisation (Figure 4.35). The induction time is slightly reduced, but in the propagation stage the effect is

more notorious, has can be saw on the slope of the corresponding curves. The vitrification phenomenon starts to be visible sooner due to the higher reaction rates however it happens for similar values of fractional conversion. Thus, the increase of viscosity due to higher values of initiator concentration is attenuated by the presence of high values of thermal energy promoting the mobility of polymeric chains. It is the increase of fractional conversion and the correspondent increase of viscosity that leads to the lack of mobility of polymeric chains and consequently to vitrification effects.

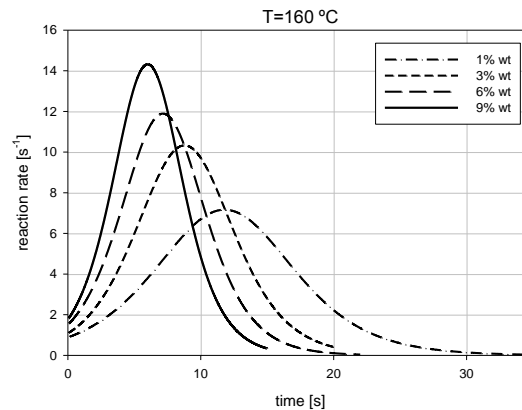


Figure 4.36 – Case II: variation of the reaction rate versus heating time for different initial concentrations of initiator (temperature of 160 °C)

Also for reaction rate versus curing time the effect of initiator concentration is relatively gradual (Figure 4.36). Progressively higher peaks of reaction rate are attained for shorter periods of time. Only for the lowest value of initiator concentration (1 %wt) the reaction rate increases and decreases smoothly owing to the presence of fewer reactive elements. For higher values of initiator concentration and also because of high energy value involved, the reaction rate increases more suddenly as a result of more reactive spots scattered by the resin. Then, the fast consumption of reactive elements along with the accentuated rise of fractional conversion originates a sharply decrease of reaction rate.

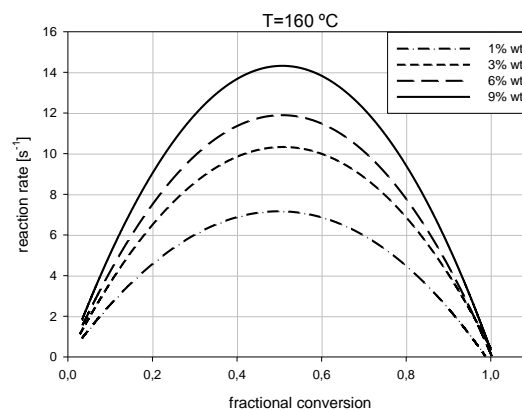


Figure 4.37 – Case II: variation of the fractional conversion versus heating time for different initial concentrations of initiator (temperature of 160 °C)

Progressively high values of reaction rate versus fractional conversion are attained for higher values of initiator concentration (Figure 4.37). However the maximum value for each case is obtained for similar values of fractional conversion. Total conversion was achieved owing to the presence of a high value of energy. Only for the lowest concentration of initiator the final value of fractional conversion was slightly below 1 because there were less reactive elements present in the resin.

4.2.3 - Vyazovkin model

Non-isothermal cure reactions were performed using the DSC apparatus Mettler Toledo Star^e system DSC823^e, equipped with a liquid Nitrogen cooling system, a TSO 800 GC1 Gas controller, and a Crucible Sealing Press (Figure 4.38). The system was controlled by the software Mettler Toledo Star^e Thermal Analysis System Version 9.01 and the results were analysed with the Model Free Kinetics from Mettler Toledo.

The software for analysis based on Vyazovkin model allows the prediction of the reaction rate and fractional conversion performing three dynamic measurements at different heating rates.



Figure 4.38 – Mettler Toledo Star^e system DSC823^e

The Vyazovkin model is based on two assumptions; the activation energy is not a constant, but constant only for a particular conversion; and the Arrhenius expression for the temperature dependence of the rate coefficient retain its validity [2, 3]:

$$\frac{d\alpha}{dt} = k_0 \cdot e^{\frac{-E(\alpha)}{R.T}} \cdot f(\alpha) \quad (4.1)$$

where $d\alpha/dt$ is the reaction rate, k_0 is the rate constant at infinite temperature, $f(\alpha)$ is the reaction model, $E(\alpha)$ is the activation energy as a function of the conversion, R is the universal gas constant, and T is the absolute temperature.

The so called iso-conversional methods are based on several measurements using different heating rates. The Model Free Kinetics (MFK) software (applying the Vyazovkin model), is a iso-conversional kinetic analysis that uses multiple dynamic DSC measurements, at least three, with different heating rates for making kinetic predictions and for exploring the mechanisms of thermally stimulated processes. It is based on evaluating a dependence of the effective activation energy (E) on conversion (α) or temperature. The MFK model is based on the temperature at a certain conversion, each conversion delivers a value of the activation energy, which is a function of the conversion and reflects complex reactions.

The equation (4.1) can be expressed by:

$$\frac{d\alpha}{dt} = k(T) \cdot f(\alpha) \quad (4.2)$$

Separating the variables of the equation and integrate with respect of time, a new integral function $g(\alpha)$ is obtained:

$$g(\alpha) = \int_0^\alpha \frac{1}{f(\alpha')} d\alpha' = \int_{t_0}^{t_\alpha} k dt \quad (4.3)$$

Introducing the Arrhenius equation and the definition equation of the heating rate β results:

$$g(\alpha) = \frac{k_0}{\beta} \underbrace{\int_0^{T_\alpha} \exp\left[-\frac{E(\alpha)}{RT}\right] dT}_{Integral I(E_\alpha, T_{\alpha, \beta i})} \quad (4.4)$$

$g(\alpha)$ is assumed to be heating rate independent.

Based on several experiments with different heating rates β_i the equation is solved numerically (Vyazovkin procedure) [4]:

$$g(\alpha) = \frac{k_0}{\beta_1} I(E_\alpha, T_{\alpha, \beta_1}) = \frac{k_0}{\beta_2} I(E_\alpha, T_{\alpha, \beta_2}) = \dots = \frac{k_0}{\beta_n} I(E_\alpha, T_{\alpha, \beta_n}) \quad (4.5)$$

4.2.3.1 - Results and discussion

A required amount of sample was weighted into a sample pan which was then sealed and placed in the DSC for each measurement. After each run the weight of the sample was determined again to check any weight loss due to evaporation of the styrene monomer. Dynamic scans from -10 °C to +250 °C were performed for each resin composition in the DSC using a nitrogen atmosphere and three different heating rates (5, 10 and 15 °C/min) recording three dynamic curves.

These curves were analysed using the model-free kinetics and the activation energy calculated as a function of the conversion. These data allow prediction of the conversion as a function of

the time at different temperatures or heating rates. Thus, it is possible to use the three dynamic measurements to predict the conversion as a function of time at different temperatures.

Four different amounts of percentage in weight of initiator were tested and the obtained results were as follow.

Figure 4.39 shows that for a certain amount of initiator, different conversions are obtained depending on the temperature. For lower temperatures ($T=80\text{ }^{\circ}\text{C}$) unsatisfactory values of fractional conversion were attained after 25 minutes of cure reaction. For values of fractional conversion under 0,5 a solid and a gel phases coexists corresponding to the generation of an incipient solid with low mechanical properties.

It is notorious that fractional conversion increases with temperature. The increase is more significant for lower temperatures, since induction time is significantly abbreviated. Therefore, propagation stage begins earlier and with progressively higher reaction rate for higher temperature. For temperatures of $120\text{ }^{\circ}\text{C}$ and above, fractional conversion increases more moderately due to vitrification phenomenon. The effect of higher thermal energy available is attenuated by the loss of mobility of polymeric chains due to increase of viscosity and consumption of reactive species. However, for this amount of initiator, the improvement on final value of fractional conversion clearly compensates the increase of energy provided.

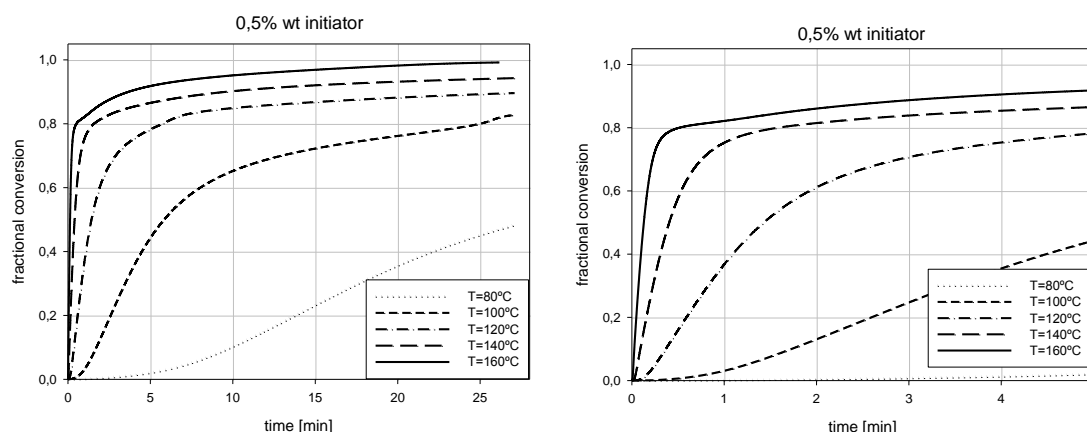


Figure 4.39 – Variation of the fractional conversion versus time for different temperatures (0,5% wt of thermal-initiator)

As shown in Figure 4.40, reaction rate increases with temperature and peak values are attained sooner for higher temperatures. Therefore, the reaction is accelerated since more thermal energy is present in the polymeric system to activate initiator species. The deceleration begins earlier because of vitrification phenomenon, as a result of the consumption of reactive elements and increase of fractional conversion.

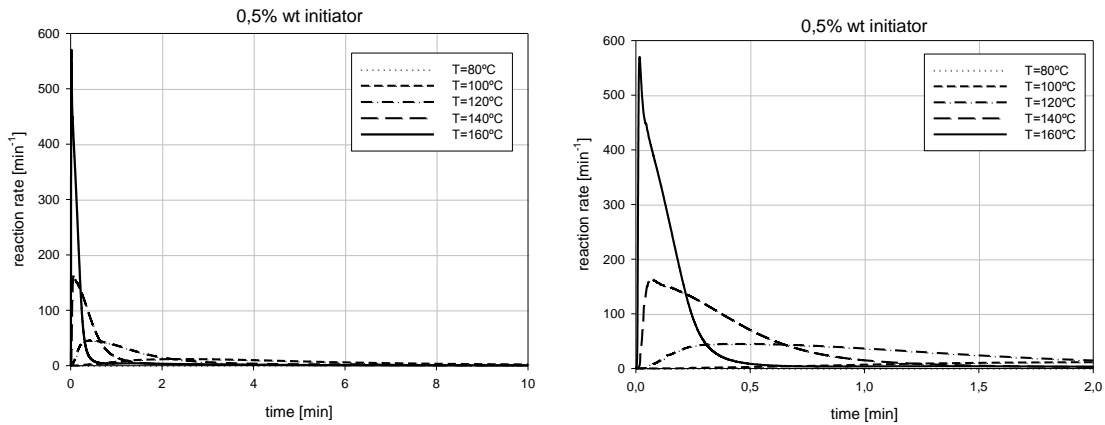


Figure 4.40 – Variation of the reaction rate versus time for different temperatures (0,5% wt of thermal-initiator)

Deceleration as a consequence of vitrification phenomenon is evident in Figure 4.41. For values of fractional conversion greater than 0.80 the deceleration becomes critical resulting in final values of fractional conversion far below 1 and consequently obtaining solids with poor mechanical properties and requiring post-cure operations.

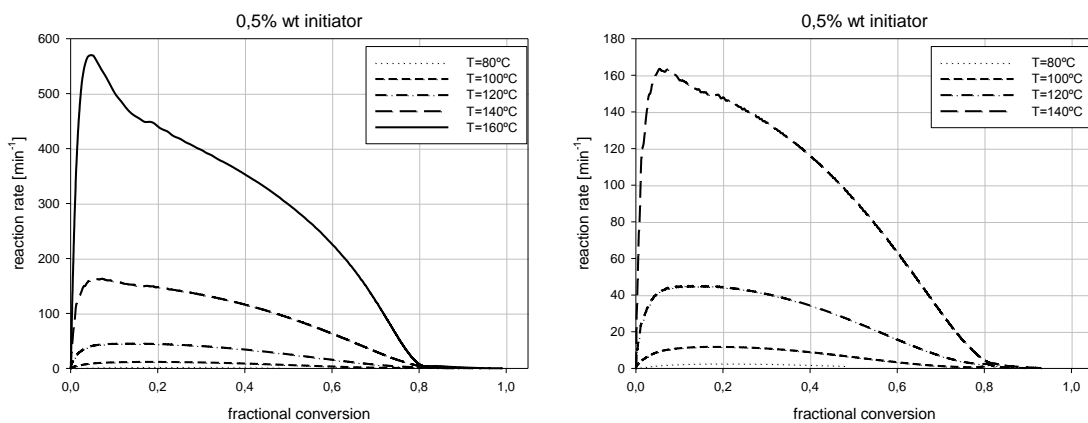


Figure 4.41 – Variation of the fractional conversion versus reaction rate for different temperatures (0,5% wt of thermal-initiator)

A lower peak value in activation energy versus fractional conversion is observed closer to 0.8 of fractional conversion (Figure 4.42). As previously stated, this is precisely the point at which the reaction decelerates significantly.

The analysis of iso-conversion curves shown in Figure 4.43 allow realizing that similar results can be obtained increasing temperature or exposure time. For this particular case of 0,5% in weight of thermal initiator, low values of fractional conversion were attained, clearly beneath total conversion. Hence, the highest iso-curve represented corresponds to 0.9 of fractional conversion.

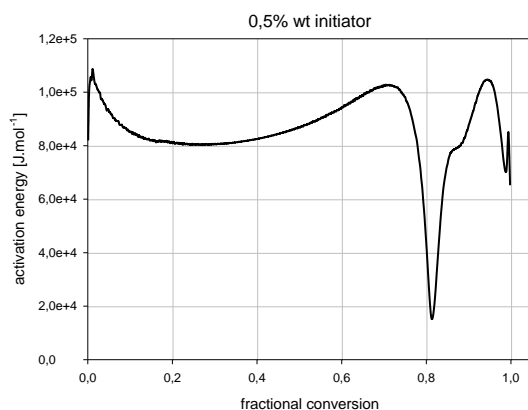


Figure 4.42 – Variation of the activation energy versus fractional conversion (0,5% wt of thermal-initiator)

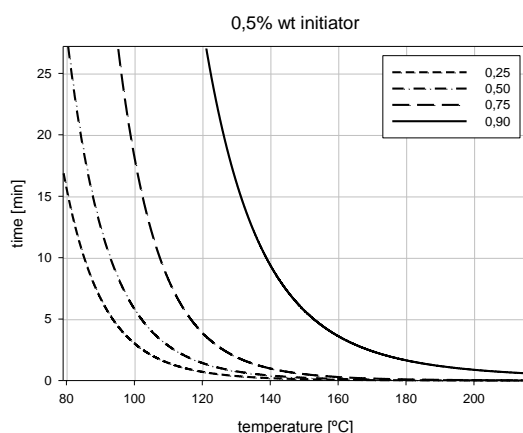


Figure 4.43 – Iso-conversion curves for time versus temperature (0,5% wt of thermal-initiator)

The results of fractional conversion using 1% in weight of initial concentration of initiator are shown in Figure 4.44. It can be observed that better results were attained for higher temperatures. The presence of higher levels of thermal energy has implications in the cure process, reducing the induction time and accelerating the propagation reaction. In this case, due to the presence of more reactive species, values near total conversion, were obtained for the highest temperature ($T=160\text{ }^{\circ}\text{C}$). Although the increment of fractional conversion for higher values of temperature, it is notorious that relatively smaller benefits are achieved when the temperatures involved are already high. Thus, when comparing temperatures of $140\text{ }^{\circ}\text{C}$ and $160\text{ }^{\circ}\text{C}$, there is a slight increase in the value of final fractional conversion, however the benefits are also reflected in the reaction rate. For those temperatures induction time was very short.

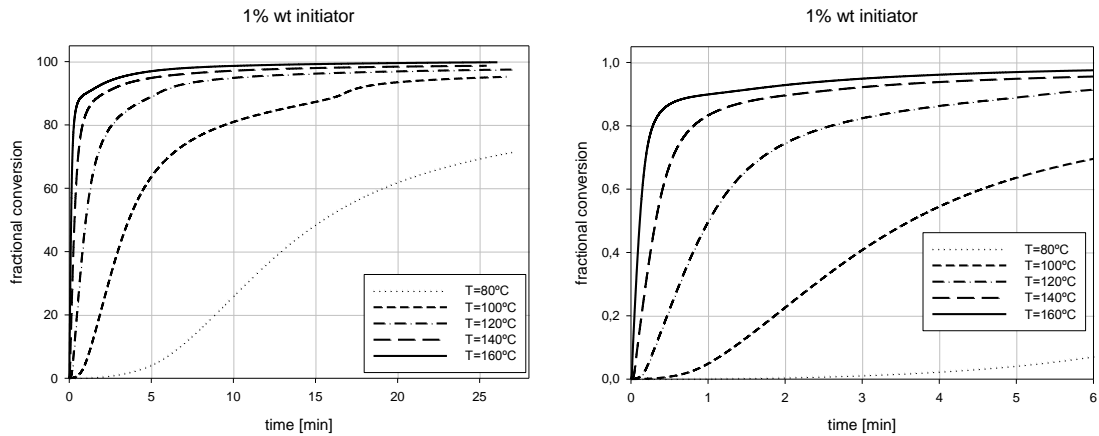


Figure 4.44 – Variation of the fractional conversion versus time for different temperatures (1% wt of thermal-initiator)

As shown in Figure 4.45, for higher temperatures, polymerisation reactions starts sooner denoting a shorter induction period. Also the propagation stage begins earlier and evolves more rapidly. Therefore, for those temperatures, the polymerisation reaction is very fast and the vitrification occurs in a short period of time as a consequence of the sharp increase in the fractional conversion.

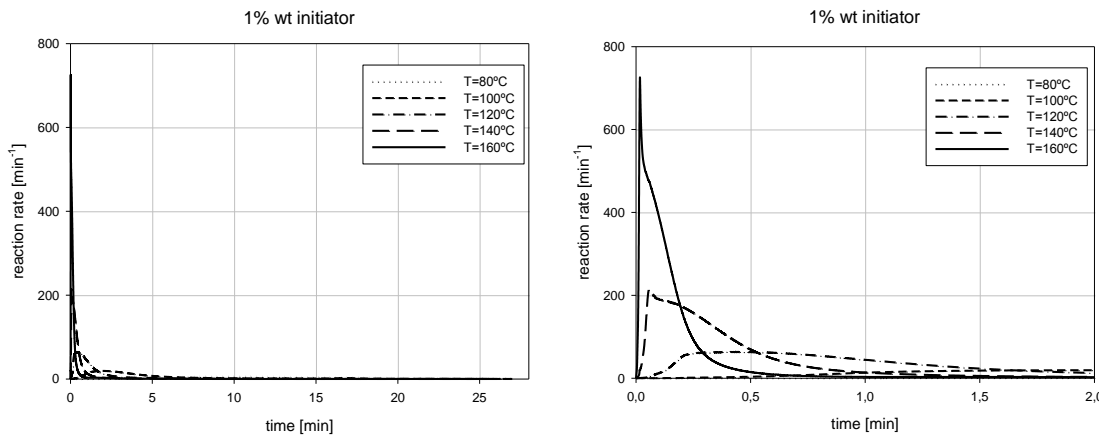


Figure 4.45 – Variation of the reaction rate versus time for different temperatures (1% wt of thermal-initiator)

As can be seen in Figure 4.46, vitrification phenomenon is more accentuated for values of fractional conversion near 0.9. However, despite of decelerating the reaction, polymerisation continues due to the existence of reactive centres available. Thereby, for the highest temperatures values closer to total conversion are achieved and therefore solids with good mechanical properties can be generated.

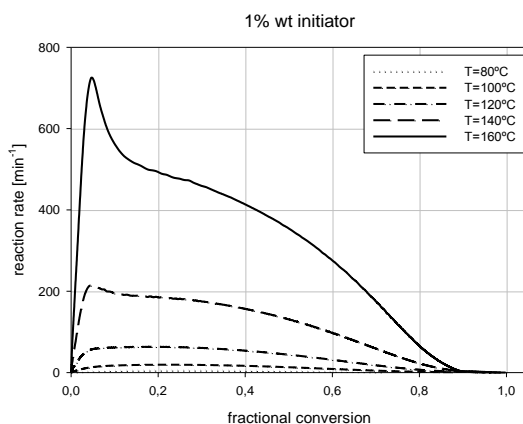


Figure 4.46 – Variation of the fractional conversion versus reaction rate for different temperatures (1% wt of thermal-initiator)

Analysed data is in accordance with the previously stated for different concentration of initiator. Curves shown in Figure 4.46 are approaching to zero at a convergence point with values of fractional conversion near 0.9. For this point, a lower peak value for activation energy is observed in Figure 4.47. When compared with previous case, a similar behaviour was detected.

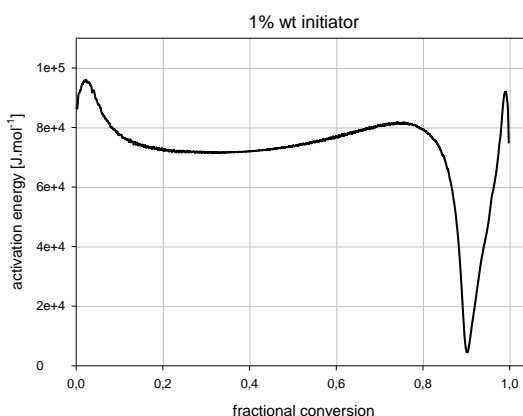


Figure 4.47 – Variation of the activation energy versus fractional conversion (1% wt of thermal-initiator)

The theoretical iso-conversion curves shown in Figure 4.48 reflect the effect of time and temperature over the final value of fractional conversion obtained. It is notorious that the curve for fractional conversion 1.0 is quite distant from the 0.9 curve, reflecting the fact that, above this value, the polymerisation reaction faces difficulties to propagate. Two major issues contribute to this situation. The lower amount of reactive species present in the resin, since they were already consumed in the process, and also the increase of viscosity of resin and consequently loss of mobility of the polymeric chains making difficult that those reactive centers are in the same zone. Therefore, vitrification phenomenon predominates at this stage of the process, and consequently more energy has to be supplied to the system, increasing the time of exposure or the temperature.

It can also be noted that similar results can be obtained either by increasing the exposure temperature or the curing time of the resin. An optimized solution must be found regarding

intended purposes for the solidified part since both parameters represents resources consumption.

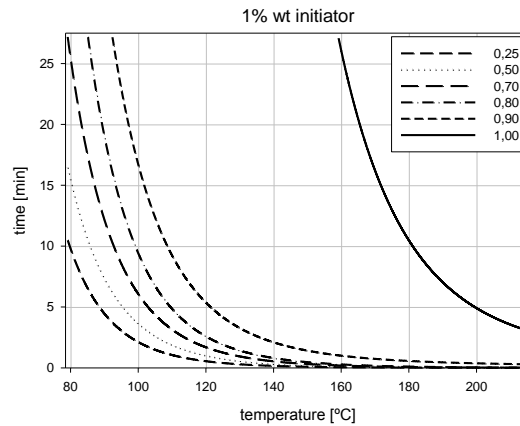


Figure 4.48 – Iso-conversion curves for time versus temperature (1% wt of thermal-initiator)

The results shown in Figure 4.49, with 2% in weight of thermal initiator, demonstrate a similar behaviour to the previously analysed with different amounts of initiator. For longer periods of time exposure, final conversion attained is almost total conversion since thermal energy exposure enables to maintain mobility of polymeric chains, and thereby counteract the effects of vitrification.

Although temperature accelerates reaction, reducing induction time and increasing reaction rate, after a certain period of time effects for higher temperatures are smoothed. Likewise, induction time cannot be shortened since it is already very low.

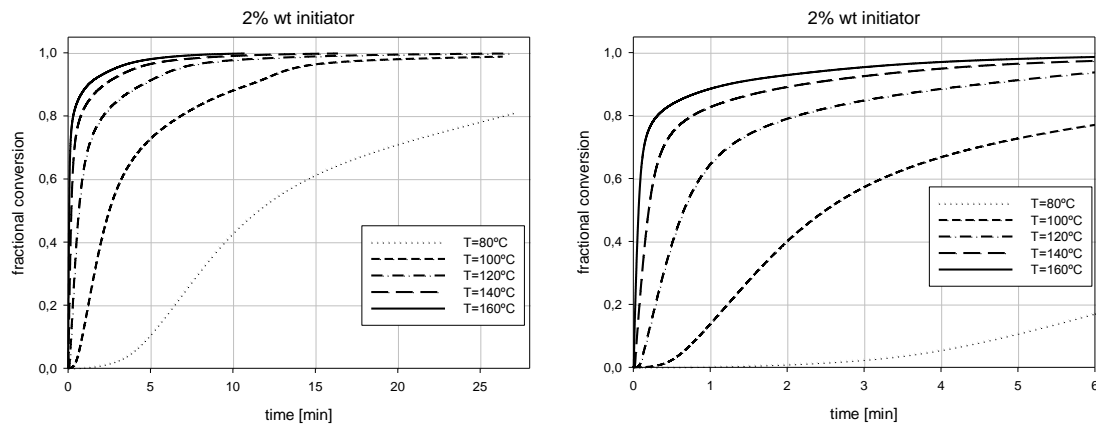


Figure 4.49 – Variation of the fractional conversion versus time for different temperatures (2% wt of thermal-initiator)

As can be seen in Figure 4.50, there is a huge difference for the highest temperatures; the reaction rate reaches a very high value and that peak point is attained in a very short period of time. Two situations contribute to this fact; the induction time is very short for the reason that there is a high level of energy present in the system, and the propagation of the polymerisation

reaction is very fast not only because of the energy level but also because there are many focuses of reaction as a result of the abundance of initiator.

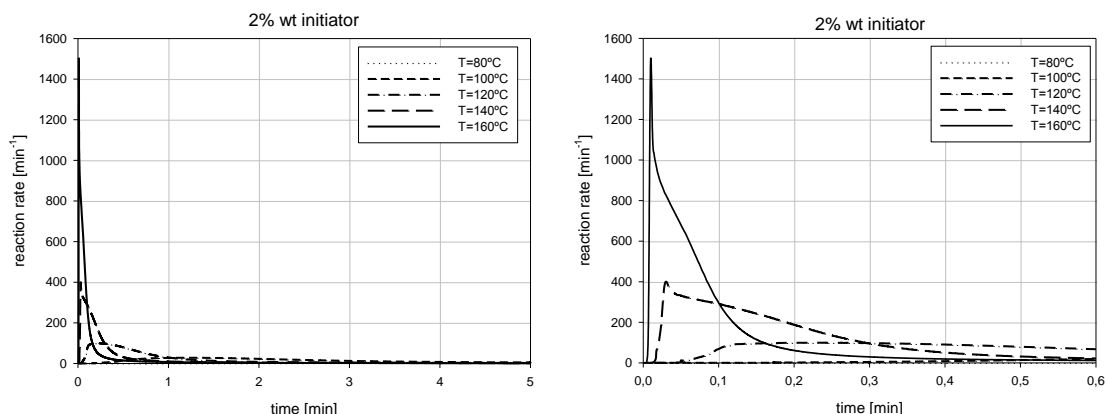


Figure 4.50 – Variation of the reaction rate versus time for different temperatures (2% wt of thermal-initiator)

Curves for reaction rate versus fractional conversion (Figure 4.51) shown that for higher temperatures the reaction is faster, and achieves the peak value sooner. Since temperature accelerates polymerisation reaction, reactive species are consumed sooner and thereby peak of reaction rate is attained earlier.

The results also shown that, despite values for reaction rate start to decrease strongly before 0.8 of fractional conversion, they come close to zero just for a value near 0.9 (Figure 4.51). A lower peak value for activation energy can be found around the same value of fractional conversion (Figure 4.52). Also the decrease in the activation energy values is verified before 0.8, confirming this correlation.

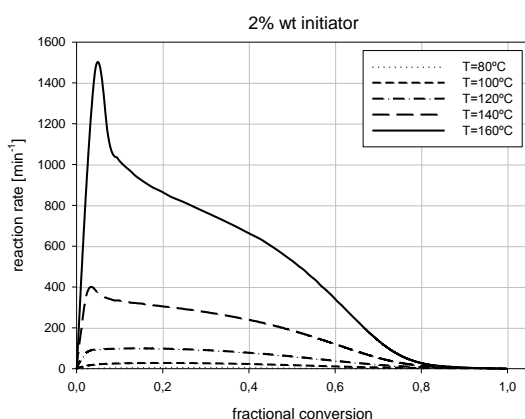


Figure 4.51 – Variation of the fractional conversion versus reaction rate for different temperatures (2% wt of thermal-initiator)

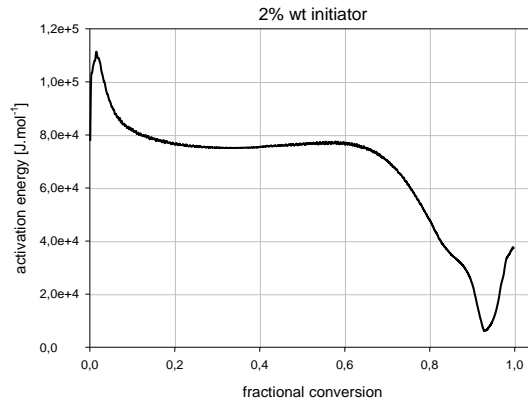


Figure 4.52 – Variation of the activation energy versus fractional conversion (2% wt of thermal-initiator)

In the iso-conversion curves shown in Figure 4.53 is notorious that the total conversion curve is quite isolated from the other curves. Nevertheless, for this percentage of initiator the difference has decreased when compared with previous cases due to the presence of more reactive spots dispersed in the resin. This gap reflects the effect of vitrification, which effectively means greater difficulty in raising the value of fractional conversion when we are in the presence of an already high value. In order to oppose to this loss of mobility of polymeric and rise of viscosity, and this way obtain a better fractional conversion a compromise solution can be done applying higher values of energy to the system or increasing the curing time.

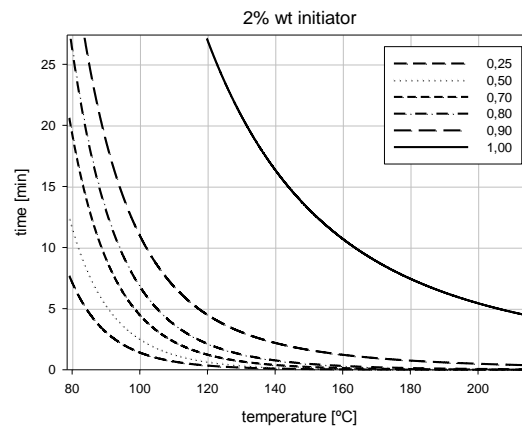


Figure 4.53 – Iso-conversion curves for time versus temperature (2% wt of thermal-initiator)

Figure 4.54 show the effect of temperature in cure kinetics using large amounts of thermal initiator (5% in weight). Temperature accelerates the reaction, reducing induction time and increasing reaction rate during propagation stage of the process. Vitrification phenomenon is verified for higher values of fractional conversion since more energy is present in the polymeric system. Overall, since large quantities of reactive elements are present, increasing the temperature, leads to faster reactions and better final results in terms of fractional conversion.

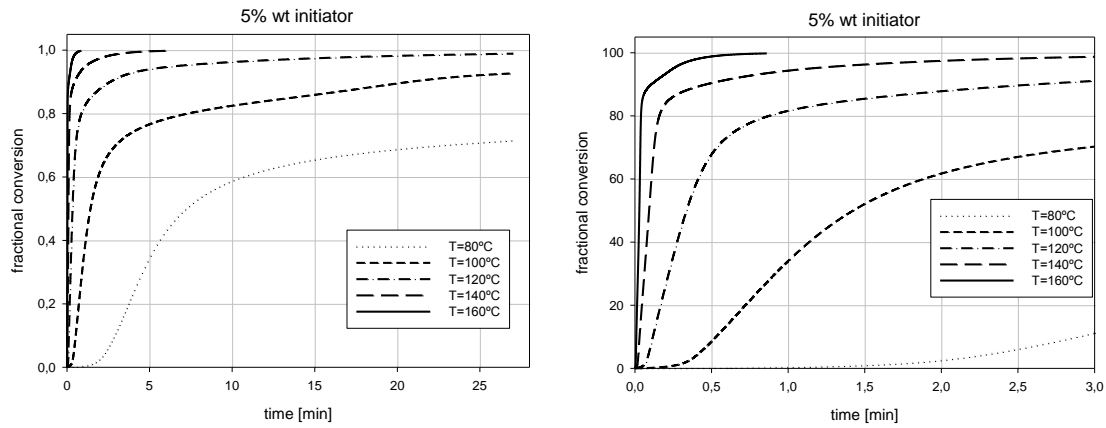


Figure 4.54 – Variation of the fractional conversion versus time for different temperatures (5% wt of thermal-initiator)

Since large amounts of thermal initiator are present in the resin, for high temperatures ($T=160\text{ }^{\circ}\text{C}$) the polymerisation reaction is extremely fast. As can be seen in Figure 4.55, the peak value for reaction rate happens to a curing time of less than 0.05 minutes (3 seconds). It is also notorious the huge increment obtained in reaction rate for the higher temperatures.

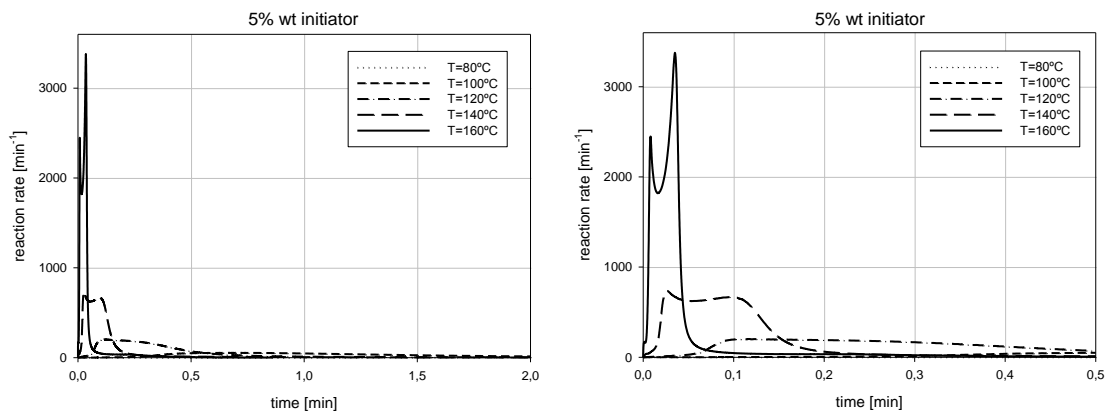


Figure 4.55 – Variation of the reaction rate versus time for different temperatures (5% wt of thermal-initiator)

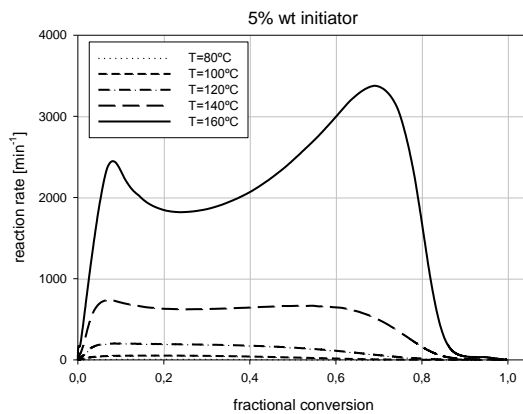


Figure 4.56 – Variation of the fractional conversion versus reaction rate for different temperatures (5% wt of thermal-initiator)

Reaction rate starts to decrease for values of fractional conversion around 0.8. However, is for fractional conversion near 0.9 that begins to tend to zero (Figure 4.56). The presence of many reactive spots dispersed in the resin as a consequence of the large amount of initiator user, allows the reaction to continue until total conversion is obtained when high values of energy are used ($T=160\text{ }^{\circ}\text{C}$).

The activation energy has an inferior peak value for values of fractional conversion around 0.9, precisely when the vitrification effects act more strongly (Figure 4.57).

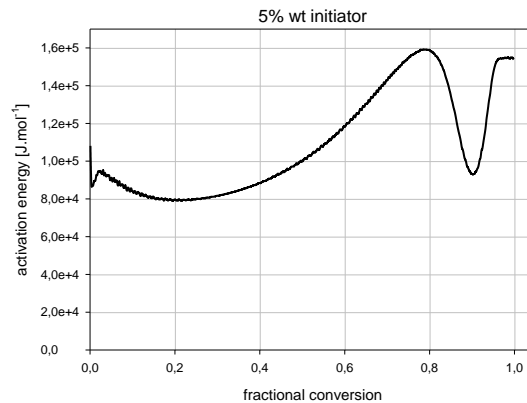


Figure 4.57 – Variation of the activation energy versus fractional conversion (5% wt of thermal-initiator)

Since large amounts of initiator were used (5% in weight), when compared with previous cases, the iso-curve of total conversion is closer to the iso-curve of fractional conversion equal to 0.90 (Figure 4.58). For temperatures above $150\text{ }^{\circ}\text{C}$ is possible to obtain total conversion in short periods of time (less than 2 minutes) or even in 6 minutes using a temperature of $140\text{ }^{\circ}\text{C}$. Slightly lowering the temperature, the time necessary to reach total conversion increases considerably because there is not enough energy to promote the mobility of polymeric chains and overcome the effects of vitrification.

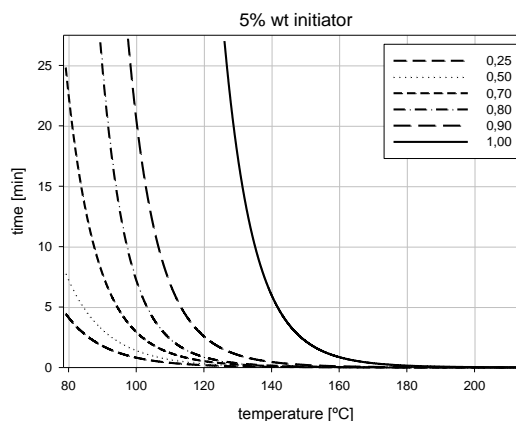


Figure 4.58 – Iso-conversion curves for time versus temperature (5% wt of thermal-initiator)

4.2.3.2 - Results and discussion (with the use of silica)

With the purpose of controlling the curing region, silica was added to polymeric compound to concentrate the thermal energy avoiding unwanted polymerisation at surrounding areas.

Extensive investigation work was carried out, using different amounts of silica for resins containing 2% in weight of thermal initiator. The results obtained are shown and analysed in detail in this section.

Results for 0.5% in weight of silica are shown in Figure 4.59. The effect of temperature was accentuated by the use of silica due to its characteristic of focusing heat. Silica acting as a heat concentrator promotes the polymerisation reaction in the area where particles are present but on the other hand enhances vitrification phenomenon and consequently favour the end of reaction achieving lower values of fractional conversion. These remarks are evident from the graphics where there is a clear gap between the curves of each temperature because the energy promotes mobility and contribute to attenuate the effects of vitrification.

For lower temperatures, the vitrification effects are accentuated by the silica particles. Two main reasons contribute to this fact, the increase of viscosity as a consequence of the addition of silica particles, and the ability to focus the heat energy in the surrounding areas and consequently avoiding the dispersion of heat energy.

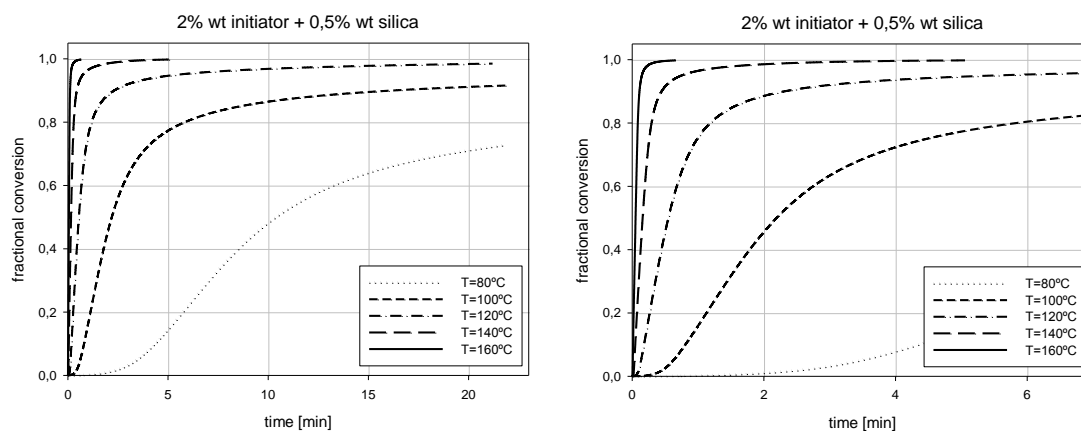


Figure 4.59 – Variation of the fractional conversion versus time for different temperatures (2% wt of thermal-initiator and 0,5% wt of silica)

Once more, it is notorious in the graphs of Figure 4.60 that temperature provides a more pronounced peak of reaction rate and that point occurs sooner. More energy is present, but it is focused in small spots corresponding to the presence of silica particles. This fact is favourable to vitrification since mobility of polymerised chains is affected, not only because silica increase viscosity of resin but mainly because energy is not dispersed in a continuous way in the resin.

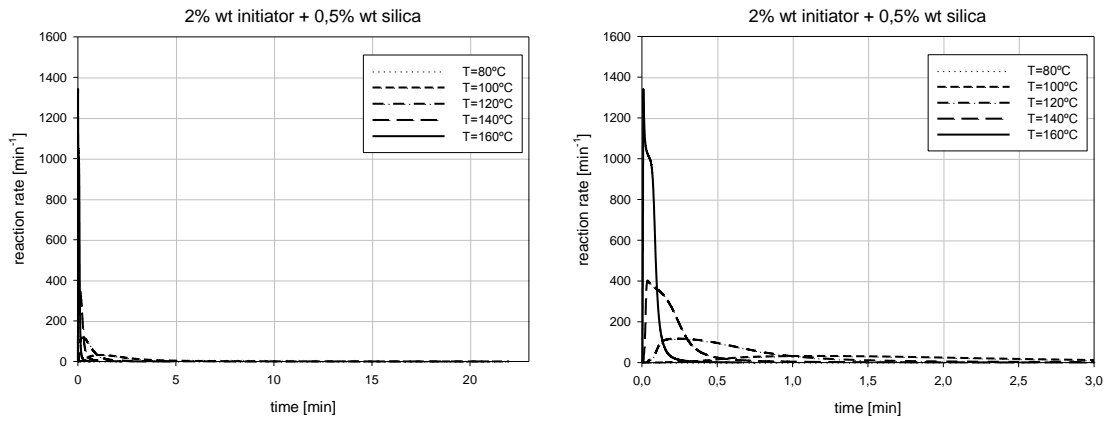


Figure 4.60 – Variation of the reaction rate versus time for different temperatures (2% wt of thermal-initiator and 0,5% wt of silica)

Figure 4.61 show that higher values of reaction rate are attained for higher temperatures and reactions decelerates and stops achieving better values of fractional conversion. For the highest value ($T=160\text{ }^{\circ}\text{C}$), the effects of vitrification almost did not were observed since enough energy was present to consume almost all reactive species. Thus, almost total conversion was achieved.

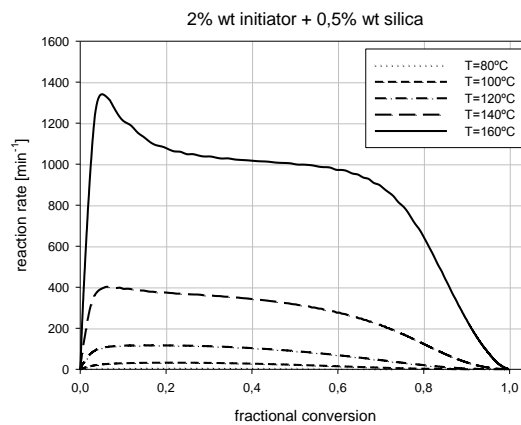


Figure 4.61 – Variation of the fractional conversion versus reaction rate for different temperatures (2% wt of thermal-initiator and 0,5% wt of silica)

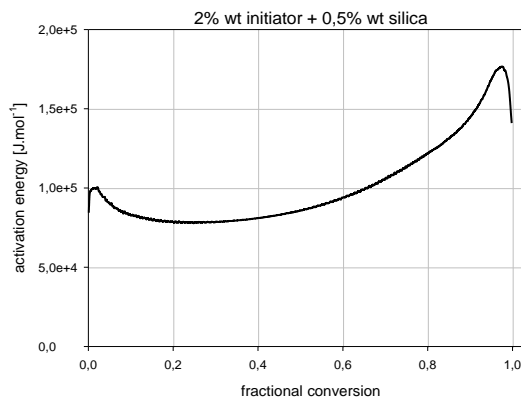


Figure 4.62 – Variation of the activation energy versus fractional conversion (2% wt of thermal-initiator and 0,5% wt of silica)

Activation energy versus fractional conversion is shown in Figure 4.62. It is notorious that, merely for values of fractional conversion closer to total conversion, activation energy start to decrease, reflecting the fact that reaction rate tends to zero near total conversion.

In Figure 4.63 can be observed that total conversion can be attained in short periods of time only for high values of energy ($T=160\text{ }^{\circ}\text{C}$). A small decrease in the supplied energy causes a huge increase in the time necessary to obtain a similar ending result in terms of fractional conversion. Only for high values of energy, starting at about $T=130\text{ }^{\circ}\text{C}$, total conversion can be achieved, reinforcing the previous conclusion that the silica acting as a thermal energy concentrator promote the vitrification phenomenon due to the raise of viscosity and mainly by preventing the energy to be dispersed in the resin.

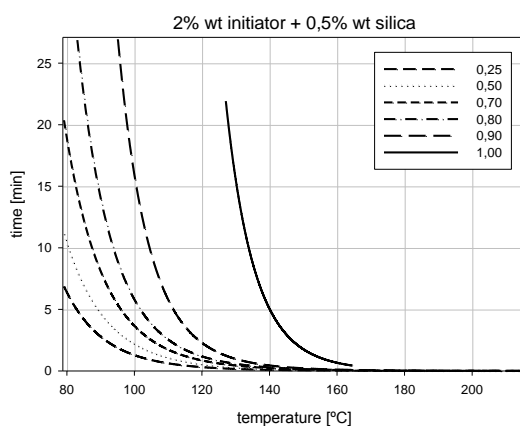


Figure 4.63 – Iso-conversion curves for time versus temperature (2% wt of thermal-initiator and 0,5% wt of silica)

Results for fractional conversion versus time for different temperatures, using 1% in weight of silica, are shown in Figure 4.64. Also in this case it is notorious a clear separation between curves enhancing the effect of temperature in cure kinetics. For temperatures of $120\text{ }^{\circ}\text{C}$ and above the induction time is extremely short. The thermal energy was instantly captured by silica particles dispersed in the resin and those focused spots of energy accelerated the process of initiation.

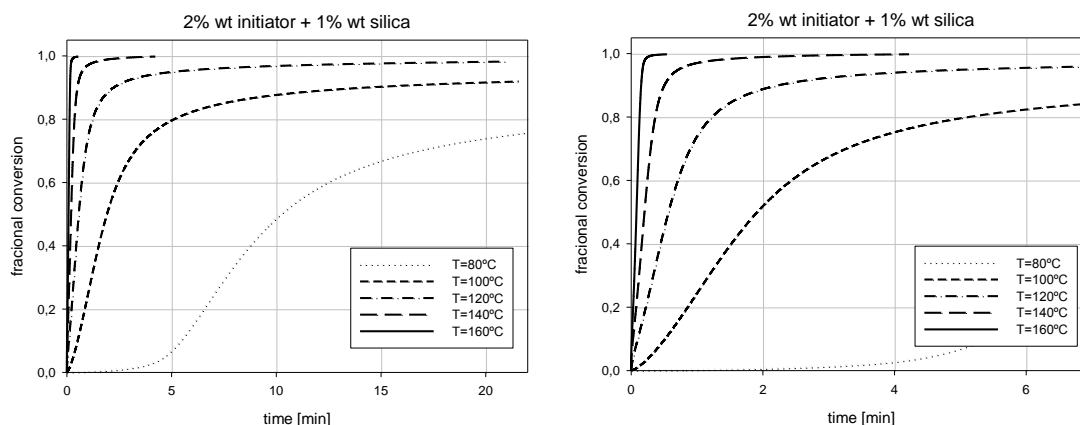


Figure 4.64 – Variation of the fractional conversion versus time for different temperatures (2% wt of thermal-initiator and 1% wt of silica)

For higher temperatures, reaction rate reaches its peak value very early (see Figure 4.65) according to previous conclusion that induction time was extremely brief. Higher peak values of reaction rate were obtained for higher temperatures since more energy is present in the polymeric system favouring the reaction.

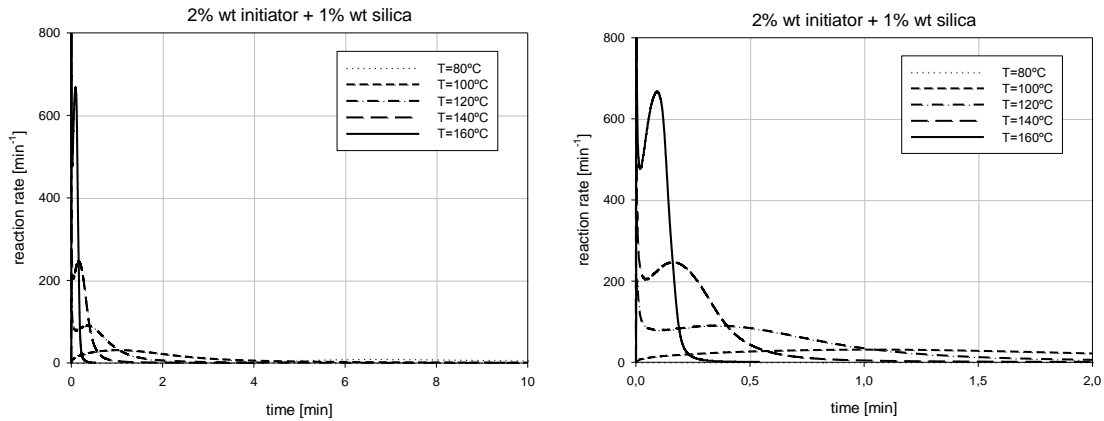


Figure 4.65 – Variation of the reaction rate versus time for different temperatures (2% wt of thermal-initiator and 1% wt of silica)

Higher values of reaction rate versus fractional conversion were obtained for higher temperatures reflecting the presence of higher values of energy in polymeric system (Figure 4.66). It can be observed that, only for higher values of temperature, were achieved fractional conversion values near total conversion. In those cases, the deceleration of reaction rate occurs later and in an abrupt way because is caused by the consumption of reactive species in contrast with the other cases where the increase of viscosity leading to vitrification phenomenon and consequently to the ending of reaction prematurely. Results also show that the increase in the values obtained in consequence of rising the temperature is more pronounced for the highest values of temperatures (from 140 °C to 160 °C).

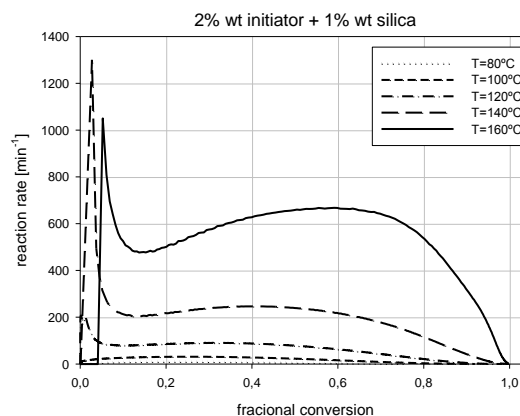


Figure 4.66 – Variation of the fractional conversion versus reaction rate for different temperatures (2% wt of thermal-initiator and 1% wt of silica)

Activation energy versus fractional conversion increases until nearly total conversion (Figure 4.67). The deceleration of reaction occurs as a result of consumption of reactive species due to the rapid polymerisation and leading to the end of reaction.

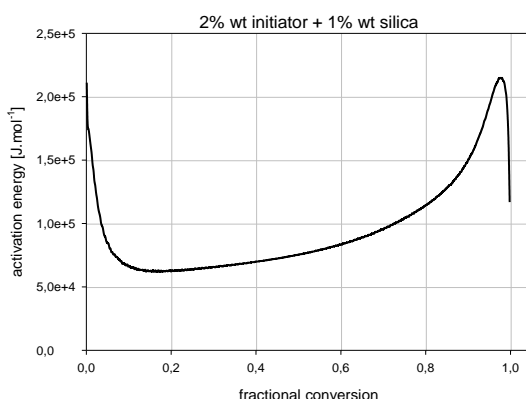


Figure 4.67 – Variation of the activation energy versus fractional conversion (2% wt of thermal-initiator and 1% wt of silica)

For lower temperatures, the vitrification effects predominate. However, for higher temperatures, unimolecular termination no longer prevails due to overlapping of the effects of rapid polymerisation. Therefore it is possible to achieve total conversion for temperatures over 130 °C (Figure 4.68). The effect of temperature in the final result of fractional conversion, looking for the aim of achieving total conversion, is more pronounced for temperatures above 150 °C.

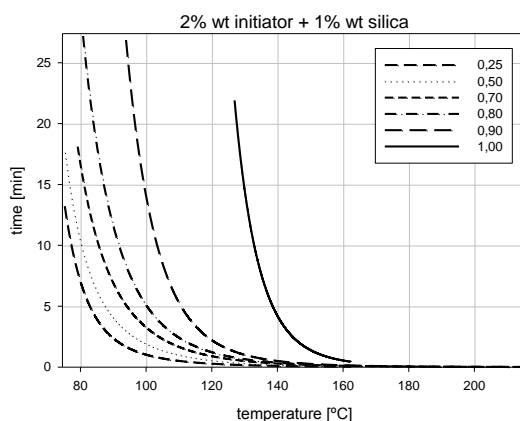


Figure 4.68 – Iso-conversion curves for time versus temperature (2% wt of thermal-initiator and 1% wt of silica)

Figure 4.69 shown results obtained for 2% in weight of silica. For almost all the researched temperatures it was achieved total conversion due to the presence of higher amounts of silica corresponding to more spots of energy concentration and consequently more active points of reaction. However, the viscosity of resin as increased significantly due to the presence of higher amounts of silica and therefore the recoat time also increases.

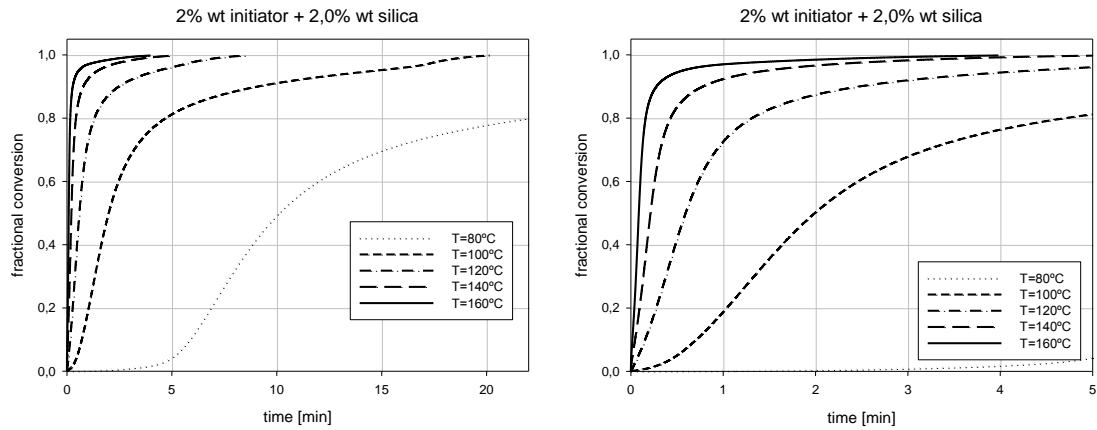


Figure 4.69 – Variation of the fractional conversion versus time for different temperatures (2% wt of thermal-initiator and 2% wt of silica)

Induction time is shortened and the peak value of reaction rate occurs soon (Figure 4.70) due to the presence of a large quantity of reaction spots corresponding to the presence of powder silica and initiator. The silica particles capture the heat energy promoting the polymerisation reaction. Since the chain reaction is initiated in many spots simultaneously, the reaction rate increases in a short period of time attaining its peak value soon because of consumption of reactive species.

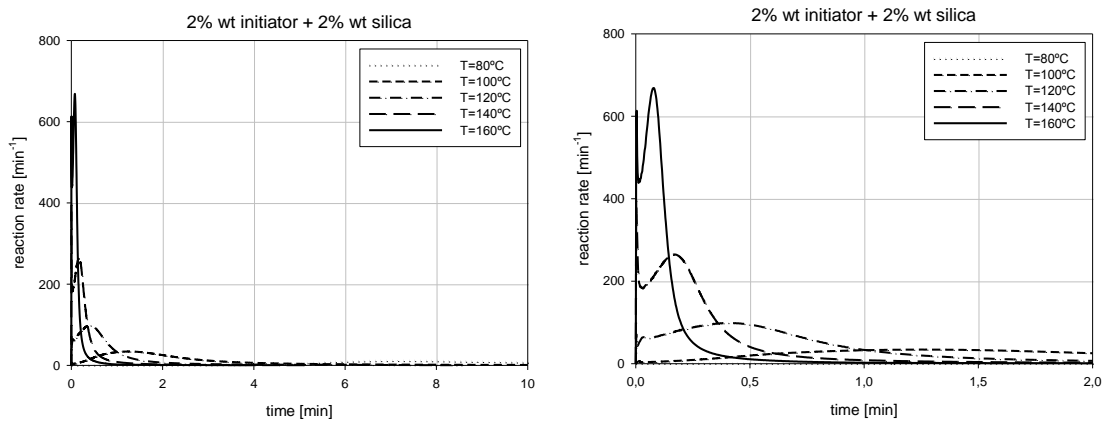


Figure 4.70 – Variation of the reaction rate versus time for different temperatures (2% wt of thermal-initiator and 2% wt of silica)

Despite of peak value of reaction rate was achieved for a short period of time, for almost all the temperatures tested was obtained total conversion (Figure 4.71). This can be explained with the fact of reaction rate deceleration was not due to vitrification phenomenon but otherwise due to the consumption of reactive species. In fact, the presence of huge quantities of silica particles acting as heat concentrators dispersed in to the resin, has promoted the polymerisation reaction at numerous locations dispersed in the resin.

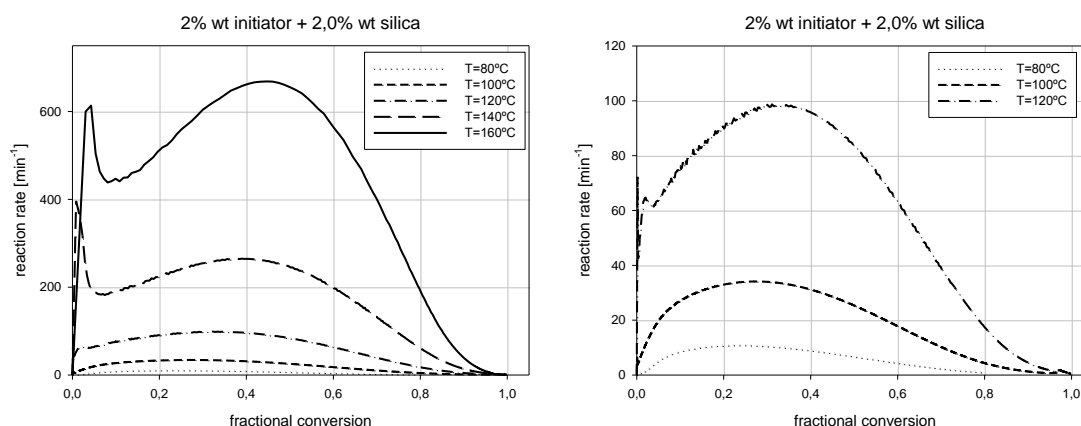


Figure 4.71 – Variation of the fractional conversion versus reaction rate for different temperatures (2% wt of thermal-initiator and 2% wt of silica)

Activation energy tends to zero before total conversion is achieved (Figure 4.72) denoting the behaviour also verified in Figure 4.71. Due to high values of reaction rate, the reactive species were consumed and consequently the reaction decelerates and the viscosity increases dramatically attaining high values of fractional conversion. However, the presence of silica particles concentrating the heat provides the necessary energy to allow the reaction to proceed and this way obtaining total conversion, slowly at this stage of reaction. Therefore activation energy versus fractional conversion tends progressively to zero and not abruptly as in the previous cases.

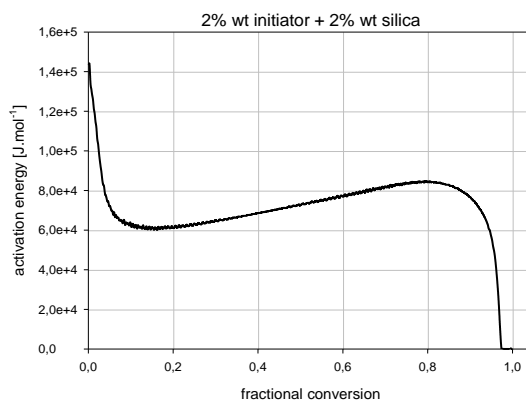


Figure 4.72 – Variation of the activation energy versus fractional conversion (2% wt of thermal-initiator and 2% wt of silica)

With this resin composition, it is possible to achieve total conversion in short periods of time using temperatures above 140 °C or even using low exposure temperatures (100 °C) during a long period of time (Figure 4.73). It can be seen that above 150 °C there are no significant reductions in the time necessary to obtain total conversion and therefore no benefits are obtained of the extra energy expenditure. Likewise, below 120 °C a small decrease in the energy supplied has a huge impact in increasing the time of cure necessary to obtain total conversion.

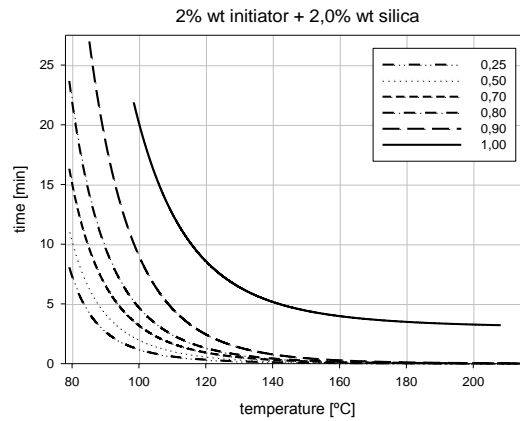


Figure 4.73 – Iso-conversion curves for time versus temperature (2% wt of thermal-initiator and 2% wt of silica)

One other resin composition was tested this time using 4% in weight of silica powder. Although it was silica with nano sized particles, the viscosity of the polymeric resin had a significant increase, with obvious repercussions in the preparation and processing of material. Not only is difficult to obtain a homogeneous and well-mixed resin as the multi-layer process is hindered by significant increase in the time necessary to recoat process. Also obtaining such a thin layer is more difficult to attain.

Due to the presence of large amounts of silica spread in the resin, the heat is captured and maintained. This energy enhanced medium acts with a catalytic behaviour, accelerating all the stages of the polymerisation reaction. Figure 4.74 show that, in the presence of the highest energy levels, corresponding to temperatures over 120 °C, the reaction is highly accelerated achieving total conversion in short periods of time. Values of fractional conversion over 0,80 are attained very fast, then there is a slowdown in reaction rate in part due to the sudden increase in viscosity of resin.

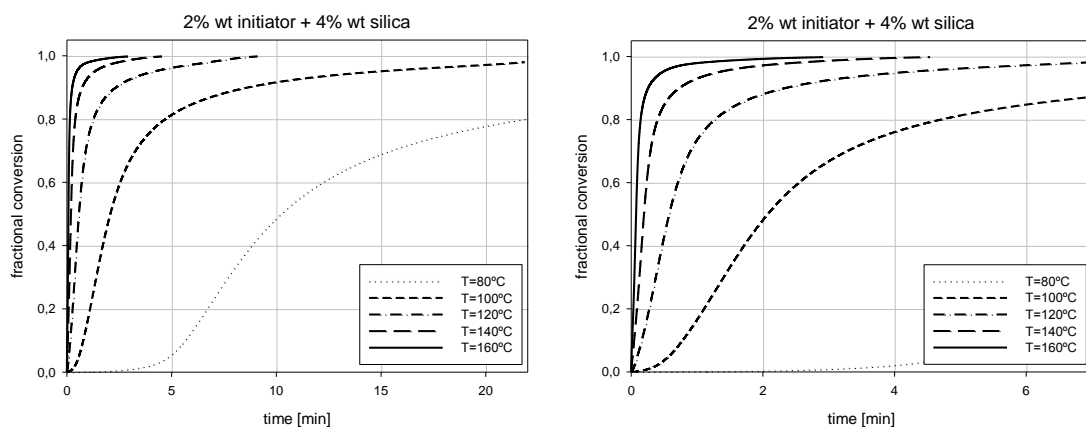


Figure 4.74 – Variation of the fractional conversion versus time for different temperatures (2% wt of thermal-initiator and 4% wt of silica)

It can be seen, in Figure 4.75, that reaction rate peak occurs very soon and not so pronounced as in previous cases. The acceleration of the reaction is very pronounced, with short induction

periods, but the deceleration is less sharply due to the increase of viscosity and existence of reactive species. The presence of heat energy concentrated in silica particles enhances the reaction until total conversion is achieved. Thus, the curve of reaction rate tends smoothly to zero.

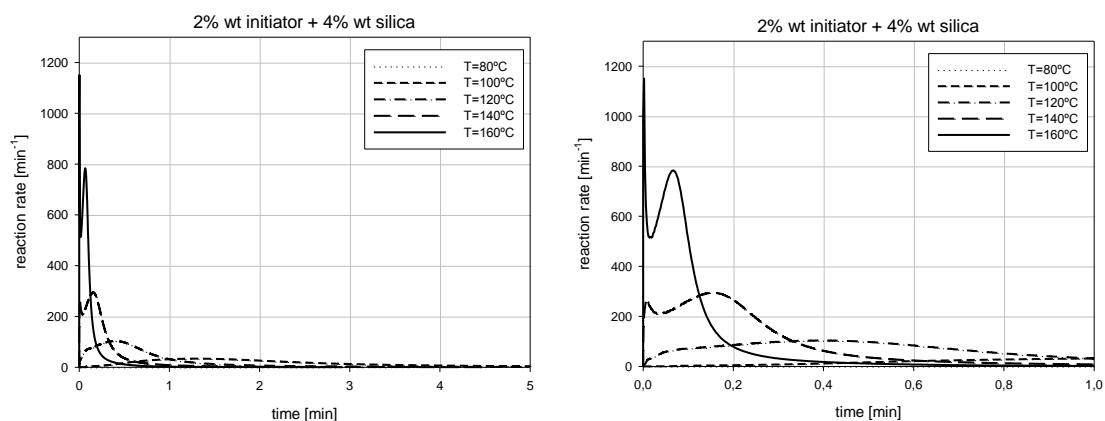


Figure 4.75 – Variation of the reaction rate versus time for different temperatures (2% wt of thermal-initiator and 4% wt of silica)

Similar behaviour is detected in Figure 4.76, the curves of fractional conversion versus reaction rate tend to zero smoothly, denoting that total conversion is achieved slowly. The increasing of viscosity is counterpoised by the presence of heat in the silica particles scattered in the resin. The mobility of the chains is affected by the increase of viscosity but the presence of energy enhances the continuation of polymerisation reactions slowly but sufficient to achieve total conversion.

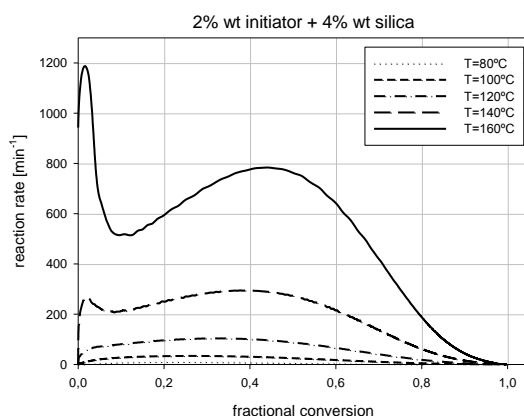


Figure 4.76 – Variation of the fractional conversion versus reaction rate for different temperatures (2% wt of thermal-initiator and 4% wt of silica)

Also in this case, activation energy approaches to zero from the left and not from the top, in accordance to the previous statement that the final stage of reaction is slowed and total conversion is achieved with lower reaction rate values (Figure 4.77).

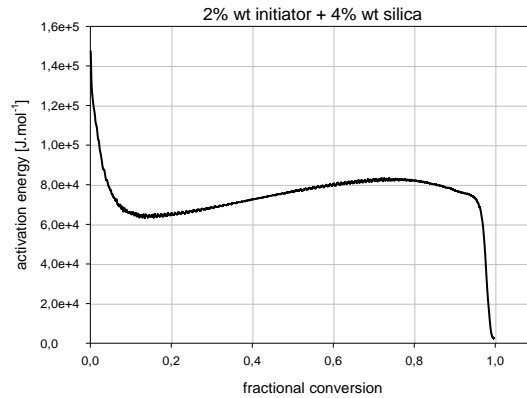


Figure 4.77 – Variation of the activation energy versus fractional conversion (2% wt of thermal-initiator and 4% wt of silica)

Total conversion can be achieved in short periods (less than 300 seconds) for temperatures above 140 °C. For lower temperatures, the period of time necessary to achieve total conversion increases significantly (Figure 4.78). In the graph is also notorious the separation between the iso-curves corresponding to conversion value of 0.90 and total conversion, which is in accordance with previous remarks that above that value the reaction rate decreases significantly and total conversion is achieved slowly. The mobility of reactive chains is dramatically affected by the high value of viscosity, but in the other hand the presence of heat in silica particles enables the reaction to progress, slowly but sufficient to obtain total conversion for the higher temperature cases.

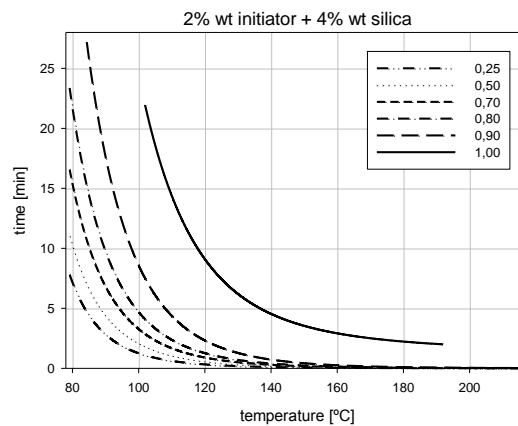


Figure 4.78 – Iso-conversion curves for time versus temperature (2% wt of thermal-initiator and 4% wt of silica)

4.2.3.3 - Case III: the effect of initiator concentration

The results, obtained using Vyazovkin model, are shown in Figures 4.79 to 4.81 for curing temperatures of 100 °C and 120 °C. The induction time is shortened with the increase of initiator concentration. The presence of larger quantities of reactive species enables the polymerisation reaction to start at more spots dispersed in the resin. Consequently also the propagation stage of reaction is accelerated since more reactive spots are present and also more reactive species

are available to continue the polymerisation. However, for larger amounts of initiator (5,0 % wt) the vitrification phenomena prevails derived by the very higher viscosity, and the final results in terms of fractional conversion, are affected. Therefore, better results were obtained for 2% in weight of initiator concentration because of the polymeric chain loss of mobility due to the high viscosity of the resin. The reactive spots became imprisoned and it was not possible to continue the reaction.

Similar behaviour was detected in both temperatures, however in the case of 120 °C, the presence of higher energy has softened the effect and has approximated the curves originating smaller differences in the final results of fractional conversion obtained.

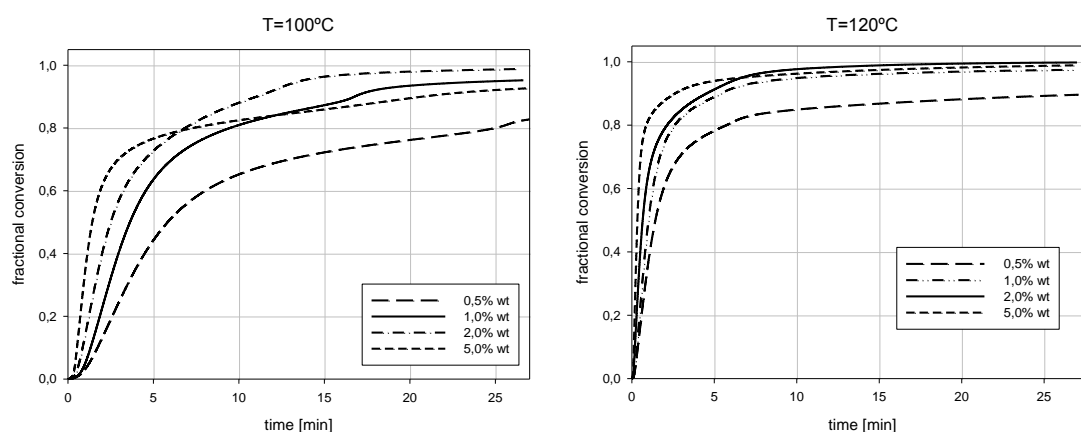


Figure 4.79 – Case III: variation of the fractional conversion versus time for different initial concentrations of initiator (temperatures of 100 °C and 120 °C)

The described effects are notorious in Figure 4.80, where can be noticed the reduction of induction time and the increase in the reaction rate due to higher initiator concentration. Higher peaks of reaction rate are obtained and the curing time to reach them is reduced. Then the reaction decelerates because of the consumption of reactive elements and to the increase of viscosity.

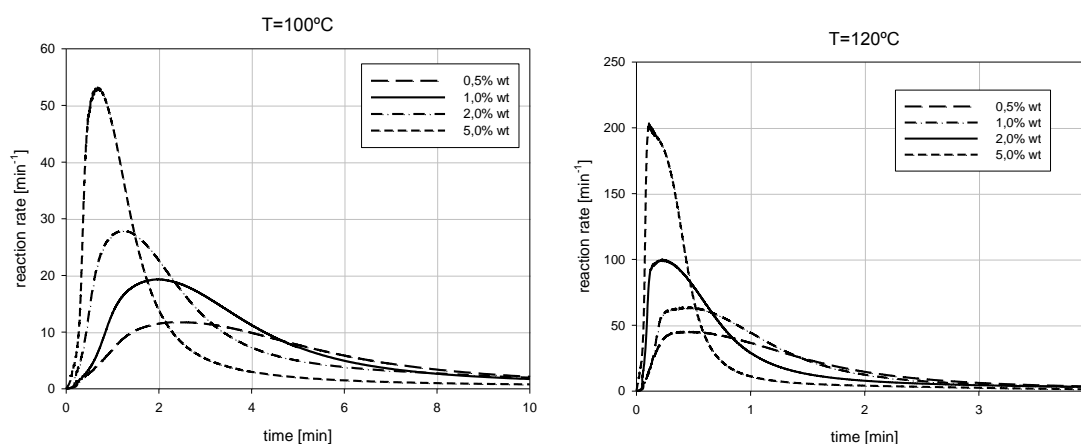


Figure 4.80 – Case III: variation of the reaction rate versus time for different initial concentrations of initiator (temperatures of 100 °C and 120 °C)

After the deceleration, as a result of vitrification, reaction rate is lower for the higher amount of initiator due to loss of mobility of polymerised chains as a consequence of high viscosity as previously described. It can be observed that the reaction is able to continue for a long period of time with reduced reaction rate. Despite of reduced mobility of polymeric chains, locally there is enough energy to allow the reaction to proceed.

Reaction rate versus fractional conversion increases with the initiator concentration (Figure 4.81). Vitrification phenomena starts to be more evident for values of fractional conversion over 0,80. After this point, the initiator concentration maintains its influence in the polymerisation reaction, but the curves are closer. This fact, together with the evidence of lower values obtained for the higher initiator concentration (5,0 %wt), leads to the assumption that, for very high concentrations of initiator, the influence of significant increase of viscosity due to higher initiator concentration prevails over the increase of viscosity due to polymerisation process.

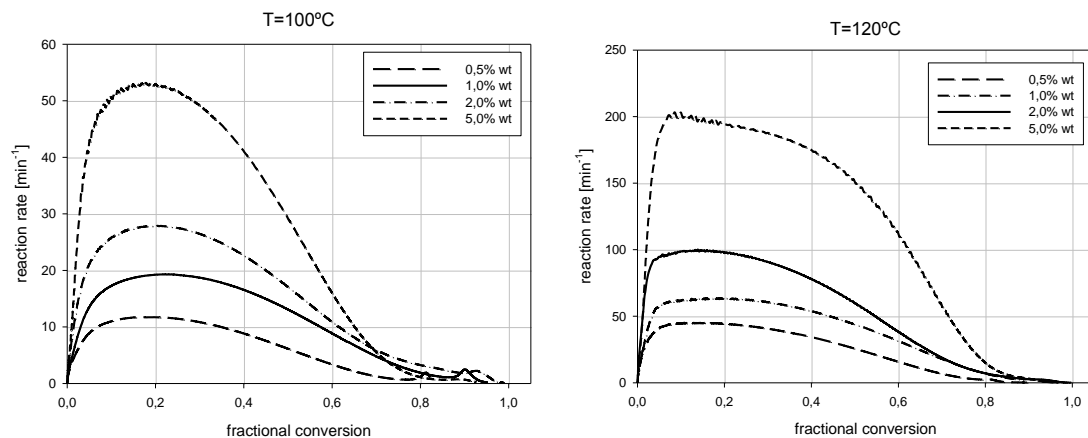


Figure 4.81 – Case III: variation of the reaction rate versus fractional conversion for different initial concentrations of initiator (temperatures of 100 °C and 120 °C)

4.2.3.4 - Case IV: the effect of silica concentration

The influence of silica concentration over the curing process is shown in Figures 4.82 to 4.84. For temperature of 100 °C the presence of silica accelerate the reaction since the particles of silica act as a heat concentrator and consequently enables the reaction due the presence of energy in localized spots dispersed in the resin. On the other hand, since the value of energy is relatively low and the powder silica contributes to the significantly increase of the resin viscosity, total conversion was achieved only in the absence of silica. However, with the presence of silica, better results in terms of fractional conversion were obtained for higher concentrations of silica, in accordance with previous conclusions.

With the presence of high values of energy (T= 120 °C) total conversion is obtained for higher values of silica concentration. This fact can be explained with presence of energy retained in the silica particles and dispersed in the resin. This energy enables the reaction to continue overlapping the effect of vitrification. It is interesting to notice that, this effect is only possible

for larger quantity of silica present in the resin and thus a higher number of reaction points corresponding to a denser mesh of energy (Figure 4.82).

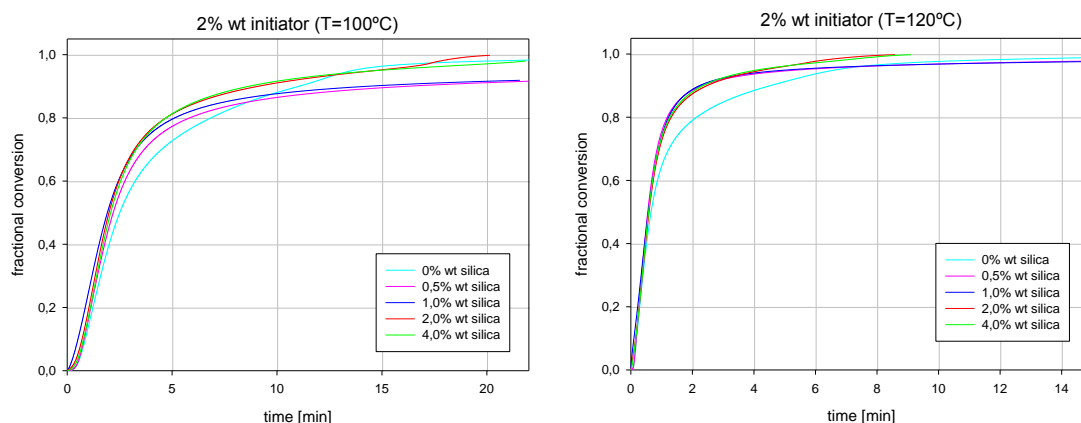


Figure 4.82 – Case IV: variation of the fractional conversion versus time for different concentrations of silica (2% wt of initiator and temperatures of 100 °C and 120 °C)

The presence of silica reduces induction time and accelerates the reaction during propagation stage of reaction. The energy is captured by the silica particles and this way promoting the activation of initiator elements nearby those particles.

The evidence of vitrification effects start to be visible for higher values of fractional conversion when silica is used. The energy retained in the silica particles makes possible to continue the polymerisation reaction counteracting the effects of the increase of viscosity. Only later, the reaction decelerates mainly because of reactive elements consumption as can be realised by the high value of fractional conversion already attained.

Higher values of silica accentuate the described effect due to a larger and denser net of spots of energy concentrated in the silica particles. However, for the highest values of silica concentration tested (4 %wt) the effect of vitrification is more accentuated for the reason that the polymeric compound has a very high viscosity as a result of large amounts of silica powder used. Furthermore, those silica particles concentrate the heat and affect the dispersion of energy by the resin. The energy is dispersed by the resin but concentrated in small spots corresponding to the silica particles. Therefore the reaction is promoted in a more localized manner, allowing vitrification effects to arise. Consequently, better results were obtained for 2% in weight of silica powder because was achieved a most effective balance between heat concentration and viscosity increase effects.

Figure 4.83 shows reaction rate versus time of cure. For temperature of 100 °C, for higher values of silica concentration consecutively larger values of reaction rate were obtained. The time requires to reach these peak values does not register significant variations. Nevertheless, the tendency is to be slightly increased with the increase of silica concentration, denoting a slight delay in the start of vitrification effects. Once more, the huge increase of silica viscosity causes that the higher value of reaction rate is obtained for 2% wt in weight of silica.

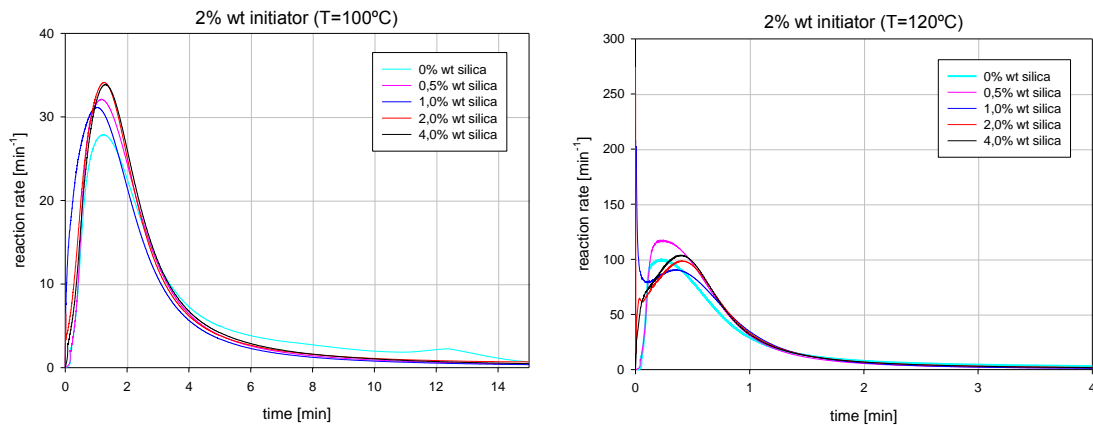


Figure 4.83 – Case IV: variation of the reaction rate versus time for different concentrations of silica (2% wt of initiator and temperatures of 100 °C and 120 °C)

Reaction rate versus fractional conversion is shown in Figure 4.84. Higher peak values of reaction rate were obtained for 2 % wt of silica. The reaction stops accelerating for values of fractional conversion of approximately 0.3, but only near fractional conversion of 0.9 the vitrification effects are stronger and the deceleration is more accentuated, also due the consumption of reactive elements. The polymerisation reaction continues above this value of fractional conversion, even if very slowly. This is due to the presence of the silica particles and the heat which they retain. The energy has a localized effect, and while the mobility of polymer chains is reduced, locally exist enough energy for the reaction to proceed slowly.

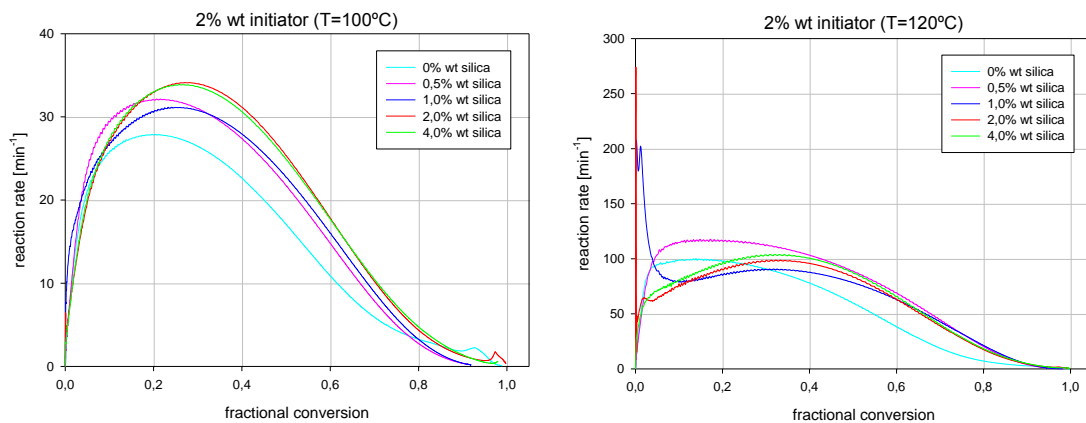


Figure 4.84 – Case IV: variation of the reaction rate versus fractional conversion for different concentrations of silica (2% wt of initiator and temperatures of 100 °C and 120 °C)

4.2.3.5 - Case V: effect of silica particle size

To understand the effect of silica particle size in the cure kinetics, two different types of silica were considered to this research work, a colloidal silica and a fumed silica. Both materials were characterised in section 3.4.3 and will be analysed in current section from de point of view of particle size. The fumed silica, henceforward designated as silica A, has an average particle length of 0.2 to 0.3 microns, and the colloidal silica, hereafter designated as silica B has an average particle size of approximately 65 microns.

Figure 4.85 shows the variation of fractional conversion versus curing time for silica A and B analysed at different temperatures. Different tendencies were detected depending on the range of temperatures used. For higher values of energy (starting at 100 °C) the induction time was shortened, in the case of silica A, since the heat is attracted and maintained in the silica particles. They are smaller but they are present in larger quantity and therefore the heat is dispersed in more spots within the resin enabling the polymerisation reaction to start at more points and consequently reducing the induction time. Nevertheless, the presence of larger particles of silica (silica B) as promoted the reaction during the propagation stage since reaction rate has increased at this stage. Actually, the presence of larger particles allows the energy to be more focused and therefore with positive influence over the reaction rate. Vitrification effects are visible sooner for silica B as a result of larger particles and therefore higher viscosity. However, slightly higher values of fractional conversion were obtained when silica B was used since energy is not so dispersed as in the case of silica A. Generally, the presence of smaller particles has enabled the reaction to start at more spots due to the dispersion of energy in smaller but more points. Then, during propagation and vitrification, the opposite effect prevailed and the reaction has benefited with the concentration of energy in less but larger spots.

For lower values of energy ($T = 80\text{ °C}$) a different behaviour was detected. In fact, the value of energy is insufficient to obtain a proper fractional conversion leading to a solid with good mechanical properties. Moreover, the reaction is very slow when compared with previous cases. Thus, the concentration of heat in the silica particles was not enough to triggers the described effects for higher temperatures. At final stages of reaction, the energy is not enough to promote polymeric chains mobility in order to oppose to vitrification effects and therefore the higher viscosity of resin B leads to lower final values of fractional conversion obtained.

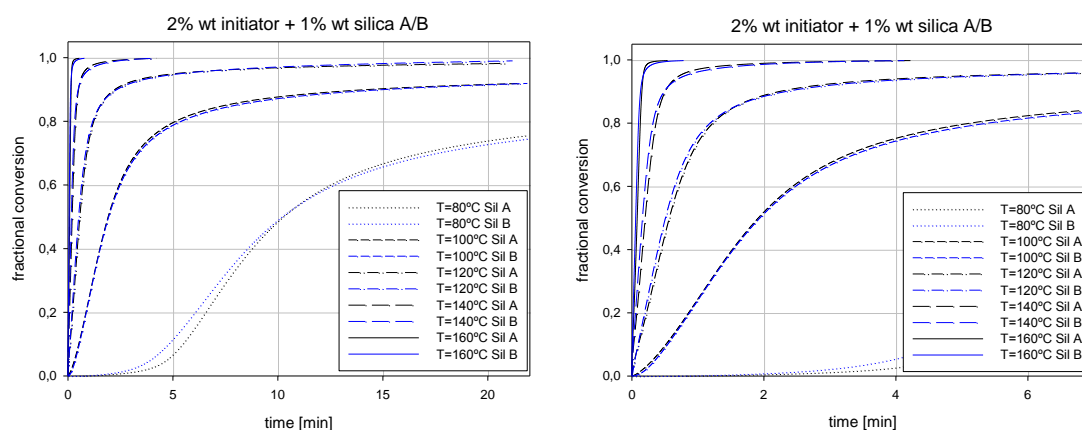


Figure 4.85 – Case V: variation of the fractional conversion versus time for different temperatures (2% wt of thermal-initiator and 1% wt of silica type A and B)

The peak value of reaction rate is higher and occurs sooner for silica B since heat is more focused in its larger particles (Figure 4.86). The reaction propagates with higher reaction rate and starts to slow down sooner due to the reactive elements consumption. Then the vitrification effects

are predominant and the reaction stills active but with low reaction rates. The influence of silica particle size increases with temperature for the reason that higher values of energy are focused at the particles and therefore the acceleration of the reaction is amplified. Once more, for the lower value of temperature ($T= 80\text{ }^{\circ}\text{C}$) a different behaviour was detected since energy is insufficient to counteract the higher viscosity of resin B.

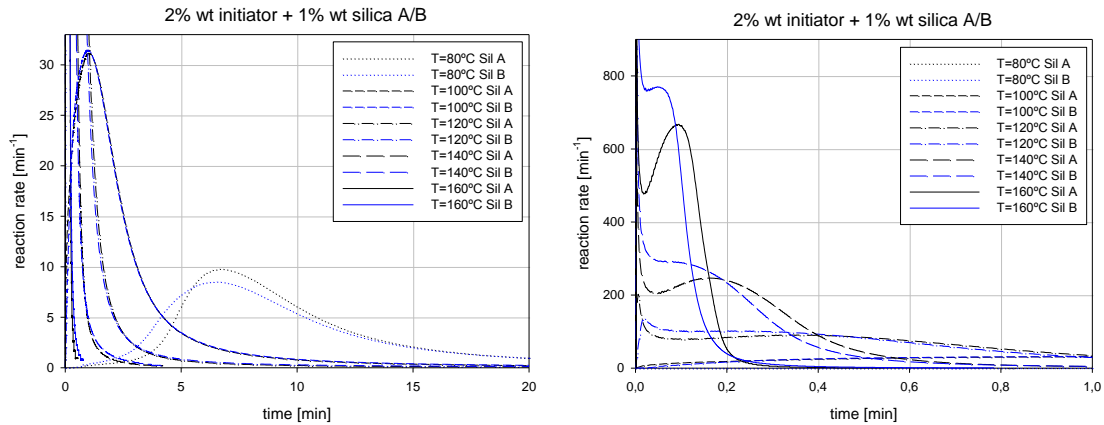


Figure 4.86 – Case V: variation of the reaction rate versus time for different temperatures (2% wt of thermal-initiator and 1% wt of silica type A and B)

Reaction rate versus fractional conversion is higher for silica B due to the same reason as previously explained; heat is more focused in its larger particles promoting the polymerisation reaction (Figure 4.87). Since viscosity increase dramatically with fractional conversion, there is a point from which the temperature effect is overcome by the effect of vitrification phenomenon. The increase of fractional conversion affects both resins however the resin B has a higher viscosity due to the size of the silica particles. This inversion point, where the curves intersect, occurs for values of fractional conversion increasingly higher depending if higher temperatures are used. Thus, the higher is the energy present in the resin, the more pronounced is the effect of heat concentration in the silica particles counteracting the loss of mobility of the polymeric chains. Again, for $T= 80\text{ }^{\circ}\text{C}$ the low energy is not enough to act as described for higher temperatures and the lower viscosity of resin A is the predominant effect causing that reaction rate is superior during all the reaction when compared with resin B.

Figure 4.88, shows activation energy versus fractional conversion for both silica A and B, underlining the previously described effects. For lower fractional conversion values, corresponding to the induction time, silica A has higher activation energy due to dispersion of energy for more spots scattered by the resin promoting the activation of the initiator. Then, as a consequence of larger particle size and therefore more focused energy, the reaction propagates with higher reaction rate for silica B and activation energy becomes larger. For high values of fractional conversion, due to the increase of viscosity the smaller particle size of silica A leads, once more, to upper values of activation energy. For the conditions under analysis, total conversion was achieved and consequently activation energy tends to zero for fractional conversion of 1.

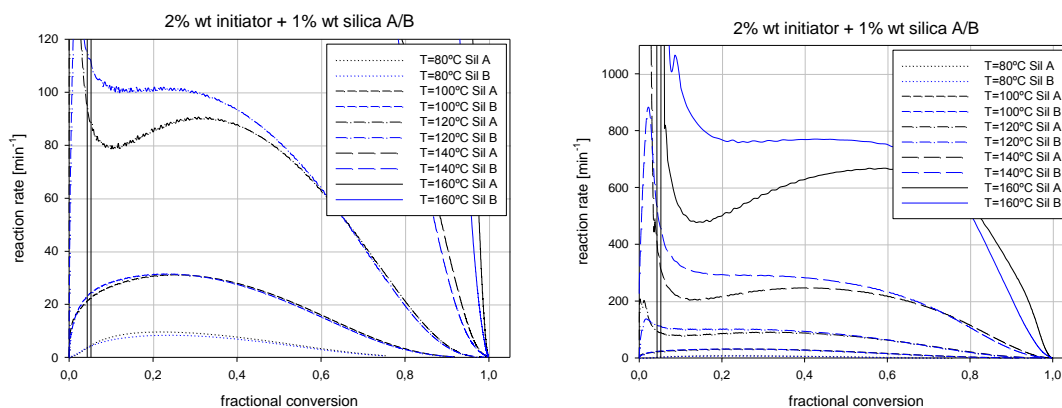


Figure 4.87 – Case V: variation of the fractional conversion versus reaction rate for different temperatures (2% wt of thermal-initiator and 1% wt of silica type A and B)

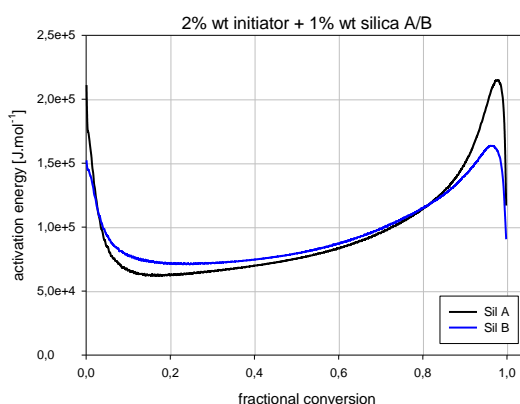


Figure 4.88 – Case V: variation of the activation energy versus fractional conversion (2% wt of thermal-initiator and 1% wt of silica type A and B)

For lower values of fractional conversion (beneath 0.90) silica B requires more time or more energy to attain the same value of fractional conversion partly due to its high viscosity (Figure 4.89). Analysing the curves of total conversion, a turning point was detected corresponding to approximately 140 °C and 4 minutes. Below this point, silica A, requires more time of reaction or more temperature of exposure to achieve total conversion. On the opposite, above that threshold of energy (T= 140 °C), silica A attains total conversion for lower temperatures and exposure times.

The results suggests that, in the presence of lower values of energy, the influence of larger particles size has a beneficial effect due to the concentration of energy in those bigger particles and therefore maintaining heat more efficiently and with a larger area of influence. For higher values of temperature, because energy is in itself high, the effect of particle size is supplanted by the benefits of having the particles, although smaller, but more widely spread by the resin and therefore maintaining energy dispersed by the entire region.

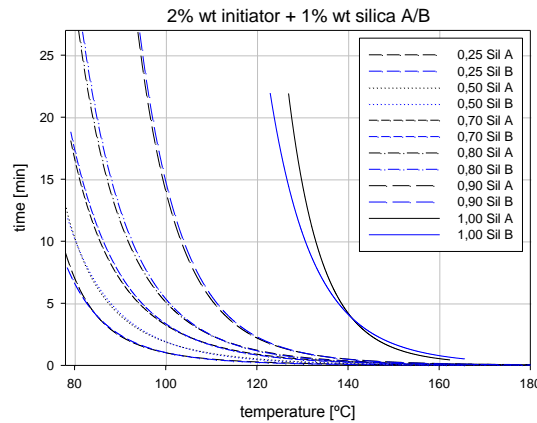


Figure 4.89 – Case V: iso-conversion curves for time versus temperature (2% wt of thermal-initiator and 1% wt of silica type A and B)

In addition to the analysis concerning the influence of the silica particle size on the cure kinetics cannot be overlooked that, in the case of silica B, larger particle size lead to significantly higher viscosity as well as reduce the geometric and dimensional accuracy. These aspects are of particular importance since viscosity not only influences the recoat time but also the ability to obtain uniform layers of very low thickness. Further, the resolution of the cured part is also affected because larger particles concentrate the energy in larger regions and therefore the control of the curing zone is limited to those dimensions.

4.3 - Modelling the curing kinetics

Kinetic models result in the evolution of reactive species concentration as a function of time using a reactive rate expression [5, 6]. Two different approaches are applied: using the concept of free-radical polymerisation (mechanistic models) or based on empirical kinetic models (phenomenological models) [7].

Mechanistic models are based on both the concept of free-radical polymerisation and the mechanisms of reactions with diffusion, requiring assumptions and approximations to simplify the complexity of the curing reaction [8, 9]. Several advantages are recognised to these models, however, the model equations include many parameters whose calculation involves the resolution of complex numerical optimisation schemes [9]. Thus, due to the complex nature of the curing reaction of thermosetting resins, commonly are used phenomenological models to describe these systems.

Phenomenological models assume that the curing process can be represented by one reaction, given by the following equation [5, 6]:

$$\frac{d\alpha}{dt} = k(T)f(\alpha) \quad (4.6)$$

where $d\alpha/dt$ is the reaction rate, $f(\alpha)$ is a function of conversion, and $k(T)$ is the chemical-controlled rate constant, function of temperature.

When non-isothermal experiments are performed, the function $f(\alpha)$ has to be specified, and is given by [5, 6]:

$$f(\alpha) = (1 - \alpha)^n \quad (4.7)$$

where n is a constant corresponding to the reaction order.

The rate constant observes an Arrhenius law and therefore is expressed by [5, 6]:

$$k(T) = k_0 \exp\left(\frac{-E}{RT_{abs}}\right) \quad (4.8)$$

where k_0 is a pre-exponential factor, E is the activation energy, R is the gas constant, T is the temperature in °C, and T_{abs} is the absolute temperature.

If an isothermal process showing a maximum value of reaction rate at a specific point is used, the previous model, so-called n th order kinetic, cannot be applied. In these case are used models based in autocatalytic mechanisms of reaction, resulting in the following equation [5, 6]:

$$\frac{d\alpha}{dt} = k_0 \exp\left(\frac{-E}{RT_{abs}}\right) \alpha^m (1 - \alpha)^n \quad (4.9)$$

where m and n are constants whose sum is the overall reaction order.

Autocatalytic models do not include the effects of the initiator concentration on the reaction rate requiring that the kinematic parameters must be recalculated for each resin composition. Another limitation is the inability to predict the diffusion-controlled effects after vitrification [6].

4.3.1 - Reaction order

The time required to reach the maximum value of reaction rate with isothermal curing temperature, t_p , is shown in Table 4.1. It is possible to observe that the maximum value of the rate of gel formation is attained for shorter reaction times as the isothermal curing temperature increases. It was found that this peak time decreases with the isothermal cure temperature in an exponential decay form ($r^2 = 1.000$ for the four cases) as shown in Figure 4.90.

The variation of the maximum rate of gel formation with isothermal curing temperatures is shown in Figure 4.91 for two different concentrations of initiator. The curves were fitted using sigmoidal equation ($r^2 = 0.9999$ for both cases) and expose three distinct regions. In region I, corresponding to low isothermal curing temperatures, it is possible to observe a small increase in the maximum value of reaction rate with temperature. The diffusion control effects appear early in the process which results in vitrification of reaction at an earlier stage. Also contributing

to the noticed effect, is the fact that the diffusivity of the reactive elements depends on the difference between the reaction temperature and the glass transition temperature [6, 10]. In region II the reactions occur closer to glass transition temperature and therefore the temperature has a great impact on the maximum value of gel formation rate. The diffusion control effects become less important and higher values of reaction rate and fractional conversion were obtained. In region III the impact of temperature is lower. The reaction proceeds in a more chemically controlled way since a dense network is formed and the larger polymer chains have reduced mobility and, therefore, the reaction rate cannot be significantly accelerated.

Table 4.1 – Summary of maximum conversion rate values and time to reach those values for different initiator concentrations

<i>Initiator concentration [%wt]</i>	<i>Cure temperature [°C]</i>	<i>(da/dt)_{max} [s⁻¹]</i>	<i>t_p [s]</i>
1	160	7,163	11,859
	140	4,769	16,434
	120	1,942	31,562
	100	0,344	148,651
3	160	10,328	8,822
	140	6,727	13,354
	120	4,332	21,329
	100	1,172	70,765
6	160	11,891	7,196
	140	7,448	10,075
	120	5,129	17,561
	100	1,511	48,680
9	160	14,320	6,037
	140	11,411	7,162
	120	6,272	11,561
	100	1,806	33,219

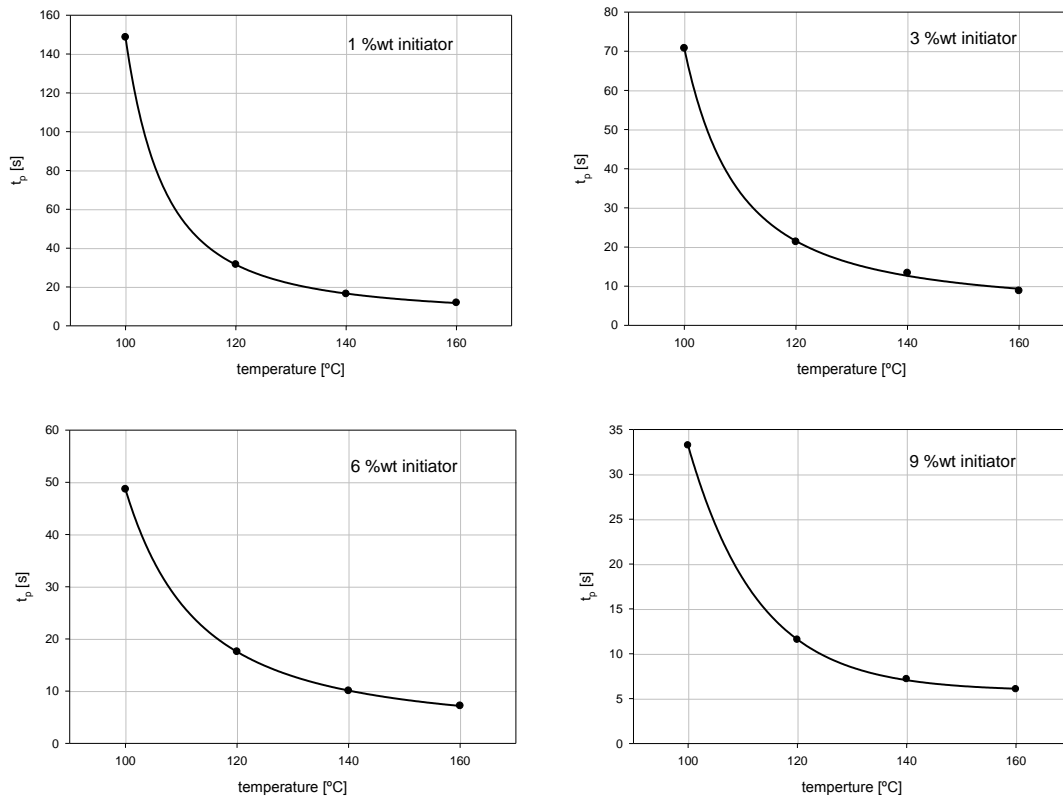


Figure 4.90 – Time to reach maximum values of conversion rate versus isothermal curing temperature for four different initiator concentrations

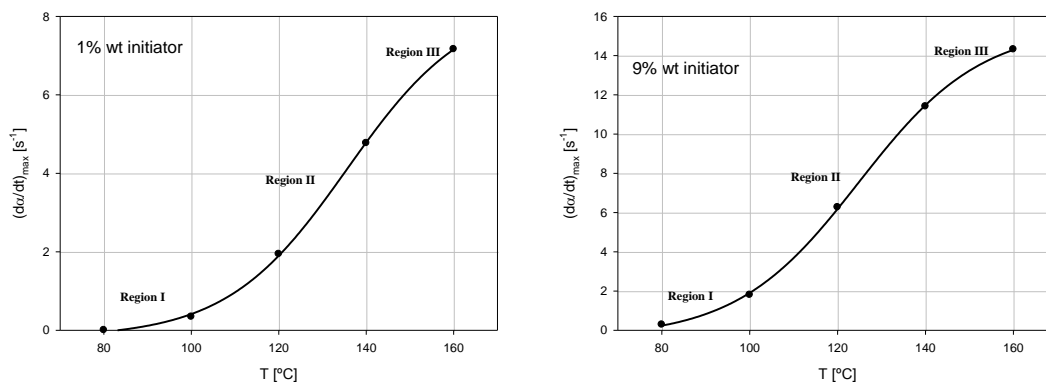


Figure 4.91 – Variation of the maximum value of gel formation rate versus curing temperature for 1% wt and 9% wt of initiator

In the Figure 4.92 is presented the time necessary to reach the reaction rate peak versus the initiator concentration for four different temperatures. Once more, it was found that this peak time decreases with the initiator concentration in an exponential decay form ($r^2= 0.997$ for $T=100$ °C, 0.986 for $T=120$ °C, 1.000 for $T=140$ °C, and 0.988 for $T=160$ °C).

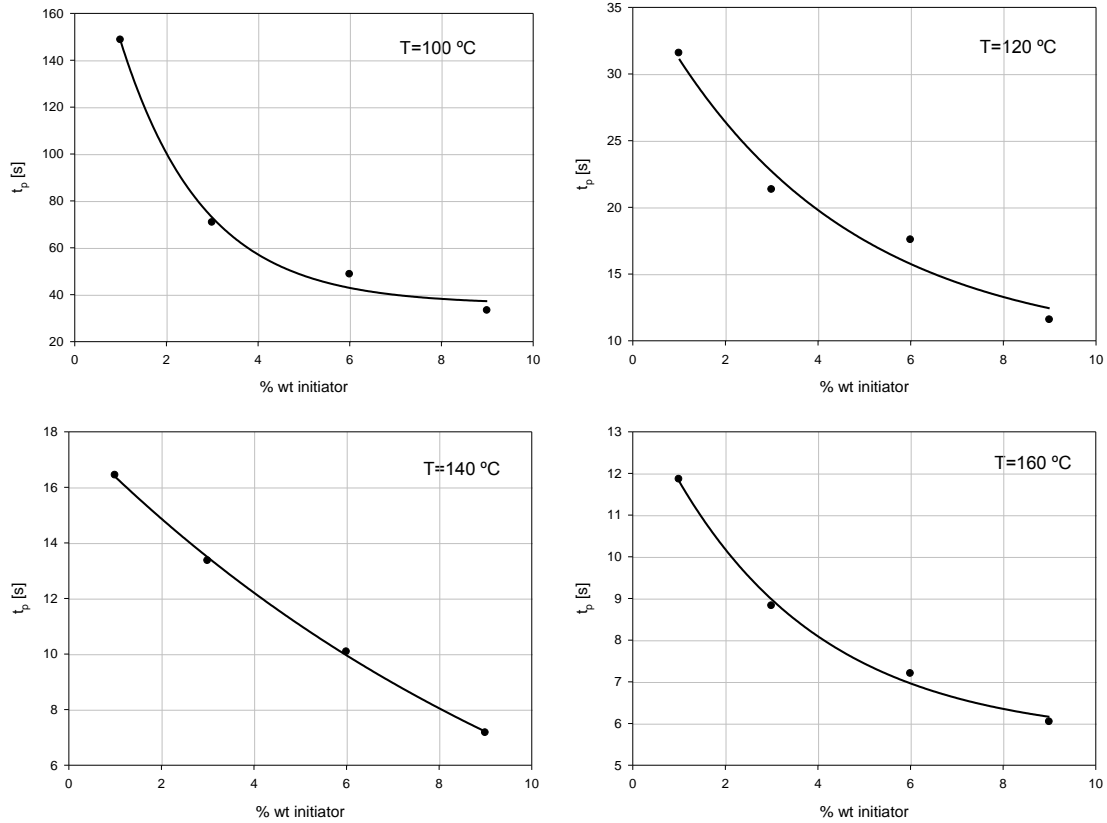


Figure 4.92 – Time to reach maximum values of conversion rate versus initiator concentration for four different temperatures

The rate of gel formation ($d\alpha/dt$) was analysed and the kinetic parameters were evaluated considering the maximum value of reaction rate defined by [6, 11, 12]:

$$\frac{d^2\alpha}{dt^2} = 0 \Rightarrow \alpha_p = \frac{m}{m+n} \quad (4.10)$$

where α_p is the fractional conversion that corresponds to the maximum value of reaction rate.

The overall reaction order is assumed to be two, therefore expressing a second order mechanism [6, 11, 12]:

$$m+n=2 \quad (4.11)$$

Reaction order, m and n , was computed according to experimental results and is shown in Figures 4.93 to 4.96. It can be verified that, for this temperature, there is no significant variation for reaction order for values of initiator concentration from 3 to more.

Infrared Stereolithography

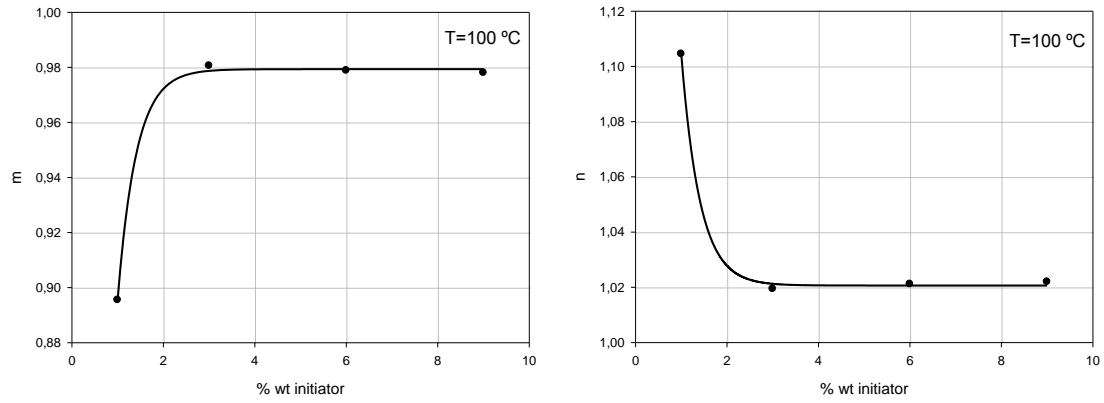


Figure 4.93 – Reaction order, m and n , versus initiator concentration for $T=100\text{ }^{\circ}\text{C}$

Similar behaviour was found for both computed temperatures $120\text{ }^{\circ}\text{C}$ and $140\text{ }^{\circ}\text{C}$, as shown in Figures 4.94 to 4.95. The value of reaction order m increases for increasing values of initiator concentration above 6 %wt. After this threshold, the reaction order starts to decrease.

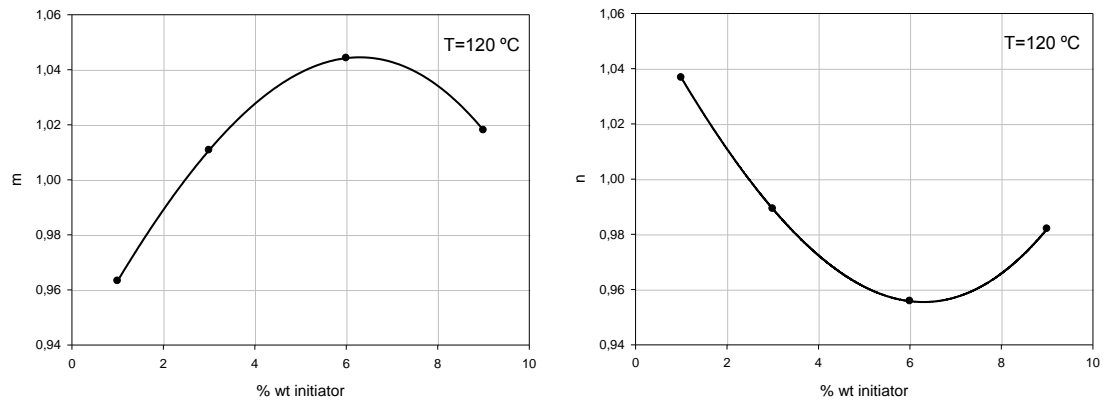


Figure 4.94 – Reaction order, m and n , versus initiator concentration for $T=120\text{ }^{\circ}\text{C}$

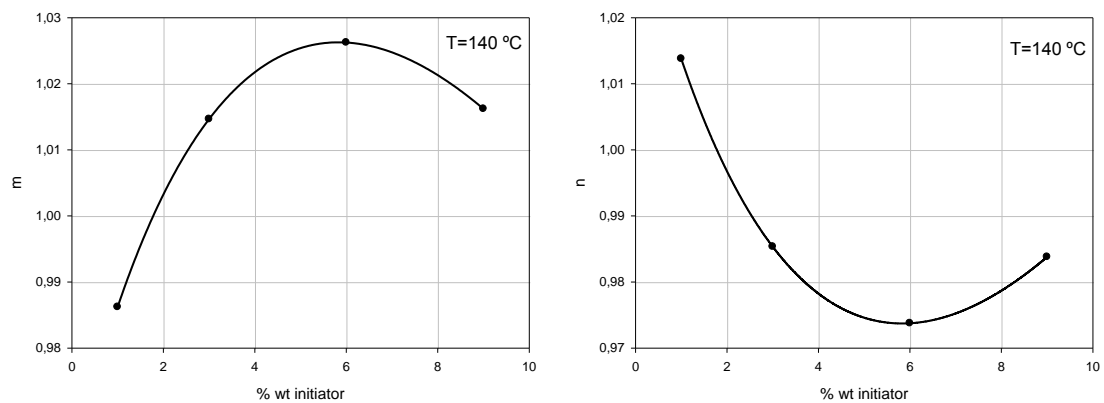


Figure 4.95 - Reaction order, m and n , versus initiator concentration for $T=140\text{ }^{\circ}\text{C}$

Despite of small differences observed, the tendency found for temperature of $160\text{ }^{\circ}\text{C}$ can be described as being similar to the observed for the previous temperatures since the calculated value m is approximately 1,025.

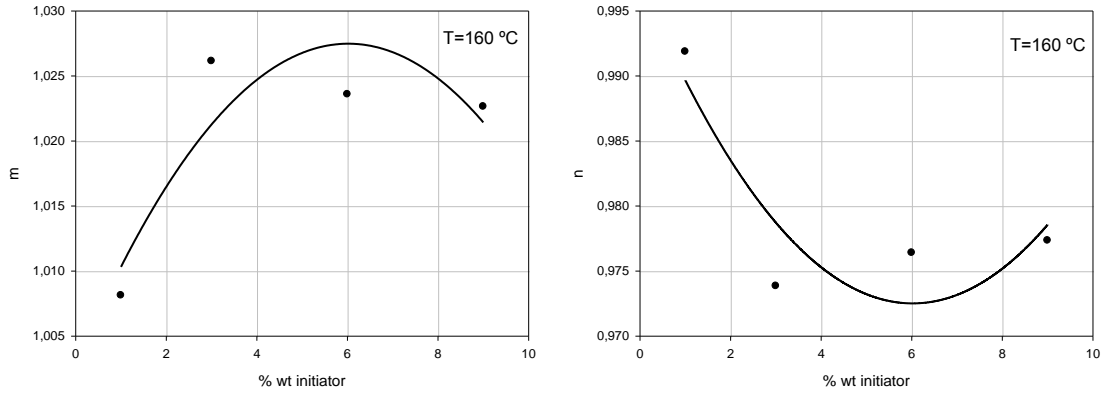


Figure 4.96 – Reaction order, m and n , versus initiator concentration for $T=160\text{ }^{\circ}\text{C}$

Usually reaction orders were considered as constants, *e.g.* independent of temperature and initiator concentration [11, 12], or in other cases, as linear functions of the temperature only [13], or even as functions of both the isothermal cure temperature and thermal initiator concentration [6]. The obtained results in this research, shown in Table 4.2, also suggest that the reaction orders are functions of both the isothermal cure temperature and thermal initiator concentration.

Table 4.2 – Summary of the kinetic parameters m and n

Initiator concentration [%wt]	Cure temperature [$^{\circ}\text{C}$]	Reaction orders	
		m	n
1	160	1,008	0,992
	140	0,986	1,014
	120	0,963	1,037
	100	0,895	1,105
3	160	1,026	0,974
	140	1,015	0,985
	120	1,010	0,990
	100	0,980	1,020
6	160	1,024	0,976
	140	1,026	0,974
	120	1,044	0,956
	100	0,979	1,021
9	160	1,023	0,977
	140	1,016	0,984
	120	1,018	0,982
	100	0,978	1,022

Figure 4.97 shows the reaction orders, m and n , as a function of isothermal cure temperature for 1% in weight of thermal initiator concentration. The reaction orders dependencies with the

temperature were fitted using a quadratic polynomial regression ($r^2=0,99$). The effect of temperature is more pronounced for lower temperatures. However, for the range of temperatures researched, the reaction order m continues to increase with temperature, although more smoothly. On the other hand the curing temperature has the opposite effect on reaction order n , which decreases with temperature.

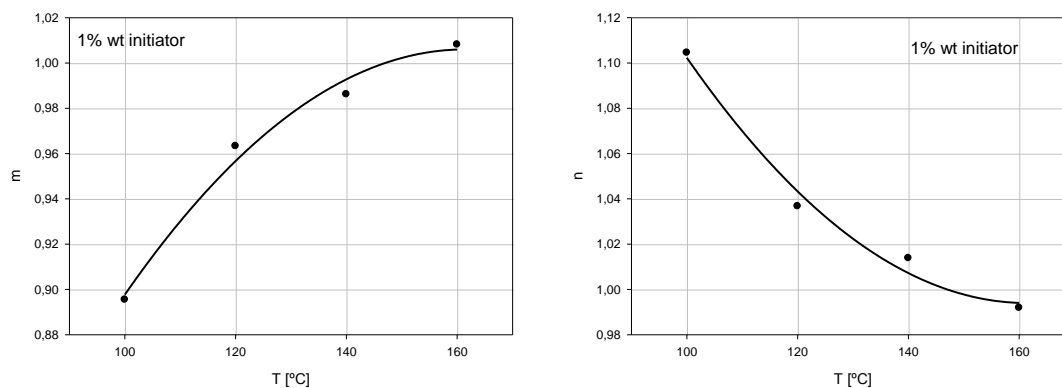


Figure 4.97 – Reaction orders m and n versus temperature for 1% wt of initiator concentration

The order of the reaction, according to its definition, indicates the number of atoms, molecules or reactive groups whose concentration determines the reaction rate [6]. Thus, for lower temperatures prevails the effect of vitrification. Increasing the curing temperature the mobility of the reactive elements is also increased and, therefore, the reaction rate increases reducing the diffusion-controlled effect over the cure reaction. Accordingly, the reaction order m increases with temperature.

4.3.2 - The activation energy

Kinetic information can be extracted from experimental data by means of various methods. One of those methods is based on Arrhenius equation, and assumes a single activation energy for the whole reactive process [6, 12-14]. This method is very useful to obtain accurate measures of activation energy and pre-exponential factor. To determine this kinetic parameters the expression (4.9) can be written in the logarithmic form [5]:

$$\ln\left(\frac{d\alpha}{dt}\right) = \ln k + m \ln \alpha + n \ln(1 - \alpha) \quad (4.12)$$

A multi-linear regression, using the least-squares method, of the triplets $(d\alpha/dt, \alpha, T)_i$ obtained by experimental measurements allow to determine the kinetic parameters. A linear representation of $\ln(k)$ against $1/T_{abs}$ makes possible to evaluate both the activation energy from the slope (E/R), and the pre-exponential factor from the ordinate at the origin.

The deviations from linearity indicated in Figure 4.98 reveals that it does not appear to exist a perfect correlation between experimental data and the Arrhenius approximation. A changeover point, for temperature around 130 °C, can be identified in the plots. For lower temperatures

$\ln(k)$ is highly dependent on the isothermal curing temperature. This dependence decreases for higher temperature in accordance with previous conclusions for region III of Figure 4.91. Similar behaviour was previously reported by Doornkamp and Tan [15], and Bártolo [6].

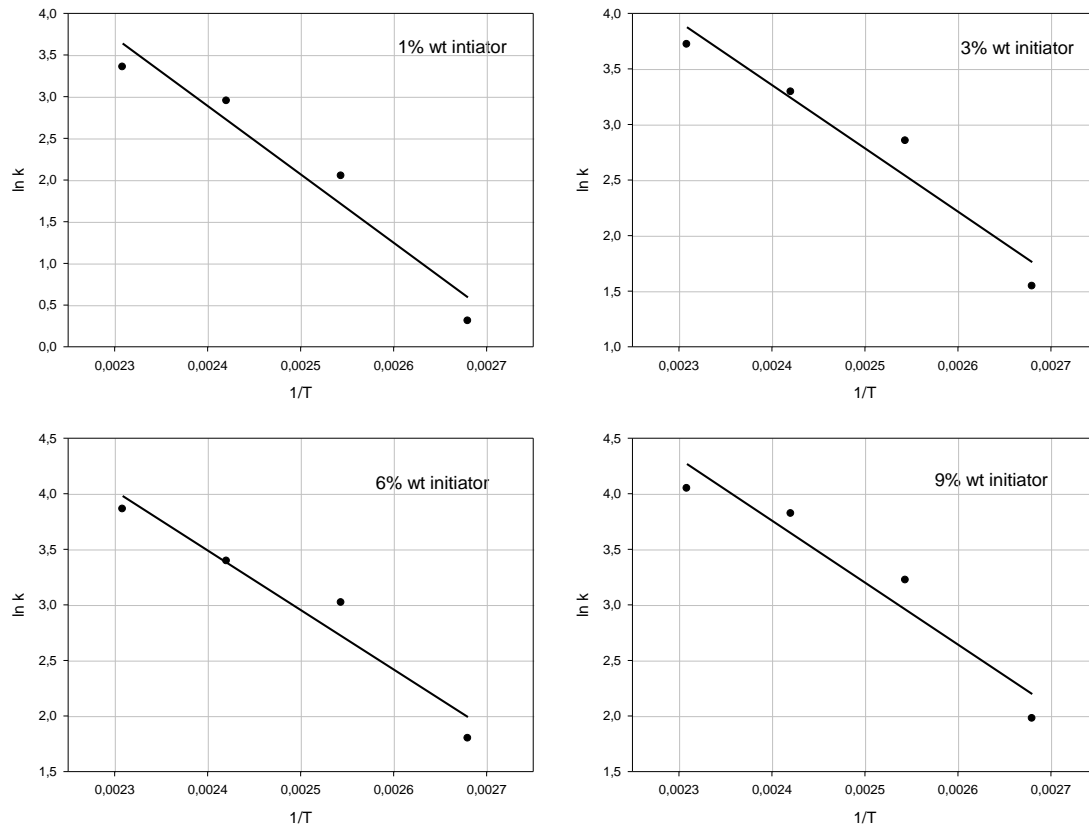


Figure 4.98 – Arrhenius plot of $\ln k$ versus $1/T$ for different concentrations of initiator

Values obtained for activation energy and pre-exponential factor, as well as the regression coefficients are indicated in Table 4.3.

Table 4.3 – Summary of activation energy and pre-exponential factor

<i>Initiator concentration [%wt]</i>	<i>E [kJ/mol]</i>	<i>K₀ [s⁻¹]</i>	<i>r²</i>
1	82,1	2,2x10 ⁵	0,941
3	56,9	1,7x10 ⁵	0,935
6	53,6	1,6x10 ⁵	0,940
9	55,8	1,7x10 ⁵	0,923

4.3.3 - The dependence of the rate constant with the initiator concentration

The chemical-controlled reaction rate (k) is dependent on the thermal initiator concentration as indicated in Figure 4.99 which plots the $\ln(k)$ as a dependent variable of $\ln(\text{thermal initiator concentration})$. Despite of that evidence, during many years this effect was not explicitly incorporated in the phenomenological models who considered k to be only temperature dependent. An expression to solve this limitation was proposed by Bártolo based on the plot of results of linear dependence of the type expressed in Figure 4.99 [6]:

$$k = \varphi \exp\left(\frac{-E}{RT_{abs}}\right) [\beta]^q \quad (4.13)$$

where φ is the pre-exponential factor of rate constant, q is an exponential parameter describing the initiator concentration dependence on the chemical-controlled rate constant, and $[\beta]$ is the thermal initiator concentration (in % wt).

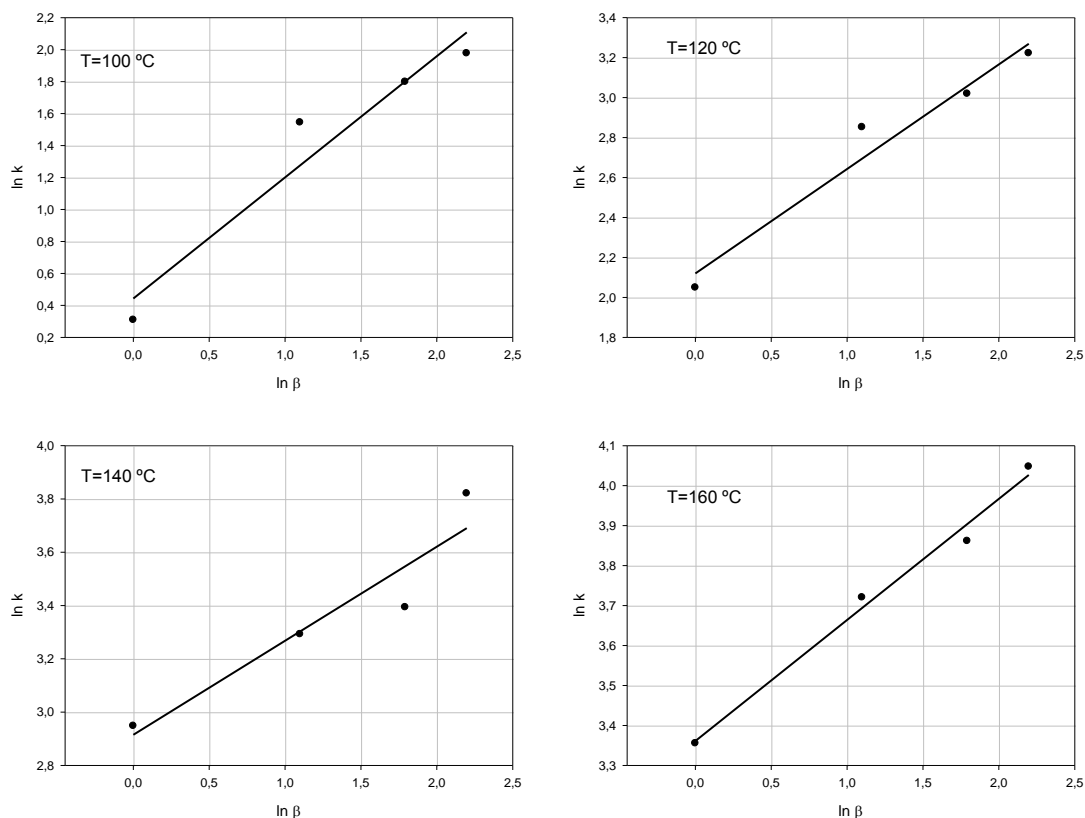


Figure 4.99 – Variation of $\ln k$ versus $\ln \beta$ for four different isothermal temperatures

Taking the equation (4.13) in the logarithmic form, the following expression is obtained:

$$\ln k = \ln \varphi + q \ln [\beta] - \frac{E}{RT_{abs}} \quad (4.14)$$

Considering that $\ln(\varphi)$ and $[-E/(RT_{abs})]$ are constants and can be incorporated into a single constant, Z :

$$\ln k = Z + q \ln[\beta] \quad (4.15)$$

Equation (4.15) corresponds to the lines plotted in Figure 4.99, where q is the slope and Z is the ordinate at the origin. The values obtained for each isothermal curing temperature are presented in Table 4.4 and the corresponding curve is plotted in Figure 4.100.

Table 4.4 – Summary of q values obtained for each temperature

Cure temperature [°C]	q	R^2
160	0,303	0,989
140	0,353	0,892
120	0,523	0,958
100	0,758	0,937

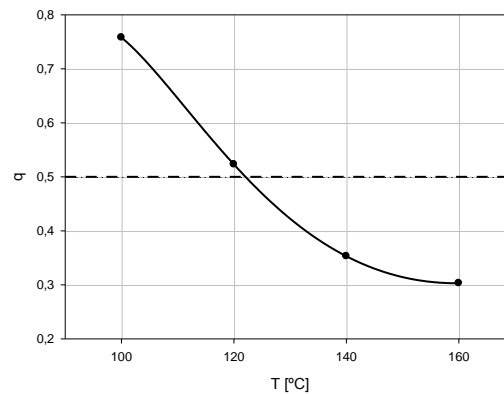


Figure 4.100 – Exponential parameter q versus temperature

Figure 4.100 puts in evidence the deviation from the classical 0,5 order of dependence of the polymerisation reaction rate relatively to the initiator concentration corresponding to unimolecular termination. For lower isothermal curing temperature ($T= 100\text{ }^{\circ}\text{C}$) the dependence obtained ($q= 0,758$) indicates that the reaction of polymerising chains terminate by two types of reaction; the usual bimolecular termination mechanism and a first order process involving only one polymer radical as a result of radical trapping or unimolecular termination. This type of termination occurs in the sequence of the increase of viscosity during the course of curing reaction. Initially, the bimolecular termination mechanism is the predominant process. However, as the viscosity increases the chains mobility is severely reduced and it starts to prevail radical termination by occlusion [6, 16]. The exponent obtained for the temperature of $100\text{ }^{\circ}\text{C}$ ($q= 0,758$) indicates that the radical trapping or unimolecular termination mechanisms is significant during the all reaction, i.e. vitrification effects prevail. For higher temperatures ($T= 140\text{ }^{\circ}\text{C}$ and $160\text{ }^{\circ}\text{C}$) unimolecular termination no longer prevail due to the fast polymerisation promoted by those elevated values of temperature and therefore values lower than 0,5 where obtained for the dependence factor ($q= 0,353$ and $0,303$).

4.3.4 - Prediction of fractional conversions

The prediction of the global temperature, due to the chemical reaction and the laser irradiation effect, is crucial for the design and optimisation of any stereolithographic system. The value of the fractional conversion, obtained at a specific time during the course of the chemical reaction represents another important parameter to be determined.

Several kinetic models have been proposed to simulate thermosetting cure reactions. The most complex models, based on a mechanistic approach of cure reactions, are developed based on the concepts of free radical polymerization and the mechanism of reactions with diffusion. However, mechanistic models are usually quite impractical for engineering purposes because of the difficulty in obtaining the model parameters. An alternative to these mechanistic models are the phenomenological models, formulated in terms of the degree of cure and much easier to apply. Phenomenological models have been largely used to study thermal-initiated cure reactions.

Computational modelling of stereolithographic processes

To simulate the curing process of stereolithographic applications a proper model was developed based on the fundamental physical and chemical phenomena that govern the behaviour of a thermosetting material in both thermal-initiated and photo-initiated curing applications. A number of assumptions were made for its development:

- a simplified isotropic/orthotropic material, whose properties are independent of the curing stage;
- a well-mixed and homogeneous initial system;
- any optical scattering effects and the flow of material due to convection or diffusion are both considered negligible;
- the internal heat generation is only due to the heat of polymerisation; and
- the absorption of radiation is defined by the Beer-Lambert law.

According to the model, the temperature field in the exposed region of the polymeric material is described by the following heating conduction equation in cylindrical coordinates (r, z):

$$\frac{1}{r} \frac{\partial}{\partial r} \left(r k_r \frac{\partial T}{\partial r} \right) + \frac{\partial}{\partial z} \left(k_z \frac{\partial T}{\partial z} \right) + \dot{Q} = \rho C \frac{\partial T}{\partial t} \quad (4.16)$$

where k is the thermal conductivity, T is the temperature, ρ is the density, C is the specific heat of the material, and t is the time. \dot{Q} describes the heat generation rate due to the exothermic polymerizing reaction and is obtained by the following equation:

$$\dot{Q} = \rho H \frac{d\alpha}{dt} \quad (4.17)$$

where H is the total heat release, and $d\alpha/dt$ corresponds to the kinetic model.

The solution of equation (4.16) requires both knowledge of the initial temperature, T_i , and the initial value of the fractional conversion, α_i , in the domain Ω being studied:

$$T(\nu, 0) = T_i \quad (4.18)$$

$$\alpha(\nu, 0) = \alpha_i \quad (4.19)$$

where ν represents a generic point in the space.

Additionally, the solution of equation (4.16) must satisfy the following boundary conditions:

$$(1) \text{ Specified temperature: } T_s = T(\nu, t) \quad (4.20)$$

$$(2) \text{ Specified light intensity: } k_n \frac{\partial T}{\partial n} - I(\nu, t) = 0 \quad (4.21)$$

$$(3) \text{ Convection boundary conditions: } k_n \frac{\partial T}{\partial n} + h[T(\nu, t) - T_\infty] = 0 \quad (4.22)$$

where T_s is the specified temperature, I is the light intensity, $\partial T/\partial n$ is the derivative of temperature in the direction normal to the surface, h is the coefficient of heat transfer, and T_∞ is the temperature of the surrounding space. As a final remark, it is worth noting that the term $k_n \partial T/\partial n$ is given by:

$$k_n \frac{\partial T}{\partial n} = k_r \frac{\partial T}{\partial r} \cos(n_r) + k_z \frac{\partial T}{\partial z} \cos(n_z) \quad (4.23)$$

Light intensity values at the resin surface, I_s , are defined by assuming a Gaussian intensity distribution as follows:

$$I_s(\nu, t) = I_0 \exp \left[-2 \left(\frac{s(\nu, t)}{w_0} \right)^2 \right] \quad (4.24)$$

whit I_0 being the peak light intensity, $s(\nu, t)$ representing the position in time of a point under irradiation, and w_0 corresponding to the beam radius. The decrease in light intensity with depth is assumed to obey the Beer-Lambert law according to the following equation:

$$I_d(\nu, t) = I_s(\nu, t) \exp[-\varepsilon[\beta]y] \quad (4.25)$$

where I_d represents the variation of the light intensity along the thickness of the resin layer, ε is the absorptivity of the initiator, $[\beta]$ is the initiator concentration, and y represents the penetration depth. For irradiation problems through masks, Fresnel's diffraction theory is applied to evaluate the effect of diffraction.

The kinetic models considered, representing a realistic approach to describe the major phenomena (vitrification, incomplete conversion, radical trapping, etc.) occurring during curing reactions, is represented by the following equations [8]:

- thermal-initiated curing reactions:
$$\frac{d\alpha}{dt} = \varphi \exp\left(\frac{-E}{RT_{abs}}\right) [\beta]^q \alpha^m (1-\alpha)^n \quad (4.26)$$

- photo-initiated curing reactions:
$$\frac{d\alpha}{dt} = \varphi I^p \exp\left(\frac{-E}{RT_{abs}}\right) [\beta]^q \alpha^m (1-\alpha)^n \quad (4.27)$$

where φ is the pre-exponential factor of the rate constant, I is the light intensity, E is the activation energy, R is the gas constant, T_{abs} is the absolute temperature, p and q are constants, and the exponents m and n represent the reaction orders, with the sum $(m + n)$ being the overall reaction order. The kinetic parameters, m , n , and E , are not constants for this equation. Diffusion-controlled effects were not included in the kinetic equations.

The photo-thermal-kinetic model is solved using the finite element method (FEM), with linear rectangular elements and an appropriate time marching scheme as described later. Fractional conversions are evaluated by integrating (with respect to time) the rate of gel formation equation using the fourth-order fixed step-size Runge-Kutta technique.

The basic concept in FEM is the discretization of a general domain (continuum domain) into a finite number of subdomains, called elements. These elements are connected to each other by points called nodes, forming a grid of cells named as finite element mesh. The parameters assigned to each element or nodal variable are called degrees of freedom of the element. In a continuum domain, a field variable has an infinite number of unknowns because it is a function of each generic point in the domain. The finite element discretization will reduce the problem to one of a finite number of unknowns, with the behaviour of the field variable within an element being represented through approximating functions called shape or interpolation functions. Through the FEM, the governing equations, usually in differential or integral form, are transformed into a set of algebraic equations, which are easier to manipulate. The solution of these equations gives the approximate behaviour of the continuum medium.

The numerical solution of equation (4.16), subjected to initial conditions, equations (4.18) and (4.19), and to boundary conditions, equations (4.20) to (4.22), involves two stages of approximation:

- spatial approximation using the Galerkin method; and
- temporal approximation using the Crank-Nicolson method.

The discretisation of equation (4.16) in space is accomplished by the discretisation of the generic domain Ω into an appropriate collection of finite elements, Ωe_i , connected at nodes as follows:

$$\Omega = \sum_{i=1}^k \Omega e_i \quad (4.28)$$

with k being the number of elements and Ωe representing each element domain.

The element shape functions N_i are used to interpolate the temperature [17]:

$$T(\nu, t) = \sum_{i=1}^j N_i(\nu) T_i(t) \quad (4.29)$$

where j represents the number of nodes of the considered element, and T_i are the nodal temperatures (in this case, $j = 4$ as linear rectangular elements are considered).

Using the Galerkin method, equation (4.16) can be rewritten at the element level in the following form:

$$\int_{\Omega_e} N_i^e \left\{ \left[\frac{\partial}{\partial x} \left(k_x \frac{\partial}{\partial x} \right) + \frac{\partial}{\partial y} \left(k_y \frac{\partial}{\partial y} \right) \right] N_j^e T_j^e + \rho H \frac{d\alpha}{dt} - \rho C \frac{\partial}{\partial t} N_j^e T_j^e \right\} d\Omega = 0 \quad (4.30)$$

Applying Gauss's theorem to the equation and after insertion of boundary conditions, the following relation is obtained:

$$\begin{aligned} & - \int_{\Omega_e} \left(\frac{\partial N_i^e}{\partial x} k_x \frac{\partial N_j^e}{\partial x} + \frac{\partial N_i^e}{\partial y} k_y \frac{\partial N_j^e}{\partial y} \right) T_j^e dxdy + \int_{\Omega_e} N_i^e \rho H \frac{d\alpha}{dt} dxdy \\ & - \int_{\Omega_e} N_i^e \rho C N_j^e \dot{T}_j^e dxdy + \oint_{\Gamma_e} N_i^e \left[I - h(N_j^e T_j^e - T_\infty) \right] d\Gamma = 0 \end{aligned} \quad (4.31)$$

where the dot denotes the time differentiation. After some manipulations, equation (4.31) becomes:

$$\begin{aligned} & \int_{\Omega_e} N_i^e \rho C N_j^e \dot{T}_j^e dxdy + \int_{\Omega_e} \left(\frac{\partial N_i^e}{\partial x} k_x \frac{\partial N_j^e}{\partial x} + \frac{\partial N_i^e}{\partial y} k_y \frac{\partial N_j^e}{\partial y} \right) T_j^e dxdy \\ & + \oint_{\Gamma_e} N_i^e h N_j^e T_j^e d\Gamma = \int_{\Omega_e} N_i^e \rho H \frac{d\alpha}{dt} dxdy + \oint_{\Gamma_e} N_i^e I d\Gamma + \oint_{\Gamma_e} N_i^e h T_\infty d\Gamma \end{aligned} \quad (4.32)$$

Equation (4.32) can also be expressed in a matrix form, using the following equation:

$$[C]\{\dot{T}\} + [K]\{T\} = \{F\} \quad (4.33)$$

where C is the heat capacity matrix, K is the conductivity matrix and F is the equivalent nodal heat flow vector. In irradiated processes, because of the shape of the light beam, a cylindrical coordinate system (r, θ, z) must be used. For this situation, assuming that the resin is spatially homogeneous, cylindrical symmetry can be assumed. This means that both the geometry and

boundary conditions are independent of the angular coordinate θ . This allows light intensities, fractional conversions, rates of gel formation, and temperatures to be functions of the two spatial coordinates (r, z) and time. In these cases, the integration with respect to θ yields a multiplicative constant 2π , and the matrix elements in the equation (4.33) become:

$$C_{ij}^e = 2\pi \int_{\Omega_e} N_i^e \rho C N_j^e r dr dz \quad (4.34)$$

$$K_{ij}^e = 2\pi \int_{\Omega_e} \left(\frac{\partial N_i^e}{\partial r} k_r \frac{\partial N_j^e}{\partial r} + \frac{\partial N_i^e}{\partial z} k_z \frac{\partial N_j^e}{\partial z} \right) r dr dz + 2\pi \oint_{\Gamma_e} N_i^e h N_j^e r d\Gamma \quad (4.35)$$

$$F_i^e = 2\pi \int_{\Omega_e} N_i^e \rho H \frac{d\alpha}{dt} r dr dz + 2\pi \oint_{\Gamma_e} N_i^e I d\Gamma + 2\pi \oint_{\Gamma_e} N_i^e h T_\infty r d\Gamma \quad (4.36)$$

The two-time-level Crank-Nicolson algorithm method of unconditional stability was used to integrate equation (4.33) with respect to time [17, 18]. According to this algorithm, the unknown values of temperature at time point t_{n+1} are determined by the known temperatures at time point t_n , considering the following temporal approximation:

$$\{T\}_{n+1}^e = \{T\}_n^e + \theta \Delta t \left(\{\dot{T}\}_{n+1}^e + \{\dot{T}\}_n^e \right) \quad (4.37)$$

Depending on θ values different methods can be considered:

$$\theta = \begin{cases} 0 & \text{Progressive differences method} \\ 1/2 & \text{Crank-Nicolson method} \\ 2/3 & \text{Galerkin method} \\ 1 & \text{Regressive differences method} \end{cases}$$

Equation (4.37) can be applied to the matrix equation (4.33) that becomes:

$$(C + \theta \Delta t K) T_{n+1} = [C - (1 - \theta) \Delta t K] T_n + \Delta t [\theta F_{n+1} + (1 - \theta) F_n] \quad (4.38)$$

where the subscript denotes the time at which the corresponding term must be evaluated, and Δt is the time step.

Linear rectangular elements were considered and the concept of isoparametric formulation was used [17, 18].

Numerical integration is used to evaluate equations (4.34) to (4.36). The Gauss-Legendre quadrature rules were used to perform such a numerical integration. Numerical quadrature formulas in quadrilateral elements have the following form [17, 18]:

$$\int_{\Omega_e} F(\xi, \eta) d\xi d\eta = \int_{-1}^1 \int_{-1}^1 F(\xi, \eta) d\xi d\eta \approx \sum_{i=1}^k \sum_{j=1}^k F(\xi_i, \eta_j) W_i W_j \quad (4.39)$$

where W_i and W_j are the weighting gauss factors and k is the number of integration or gauss points. A 2 x 2 integration rule for linear rectangular elements is used. The corresponding values for quadrature points and weighting factors are indicated in Table 4.5 [19].

Table 4.5 – Values for the Gauss points and weighting factors

$k \times k$	ξ_i	η_j	W_i	W_j
2 x 2	-0.57735	-0.57735	1	1
	-0.57735	0.57735		
	0.57735	-0.57735		
	0.57735	0.57735		

Simulation of isothermal reactions in thermo-initiated processes

The proposed model was used to predict curing profiles for samples of unsaturated polyester resin (UP resin) containing 2 and 0.5 wt% of thermo-initiator, cured at different temperatures. Material parameters values used in these simulations are summarised in Table 4.6. Some of these values were experimentally determined, whereas others were obtained from relevant literature sources [6, 20, 21].

Table 4.6 – Material properties used in the simulations

<i>Property</i>	<i>Value</i>
Density	1.1 g/cm ³
Heat of polymerisation	335 J/g
Glass transition temperature of the fully cured polymer	125 °C
Specific heat	1.674 J/(g °C)
Thermal conductivity	0.0017 W/(cm °C)
Heat transfer	0.002 W/(cm ² °C)
Heat of reaction	335 J/g
Absorptivity of photo-initiator	5 (wt % of PI cm) ⁻¹

The effect of the curing temperature and initiator concentration on the curing kinetics is shown in Figures 4.101 and 4.102. Results show that, after an initial period, called induction time [1], more significant for samples cured at low temperatures and containing low amounts of thermo-initiator, the conversion rate increases rapidly followed by a progressive slowing down, until the cure profile reaches a plateau corresponding to the maximum value of the fractional conversion.

This progressive slowing down is due to diffusion constraints on the mobility of the reacting species. The viscosity increases as the solidification progresses and, at the vitrification point, the viscosity of the medium is so high that the diffusivity of reactive groups becomes seriously restricted, so the reaction eventually stops. Results also show that, by increasing both temperature and initiator concentration both the reaction rate and the fractional conversion increase while the induction time decreases as well the need of post-curing operations.

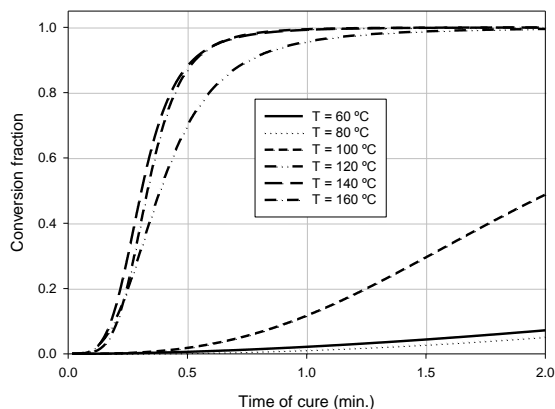


Figure 4.101 – Profiles of fractional conversion versus curing time for UP resin samples containing 2% wt of thermal-initiator cured at different temperatures

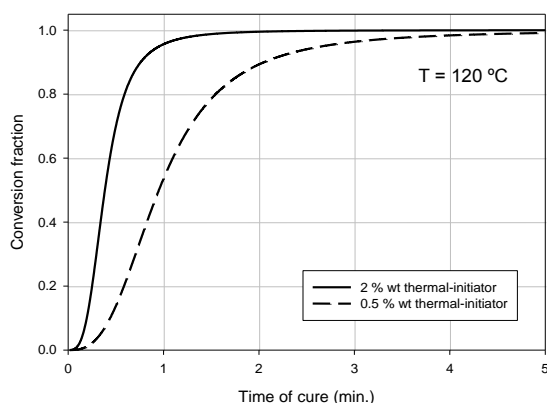


Figure 4.102 – Profiles of fractional conversion versus curing time for UP resin samples containing 2% wt and 0.5% wt of thermal-initiator cured at 120 °C

The variation of the reaction or conversion rate, as a function of time for different curing temperatures is shown in Figure 4.103. It is possible to observe that, at the lowest temperatures, the conversion rate is low but increases rapidly by increasing the curing temperature. Figure 4.104 shows the variation of conversion rate with the fractional conversion for different curing temperatures. Results show that, by increasing the curing temperature, the maximum value of conversion rate occurs also for higher fractional conversion values, owing to an increase on the mobility of reactive species and reduction of vitrification effects.

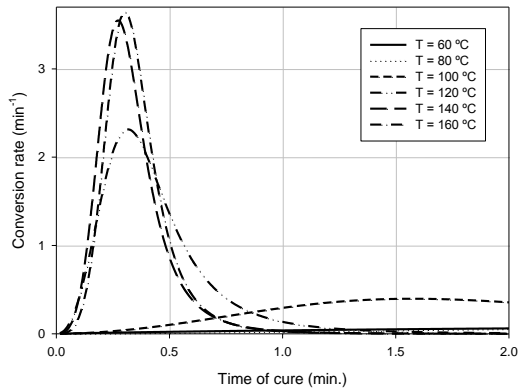


Figure 4.103 – Conversion rate versus curing time for UP resin samples containing 0.5% wt of thermal-initiator cured at different curing temperatures

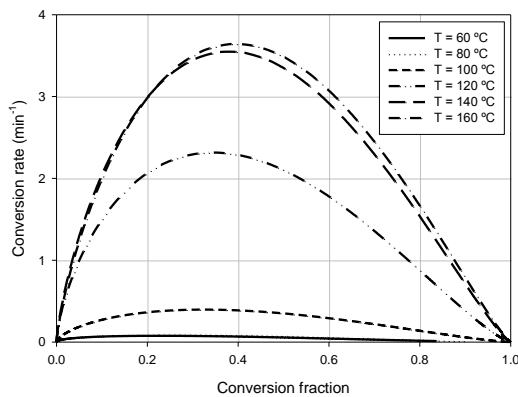


Figure 4.104 – Conversion rate versus fractional conversion for UP resin samples containing 0.5% wt of thermal-initiator cured at different curing temperatures

Simulation of photo-initiated processes in polymeric systems submitted to constant intensities of radiation

In this case UP resin samples containing 0.2% wt of photo-initiator were irradiated at different light intensities. All curing reactions are conducted at 25 °C. The obtained conversion profiles are shown in Figure 4.105. Results show that, after an induction time more evident for low light intensity values, the reaction rate increases rapidly. The maximum conversion is earlier achieved for higher light intensities.

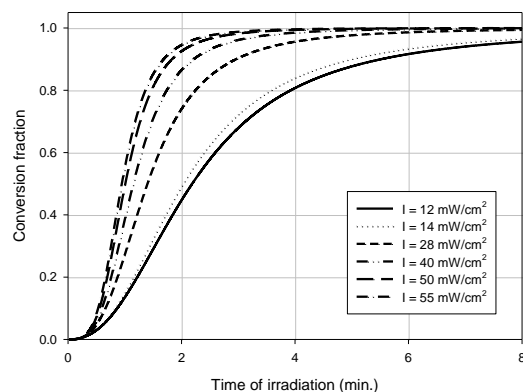


Figure 4.105 – Fractional conversion versus curing time for UP resin samples containing 0.2% wt of photo-initiator cured at different light intensities

Simulation of photo-initiated processes at polymeric systems submitted to a radiation profile

The model was first used to predict the necessary time to achieve a complete cure (no diffusion-controlled effect were considered) for a UP resin layer containing 0.2% wt of photo-initiator, which was irradiated at room temperature using an UV lamp. A resin layer with 0.9 cm thickness and 0,7 cm length was considered. In addition, the centre of the layer and the centre of the light beam, which has a Gaussian distribution profile (see Figure 4.106), were assumed to be coincident. Consequently, only one half of the resin layer was considered for simulation purposes because of the geometry and light distribution symmetry of the problem. For simulation purposes, a mesh of 210 linear rectangular elements was used (7 elements along the radial direction and 30 along the thickness direction), with dimensions of 0.05 cm x 0.03 cm.

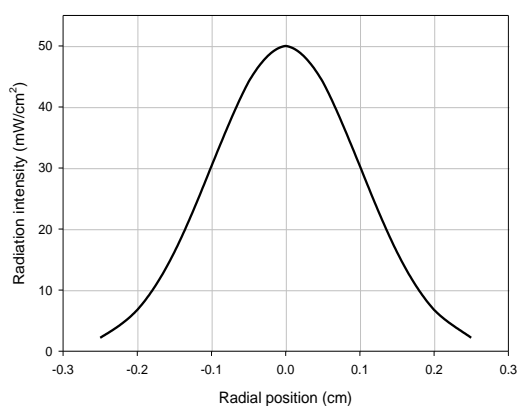


Figure 4.106 – Light intensity profile at the resin surface

Figure 4.107 shows contour plots of fractional conversion for different exposure times. The fractional conversion contour indicates a conical variation, which can be an important factor in terms of the quality of the final models. Higher fractional conversions are obtained at the resin surface because of the high light intensity values. For longer exposure times, it is possible to observe an increase of the fractional conversion with depth because of an increase of the energy

values supplied to the resin layer. As a consequence of the decrease of light intensity with depth according to Beer-Lambert law, it is possible to observe that with both the light intensity and the photo-initiator concentration considered in this case, it is not possible to solidify all the thickness.

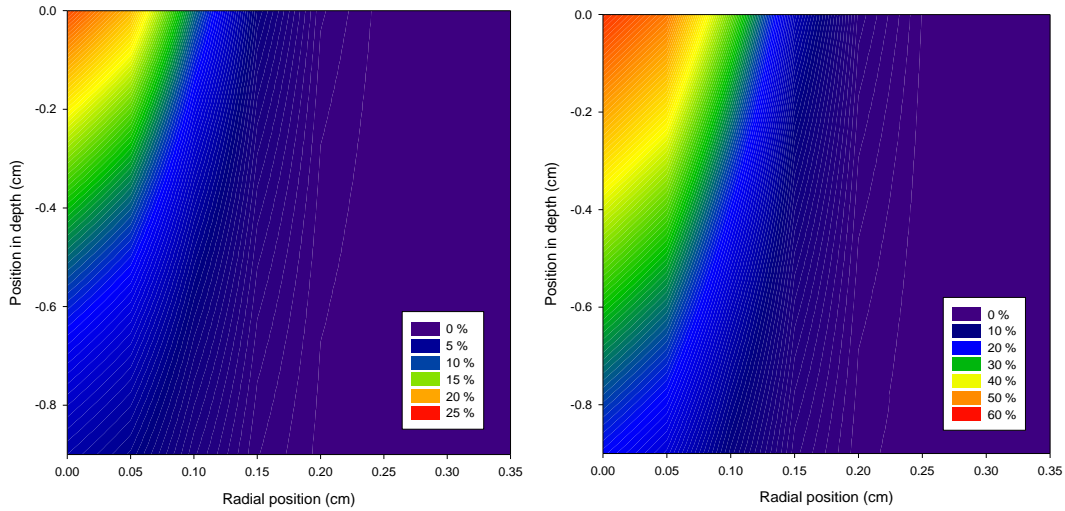


Figure 4.107 – Contour plot showing the variation of fractional conversion as a function of position. Irradiation times: (a) 10 and (b) 15 min. Light intensity: 50 mW/cm² of intensity. UP sample containing 0.2% wt of photo-initiator

Figures 4.108 and 4.109 illustrate the effect of both light intensity and photo-initiator concentration on the curing process. The reaction rate increases by increasing both light intensity and initiator concentration as expected. However, the increase of the photo-initiator concentration decreases the light penetration depth due to shadow effect.

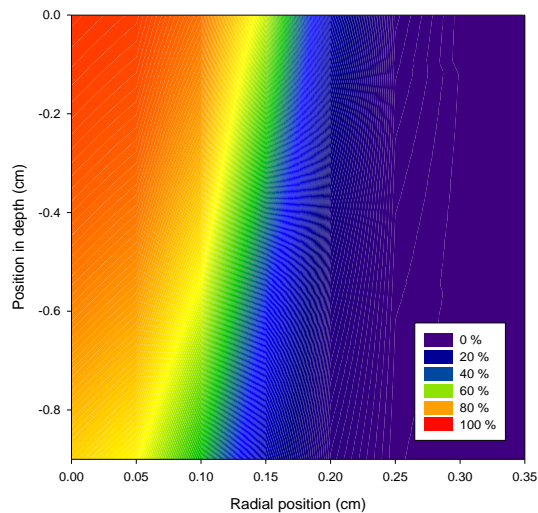


Figure 4.108 – Contour plot showing the variation of fractional conversion as a function of position. Irradiation time: 10 min. Light intensity: 100 mW/cm² of intensity. UP sample containing 0.2% wt of photo-initiator

Infrared Stereolithography

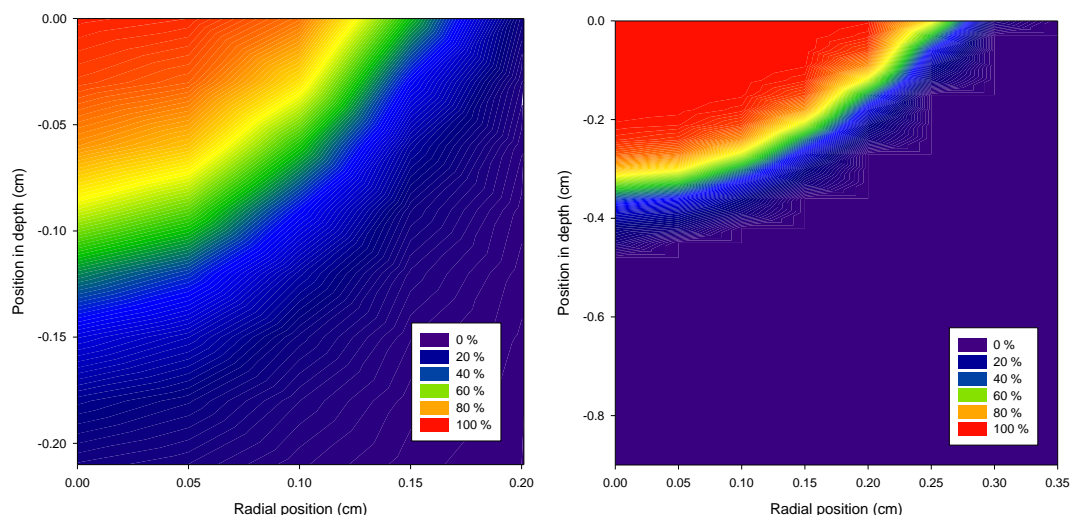


Figure 4.109 – Contour plot showing the variation of fractional conversion as a function of position. Irradiation times: (a) 1 and (b) 5 min. Light intensity: 100 mW/cm^2 of intensity. UP sample containing 2% wt of photo-initiator

The photo-thermal-kinetic model was also used to study the effect of the irradiation from two different light sources having both a maximum light intensity of 100 mW / cm^2 . The relative position between the two light sources is shown in Figure 4.110 and the irradiation time was 1 minute. The conversion profile is indicated in Figure 4.111 (a). As in the previous case, results show a parabolic profile for the curing process and, in this particular case, symmetry due to the two irradiation sources (w-like profile of fractional conversion). Maximum values of fractional conversion are also observed at the centre of each irradiation profile. The w-like profile of fractional conversion for two light sources can be improved by reducing the distance between the centres of each irradiation profile (Figure 4.111 (b)) or by increasing the difference of maximum light intensities between the two irradiation profiles (Figure 4.112).

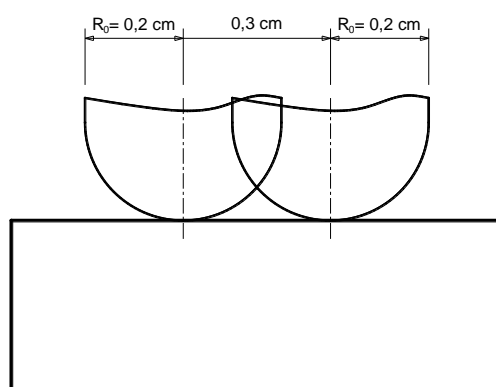


Figure 4.110 – Irradiation through two light sources

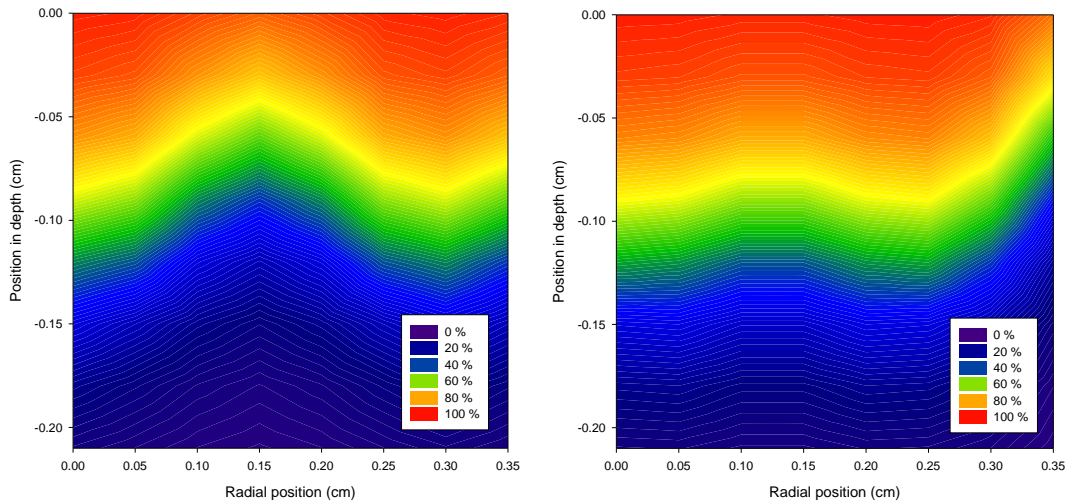


Figure 4.111 – Contour plot showing the variation of fractional conversion as a function of position for an irradiation process using two light beams of same intensity. Distance between the centres of the light beams: (a) 0.30 cm and (b) 0.25 cm

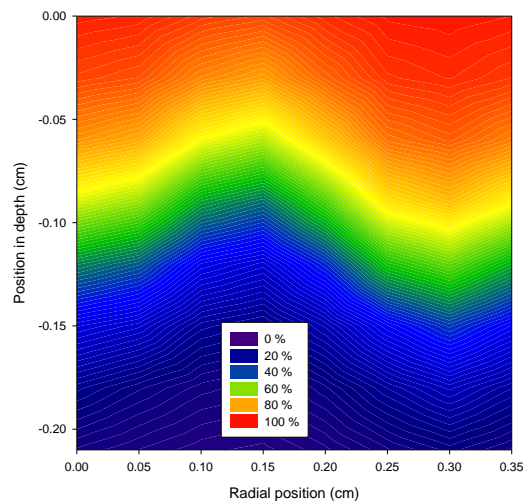


Figure 4.112 – Contour plot showing the variation of fractional conversion as a function of position for an irradiation process using two light beams of different intensities. Distance between the centres of the light beams: 0.25 cm. Maximum light intensity: 100 mW/cm² (left beam) and 120 mW/cm² (right beam)

Based on the understanding of the fundamental physical and chemical phenomena governing the curing behaviour of an UP resin, a photo-thermal-kinetic model was used for simulation purposes. This model assumes a Gaussian intensity distribution of light at the resin surface, the Beer-Lambert law to model the decrease in light intensity with depth, and Fresnel's diffraction theory to evaluate the effect of diffraction. The model has been numerically solved using the finite element technique. The finite element model has been developed by using the Galerkin method for spatial discretisation and the Crank-Nicolson method for temporal discretisation. Linear rectangular elements have been considered and the concept of isoparametric formulation used. This model describes the major events occurring during the chemical process of liquid resin solidification, enabling to control and optimise the most important curing parameters.

Results show that, by increasing the temperature, light intensity and initiator, the reaction rate increases while the induction time decreases. For radiation profiles, because of the decrease in light intensity with depth, fractional conversion contours show a conical variation, which could be an important factor in terms of the quality of the obtained models. This effect can be minimised by decreasing the concentration of photo initiator because more light can be absorbed along the thickness of the resin layer. Light intensity increases the rate of gel formation. Consequently, higher values of fractional conversion are obtained and the necessary exposure time is reduced.

4.4 - Summary

Experimental techniques to study cure kinetics are described and experimental results are presented and discussed. The effect of parameters, such as temperature, initiator concentration, and silica content are discussed as well as the dependence between the curing kinetic parameters and those factors. Both gel content method and Vyazovkin model were used in this extensive experimental work.

Thermal-initiated reactions were performed to evaluate and model the effect of specific parameters over the cure kinetics. Five cases are used to analyse and discuss the effect of those parameters, namely curing temperature, initiator concentration, initiator concentration using Vyazovkin model, silica concentration and silica particle size.

Phenomenological models used to describe cure kinetics were presented. The model considers samples with different amounts of initiator concentration and cure reactions performed under different conditions of irradiation. In order to solve the models, the parameters involved were calculated based in experimental data presented previously.

To simulate the curing process of stereolithographic applications a proper model was developed based on the fundamental physical and chemical phenomena that govern the behaviour of a thermosetting material in both thermal-initiated and photo-initiated curing applications. The model has been numerically solved using the finite element technique.

Finally, simulations were performed with the presented model, including the cases of polymeric systems submitted to a single or multiple radiation profiles.

4.5 - References

1. Fouassier, J.P., *Photoinitiation, Photopolimerization, and Photocuring: Fundamentals and Applications*. 1995: Hanser Gardner Pubns.
2. Vyazovkin, S. and C.A. Wight, *Model-free and model-fitting approaches to kinetic analysis of isothermal and nonisothermal data*. *Thermochimica Acta*, 1999. **340–341(0)**: p. 53-68.

3. Vyazovkin, S. and N. Sbirrazzuoli, *Kinetic methods to study isothermal and nonisothermal epoxy-anhydride cure*. Macromolecular Chemistry and Physics, 1999. **200**(10): p. 2294-2303.
4. Vyazovkin, S., *A unified approach to kinetic processing of nonisothermal data*. International Journal of Chemical Kinetics, 1996. **28**(2): p. 95-101.
5. Yousefi, A., P.G. Lafleur, and R. Gauvin, *Kinetic studies of thermoset cure reactions: A review*. Polymer Composites, 1997. **18**(2): p. 157-168.
6. Bártolo, P.J., *Optical Approaches to Macroscopic and Microscopic Engineering*. 2001, Reading University, UK.
7. Martin, J.L., A. Cadenato, and J.M. Salla, *Comparative studies on the non-isothermal DSC curing kinetics of an unsaturated polyester resin using free radicals and empirical models*. Thermochimica Acta, 1997. **306**(1-2): p. 115-126.
8. Stevenson, J.K., *Free radical polymerization models for simulating reactive processing*. Polymer Engineering & Science, 1986. **26**(11): p. 746-759.
9. Han, C.D. and D.-S. Lee, *Analysis of the curing behavior of unsaturated polyester resins using the approach of free radical polymerization*. Journal of Applied Polymer Science, 1987. **33**(8): p. 2859-2876.
10. Gordon, M. and W. Simpson, *The rate of cure of network polymers and the superposition principle*. Polymer, 1961. **2**(0): p. 383-391.
11. Kamal, M.R. and S. Souror, *Integrated Thermo-Rheological Analysis of the Cure of Thermosets*. SPE ANTEC Technical Paper, 1972. **18**(93).
12. Kamal, M.R. and S. Sourour, *Kinetics and thermal characterization of thermoset cure*. Polymer Engineering & Science, 1973. **13**(1): p. 59-64.
13. Mijović, J., J. Kim, and J. Slaby, *Cure kinetics of epoxy formulations of the type used in advanced composites*. Journal of Applied Polymer Science, 1984. **29**(4): p. 1449-1462.
14. Núñez, L., et al., *Activation energies and rate constants for an epoxy/cure agent reaction*. Journal of thermal analysis, 1996. **47**(3): p. 743-750.
15. Doornkamp, A.T. and Y.Y. Tan, *Kinetic study of the ultraviolet initiated polymerization of a polyester urethane diacrylate by differential scanning calorimetry*. Polymer Communications, 1990. **31**: p. 362-366.
16. Selli, E. and I.R. Bellobono, *Radiation Curing in Polymer Science and Technology*, in *Polymerisation Mechanisms*, J.P. Fouassier and J.F. Rabek, Editors. 1993, Elsevier Applied Science: London. p. 1-32.
17. Lewis, R.W., et al., *The Finite Element Method in Heat Transfer Analysis*. 1996, Chichester: Wiley.
18. Reddy, J.N. and D.K. Gartling, *The Finite Element Method in Heat Transfer and Fluid Dynamics*. Third ed. 2010, Boca Raton, FL: CRC Press.

19. Reddy, J.N., *An Introduction to the Finite Element Method*. Third ed. 2005: McGraw-Hill Science/Engineering/Math.
20. Matias, J.M., *Simulation and Optimisation of Stereolithographic Processes*. 2007, University of Aveiro: Aveiro.
21. Matias, J.M., P.J. Bartolo, and A.V. Pontes, *Modeling and simulation of photofabrication processes using unsaturated polyester resins*. *Journal of Applied Polymer Science*, 2009. **114**(6): p. 3673-3685.

5

Fabrication process by infrared stereolithography

5.1 - Introduction

As explained in chapter 2, the stereolithographic processes can be classified in two groups: direct irradiation processes with the use of a laser device to scan the resin surface, and mask irradiation processes where resin surface is irradiated at once (see Figure 2.10). In the beginning stage of the present research work was used the mask irradiation concept. An apparatus was developed to obtain microstructures by mask irradiation including a construction platform, an optic system, a Digital Micromirror Device (DMD), a light source and a computer (Figure 5.1).

The structural elements and the construction platform of the apparatus were developed for universal use regardless of the type of radiation involved. However it was used UV radiation to assemble and refine the process because were available irradiation source, optical systems and DMD device for this type of radiation.

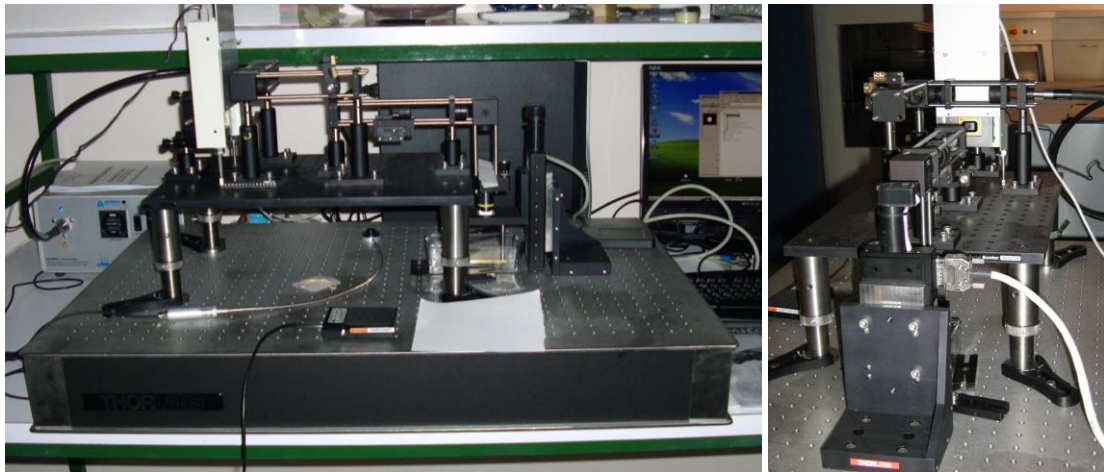


Figure 5.1 – Microstereolithography apparatus developed at CDRsp (Leiria, Portugal)

The construction platform is immersed in a vat containing the resin allowing the recover stage of the process. The construction platform is assembled to a translation stage Micos® VT-80 that performs the z motion (Figure 5.2). This system enables z-steps of 1 μm with a velocity of 0.001-20 mm/s and ensures an accuracy of 100 μm for each 50 mm of amplitude. An RS232 interface enables the control of the system using the software MoCo.



Figure 5.2 – Construction platform and MoCo control software

The dynamic mask generator system used was a DMD Discovery™ 1100 from Texas Instruments controlled by specific software provided by the manufacturer of the equipment. This device consists of an array of micro mirrors individually controlled allowing to generate a bitmap with 1024 x 768 pixels dimension. The dimension of each mirror is 14 μm . Mirrors can actually take two positions: reflect the light to an angle of 30 degrees or deflect the light to other direction. This way, the intended image corresponding to the cross-section of the geometry to be cured can be reproduced by the light beam (Figure 5.3).

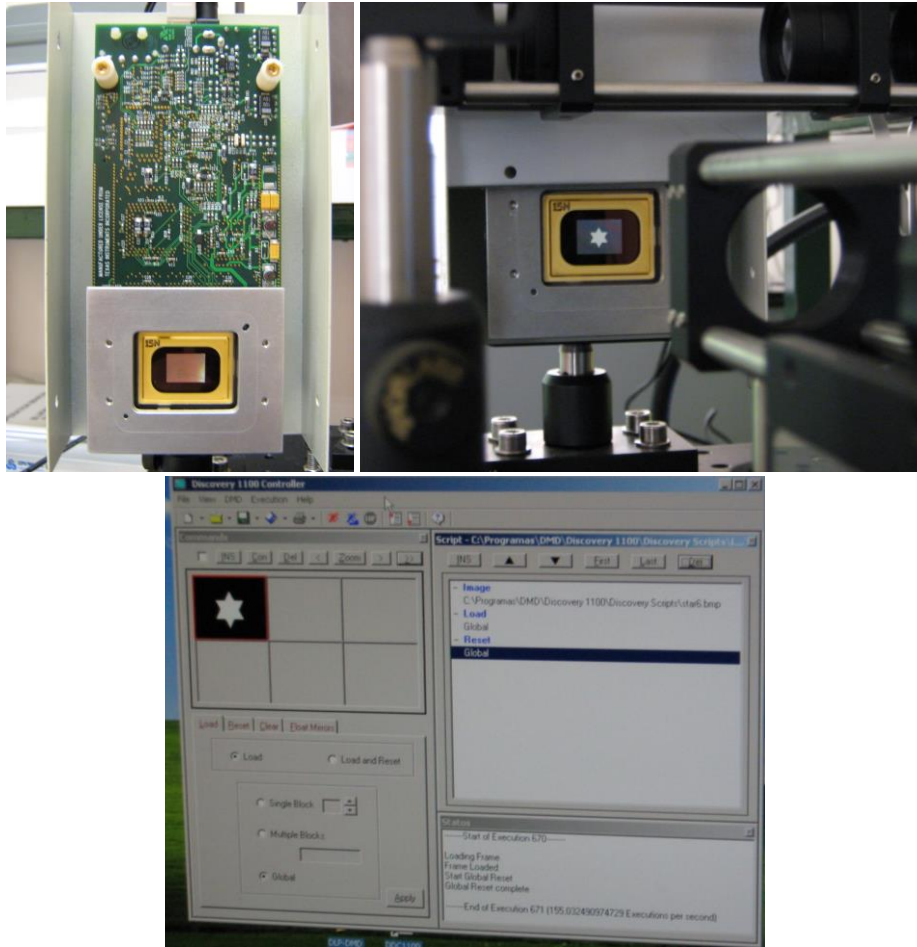


Figure 5.3 - Digital Micromirror Device DMD 0.7 XGA 12° DDR, image being reproduced and control software

The irradiation source used was a light curing system Dymax Bluewave™ 200 consisting on a 200 W mercury bulb with three fundamental peaks of irradiation: 320-390 nm with an intensity of 17 W/cm² irradiation, 390-450 nm with an intensity of 20 W/cm² irradiation, 280-320 nm with an intensity of 7 W/cm² irradiation; a shutter for radiation on-off; a set of filters that ensure control over the wavelength; and a liquid medium lightguide to deliver radiation.

The optic system is composed by following types of lenses from Thorlabs®: bi-convex, plano-convex, meniscus – negative, meniscus – positive. A reduction lens (10x) from Zeiss® is also available to improve the resolution of the system.

Were used structural and positioning elements from Thorlabs®.

The apparatus was used to cure unsaturated polyester resins by UV radiation (Figure 5.4). During this development stage improvements and refinements were made to the system as well as the establishment of procedures for the operations process control of the device.

Small structures were cured by photo-initiated reactions. The control of the cross-section to be cured is made via images sent to the DMD device, the exposure time is controlled by the shutter present in the radiation source and the correct positioning of the material under fabrication is guaranteed by the manipulation of construction platform. The DMD and construction platform

Infrared Stereolithography

are controlled by software while the shutter that determines the exposure time is triggered by a pedal. However this equipment is also endowed with the ability to integrate programmable logic controller (PLC). This way, it is possible to integrate the control of the entire process in a common interface.

The results obtained shown that the apparatus has a proven design and allows to obtain micro structures with controlled geometry with an effective and automated process. In Figure 5.4 can be seen the operation in progress; the first picture in the zone of the light beam collimation and the second picture in the construction zone of the parts, where is visible the geometry of the light beam that reaches the resin surface.



Figure 5.4 – Microstereolithography apparatus in operation curing a photo-sensitive resin

In the Figure 5.5 are shown examples of micro structures with constant cross-section obtained by photo curing of unsaturated polyester resins. In both cases, the parts still present a basic level of cleanliness without the use of appropriate solvents.

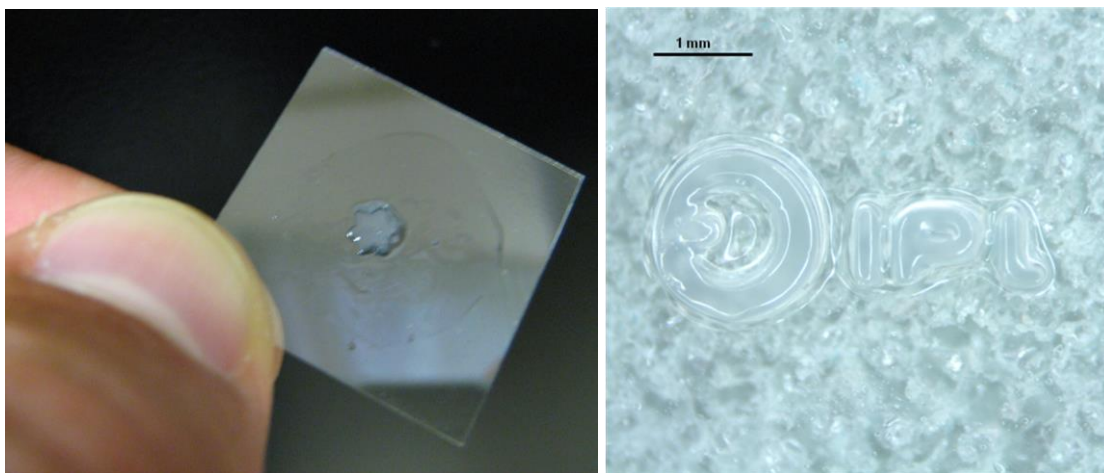


Figure 5.5 – Examples of micro structures obtained by photo curing process

For several reasons it was not possible to adapt the developed equipment to be used with thermo-initiated cure. Thus, the presented work is useful to demonstrate the feasibility, effectiveness and versatility of the manufacturing process designed and assembled. To adapt the

apparatus to thermo-initiated cure some changes are required involving expensive parts. It would be necessary to replace the source of irradiation by another suitable to the desired wavelength. The DMD device used, proper for UV irradiation, would also have to be replaced by an equivalent for use with IR irradiation. Finally, the lenses used were coated for UV irradiation and would have to be replaced by lenses more efficient for IR irradiation.

For the fabrication process using thermo-initiated cure was used an equipment containing a CO₂ laser source at Unicamp (Campinas, Brazil) which was specifically adapted for this purpose.

5.2 - The infrared stereolithography system

An infrared stereolithography apparatus was developed to perform experimental research work with the aim of obtain small sized parts. The apparatus will be described in the following chapters. A general overview is presented in Figure 5.6.



Figure 5.6 – Infrared stereolithography apparatus

5.2.1 - Light source

In this experimental work was used a CO₂ laser device emitting infrared radiation with wavelength of 10.6 μm and a maximum power of 100 Watts. The CO₂ laser has a tube filled with a gas mixture, generally comprised of carbon dioxide, nitrogen, hydrogen and helium, with a transparent mirror on one end and a fully reflective mirror on the other end (Figure 5.7). When electricity is run through the gas mixture, the particles of nitrogen become excited and the excited vibrations of nitrogen cause the carbon dioxide to become excited as well. This effect known as population inversion was described in detail in chapter 2. When the excited nitrogen atoms contact the very cold helium atoms they lose their excited state releasing energy in the form of photons. The light produced is then amplified as it travels through the gas tube reflected by surrounding mirrors. This reflection of light causes the light waves being produced by the nitrogen to reinforce themselves. Thus, the light is amplified as it travels through the gas tube

becoming extremely powerful. The laser beam produced is in the infrared part of the spectrum therefore has a very high wavelength, around 10.6 micrometers.



Figure 5.7 – CO₂ laser device: (a) gas tube and galvanometric mirrors; (b) power unit, control unit and water chiller

5.2.2 - Optical system

For this experimental work was used the direct irradiation stereolithography concept. The resin surface is scanned by the laser beam driven and focused through galvanometric mirrors to cover the intended geometry for each cross-section.

The generation of the laser path was done in the vector graphics editor CorelDRAW following the contour equidistant paths strategy shown in Figure 2.8 of Chapter 2. This strategy prevents the over exposure of the resin avoiding crossing points of the laser path. The distance between two adjacent paths is estimated taking into account the laser beam spot dimension. The path is generated with the purpose of exposing the entire region to be cured at the same energy level (Figure 5.8).

172

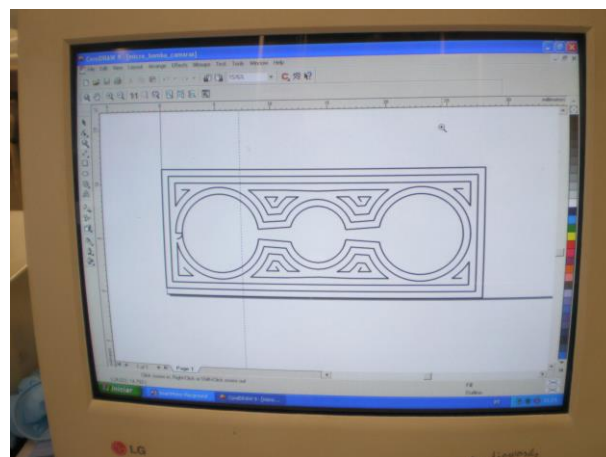


Figure 5.8 – Path generation of a micro-pump cross-section using vector graphics editor CorelDRAW

The information is then exported to RangeScan. This software is responsible for monitoring and setting of the laser device and also for reproducing the programmed path through the control of the galvanometric mirrors (Figure 5.9).

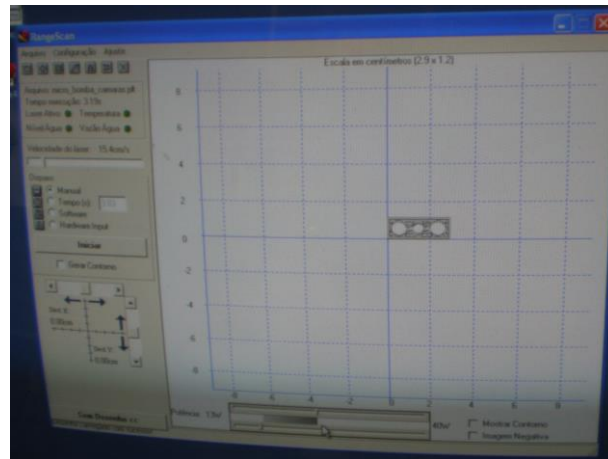


Figure 5.9 – RangeScan software

5.2.3 - Vat control

As previously explained, the xy degrees of freedom are executed by laser beam scanning. Thus the construction platform only has movement in z direction. The construction platform is attached to a slide bars structure moved by a precision step motor and controlled by the SmartMotor software (Figures 5.10 and 5.11). The system allows positioning the construction platform at every 2.5 micrometers.



Figure 5.10 – Construction platform with recoat; z movement system attached to construction platform

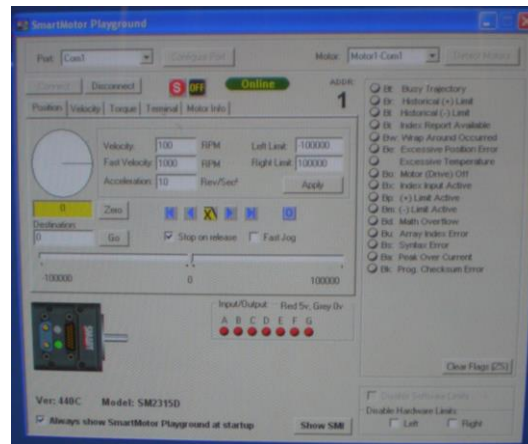


Figure 5.11 – Interface of the control software for positioning system

The recoat system consists of a leveller attached to a step motor and operated sequentially by the user with switches on / off and forward / backward. The deposition of the resin is carried out manually and the excess of resin is scraped off gradually with small decrements until it reaches the level defined for layer thickness (Figure 5.12).



Figure 5.12 – Resin leveller; construction area

5.2.4 - Operating parameters and layer thickness

The operating parameters of the process are the power of the laser, the scanning speed, the dwell time, the repetition rate (number of pulses), and the diameter of the laser beam.

The dwell time represents the average time of interaction between laser beam and resin surface at a specific spot, and is obtained by dividing the beam diameter (2ω) by the scanning speed (v):

$$t_d = \frac{2\omega}{v} \quad (5.1)$$

Because the resin is highly absorptive at the CO₂ laser wavelength (10.6 μm), during dwell time, nearly all the beam energy is absorbed by the resin within a distance from the surface equivalent to the absorption depth δ [1, 2] (Figure 5.13).

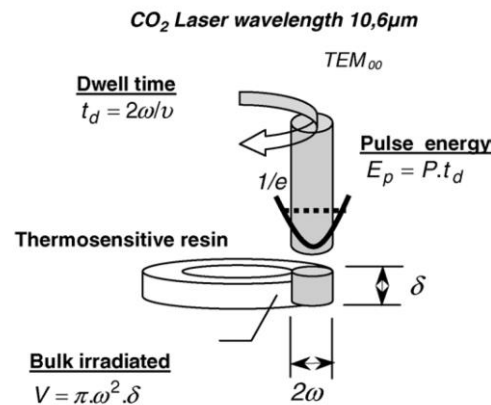


Figure 5.13 – Simple model of the heat flow in laser-induced localized curing [1, 2]

5.3 - Experimental results

Experimental work was carried out using the equipment described in previous chapters with the aim of producing small prototypes. The materials used were: polyester resin AROPOL FS 6902 (Ara Ashland), thermo-initiator Peroxan BP-Paste 50 PF (Pergan), and fumed silica CAB-O-SIL type M-5 (Cabot).

Preliminary studies were conducted at the initial stage of this experimental work attempting to establish an approximation to initial conditions of the process. Samples of the polymeric compound with different compositions were scanned in circular paths by a laser beam with different operating parameters.

It was possible to observe that, in some cases, the value of energy to which the sample was exposed to was insufficient to obtain a significant value of fractional conversion. Likewise, by visual inspection of some samples it is possible to detect an over-exposure of energy that may have led to degradation of the material (Figure 5.14). For example, in the samples L1 to L4, with the same resin composition (polyester resin, 2% wt of thermo-initiator, 0.5% wt of silica) submitted to a 15W power laser beam, it is possible to observe that for higher scanning speeds ($v = 17.5$ cm/s) the result obtained was poor while at low speeds ($v = 8.6$ cm/s) can be notice some over-exposure. For this resin composition, the best sample (L4) was obtained at intermediate speeds ($v = 11.8$ cm/s). As shown in equation (5.1) and Figure 5.13, the scanning speed is inversely proportional to dwell time and the energy release in a small cylindrical volume (V) by the laser beam is the product of the laser power by dwell time [1, 2]:

$$E = P \cdot t_d \tag{5.2}$$

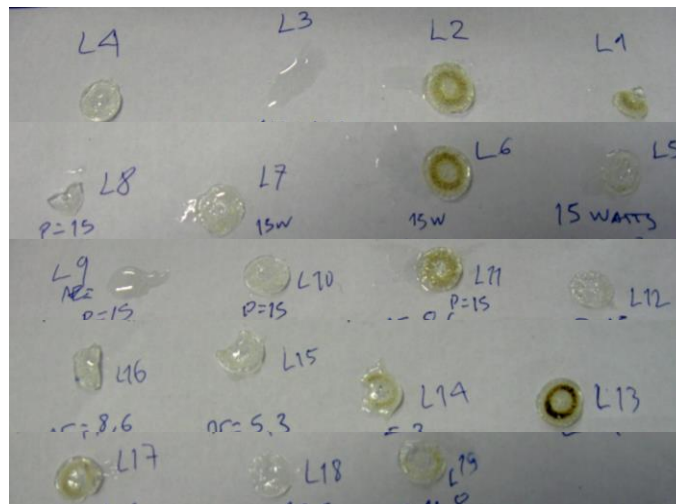


Figure 5.14 – Samples of the polymeric compound submitted to a laser beam scanning

Similar results for ν parameter were observed for different resin compositions. It should be noted, however, that between samples L6 and L7 and between samples L11 and L10 the only parameter modified was the reduction of the number of pulses from 8 to 4, with direct implications in the results obtained: it is visible that the over-exposure is no longer present in samples L7 and L11 obtained with 4 pulses.

Samples L2 and L7 were obtained with the same laser operating parameters but with different resin compositions: L2 (polyester resin, 2% wt of thermo-initiator, 0.5% wt of silica) and L7 (polyester resin, 2% wt of thermo-initiator, 1% wt of silica). It is visible that the effect of over-exposure has disappeared from samples L2 to L7. This is explained by the presence of higher amount of silica particles in the sample L7, who acted as concentrators of energy agents. The heat was absorbed by silica particles preventing degradation of the resin by over-exposure.

The resin does not degrade (despite the high temperature) because of the low exposure time and also due to the high thermal resistance coefficient (K) of silica that captures the energy (heat).

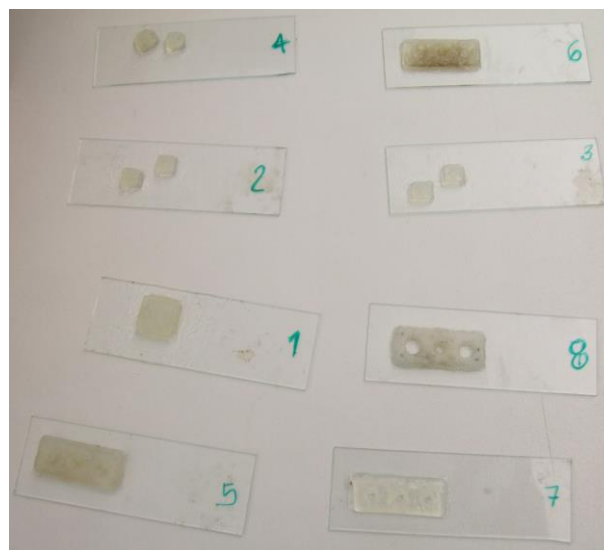


Figure 5.15 – Prototypes produced by infrared stereolithography

The second stage of experimental work was carried out with the purpose of obtain small structures to evaluate and characterise in terms of mechanical properties, and dimensional and geometric accuracy. It was used a polymeric compound with polyester resin, 2% wt of thermo-initiator and 2% wt of silica. An overview of the results obtained is shown in Figure 5.15 and a closer look at Figure 5.16. The small parallelepiped (12 mm x 12 mm x 4 mm) was obtained using a 12W power laser beam with a scanning speed of $v = 15.4$ cm/s. It was produced with 32 layers of 0,125 mm thickness with a constant cross section.



Figure 5.16 – Prototypes produced by infrared stereolithography

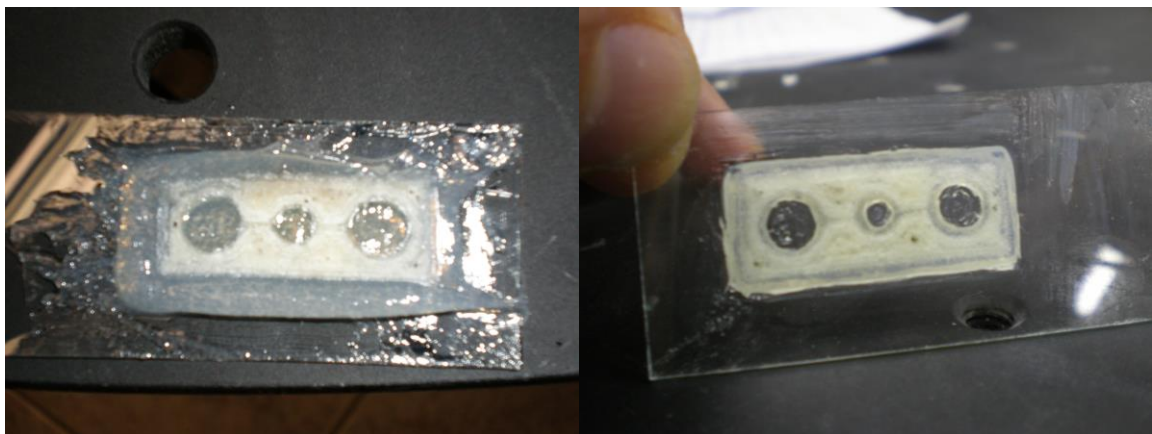


Figure 5.17 – Micro-pump obtained by infrared stereolithography

Figure 5.17 shows a micro-pump obtained by infrared stereolithography before and after being cleaned of uncured material using a proper solvent. It is notorious the micro channels inside the prototype connecting the three chambers. It was used a polymeric compound with polyester resin, 2% wt of thermo-initiator and 2% wt of silica submitted to a 12W power laser beam with a scanning speed of $v = 15.4$ cm/s. It is composed by 37 layers of 0.125 mm thickness and a total

Infrared Stereolithography

of 4 different cross sections, corresponding to the base, the chambers, the in/out channels and the top of the micro pump.

Figure 5.18 shows small holes in the micro-pump. The measure diameter was 2.8 millimetres, nevertheless the overall quality of the walls was very satisfying.

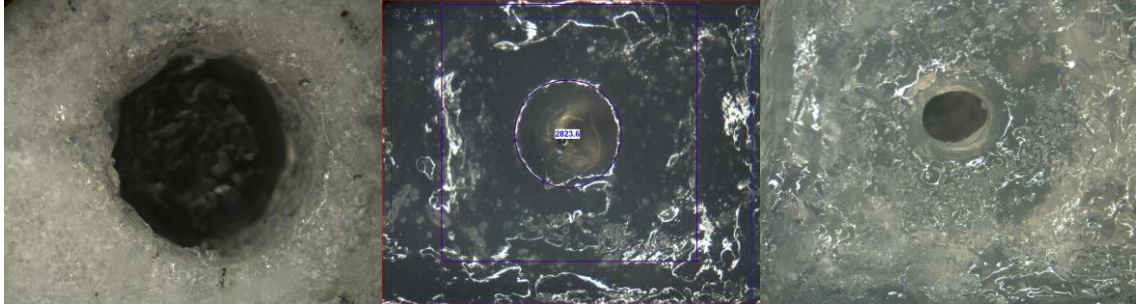


Figure 5.18 – Small hole of the micro-pump

In Figure 5.19 are illustrated three small sized parts with dimension of 6.7 millimetres. The protruded corner was produced to evaluate the spot dimension of the laser beam. It was used a polymeric compound with polyester resin, 2% wt of thermo-initiator and 2% wt of silica submitted to a 12W power laser beam with a scanning speed of $v = 15.4$ cm/s. It is composed by 25 layers of 0.125 mm thickness with a constant cross section.

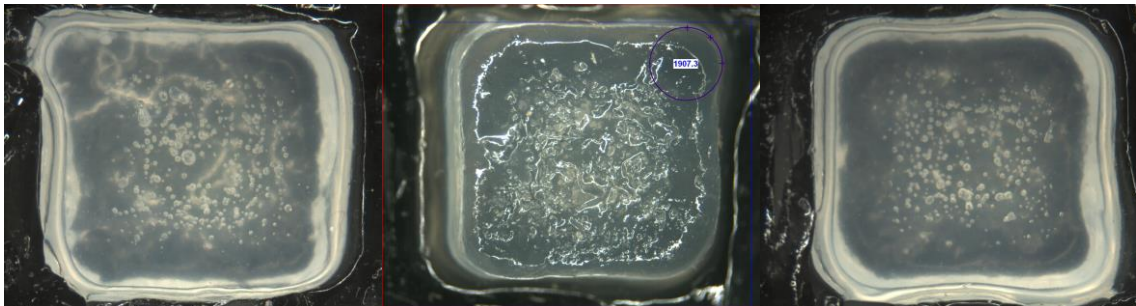


Figure 5.19 – Prototypes produced by infrared stereolithography

In Figure 5.20 is represented the dimensions, the corner angle and the corner radius of the small parallelepiped. There are small deviations in the dimensions and geometry obtained however the overall quality is satisfactory.

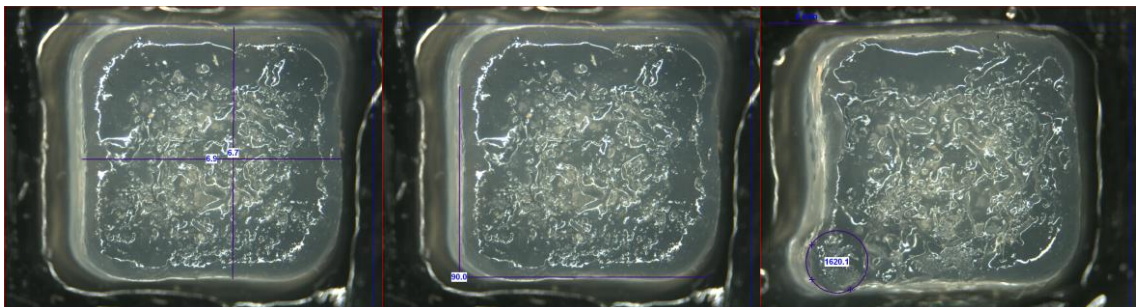


Figure 5.20 – Overall dimensions; corner angle; and corner radius

In Figure 5.21 is visible the difference in the final results for different process parameters and scanning conditions. In the first pictures, there very small visible bubbles randomly dispersed and in the others pictures the visual effect is clearly dominated by the laser beam path.

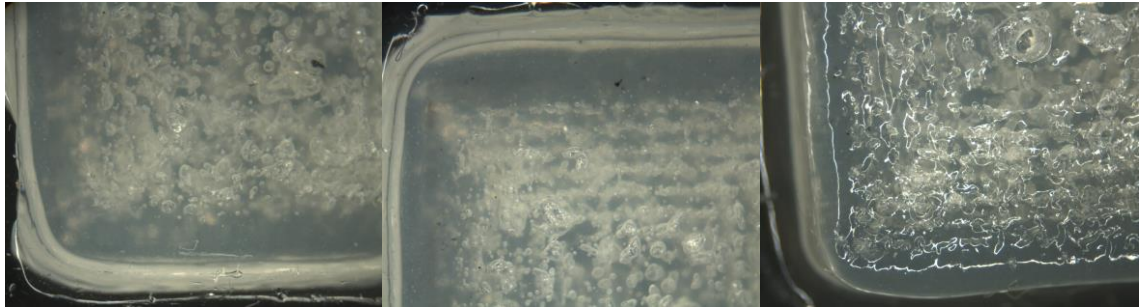


Figure 5.21 – Different parameters and scanning strategies

Figure 5.22 shows images of the prototypes obtained by scanning electron microscope (SEM). The composition of the polymeric compound used to obtain the analysed prototypes was polyester resin, 2% wt of thermo-initiator and 2% wt of silica. Nanoparticles of silica randomly dispersed are visible in the top right figure.

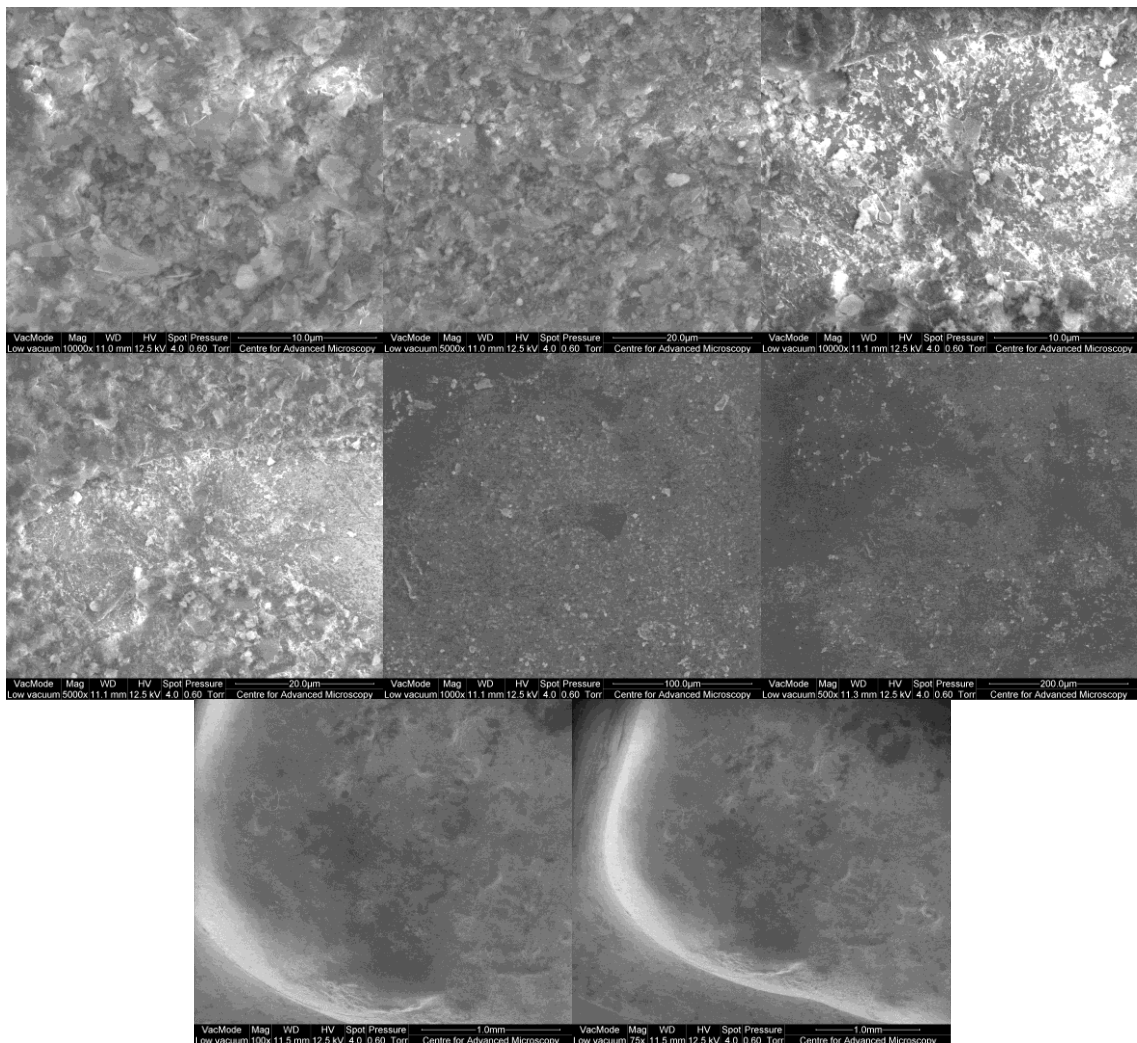


Figure 5.22 – Prototypes analysed by SEM

5.4 - Summary

In this Chapter was described the implementation of an infrared stereolithography system. For this purpose a device was manufactured and tested. The first prototyped equipment is composed by a light source, a shutter to switch on-off the radiation, a set of filters and lenses that ensure control over the wavelength, a DMD™ to define the micro-image of each layer of the model, a ZEISS® lens to reduce the layer image (maximum 10x) and the construction area. Micro sized prototypes were produced by UV radiation.

A second apparatus was adapted in order to produce parts by infrared radiation. It is composed by a CO₂ laser device emitting infrared radiation with wavelength of 10.6 μm and a maximum power of 100 Watts, an optical system to control the laser beam, and a vat control system to positioning the surface of the resin to be polymerised.

The laser system and the positioning system were fine-tuned in order to obtain a good resolution. The operating parameters were tested and it was determined proper conditions for obtain prototypes. Several obtained prototypes were presented in detail.

5.5 - References

1. Jardini, A.L.M., et al., *Improvement of the spatial resolution of prototypes using infrared laser stereolithography on thermosensitive resins*. Journal of Materials Processing Technology, 2006. **172**(1): p. 104-109.
2. S. R. Andrade, A.L.J., M. R. Wolf Maciel, R. Maciel Filho,, *Numerical simulation of localized cure of thermosensitive resin during thermo stereolithography process (TSTL)*. Journal of Applied Polymer Science, 2006. **102**(3): p. 2777-2783.

6

Conclusions

6.1 – Introduction

The theoretical and practical bases of a new stereolithographic approach using infrared radiation to produce small sized prototypes were researched. Due to extensive experimental work carried out was possible to develop a better understanding relating to the physical and chemical transformations associated with the cure process.

Furthermore, polymeric systems suitable for being used in the construction of prototype models obtained by infrared stereolithography were studied and developed. Thus, it was possible to understand the influence of process parameters, such as, light intensity or temperature, irradiation time, and initiator concentration in the cure kinetics and in the mechanical properties of the cured parts. The effect of silica was subject of an intensive research which allowed to know its influence in the process.

Prototype systems were developed. Firstly, an apparatus capable of producing micro parts using UV radiation was obtained. It has been demonstrated the suitability of the equipment to operate with the mask irradiation technique. Then, an infrared stereolithographic system

capable of produce small sized parts was developed using a laser device to scan the resin surface.

Phenomenological models were used to describe thermal-initiated curing reactions. These models make it possible to control several kinds of information: the progress of the cure reaction for estimating the time to produce a physical model, the spatial solidification profile for controlling the precision of the process and diffusion control effects to evaluate the need of post-curing operations.

6.2 – Summary and conclusions

The main conclusions of the research work are:

Significant benefits can be achieved with the use of infrared radiation. Since the reaction is thermal induced, shadow effects are avoided and therefore opaque additives can be added to resin composition with potential advantages in mechanical properties or others.

Two different types of thermal-initiator were investigated, a methyl ethyl ketone and a benzoyl chloride, submitted to an isothermal situation. The resin containing benzoyl chloride thermal-initiator has achieved higher values of fractional conversion for the same curing time. The curing reaction has started earlier, therefore with a shorter inducing period. Also during the propagation phase of the reaction, the resin containing benzoyl chloride has revealed faster conversion rates. For the time periods investigated, the same polymeric compound has achieved higher fractional conversion values at final stages of reaction.

Temperature as a strong influence in cure kinetics accelerating the reaction and leading to higher values of fractional conversion obtained. More energy present in the resin means lower induction time, higher reaction rate and also reduces the vitrification phenomenon increasing the conversion of material.

Above certain value of curing temperature, the increasing of temperature does not have significant effects in terms of final fractional conversion obtained. In fact, values near total conversion are achieved and this way there are not more reactive centres available to continue the reactions. Although the increment of fractional conversion for higher values of temperature, it was notorious that relatively smaller benefits are achieved when the temperatures involved are already high.

Higher peak values of reaction rate are achieved for higher temperatures and those values are attained in shorter periods of time.

Using gel content method, shadows effects were not detected since initiator species are thermo-sensitive and heat source was not irradiation, but rather isothermal chamber, i.e. the heat energy could reach the inside zones of resin without being blocked by more external initiator species.

The theoretical iso-conversion curve for fractional conversion 1.0 is quite distant from the 0.9 curve, reflecting the fact that, above this value, the polymerisation reaction faces difficulties to propagate. Two major issues contribute to this situation. The lower amount of reactive species present in the resin, since they were already consumed in the process, and also the increase of viscosity of resin and consequently loss of mobility of the polymeric chains, makes it difficult reactive centres to be in the same zone. Therefore, vitrification phenomenon predominates at this stage of the process, and consequently more energy has to be supplied to the system, increasing the time of exposure or the temperature.

Similar results, in terms of fractional conversion, can be obtained either by increasing the exposure temperature or the curing time of the resin. An optimized solution must be found regarding intended purposes for the solidified part since both parameters represents resources consumption.

The concentration of initiator accelerates the cure reaction, reducing the induction time since there are more reactive centres available to start the polymerisation reaction. Also the propagation stage occurs with higher reaction rates, peak values of reaction rate are higher and are achieved sooner. Hence, the vitrification occurs sooner for higher initiator concentrations as a result of consumption of initiator species and decreasing mobility of polymeric chains.

Although all stages of polymerisation reactions occur sooner and faster, the effect of the initiator concentration in the fractional conversion obtained is evident for lower percentages of initiator but not so obvious for higher amounts. In that case, there is a slightly increase due to near 1 values are already achieved.

A very high value of initiator concentration leads to more expensive resins and as a strong effect on the raise of resin viscosity with prejudice in the process time, mainly in deposition of the resin and in the recoat. As stated previously, above certain values there is no significant advantage in having higher values of initiator concentration.

Adding silica to the polymeric system enables to control the curing region, since silica concentrate the thermal energy avoiding unwanted polymerisation at surrounding areas.

The presence of silica in the polymeric system enhances the cure reaction since thermal energy captured by silica particles promotes thermal initiated reactions.

For low concentrations of silica, vitrification is promoted since mobility of polymerised chains is affected, not only because silica increase viscosity of resin but mainly because energy is not dispersed in a continuous way in the resin but focused in the silica particles scattered by the resin.

With higher concentrations of silica, for almost all the temperatures tested was obtained total conversion. Despite of peak value of reaction rate is achieved for a short period of time, the reaction rate deceleration is not due to vitrification phenomenon but otherwise due to the consumption of reactive species. In fact, the presence of huge quantities of silica particles acting

has heat concentrators dispersed in to the resin, promotes the polymerisation reaction at numerous locations.

For very high values of silica concentration, and although using silica with nano sized particles, the viscosity of the polymeric resin increase significantly, with obvious repercussions in the preparation and processing of material. Not only is difficult to obtain a homogeneous and well-mixed resin as the multi-layer process is hindered by significant increase in the time necessary to recoat process. Also obtaining such a thinner layer is more difficult to attain.

Particle size of silica influences cure reaction. Smaller particles accelerates the reaction, reducing induction time because, for the same concentration of silica, more reactive points are available allowing a faster induction of reaction with repercussions in the following stages of reaction.

Vitrification phenomenon occurs with more consequences for smaller particles case because the energy is concentrated in more, but smaller points. This way the mobility of reactive chains is less affected with the use of larger silica particles. In this case, the thermal energy is retained in larger spots and this way dispersed by larger areas.

Therefore, silica with small sized particles leads to higher reaction rates but slightly lower fractional conversions. However, this inconvenient can be solved with the use of higher energy values.

Small sized silica particles have also positive impact in the resolution of the cured models since retain the thermal energy in more localised spots, therefore improving the accuracy of the cured geometry.

With the use of silica, the initiator concentration accelerates the reaction. The induction time is shortened because the presence of larger quantities of reactive species enables the polymerisation reaction to start at some more spots dispersed in the resin. Consequently also the propagation stage of reaction is accelerated since more reactive spots are present and also more reactive species are available to continue the polymerisation. However, for larger amounts of silica (5,0 % wt) the vitrification phenomena prevails derived by the very higher viscosity and the final results, in terms of fractional conversion, are affected. Therefore, better results were obtained for 2% in weight of initiator concentration because of the polymeric chain loss of mobility due to the high viscosity of the resin. The reactive spots became imprisoned and it was not possible to continue the reaction.

The presence of silica accelerate the reaction since the particles of silica act as a heat concentrator and consequently enables the reaction due the presence of energy in localized spots dispersed by the resin.

On the other hand, for relatively low value of energy the powder silica contributes to the significantly increase of the resin viscosity, hindering total conversion.

Modeling cure kinetics can avoid extensive experimental work. Understanding the influence of process parameters over the cure reaction allows predicting final results and therefore parameters can be fine tuned to obtain the intended final result.

Two different approaches were tested to produce micro components. It was proven that both are suitable to obtain good results. Two major difficulties were faced in the developed apparatus; for the integral exposure, the absence of a CO₂ laser device; for the laser scanning, some components were inappropriate to obtain smaller parts.

Small deviations in terms of dimensions and geometry were detected in the produced prototypes. However, satisfactory results were obtained leading to the assumption that both processes are adequate to obtain micro components by infrared stereolithography.

6.3 – Further work

Based on the results and experience gained throughout this work, the following aspects are suggested:

Study the crossed result of thermal and photo initiated polymerisation. Since the cure reaction is exothermic, can this energy be used to initiate thermal initiators?

Fine tune and improve of both prototyped apparatus. Test the use of an infrared source in the mask irradiation system. Improve the accuracy of components in the laser scanning system.

Study the limits in terms of accuracy and resolution with the use of silica.

Research the use of other additives together with silica to improve mechanic, electric or magnetic properties. Understand its influence in cure kinetics and the advantages obtained.

